UNITED STATES DEPARTMENT OF THE INTERIOR

GEOLOGICAL SURVEY

PROCEEDINGS OF CONFERENCE LXII

EIGHTH JOINT MEETING of the U.S.-JAPAN CONFERENCE

ON NATURAL RESOURCES (UJNR)

PANEL ON EARTHQUAKE PREDICTIONS TECHNOLOGY

NOVEMBER 16-21, 1992

OPEN-FILE NO 93-542

MENLO PARK, CALIFORNIA

1993

Proceedings of the

Eighth Joint Meeting of the U.S.-Japan Conference on Natural Resources (UJNR)

Panel on Earthquake Prediction Technology

November 16-21, 1992

Panel Chairmen:

Robert L. Wesson
U.S. Geological Survey
Reston, Virginia 22092
U.S.A.

Yamato Miyazaki
Geographical Survey Institute
Ibaraki-Ken 305
Japan

Table of Contents

INTRODUCTION

The 8th Joint Meeting of the U.S.-Japan Natural Resources Panel on Earthquake Prediction Technology was held in Seattle, Washington and near Landers, California on November 16-21, 1992. The UJNR program fosters the exchange of scientists, information, equipment and knowledge between government agencies in Japan and the United States concerned with problems involving natural resources.

Technical sessions were held in Seattle, Washington, on November 17-18, 1992, with the scientific theme of the meeting "*Great subduction zone earthquakes*". The technical chairman for the meeting was Dr. Craig Weaver (U.S.G.S., Seattle, WA).

A field trip was taken to visit newly recognized paleoseismic sites in Puget Sound, near Seattle, on November 19, 1992, under the leadership of Dr. Robert Bucknam (U.S.G.S., Golden, CO), and Dr. Brian Atwater (U.S.G.S., Seattle, WA). The entire party travelled by ferry across Puget Sound to visit the uplifted beaches on Restoration Point. Upon returning to Seattle, some members of the party visited the site of the Seattle Sewage Treatment Plant, where excavations in progress revealed further paleoseismic evidence. All participants who visited the construction site to view evidence of tsunami (or seiche?) depoists will long remember the specialized footwear provided by Dr. Bucknam and Dr. Atwater.

The Japanese delegation continued from Seattle to Ontario, California, on November 20, 1992, where they were met by Mr. Michael Rymer (U.S.G.S., Menlo Park, CA) and Dr. Susan Hough (U.S.G.S., Pasadena, CA), who took them to visit the site of the 1992 M 7.4 Landers, California earthquake. The Landers field trip concluded on November 21, 1992.

U.S.-Side Members of the UJNR Panel on Earthquake Prediction Technology

Dr. Robert L. Wesson, Chairman
Chief
Office of Earthquakes Volcanoes and Engineering
U.S. Geological Survey
12201 Sunrise Valley Drive
Reston, Virginia 22092

Dr. James H. Dieterich
Branch of Tectonophysics
U.S. Geological Survey
345 Middlefield Road
Menlo Park, California 94025

Dr. William L. Ellsworth
Branch of Seismology
U.S. Geological Survey
345 Middlefield Road
Menlo Park, California 94025

Dr. David P. Hill
Branch of Seismology
U.S. Geological Survey
345 Middlefield Road
Menlo Park, California 94025

Mr. Gary Johnson
Assistant Associate Director,
Office of Earthquakes and Natural Hazards
Federal Emergency Management Agency
Washington, D.C. 20472

Dr. Andy Murphy
Earth Science Branch, MS 007NL
U.S. Nuclear Regulatory Commission
Washington, D.C. 20555

Mr. William Strange
Chief, Geodynamics Branch
Geodetic Research and Development Laboratory
National Geodetic Survey/NOS
6001 Executive Boulevard
Rockville, Maryland 20852

Dr. Wayne Thatcher
Branch of Tectonophysics
U.S. Geological Survey
345 Middlefield Road
Menlo Park, California 94025

Dr. Shelby G. Tilford
Director
Earth Science and Applications Division
National Aeronautics and Space Administration
Washington, D.C. 20550

Dr. James Whitcomb
National Science Foundation
1800 G Street, N.W.
Washington, D.C. 20550

Dr. Richard Wright
Director
Center for Building Technology
National Institute of Standards and Technology
Building Research Building, 226
Gaithersburg, Maryland 20899

Japan-Side Members of the UJNR Panel on Earthquake Prediction Technology

Mr. Yamato Miyazaki, Chairman
Director General
Geographical Survey Institute
Kitazato-1, Tsukuba-Shi
Ibaraki-Ken 305

Dr. Yoshitake Egawa, Secretary
Director
Crustal Dynamics Department
Geographical Survey Institute
Kitazato-1, Tsukuba-Shi
Ibaraki-Ken 305

Dr. Kazuo Hamada
Visiting Research Officer
National Research Center for Disaster Prevention
3-1, Tennodai, Tsukuba-Shi
Ibaraki-Ken 305

Dr. Katsuhiko Ishibashi
Chief
Seismology Division
International Institute of Seismology and Earthquake Engineering
Building Research Institute
Tatchara-1, Tsukuba-Shi
Ibaraki-Ken 305

Dr. Sigeru Kato
Senior Officer
Planning Division
Hydrographic Department
Maritime Safety Agency
5-3-1, Tsukiji, Chuo-Ku
Tokyo 104

Dr. Yasuo Kadokawa
Associate Director General
Communications Research Laboratory
4-2-1, Nukuikita-Machi, Koganei-Shi
Tokyo 184

Dr. Tadanao Oh'ishi
Director
Quantum Metrology Department
National Research Laboratory of Metrology
1-1-4, Umezono, Tsukuba-Shi
Ibaraki-Ken 305

Dr. Yoshihiro Kinugasa
Chief
Seismo-Tectonics Research Section
Environmental Geology Department
Geological Survey of Japan
1-1-3, Higashi, Tsukuba-Shi
Ibaraki-Ken 305

Mr. Yutaka Iida
Director
Earthquake Disaster Prevention Department
Public Works Research Institute
Asahi-1, Tsukuba-Shi
Ibaraki-Ken 305

Dr. Kenshiro Tsumura
Head
Seismological and Volcanological Management Division
Seismological and Volcanological Department
Japan Meteorological Agency
1-3-4, Ote-Machi, Chiyoda-Ku
Tokyo 100

Participants in the Eighth Joint Meeting of the UJNR Panel on Earthquake Prediction Technology

U.S. Members:

Robert L. Wesson, Chairman
U.S. Geological Survey, MS-905
12201 Sunrise Valley Drive
Reston, Virginia 22092

James H. Dieterich
U.S. Geological Survey, MS-977
345 Middlefield Road
Menlo Park, California 94025

William L. Ellsworth
U.S. Geological Survey, MS-977
345 Middlefield Road
Menlo Park, California 94025

David P. Hill
U.S. Geological Survey, MS-977
345 Middlefield Road
Menlo Park, California 94025

U.S. Observers:

Brian Atwater
U.S. Geological Survey
Geophysics Program AK-50
University of Washington
Seattle, Washington, 98195

John Booker
Geophysics Program AK-50
University of Washington
Seattle, Washington, 98195

Bob Bucknam
U.S. Geological Survey, MS-966
Box 25046
Denver Federal Center
Denver, Colorado 80225

Gary Carver
Department of Geology
Humboldt State University
Arcata, California 95521

Ken Creager
Geophysics Program AK-50
University of Washington
Seattle, Washington, 98195

Robert Crosson
Geophysics Program AK-50
University of Washington
Seattle, Washington, 98195

Jim Dieterich
U.S. Geological Survey, MS-977
345 Middlefield Road
Menlo Park, California 94025

Susan Hough
U.S. Geological Survey
525 Wilson St.
Pasadena, California 91106

Lorraine Hwang
U.S. Geological Survey
525 Wilson St.
Pasadena, California 91106

Allan G. Lindh
U.S. Geological Survey, MS-977
345 Middlefield Road
Menlo Park, California 94025

Steve Malone
Geophysics Program AK-50
University of Washington
Seattle, Washington, 98195

Karen Meagher
U.S. Geological Survey
Geophysics Program AK-50
University of Washington
Seattle, Washington, 98195

Walter Mooney
U.S. Geological Survey, MS-977
345 Middlefield Road
Menlo Park, California 94025

Alan Nelson
U.S. Geological Survey, MS-966
Box 25046
Denver Federal Center
Denver, Colorado 80225

Stuart Nishenko
U.S. Geological Survey, MS-967
Box 25046
Denver Federal Center
Denver, Colorado 80225

Anthony Qamar
Geophysics Program AK-50
University of Washington
Seattle, Washington, 98195

Michael Rymer
U.S. Geological Survey, MS-977
345 Middlefield Road
Menlo Park, California 94025

Stewart Smith
Geophysics Program AK-50
University of Washington
Seattle, Washington, 98195

Paul Somerville
Woodward-Clyde Consultants
566 El Dorado Street
Pasadena, California 91101

Chris Stephens U.S. Geological Survey, MS-977 345 Middlefield Road Menlo Park, California 94025

Craig Weaver U.S. Geological Survey Geophysics Program AK-50 University of Washington Seattle, Washington, 98195

Japanese Members:

Yamato Miyazaki
Director General
Geographical Survey Institute
Kitazato-1, Tsukuba-Shi
Ibaraki-Ken 305

Yoshitake Egawa
Director
Crustal Dynamics Department
Geographical Survey Institute
Kitazato-1, Tsukuba-Shi
Ibaraki-Ken 305

Kazuo Hamada
National Research Center for
Disaster Prevention
3-1, Tennodai, Tsukuba-Shi
Ibaraki-Ken 305

Katsuhiko Ishibashi
International Institiute of Seismology
and Earthquake Engineering
Building Research Institute
1 Tatehara, Tsukuba-Shi
Ibaraki-Ken 305

Shigeru Kato
Hydrographic Department
Maritime Safety Agency
Tsukiji 5-3-1, Chuo-ku
Tokyo 104

Yoshihiro Kinugasa
Geological Survey of Japan
1-1-3, Higashi, Tsukuba-Shi
Ibaraki-Ken 305

Japanese Observers:

Masajiro Imoto
National Research Center for
Disaster Prevention
3-1, Tennodai, Tsukuba-Shi
Ibaraki-Ken 305

Hiroki Kuroishi
Geographical Survey Institute
Geographical Survey Institute
Kitazato-1, Tsukuba-Shi
Ibaraki-Ken 305

Shouichi Matsumura
Geographical Survey Institute
Kitazato-1, Tsukuba-Shi
Ibaraki-Ken 305

Kiyoo Mogi
College of Industrial Technology
Nihon University
Izumi-Machi 1-2-1
Narashino-Shi
Chiba-Ken, 275

Noritake Nishide
Japan Meterological Agency
Seismological and Volcanological Department
1-3-4, Otemachi, Chiyodaku
Tokyo 100

Taizo Yoshino
Communications Research Laboratory
4-2-1 Nukuikita-machi, Koganei
Tokyo 184

RESOLUTION OF THE EIGTH JOINT MEETING U.S.-JAPAN PANEL ON EARTHQUAKE PREDICTION TECHNOLOGY

U.J.N.R.
November 1992

The UJNR Panel on Earthquake Prediction Technology recognizes the critical improtance of promoting prediction research in both countries. The Eigth Joint Meeting was extremely beneficial in furthering friendship and deepening understanding of the common problems of both Japan and the U.S.

Technical sessions included presentation of 27 papers, focussing on great subduction zone earthques in Japan and the U.S., including extensive discussion of national and agency programs, probabilistic methods of earthquake forecasting, earthquake precursors, fundamental earthquake studies, crustal structure and the M 7.5 Landers, California earthquake of 1992.

Discussion was extremely frutiful, and the Panel unanimously adopted the following resolutions:

1. One of the most important means of achieveing joint progress is by the long-term exchange of researchers between our two countries. Since the First Joint Meeting such exchanges have already achieved extremely valuable results. We recognize the advantages of close coopearation between governmental and academic scientists in earthquake prediction research in both the United States and Japan. Each side should investigate possibilities for widening participation in the Panel. In this respect, the panel members recognize the importance of joint activities in the form of symposia, and support the proposal of cooperative programs on earthquake prediction research under the U.J.S.T. agreement. Efforts should also be made to cooperate on instrumental development, observations, data interpretation, and earthquake prediction experience, collocation between laser ranging, GPS and VLBI techniques, development of transportable VLBI and SLR systems, research on active faults, and laboratory rock mechanics.

2. We strongly agree that exchanges of data and analysis methods are mutually beneficial, and strongly encourage these activities. In particular, the Panel empahasizes the importance of sharing experience and exchanging data in the areas of geodetic measurements, crustal deformation and monitoring, precursory phenomena, modelling techniques, and automatic processing of both seismic and crustal deformation data.

3. Advances in the archiving and retrieval of seismic waveform data has created a new envornment for collaborative research. The panel endorses and encourages cooperation in the analysis of these data, and recognizes the potential for exchange of these data through computer network connections between our two countries.

4. Cooperation in the application of space techniques to prediction research is already in progress and should continue. Information on the precision geodetic measurements and GPS measurements for the detection of crustal deformation should be exchanged. Coopearative experiments using U.S. and Japanese laser ranging and VLBI facilities should be continued.

5. The next joint meeting will be held in Japan in the autumn of 1994.

Opening Remarks
by
William L. Ellsworth

On behalf of Dr. Robert Wesson, U.S. Chairman, and the other U.S. members of the U.S.-Japan Conference on Natural Resources, I would like to welcome everyone to the 8th meeting of the Panel on Earthquake Prediction Technology. I want to extend an especially warm welcome to our guests from Japan, and wish you all a plesant stay in the Emerald City of Seattle.

Over the past 14 years, the work of this UJNR Panel, through its joint meetings, and scientist-to-scientist exchanges, has done much to improve our common understanding of earthquakes, advance the technology we use to study them, and perhaps most importantly, put this technology into practical use for the benefit of both of our societies. During our meeting these next two days, we can look forward to learning about many exciting, new results from both sides of the Pacific.

One important result that you will hear about has been a major change in our perception of earthquake hazards in Seattle, and more generally, the Pacific Northwest of the United States. Many of the scientists responsible for advancing and refining this understanding are in attendance. I am sure that they look forward to sharing their ideas with you, and will welcome your comments and questions.

Opening Remarks
by
Yamato Miyazaki

It is our honor and pleasure to be able to visit the United States and this most beautiful city of Seattle to participate in the 8th Joint Meeting of UJNR, the United States-Japan Conference on Developement and Utilization of Natural Resources Panel on Earthquake Prediction Technology.

To our pleasure this conference also gives us an opportunity to meet old friends again and make new friends.

Prediction of earthquakes, compared to other fields of science, is no easy task. Nowdays with rapid economic and urban development, the demand for prediction technology is increasingly urgent. I believe the exchange of information and opinions through the Technical Sessions will greatly help to minimize damage caused by earthquakes not only for us but also for the whole world.

Taking this opportunity I would like to express our deepest gratitude to Dr. Robert Wesson and all the staff members for organizing and inviting us to this most meaningful conference. Also please accept our special appreciation to Dr. William L. Ellsworth and Dr. Craig Weaver for their dedicated efforts. Here may I introduce the participants from Japan. Professor Kiyoo Mogi, Special Guest for today. As you may well know, Professor Mogi is leading the Coordinating Committee for Earthquake Prediction and the Panel on Earthquake and Volcano of Geodetic Council.

Paper Presented at the Eighth UJNR Meeting

Y. Miyazaki, and Y. Egawa, Activities of the Coordinating Committee for Earthquake Prediction.

B. Atwater, Surety of assertion in subduction-zone paleoseismology.

Y. Inouchi, Y. Kinugasa, and F. Kunmon, Study of turbidite as an indicator of an earthquake and its intensity.

A.R. Nelson, Great subduction-zone earthquakes in the Pacific Northwest? Differentiating coseismic from nontectonic tidal-marsh deposits along the Oregon coast.

G.A. Carver, Comparison of paleoseismic geology of subduction zone earthquakes in Alaska and Cascadia.

K. Mogi, Recent crustal activity in the Tokai (Japan) region where a large earthquake is expected in the near future.

S.P. Nishenko, and L.R. Sykes, Comment on "Seismic gap hypothesis: ten years after" by Y.Y. Kagan and D.D. Jackson.

K. Ishibashi, Review of the recurrencd history fo great subduction earthquakes along the Sagami-Nankai trough, Japan: irregularity has a definite tectonophysical reason.

P. Somerville, Strong ground motion prediction for Cascadia subduction earthquakes.

R.C. Bucknam, E. Hemphill-Haley, and E.B. Leopold, Late Holocene uplift at Puget Sound, Washington, U.S.A.

S. Matsumura, Work of the Coastal Movements Data Center.

C.D. Stephens, Seismicity, stress orientation and configuration of the Aleutian megathrust in the vicinity of the great 1964 Alaska earthquake.

S. Malone, Regional seismic network recording and analysis under technological change.

K. Hamada, The plan for intensified observational facilities for prediction research of earthquakes occurring in the Tokyo metropolitan area.

W.D. Mooney, Probing the active subduction zone of the Pacific NW, USA.

R.S.Crosson, Cascadia subduction zone: large scale structure studies.

T. Yoshino, Results of recent geodetic VLBI experiments by the Communications Research Laboratory.

J. Booker, Electromagnetic imaging of crustal structure: recent results and prospects.

S. Kato, Developement of a sea-bottom surveying and processing system on SEA BEAM 2000.

K. Hamada, Statistics of earthquake precursors in Japan in the 20 years preceeding the end of 1990.

J.H. Dieterich, Stressing rate- and state-dependence of seismicity: applications to earthquake clustering.

M. Imoto, Foreshock occurrence in Kanto, central Japan, and its performance as a precursor.

A.G. Lindh, K. Breckenridge, and M. Gladwin, Seismicity and creep at Parkfield.

K.L. Meagher, Relocation of earthquakes in the Parkfield region.

N. Nishide, and M Seino, Probability estimation of large earthquake occurrence from the viewpoint of successiveness of seismic activity.

L. Hwang, An overview of the 1992 Joshua Tree, Landers and Big Bear earthquakes.

D.P. Hill, and P.A. Reasenberg, Seismicity triggered at large distances by the M 7.5 Landers, California, earthquake of June 28, 1992.

Activities of the Coordinating Committee for Earthquake Prediction

Yamato MIYAZAKI, Yoshitake EGAWA
Geographical Survey Institute
Tsukuba, Ibaraki,305, Japan

1. Introduction

23 years have passed since the CCEP(Coordinating Committee for Earthquake Prediction) was established. The purpose of the CCEP is realization of earthquake prediction. The CCEP has been playing an important role in promoting cooperation and information exchange among scholars in related fields both from universities and governmental organizations. In May 1992, the 100th regular meeting of the CCEP was held.

In this report, first the organization of the CCEP is introduced, secondary its achievements are shown, and finally its role in the earthquake prediction system in Japan is explained.

2. The Organization of the CCEP

The CCEP is composed from about 30 researchers concerning earthquake prediction in various areas, i.e. seismology, geology, geodesy, oceanology, geochemistry, etc. from universities or governmental organizations. The Geographical Survey Institute, the secretariat of the CCEP, commissions the members of the CCEP and makes an announcement concerning important matters discussed in the CCEP. Organizations from which the CCEP members come are as follows(Table 1).

Geographical Survey Institute (Secretariat)
National Research Institute for Earth Science and Disaster Prevent
Meteorological Agency
Hydrographic Department, Maritime Safety Agency
Geological Survey of Japan
National Astronomical Observatory
Hokkaido University
Tohoku University
University of Tokyo
Nagoya University
Kyoto University
Kyushu University
Nihon University

TABLE 1 Composition of the CCEP

The chairman of the CCEP is elected among the members. Professor K. Mogi of Nihon University, originated from the head of the Earthquake Institute of Tokyo University, is the Chairman of the CCEP now. The regular meeting is generally held 4 times a year. Besides the regular meeting, the subcommittee for the Intensified Observation Areas and the Specific Observation Areas are held, as occasion demands.

The results of observations and researches by the organizations of the CCEP members are exchanged and discussed in the meeting. The most apparent difference between academic societies and the CCEP is that it is acceptable to report only observation data in the CCEP without any theoretical explanations. Data exchange would be important to study empiric and synthetic science like earthquake prediction. In Japan, especially in the CCEP, not only theoretical studies but also results of observation are valued highly, which is one of the reasons why the CCEP works well. It is another reason that contributions to the CCEP by researchers are appreciated in academic societies.

The matters presented in the meeting are also open to the researchers other than the members of the CCEP through the publication of the bulletins. The bulletins which have been generally published twice a year are widely used and often referred in seismological papers as fundamental materials. The important matters of each meeting are also notified to the public through the explanations to journalists and local government officials concerned after the meeting.

3. The Achievements of the CCEP

The activities of the CCEP has been steadily increasing since it was established. So far 48 regular bulletins were published, the total amount pages of which exceeds 13,000, besides 4 special bulletins about the Intensified Observation Areas and the Specific Observation Areas(Fig. 1). The government budget concerning earthquake prediction in 1991 fiscal year increased about 13 times more than that in 1969 when the CCEP was established(Fig. 2). It will be seen that the government has been constantly and steadily investing in the enterprise of earthquake prediction.

Several important matters concerning earthquake prediction have been discussed in the CCEP. The selection of the Intensified Observation Areas and the Specific Observation Areas has been useful from the point of view of efficiency and concentration of observations. In addition, the areas are used by the administrative organizations, for instance, to make up a countermeasure for preventing disasters(Fig. 3).

People recognize that the information of the CCEP is highly reliable. It will be because the CCEP has been showing many achievements, some examples of which are as follows.

(Example 1)

In 1969, it was made clear in the CCEP that there exists seismic gap off the Nemuro Peninsula(Fig. 4). Nemuro-hanto-oki earthquake(M7.4) occurred in the indicated area in 1973.

(Example 2)

In 1974, the CCEP decided to upgrade the Tokai district from the Specific Observation Area to the Intensified Observation Area, because of the results of the geodetic observations and the discovery of new evidence concerning the "Tokai earthquake". It made an important effect on the promulgation of the Large-Scale Earthquake Countermeasures Act in 1978.

(Example 3)

In 1974, it became clear that there is the upheaval of the ground around Kawasaki city, because of the results of releveling

made by the Geographical Survey Institute. The CCEP made an announcement that the upheaval around Kawaski city will not have no relation to big earthquakes.

(Example 4)

In 1989 July, there were a series of swarm earthquake activities in the east of Izu Peninsula, near Ito city. The Intensified Observation Area subcommittee was held on July 5 and 13. After the meeting of July 13, the comment was announced that these earthquakes are owing to the magmatic activities. About one hour after the announcement, the eruption in the sea off Ito City occurred.

(Example 5)

Though the number of big earthquakes after the establishment of the CCEP is less than the previous period, almost all big earthquakes including Nihonkai-chubu Earthquake, M7.7, happened in the Intensified Observation Areas or the Specific Observation Areas which covers about 20% areas of Japan. It is possible to say that the long-term earthquake prediction by the CCEP has been successful.

4. The Role of the CCEP in Earthquake Prediction System in Japan

Fig. 5 shows the earthquake prediction system in Japan.

The Geodesy Council which was settled in 1949 has been recommending to the Prime Minister and other Ministers concerned the 5-year plan for earthquake prediction. The first 5-year plan was made in 1963, after "Prediction of Earthquakes - Progress to Date and Plans for Further Development" or so-called the "blue print" was drafted by the seismologists and earthquake prediction researchers in 1962. Because the necessity of the coordinating organization for earthquake prediction was recommended in the second 5-year plan in 1968, the CCEP was settled in 1969. The present 6th 5-year plan has been running from 1988.

The Headquarters for Earthquake Prediction Promotion(HEPP), which was settled in 1976, is an interdepartmental conference for controlling and arranging earthquake prediction research between government organizations concerned under the 5-year plan recommended by the Geodesy Council. The head of HEPP is the Minister of Science and Technology Agency and the members are the permanent secretaries of concerning Ministries.

On June 15, 1978, the Large-Scale Earthquake Countermeasures Act was promulgated. This Act, which is intended to protect the life and property of the citizens against disaster due to large scale earthquakes, was formulated on the assumption that it is possible to predict large-scale (M8 class) earthquakes in the Areas under Intensified Measures against Earthquake Disaster. Presently only Tokai area, where Magnitude 8 class earthquake, so called "Tokai earthquake" is predicted to occur in near future, is applied to the Act. For this purpose, many data of several government organizations concerning "Tokai earthquake" are gathered to the Japan Meteorological Agency(JMA). The Earthquake Assessment Committee for the Areas Under Intensified Measures Against Earthquake Disaster, the secretary of which is JMA, was established in 1980 to assess the "Tokai earthquake". The promul-

gation of the Act is owing to the discussion in the CCEP, as stated previously.

In the earthquake prediction system in Japan, The CCEP plays a role of practical "headquarters" because all information necessary for earthquake prediction are gathered, exchanged, and discussed freely in the CCEP research and assessed from the academic point of view. Though the CCEP is operated by the government budget, it is administratively independent from government organizations.

5. Closing Remarks

Recently the circumstance around earthquake prediction in Japan seems to be slightly changing. The doubts about effectiveness and probability of earthquake prediction and the criticism on the earthquake prediction system are sometimes seen in the articles of newspapers and magazines.

Though it becomes clear that the earthquake prediction is not so easy as thought when the CCEP started, many scientific facts have been made clear by the CCEP. The CCEP is expected to make progress towards the successful earthquake prediction in Japan and will increase its activities.

1943	Tottori Earthquake	M7.2
1944	Tonankai Earthquake	M7.9
1946	Nankai Earthquake	M8.0
1948	Fukui Earthquake	M7.1
1952	Tokachi-oki Earthquake	M8.2
1953	Boso-oki Earthquake	M7.4
1960	Sanriku-oki Earthquake	M7.2
1961	Hyuga-nada Earthquake	M7.0
1961	Kushiro-oki Earthquake	M7.2
1961	Kita-Mino Earthquake	M7.0
1962	Hiroo-oki Earthquake	M7.0
1964	Niigata Earthquake	M7.5
1968	Hyuga-nada Earthquake	M7.5
1968	Tokachi-oki Earthquake	M7.9
1969	ESTABLISHMENT OF THE COORDINATING COMMITTEE FOR EARTHQUAKE PREDICTION	
1970	The CCEP selected 1 Intensified Observation Area and 8 Specific Observation Areas	
1972	Hachijo-jima-kinkai Earthquake	M7.1
1972	Hachijo-jima-toho-oki Earthquake	M7.2
1973	Nemuro-hanto-oki Earthquake	M7.4
	The CCEP announced an unified view on Nemuro-hanto-oki Earthquake	
1978	Izu-Oshima-kinkai Earthquake	M7.0
1978	Miyagi-ken-oki Earthquake	M7.4
1978	Large-Scale Earthquake Countermeasures Act was promulgated.	
1978	The CCEP revised 2 Intensified Observation Areas and 8 Specific Observation Areas	
1982	Urakawa-oki Earthquake	M7.1
1983	Nihonkai-chubu Earthquake	M7.7
1984	Hyuga-nada Earthquake	M7.1

TABLE 2 Main earthquakes in last 50 years in Japan and topics concerning the CCEP

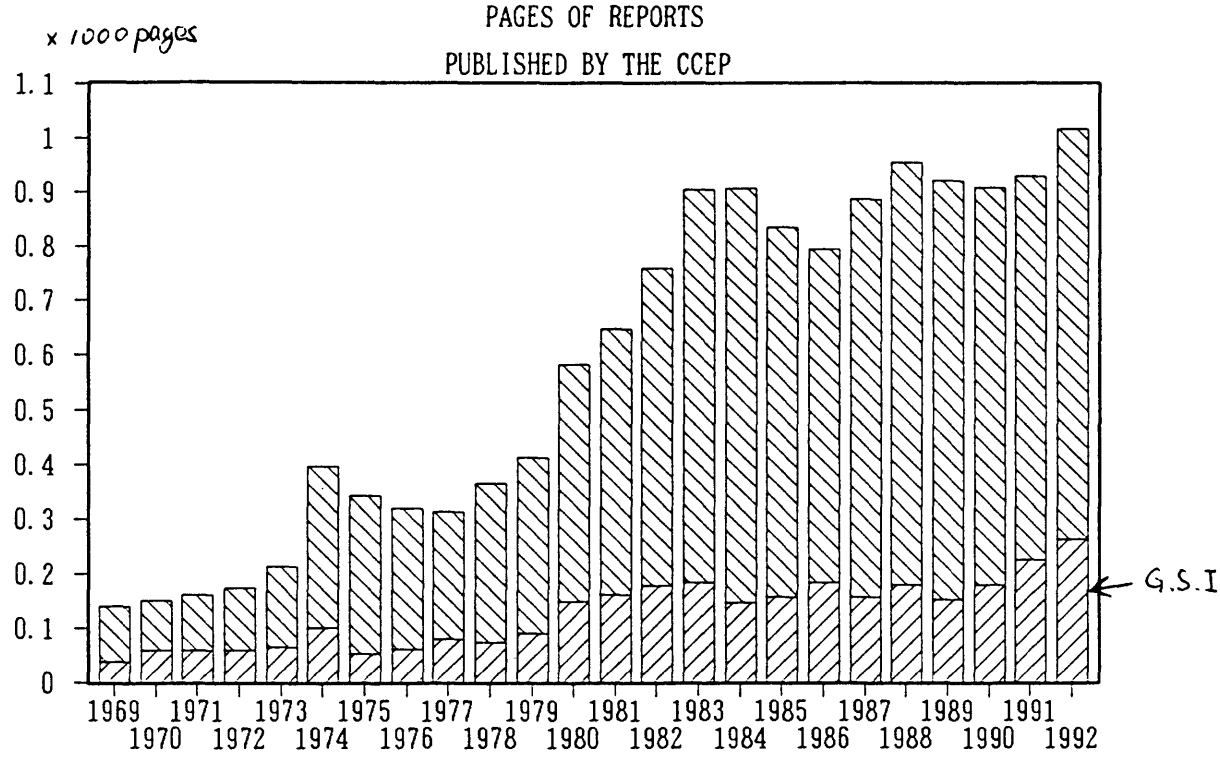

Fig. 1 Pages of Regular Bulletins Published by the CCEP

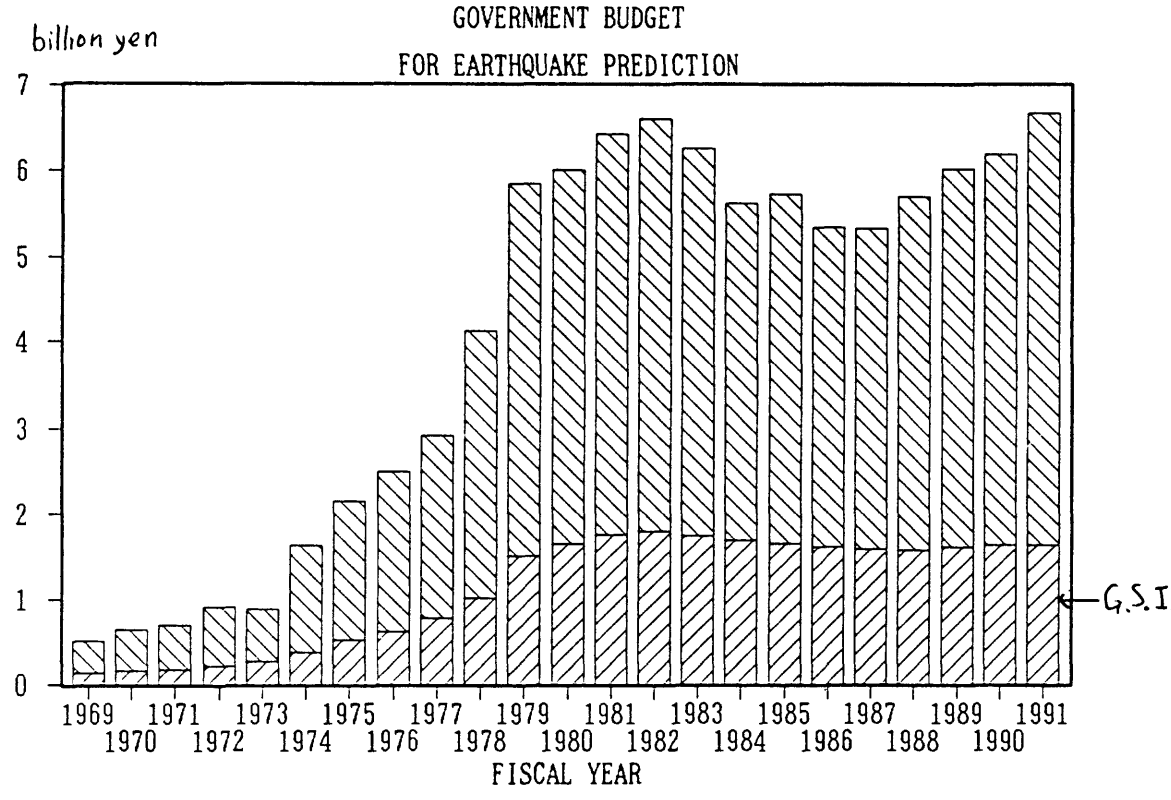

Fig. 2 Government Budget for Earthquake Prediction in Japan

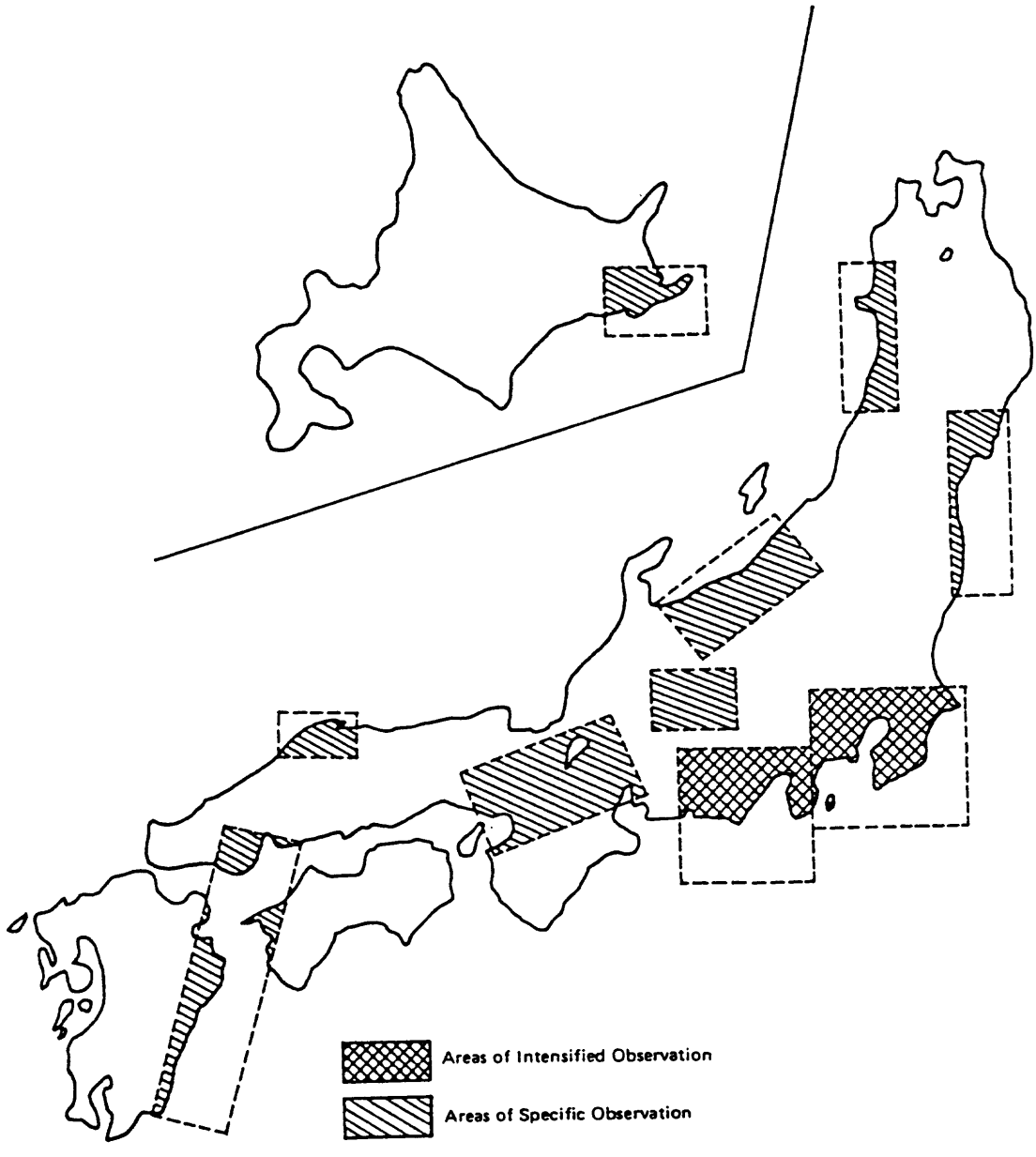

Fig. 3 The Intensified Observation Areas

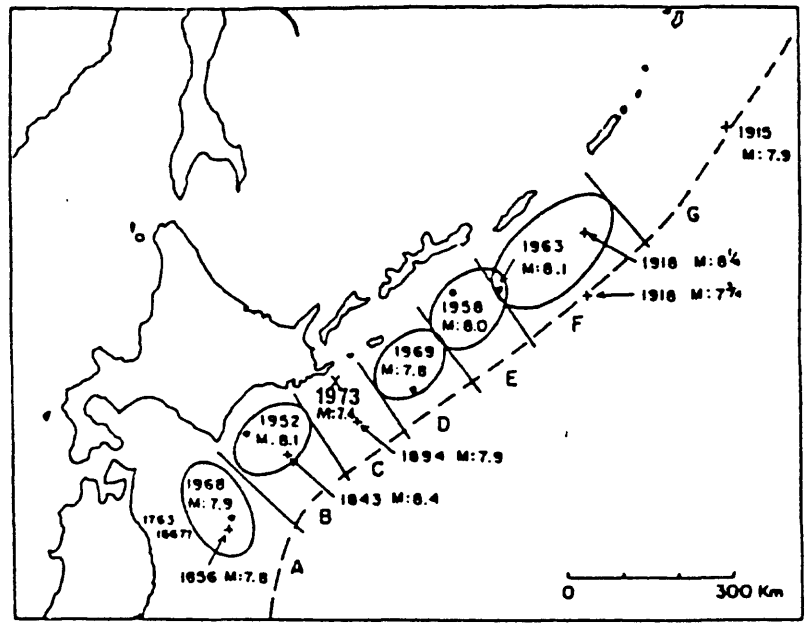

Fig. 4 Seismic Gap off Nemuro Peninsula
(after T. Utsu).

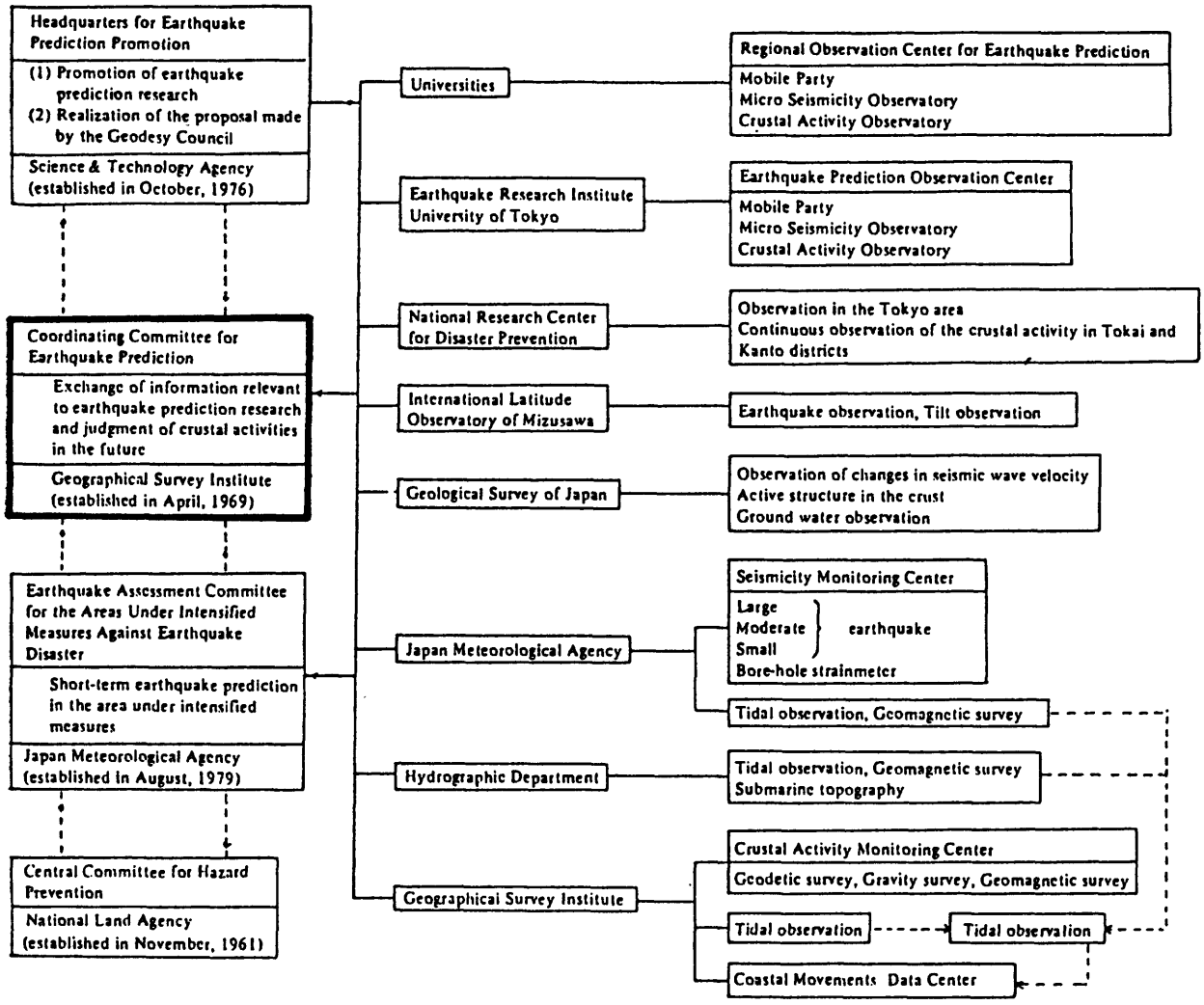

Fig. 5 Earthquake Prediction System in Japan

A Tsunami About 1000 Years Ago in Puget Sound, Washington

Brian F. Atwater and Andrew L. Moore

Water surged from Puget Sound sometime between 1000 and 1100 years ago, overrunning tidal marshes and mantling them with centimeters of sand. One overrun site is 10 kilometers northwest of downtown Seattle; another is on Whidbey Island, some 30 kilometers farther north. Neither site has been widely mantled with sand at any other time in the past 2000 years. Deposition of the sand coincided—to the year or less—with abrupt, probably tectonic subsidence at the Seattle site and with landsliding into nearby Lake Washington. These findings show that a tsunami was generated in Puget Sound, and they tend to confirm that a large shallow earthquake occurred in the Seattle area about 1000 years ago.

A large earthquake probably happened between 500 and 1700 years ago on the Seattle fault (*1*), which has been inferred to extend westward across Puget Sound from downtown Seattle (*2*). The main evidence for the earthquake consists of terraces that record meters of abrupt uplift at Puget Sound (*1*). If abrupt enough to have accompanied an earthquake, such uplift should have generated a tsunami in Puget Sound. In this report, we show that a tsunami originated in Puget Sound between 1000 and 1100 years ago (*3*) and that it probably was generated by an earthquake on the Seattle fault.

Tsunamis can deposit sand on coastal lowlands. Modern examples have been reported from Chile (*4*, *5*), Japan (*6*), and British Columbia (*7*), and ancient examples have been inferred for Chile (*5*), Japan (*6*), Scotland (*8*), Alaska (*9*), and the Pacific coast of Washington and Oregon (*10*, *11*). In most of these examples, an onshore sheet of marine or estuarine sand dates to the time of an event known or inferred to have generated a tsunami.

We found tsunami deposits at two sites north of the Seattle fault [see figure 1 in (*1*)]. One of these sites borders Cultus Bay, which opens southward from Whidbey Island, 40 km north of the fault. The other site is West Point, which juts into Puget Sound 7 km north of the fault.

B. F. Atwater, U.S. Geological Survey at Department of Geological Sciences, University of Washington, AJ-20, Seattle, WA 98195.
A. L. Moore, Department of Geological Sciences, University of Washington, AJ-20, Seattle, WA 98195.

The tsunami deposit at Cultus Bay forms a sheet of sand mostly 5 to 15 cm thick in an area at least 100 by 200 m (Figs. 1 and 2). There, wetland peat has built upward and bayward since a tidal marsh began to supplant a tidal flat about 2000 years ago. This peat contains the sand sheet, which we found in scores of auger borings and followed as a continuous bed along more than 100 m of a drainage ditch. Neither the auger borings nor the ditch revealed any other sand bed in the peat. The surface covered by the sand shows 2 m of relief: 1.5 m where the sand mantled a sloping marsh (*12*) and another 0.5 m where the sand covered colluvium of an adjacent hillside (Fig. 2). The median grain size, mostly about 0.1 mm, decreases landward and stratigraphically upward (*13*). The sand contains microscopic marine fossils (*14*).

Deposition of the sand sheet at Cultus Bay occurred sometime between 850 and 1250 years ago, and it happened while the site probably underwent little or no subsidence. We dated the sand sheet by obtaining radiocarbon ages on plant remains in growth position in the sand (Fig. 2, in ditch). The dated remains are rhizomes (below-ground stems) and attached leaf bases of arrowgrass (*Triglochin maritimum*), which at modern Cultus Bay thrives only in a 1-m range high in the intertidal zone. Because additional arrowgrass rhizomes lie both below and above the sand, we suspect that the dated rhizomes grew upward through the sand sheet within years of its deposition. Such maintenance of arrowgrass would mean that deposition of the sand attended little or no subsidence of the Cultus Bay marsh (*15*).

The sand sheet at Cultus Bay is better explained by a tsunami than by a flood or storm. The landward fining and salt water fossils of the sand implicate a surge from

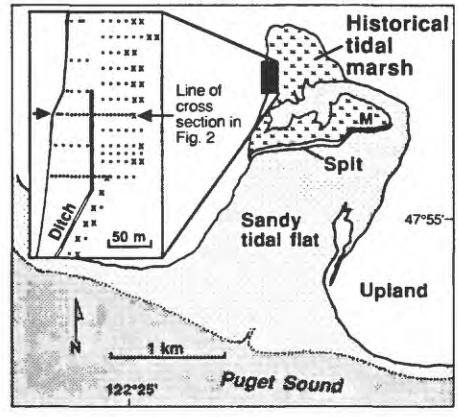

Fig. 1. Index maps of Cultus Bay. M, marsh surveyed for vertical ranges of plants plotted on right side of Fig. 2. Inset shows extent of sand sheet in peat or peaty mud, as seen in auger borings (•, sand present; **x**, absent) and in ditch (filled, present; open, absent).

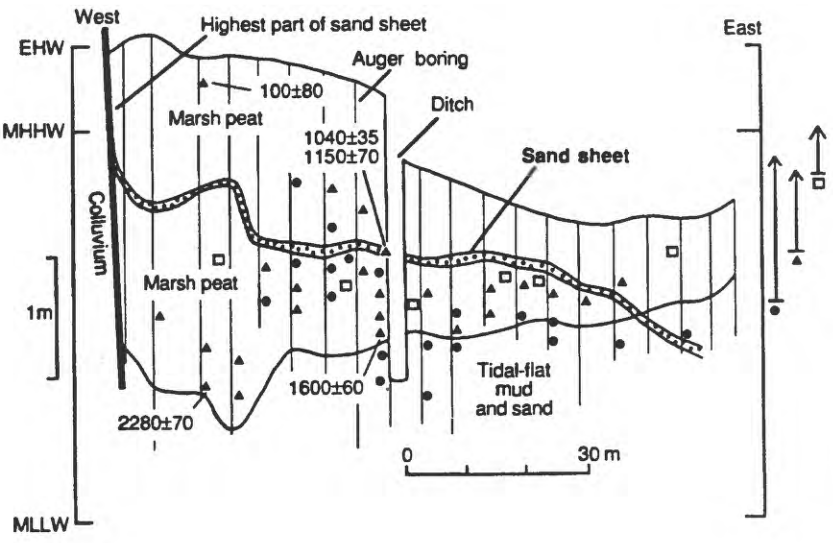

Fig. 2. Cross section along line of auger borings near Cultus Bay (vertical exaggeration ×20) (Fig. 1). Fossil rhizomes: (□), saltgrass *Distichlis spicata*; (▲), arrowgrass *Triglochin maritimum*; (●), tule *Scirpus acutus* or *S. californicus*. Radiocarbon ages (in ^{14}C yr before A.D. 1950) all measured on arrowgrass rhizomes (*25*). Vertical control from third-order leveling. Tidal datums (MHHW, mean higher high water; MLLW, mean lower low water) estimated by measuring a low slack tide on a windless sunny day, relating this tide to tide-table predictions, and extrapolating tidal datums from Hansville, which is 12 km west of Cultus Bay. EHW, extreme high water in winter of 1991–1992; denotes upper limit of flotsam in sheltered embayment. Lines at far right show vertical zonation of tule, arrowgrass, and saltgrass on tidal wetlands near M (Fig. 1): species denoted by rhizome symbol; horizontal line shows lower limit of marsh surface on which species was found living; tip of arrow shows upper limit.

Puget Sound, not a flood from the land. The lack of other sand beds distinguishes this surge from most or all storms at Cultus Bay in the past 2000 years. Because it occurred sometime between 850 and 1250 years ago, the surge may correlate with events that could have common cause with a tsunami in Puget Sound: abrupt uplift south of the Seattle fault between 500 and 1700 years ago (*1*), a landslide at Lake Washington between 1000 and 1100 years ago (*16*), rock avalanches in the Olympic Mountains between 1000 and 1300 years ago (*17*), a ground-water eruption along the Pacific coast of Washington between 900 and 1300 years ago (*11*), and abrupt subsidence at West Point between 1000 and 1100 years ago [see figure 1 of (*1*)].

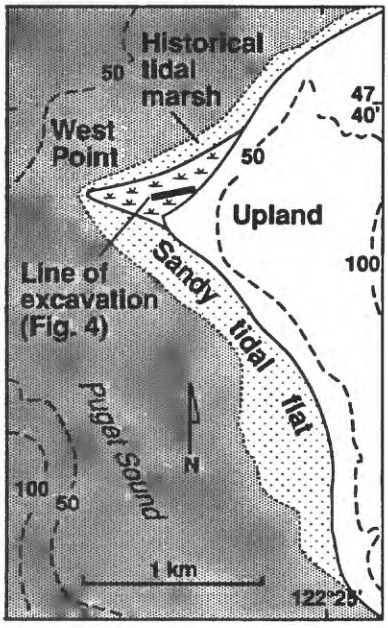

Fig. 3. Index map of West Point. Depth and elevation contours in meters.

The tsunami deposit at West Point punctuates a sequence of mostly intertidal deposits exposed in a sewer excavation 150 m long (Fig. 3). Sand and gravel low in the excavation represent a beach (*18*) on which people built fires and discarded shells before 2000 years ago (unit A, Fig. 4). The beach was eventually buried by silty debris flows from an adjacent hillside and by intertidal mud, peat, and sand. The first phase of intertidal burial, marked by unit B, lasted about 1000 years and concluded with a marsh dominated by saltgrass (*Distichlis spicata*) and bulrush (*Scirpus maritimus*). Next came the tsunami, which deposited the only widespread, tabular body of sand in the excavation (*19*). At that point the marsh and the toe of a debris flow became a short-lived tidal flat. This tidal flat, recorded by unit C, aggraded rapidly until it became a saltgrass marsh, recorded by unit D (*20*). The marsh of unit D persisted about 1000 years until it was covered by artificial fill several decades ago.

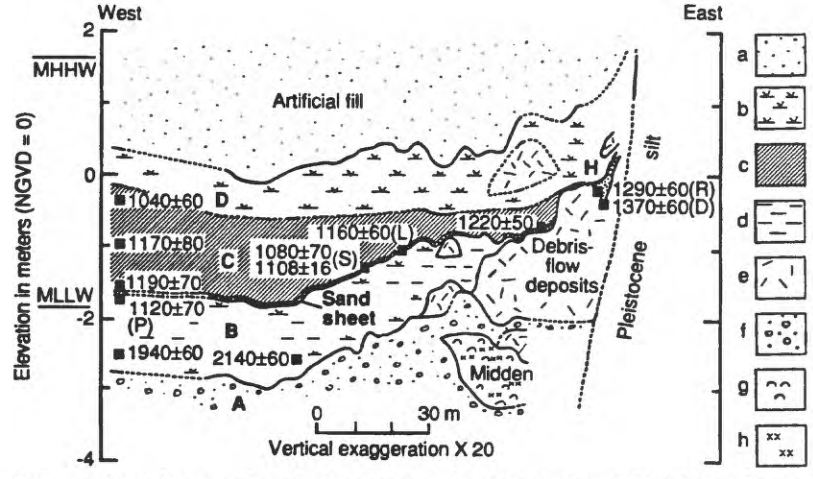

Fig. 4. Cross section along south wall of excavation for effluent pipe at West Point. Contacts solid where observed, dashed where inferred. A, B, C, and D denote stratigraphic units discussed in text. Kinds of deposits: a, stratified sand and basal mud pumped onto site in middle 1900s; b, peaty mud and peat with growth-position rhizomes of tidal-marsh plants; c, well-bedded, woody but rhizome-free mud and sand; d, nonbedded gray mud; e, sandy silt with scattered pebbles; f, sandy gravel and subordinate sand, organic in uppermost 0.1 to 0.5 m; g, disarticulated shell with minor charcoal, cracked rock, and mammal bone; h, lenses containing wood ash. Vertical control by third-order leveling from construction bench marks. Tidal datums (abbreviated as in Fig. 2) extrapolated from 10 km to southeast, at downtown Seattle, where tied by the National Ocean Survey to the National Geodetic Vertical Datum of 1929 (NGVD). Radiocarbon ages (in ^{14}C yr before A.D. 1950) on individual detrital sticks except where labeled P (peat), S (bulrush culms entombed in sand sheet and in overlying mud), L (Douglas fir log, outer 15 rings), R (shrub root in growth position), and D (multiple sticks from duff) (*26*). Location of cross section in treatment-plant coordinate system (*18*): north 850 to 900 feet, east 1365 to nearly 1900 feet.

Properties of the sand sheet at West Point vary with the kind of land that the sand covered. Where deposited on a marsh, the sheet ranges from 4 to 6 cm thick, shows little or no evidence of basal scour, grades stratigraphically upward from 0.5-mm sand to 0.1-mm sand, locally contains a basal lamina of 0.1- to 0.2-mm sand, includes sparse transported bivalves and barnacles, and surrounds culms (aboveground stems) of saltgrass and bulrush that are rooted just below the sand and extend vertically into tidal-flat mud as much as 10 cm above the top of the sand. On debris flows, the sand thickens to 40 cm in swales, disappears on rises, and contains angular clasts of debris-flow silt and rounded pebbles. The highest deposit that we assign to the sand sheet (below H, Fig. 4) contains microscopic marine fossils (*21*). Present-day relief on the sand-mantled marsh and debris flows totals 1.5 m, but this value exceeds initial relief if unit B has been compacted by its overburden.

Land at West Point underwent at least 1 m of abrupt, largely tectonic subsidence that coincided, within months, with deposition of the sand sheet. The subsidence sufficed to make room for the 1 to 1.5 m of tidal-flat deposits that widely accumulated on the sand-mantled marsh (*22*). Both the subsidence and some of the consequent tidal-flat deposition happened too abruptly for the saltgrass and bulrush culms to decompose before being buried by tidal-flat mud. Having initiated rapid tidal-flat deposition, the subsidence cannot have preceded deposition of the sand sheet by many months, for the sand accumulated on a marsh, not on a tidal flat. Nor did the subsidence follow sand-sheet deposition by more than one growing season: None of the marsh plants survived long enough after subsidence to grow rhizomes or tubers into the sand sheet, toward the aggrading tidal flat. We doubt that much of the subsidence resulted from landsliding or compaction because none of the subsided land appears to have been rotated toward the hillside and because the subsided hillside consists of scarcely compressible diamict and silt (Fig. 4).

The probable age of the sand sheet at West Point is between 1000 and 1100 years ago. This century contains the 95% confidence interval for the time of deposition, as shown by a high-precision radiocarbon age on standing, rooted bulrush culms (S, Fig. 4) (*23*) and as further shown by radiocarbon ages and matched ring-width patterns of Douglas fir. A Douglas fir log (L, Fig. 4) was deposited with the sand sheet: it rests on patches of the sand and on toppled, flattened bulrush culms. Bark on the trunk and on flexible limbs suggests that this fir died close to its time of deposition. A conventional radiocarbon age (Fig. 4) brackets the time of death between 850 and 1350 years ago. Matching of ring-width patterns shows that death of the West Point fir coincided, to the half year or less, with a landslide into Lake Washington (*16*). High-precision radiocarbon ages show that this landslide occurred between 1000 and 1100 years ago (*16*).

A tsunami explains the sand sheet at West Point because the sand contains marine fossils, mantles a former tidal marsh, ascends and incorporates hillside deposits, and dates to within months of subsidence and landsliding in the Seattle area. The tsunami probably originated in Puget Sound: Not only does the tsunami correlate closely with local subsidence and landsliding, it also left abundant deposits at sites that show no obvious sign of the largest tsunamis that probably struck the Pacific coast of Washington in the past 2000 years (*24*). We equate the tsunami at West Point with the one at Cultus Bay because the sand sheets at Cultus Bay and West Point resemble one another in graded bedding and radiocarbon age and because we recognized no evidence for any other tsunami in the past 2000 years at either site.

A large earthquake on the Seattle fault probably generated the tsunami by causing abrupt uplift south of the fault and complementary subsidence to the north (*1*). Such movement would have caused water in Puget Sound to surge northward across the fault. As it approached the West Point and Cultus Bay marshes, the tsunami probably encountered sandy shallows ancestral to modern tidal flats (Figs. 1 and 3). Sand thus suspended could have settled onto the marshes as the tsunami slowed across them. If tsunami deposits at West Point and Cultus Bay record every large earthquake on the Seattle fault in the past few thousand years, only one large earthquake has occurred on that fault since 2000 years ago.

REFERENCES AND NOTES

1. R. C. Bucknam, E. Hemphill-Haley, E. B. Leopold, *Science* **258**, 1611 (1992).
2. J. C. Yount and M. L. Holmes, *Geol. Soc. Am. Abstr. Prog.* **24** (no. 5), 93 (1992); J. C. Yount and H. D. Gower, *U.S. Geol. Surv. Open-File Rep. 91-147* (1991).
3. We use "years ago" to denote age in calibrated (approximately calendric) years before A.D. 1990. We converted from radiocarbon years to calibrated years with the bidecadal calibration data of M. Stuiver and G. W. Pearson [*Radiocarbon* **28**, 805 (1986)] and a recent version of the calibration program of M. Stuiver and P. J. Reimer (*ibid.*, p. 1022). We multiplied the laboratory-quoted error by 1.6 [high-precision age (*23*)] or by 2.0 (all other ages) because the quoted error may be smaller than one standard deviation of the age measurement [E. M. Scott *et al.*, *ibid.* **32**, 309 (1990)]. Treating the multiplied error as one standard deviation, we then calibrated at two standard deviations. While guarding against underestimation of analytical errors, this approach may also obscure differences in age between noncorrelative events.
4. C. Wright and A. Mella, *Bull. Seismol. Soc. Am.* **53**, 1367 (1963); J. Bourgeois and M. A. Reinhart, *Eos* **70**, 1331 (1989).
5. B. F. Atwater, H. Jiménez Núñez, C. Vita-Finzi, in *Impacts of Tectonics on Quaternary Coastal Evolution*, Y. Ota, A. R. Nelson, K. Berryman, Eds. (*Quat. Int.* **15/16**, 1992), pp. 77–85.
6. K. Minoura and S. Nakaya, *J. Geol.* **99**, 265 (1990).
7. P. T. Bobrowsky, J. J. Clague, T. S. Hamilton, *AMQUA Program Abstr.* **12**, 34 (1992).
8. A. G. Dawson, D. Long, D. E. Smith, *Marine Geol.* **82**, 271 (1988); D. Long, D. E. Smith, A. G. Dawson, *J. Quat. Sci.* **4**, 61 (1989).
9. P. D. Lea, *Geol. Soc. Am. Abstr. Prog.* **21** (no. 7), 344 (1989).
10. B. F. Atwater, *Science* **236**, 942 (1987); M. A. Reinhart and J. Bourgeois, *Eos* **68**, 1469 (1987); W. C. Grant and D. D. McLaren, *ibid.*, p. 1469, M. E. Darienzo and C. D. Peterson, *Tectonics* **9**, 1 (1991); B. F. Atwater and D. K. Yamaguchi, *Geology* **19**, 706 (1991).
11. B. F. Atwater, *J. Geophys. Res.* **97**, 1901 (1992).
12. At its lowest the sand overlies peaty mud with rhizomes (below-ground stems) only of the tule *Scirpus californicus* or *S. acutus*, a pioneer colonist of modern brackish-water tidal flats of Cultus Bay. At higher levels it overlies peat with rhizomes of saltgrass (*Distichlis spicata*), which does not live as low as the tules at Cultus Bay (Fig. 2).
13. Samples containing the entire thickness of the sand bed showed a westward decrease in median grain size from 0.09 to 0.07 mm along the line of the cross section shown in Fig. 2.
14. *Isthmia nervosa* and *Arachnoidiscus ehrenbergii*, diatoms that live attached to rooted or floating seaweed in Puget Sound [H. H. Gran and E. C. Angst, *Publ. Puget Sound Biol. Sta.* **7**, 417 (1931); E. E. Cupp, *Bull. Scripps Inst. Oceanogr. Tech. Ser.* **5**, 1 (1943)], and *Trochammina*, a dominant genus of salt-marsh foraminifera in the northwestern United States [A. E. Jennings and A. R. Nelson, *J. Foraminiferal Res.* **22**, 13 (1992)].
15. Locally the peat is muddier above than below the sand. This contrast, along with a scarcity of saltgrass rhizomes above the sand, may mean that slight subsidence attended deposition of the sand sheet [A. L. Moore, *Eos* **72**, 315 (1991)].
16. G. C. Jacoby, P. L. Williams, B. M. Buckley, *Science* **258**, 1621 (1992).
17. R. L. Schuster, R. L. Logan, P. T. Pringle, *ibid.*, p. 1620.
18. CH2M-Hill and Associated Firms, "Plant Site Geotechnical Data Report, West Point Treatment Plant Secondary Treatment Facilities, Liquids Stream, v. 19" (Metro, Seattle, WA, 1991).
19. Unlike the peat at Cultus Bay, the tidal deposits above unit A at West Point contain many sand bodies in addition to the sand sheet. These sand bodies are low in unit B and high in unit C and in unit D. None of them, however, show the conformable base, tabular shape, graded bedding, or wide extent of the sand sheet. Rather, the additional sand bodies above unit A are disconformable lenses of interbedded fine to very coarse sand and are restricted to the western half of the excavation.
20. We infer that unit C was deposited rapidly because it shows no upward decrease in radiocarbon ages measured on individual sticks (Fig. 4) and because, in contrast to the probably bioturbated intertidal mud in unit B, unit C is distinctly bedded.
21. *Trochammina* sp. (*14*).
22. Our assumptions are that (i) the marsh deposits below and above unit C represent similar positions high in the intertidal zone and (ii) relative sea level changed little during deposition of unit C. We interpret unit C as having formed low in the intertidal zone because it contains many transported shells of mussels (*Mytilus edulis*), clams (*Macoma* sp.), and barnacles in the western half of the excavation and because it abounds in well-preserved leaves and sticks yet lacks growth-position rhizomes. This fossil assemblage signifies salt water too deep for the growth of tidal-marsh plants.
23. *Scirpus maritimus* culms surrounded by the sand

yielded a high-precision age of 1108 ± 16 ^{14}C yr before A.D. 1950 (QL-4623), which corresponds to a 95% confidence interval between A.D. 885 and 990 (3). This interval probably includes the time when the dated culms lived. Culms of modern *S. maritimus* at Puget Sound live less than 1 year and rarely stand dead for more than 2 years. By analogy, the dated culms lived within 3 years of the abrupt subsidence that killed the *S. maritimus* and that coincided, within months, with deposition of the sand sheet.

24. Oceanic tsunamis produced sand sheets along the southern Washington coast 300 and 1400 to 1900 years ago (*10, 11*)—times when little or no sand accumulated at our Cultus Bay and West Point sites.
25. Laboratory numbers, from greatest to least age: Beta-51806, -48232, and -48231; USGS-3090; Beta-51805. Ages calculated with an assumed δ^{13}C value of −25 per mil except for USGS-3090 (1040 ± 35 ^{14}C yr B.P.), which was calculated with a measured value of −26.8 per mil. Use of this measurement reduced the age by about 30 ^{14}C yr relative to the age that would have been obtained for a value of −25 per mil.
26. As in (*25*): Beta-50841, -49193, -52626, -52627, -52625, -49614, -49196, -52539, and -49194; QL-4623; Beta-51890 and -49615. Only ages for peat (P) and bulrush stems (S) were adjusted for the measured δ^{13}C value
27. We thank D. Drake, K. Sharp, I. Khilfeh, and T. Gunstone for hospitality; B. Benson, S. Palmer, J. Bourgeois, L. Amidon, P. Atwater, P. Bierman, R. Bucknam, D. Clark, A. Eipert, B. Eipert, E. Eipert, C. Graff, B. Hallet, K. Hoppe, K. Nimz, D. Perkins, M. Reinhart, J. Shulene, R. Waitt, K. Whipple, and T. Yelin for field help; E. Hemphill-Haley and S. Cooke for fossil identifications; P. Reimer, M. Stuiver, and P. Wilkinson for high-precision radiocarbon dating; F. Bardsley for drafting, and R. Bucknam, D. Swanson, J. Bourgeois, A. Dawson, R. Waitt, and two anonymous referees for reviews.

24 July 1992; accepted 22 October 1992

Study of Turbidite as an Indicator of Earthquake and its Intensity*

Yoshio INOUCHI**, Yoshihiro KINUGASA**
and Fujio KUMON***

Sediments and other geological materials can retain evidences of earthquakes occurred in longer past, longer than written historical records and much longer than instrumental records. In this regard, study of sediments and geological materials have great advantage for studying past earthquakes and their recurrence.

We have had a chance to analyze the drilling cores and high resolution seismic profiles in Lake Biwa near Kyoto, Central Japan, obtained for other purpose than the earthquake study. At four drilling stations, we estimate the ages of some 20 turbidites within 3 meters of the lake bottom based on maker tephra layers and sedimentation rate. On the other hand, the seismic intensities of historical earthquakes which occurred in the central part of Japan are estimated using empirical relations between intensity, distance from epicenter and magnitude.

The ages of the historical earthquakes of which intensities at Lake Biwa are higher than IV (JMA), equivalent to VII (MMK), fall in the time windows of the estimated ages of turbidites. This indicates that the studies of turbidite enable us to reveal the intensity of paleoearthquakes as well as those occurrences.

* will be read by Y.KINUGASA
** Geological Survey of Japan
*** Shinsyu Univ., Japan

GREAT SUBDUCTION-ZONE EARTHQUAKES IN THE PACIFIC NORTHWEST? DIFFERENTIATING COSEISMIC FROM NONTECTONIC TIDAL-MARSH DEPOSITS ALONG THE OREGON COAST

Alan R. Nelson
U.S. Geological Survey
MS 966, P.O. Box 25046
Denver, Colorado 80225-0046

EXTENDED ABSTRACT

Has subduction of the Juan de Fuca plate beneath the North America plate in the Pacific Northwest produced great (M>8) earthquakes during the late Holocene? Historic records of the past 200 years yield no evidence of great plate-boundary earthquakes in the Cascadia subduction zone (Heaton and Hartzell, 1987). But along the coasts of Washington (Atwater, 1987, 1992; Atwater and Yamaguchi, 1991; Atwater et al., 1991), Oregon (Grant, 1989; Darienzo and Peterson, 1990; Peterson and Darienzo, 1991; Darienzo, 1991; Nelson and Personius, 1991; Nelson, 1992, in press; Fig. 1), and northern California (Vick, 1988; Clarke and Carver, 1992; Valentine, 1992), peaty, tidal-wetland soils are interbedded with mud in estuarine stratigraphic sequences (Figs. 2*B* and 3) and the submergence (relative rise of sea level) of at least two of these soils seems too widespread (>100 km), too large (>1 m), and too sudden (<10 yr) to be attributed to any process except coseismic subsidence. How large were the earthquakes that could have produced this coastal subsidence, and how often do they occur? Such questions are critical for earthquake-hazard assessment in the Pacific Northwest. In this abstract I reference many coastal process papers that bear directly on the answers to these questions but that are commonly overlooked.

Buried tidal-wetland soils in the Pacific Northwest may have been submerged by sudden coastal subsidence during three principle types of earthquakes. First, great earthquakes on one or more segments of the interface between the subducting and overriding plates may have produced a regional zone (hundreds of kilometers long) of coastal subsidence (Atwater, 1987; Nelson and Personius, 1991; Peterson and Darienzo, 1991). Tidal-wetland soils similar to those in southern Washington and northern Oregon were submerged and buried along hundreds of kilometers of coast following great subduction earthquakes in the 1960's in Alaska and Chile (Plafker, 1972). Second, deformation on faults and folds in the overriding North America plate during great earthquakes on the plate interface may have produced localized areas of coseismic coastal subsidence (McInelly and Kelsey, 1990; Kelsey, 1990; Goldfinger et al., 1992; Atwater, 1992; Clarke and Carver, 1992; Valentine, 1992). And third, some localized subsidence may have occurred during smaller earthquakes (M 6-7¾) in the overriding plate that were independent of plate-interface events (Nelson and Personius, 1991), such as the 1931 Hawkes Bay earthquake in New Zealand (Berryman et al., 1989).

At least some buried tidal-wetland soils, however, may have been submerged by nontectonic processes. Peaty soils are commonly interbedded with mud in intertidal sequences of mid-latitude passive continental margins (e.g., Tooley, 1978; Streif, 1987; van de Plassche, 1991; Fletcher et al., 1991). Many such long-term studies in northwest Europe are much more extensive than any studies in the Pacific Northwest, and they are supported by thousands of ^{14}C ages (e.g., Berendsen, 1984; Shennan, 1987).

The stratigraphy at many sites in northwest Europe indicates large ranges in local rates of sea-level rise (Shennan, 1986). Several nontectonic processes have been invoked to explain these inferred rate changes, including rapid changes in the rate of regional sea-level rise combined with changing sedimentation rates (Fig. 2*C*), or changes in the configuration of bars and channels in tidal inlets that led to local changes in tidal range. Bars can be breached suddenly during floods or storms and migration of barrier bars at the mouths of major inlets may affect tide levels in large parts of an estuary. Oscillations in late Holocene sea level are the most often cited explanation for interbedded peat and mud sequences on many coasts (e.g., Rampino and Sanders, 1981; Fairbridge, 1987; van de Plassche, 1991; Fletcher et al., 1991). Although regional oscillations of sea level have been identified (e.g., Shennan, 1986; van de Plassche, 1991), these oscillations are not necessarily synchronous from region to region (Kidson, 1982).

Other processes that may be involved in sea-level changes that produce peat-mud couplets on nontectonic coasts include (1) stormy periods with many storm

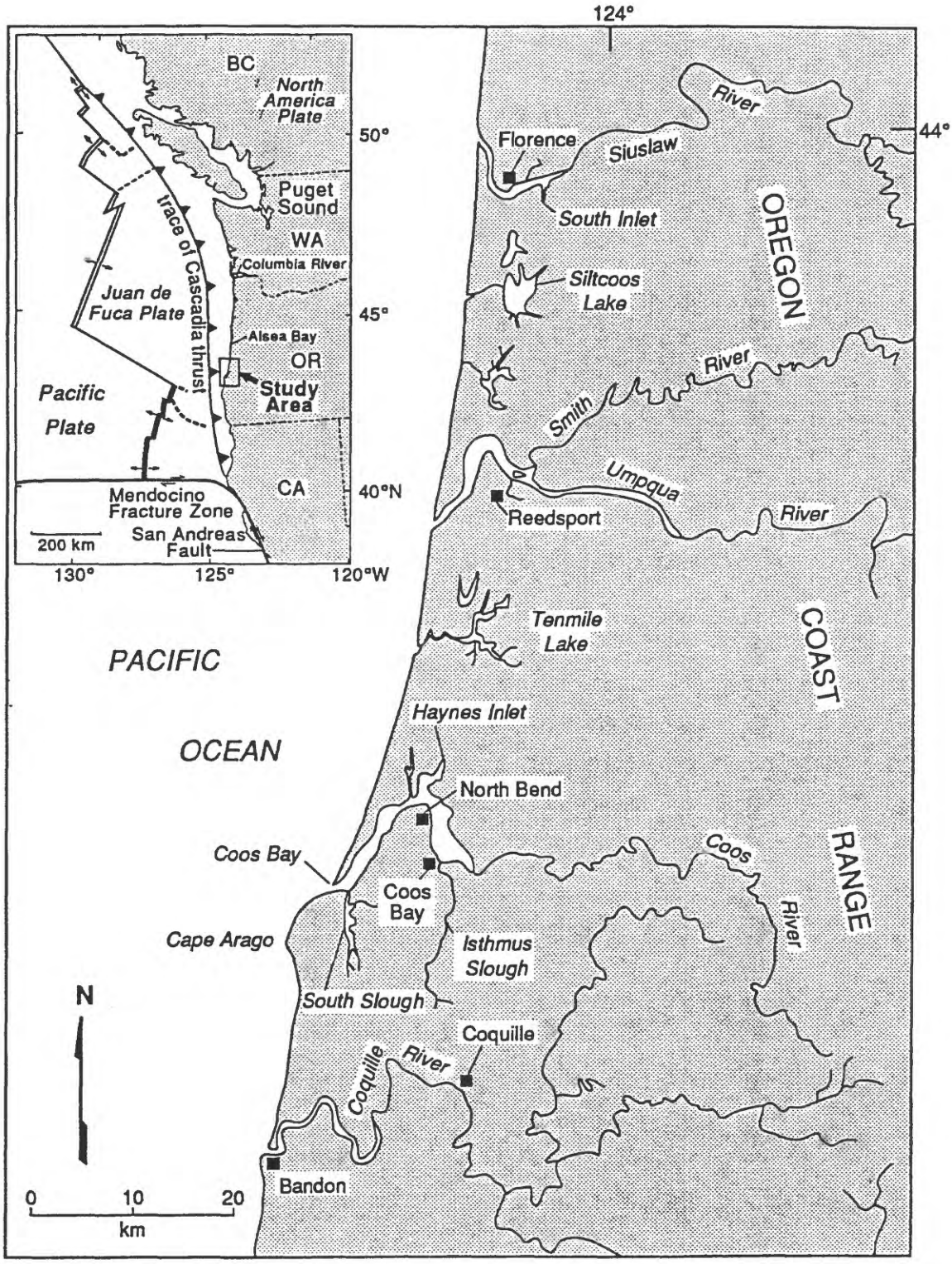

FIGURE 1.--Location map of the south-central Oregon coast. In the inset figure the trace of the Cascadia thrust fault (barbed line, barbs point downdip), where the Juan de Fuca plate is being subducted beneath the North America plate, is placed at the bathymetric boundary between the continental slope and abyssal plain; double lines are spreading ridges, solid lines are strike-slip faults, and dashed lines are other faults.

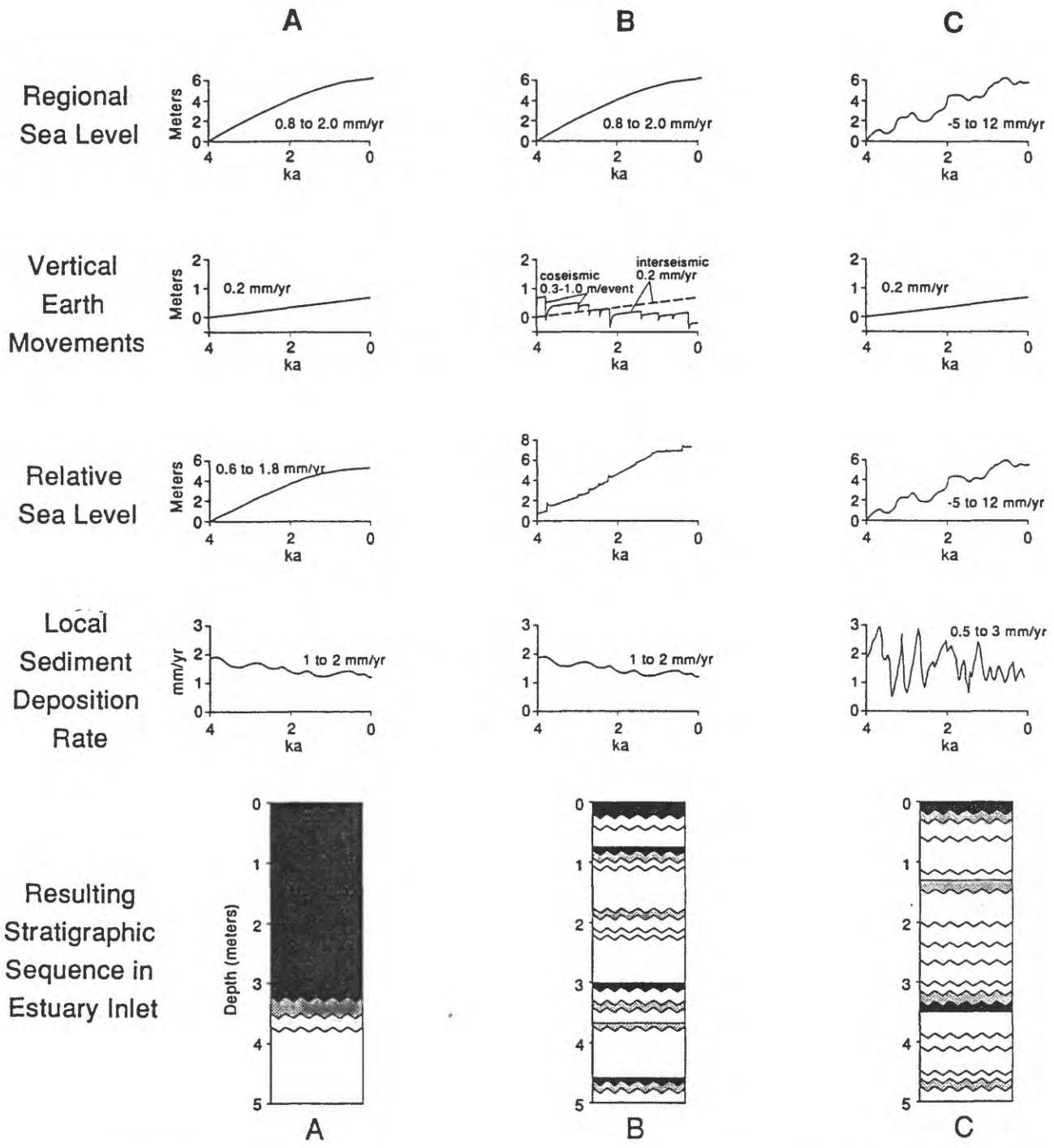

FIGURE 2.--Models of late Holocene sedimentation in tidal inlets in the Pacific Northwest. The curves illustrate how different but plausible histories of sea-level rise, coastal uplift, and sedimentation can produce different types of stratigraphic sequences in these inlets. See figure 3 for definition of lithologies and contacts. *A*) A sequence that could only be produced in an inlet that had not experienced major (>0.5 m) sudden changes in relative sea level. *B*) Abrupt upper contacts on the peat units in this sequence indicate sudden submergence, possibly as the result of coseismic subsidence. *C*) Gradational contacts are produced by fluctuating regional sea level and rapidly changing sedimentation rates. The sequence in *B* could easily be confused with *C*, which could be produced without any sudden changes in relative sea level.

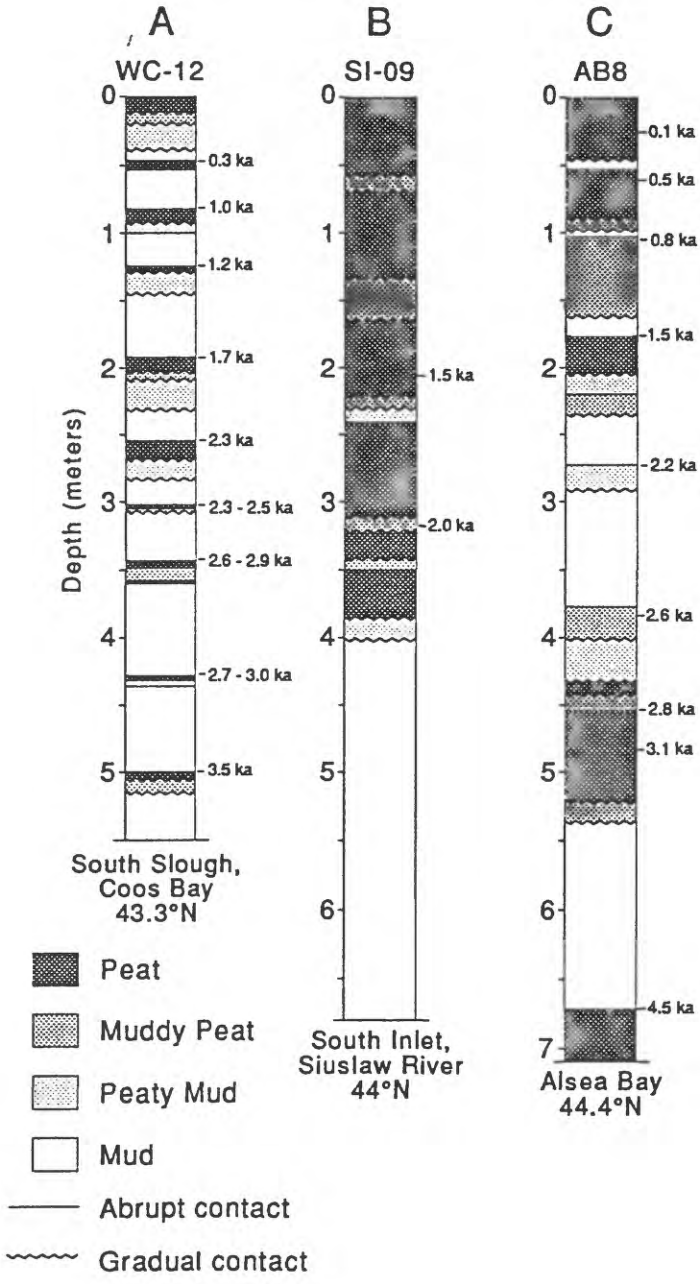

FIGURE 3.--Comparison of typical cores from estuarine sequences at three sites along the southern and central Oregon coast. Age estimates for different levels in cores are based on ^{14}C ages from these or nearby cores (Nelson, 1992, in press; Peterson and Darienzo, 1991). *A*) Core contains 9 abruptly buried peaty units--the abrupt contacts may be the result of sudden changes in tidal range caused by migration or breaching of bars, or by subsidence during local or regional earthquakes. *B*) The thick peat indicates no sudden changes in relative sea level during the past 2000 years. *C*) The abrupt contacts at the top of peaty units have been interpreted (Peterson and Darienzo, 1991) as marking regional coseismic subsidence events of about 0.5-1 m.

surges (Streif, 1979), (2) changes in the shapes and gradients of estuarine systems due to river changes and rising Holocene sea level (van de Plassche, 1982), and (3) gradual aseismic regional tectonic warping (Newman et al., 1980; Shennan, 1989). An additional interpretive problem is that lithologic changes in the peat-mud sequences are not necessarily direct proxies of small sea-level changes (e.g., Stevenson et al., 1986; Allen, 1990). Such lithologic changes do show, however, that marsh aggradation has not kept up with late Holocene sea-level rise on many nontectonic coasts (e.g., Kearney and Ward, 1986) and that, contrary to the argument of Atwater (1987), the absence of thick sequences of peat is not necessarily evidence for tectonic instability.

Submergence of tidal-wetland soils by coseismic subsidence can only be inferred where the abrupt upper transgressive contact of a widely mapped peaty soil represents a sudden, substantial change (>0.5 m) in water depth (Jennings and Nelson, 1992; Nelson, in press). The sharpness of transgressive or regressive contacts is particularly important in paleoseismic studies because subsidence or uplift during large earthquakes should produce abrupt contacts (e.g., Ovenshine and others, 1976; Atwater, 1987, 1992; Darienzo and Peterson, 1990). Few published studies of tidal-wetland stratigraphy from passive continental margins discuss the thickness or character of transgressive and regressive contacts--most contacts are gradual transitions between different types of intertidal sediment. Most of the local, regional, and global factors commonly invoked to explain intertidal facies changes involve processes that operate for decades to hundreds of years. These processes should cause gradual facies changes across contacts in protected estuarine settings (e.g., Behre, 1986, his fig. 3). Gradual contacts could also be produced by slow subsidence or uplift during interseismic accumulation of tectonic strain (Darienzo and Peterson, 1990). However, along convergent-plate margins, I know of no way to distinguish gradual contacts resulting from slow, tectonically induced changes in regional uplift from contacts produced by nontectonic factors on passive continental margins. Gradual contacts can only be attributed to tectonic processes at sites where rates of interseismic vertical movement are too high to be the result of processes that cause nontectonic sea-level fluctuations (e.g., Newman et al., 1987).

Sequences of intertidal sediment in tidal marshes show that the late Holocene history of submergence differs from north to south along the south-central Oregon coast (Nelson, in press; Fig. 1). Thick, uniform sequences of tidal-marsh peat are present in the marshes of the Siuslaw River estuary (Fig. 3*B*); acclerator mass spectrometer ^{14}C ages of samples from this peat indicate a gradual relative rise in sea level at about 1.0-1.6 mm/yr during the past 2000-2500 years. Thick muddy peat from marshes in the Umpqua River estuary also suggest a gradual sea-level rise for most of the past few thousand years, but only three sites have been investigated in this area. Peat is much less common in the marsh stratigraphy of the Coos Bay estuary. Many sites have a buried peaty soil in the upper 1.5 m that was rapidly submerged in the past 1500 years, but buried soils with peaty surface horizons at a few sites may also have developed following emergence during this period. The lower intertidal or subtidal mud that predominates in cores from eastern Coos Bay gives no clear record of sea-level change for most of the late Holocene. In contrast, multiple abrupt transgressive contacts characterize intertidal sequences in the South Slough arm of western Coos Bay (Fig. 3*A*). Some abrupt transgressive contacts may have formed following local or regional coseismic subsidence, but many soils also may have been buried as a result of localized nontectonic changes in tide levels. Very detailed stratigraphic, micropaleonotologic, and ^{14}C dating studies will be required to distinguish coseismic from nontectonic burial processes at such sites.

This research is supported by the National Earthquake Hazards Reduction Program of the U.S. Geological Survey and by the U.S. Nuclear Regulatory Commission.

REFERENCES

Allen, J.R.L., 1990, Constraints on measurement of sea-level movements from salt-marsh accretion rates: Journal of the Geological Society, London, v. 147, p. 5-7.

Atwater, B. F., 1987, Evidence for great Holocene earthquakes along the outer coast of Washington state: Science, v. 236, p. 942-944.

Atwater, B.F., 1992, Geologic evidence for earthquakes during the past 2000 years along the Copalis River, southern coastal Washington: Journal of Geophysical Research, v. 97, no. B2, p. 1901-1919.

Atwater, B.F., Stuiver, Minze, and Yamaguchi, D.K., 1991, Radiocarbon test of earthquake magnitude at the Cascadia subduction zone: Nature, v. 353, p. 156-158.

Atwater, B.F. and Yamaguchi, D. K., 1991, Sudden, probably coseismic submergence of Holocene trees and grass in coastal Washington State: Geology, v. 19, p. 706-709.

Behre, K.-E., 1986, Analysis of botanical macro-remains, *in* van de Plassche, Orson, ed., Sea-level research: a manual for the collection and evaluation of data: Norwich, U.K., Geo Books, p. 413-434.

Berendsen, H.J.A., 1984, Quantitative analysis of radiocarbon dates of the perimarine area in the Netherlands: Geologie en Mijnbouw, v. 63, p. 343-350.

Berryman, K.R., Ota, Yoko, and Hull, A.G., 1989, Holocene paleoseismicity in the fold and thrust belt of the Hikurangi subduction zone, eastern North Island, New Zealand: Tectonophysics, v. 163, p. 185-195.

Clarke, S. H., Jr., and Carver, G.A., 1992, Late Holocene tectonics and paleoseismicity, southern Cascadia subduction zone: Science, v. 255, p. 188-192.

Darienzo, M.E., 1991, Late Holocene paleoseismicity along the northern Oregon coast: unpub. Ph.D. thesis, Department of Environmental Sciences and Resources, Portland State University, 167 p.

Darienzo, M. E., and Peterson, C. D., 1990, Episodic tectonic subsidence of late Holocene salt marshes, northern Oregon coast, central Cascadia margin, U.S.A.: Tectonics, v. 9, p. 1-22.

Fairbridge, R.W., 1987, The spectra of sea level in a Holocene time frame, *in*, Rampino, M.R., Sanders, J.E., Newman, W.S., and Konigsson, L.K., eds., Climate--History, periodicity, and predictability: New York, Van Nostrand Reinhold, p. 127-141.

Fletcher, C.H., Van Pelt, J.E., Sherman, J., and Brush, G.S., 1991, High-resolution sea-level and climate history of the middle to late Holocene from wetland sediments of Delaware Bay: Geological Society of America Abstracts with Programs, v. 23, no. 5, p. A352.

Goldfinger, C., Kulm, L.D., Yeats, R.S., 1992, Transverse structural trends along the Oregon convergent margin: Implications for Cascadia earthquake potential and crustal rotations: Geology, v. 20, p. 141-144.

Grant, W.C., 1989, More evidence from tidal-marsh stratigraphy for multiple late Holocene subduction earthquakes along the northern Oregon coast: Geological Society of America Abstracts with Programs, v. 21, no. 5, p. 86.

Heaton, T. H., and Hartzell, S. H., 1987, Earthquake hazards on the Cascadia subduction zone: Science, v. 236, p. 162-168.

Jennings, A. E., and Nelson, A. R., 1992, Foraminiferal assemblage zones in Oregon tidal marshes--Relation to marsh floral zones and sea level: Journal of Foraminiferal Research, v. 22, no. 1, p. 13-29.

Kearney, M.S., and Ward, L.G., 1986, Accretion rates in brackish marshes of a Chesapeake Bay estuarine tributary: Geo-Marine Letters, v. 6, p. 41-49.

Kelsey, H. M., 1990, Late Quaternary deformation of marine terraces on the Cascadia Subduction Zone near Cape Blanco, Oregon: Tectonics, v. 9, p. 983-1014.

Kidson, C., 1982, Sea level changes in the Holocene: Quaternary Science Reviews, v. 1, p. 121-151.

McInelly, G.W., and Kelsey, H.M., 1990, Late Quaternary tectonic deformation in the Cape Arago-Bandon region of coastal Oregon as deduced from wave-cut platforms: Journal of Geophysical Research, v. 95, no. B5, p. 6699-6713.

Nelson, A.R.,1992, Discordant ^{14}C ages from buried tidal-marsh soils in the Cascadia subduction zone, southern Oregon coast: Quaternary Research, v. 38 (July issue).

Nelson, A.R., (in press), Holocene tidal-marsh stratigraphy in south-central Oregon--Evidence for localized sudden submergence in the Cascadia subduction zone, *in* Fletcher, C.P., and Wehmiller, J.F., eds., Quaternary coasts of the United States--Marine and lacustrine systems: Society for Sedimentary Geology Special Publication no. 48.

Nelson, A.R., and Personius, S. F., 1991, The potential for geat earthquakes in Oregon and Washington: an overview of recent coastal geologic studies and their bearing on segmentation of Holocene ruptures in the central Cascadia subduction zone, *in* Rogers, A.M., Kockelman, W.J., Priest, George, and Walsh, T.J., eds., Earthquake hazards in the Pacific Northwest of the United States: U.S. Geological Survey Open-File Report 91-441A (Preliminary version of chapter in U.S. Geological Survey Professional Paper 1560), 29 p.

Newman, W.S., Cinquemani, L.J., Pardi, R.P., and Marcus, L.F., 1980, Holocene deleveling of the United States east coast: *in*, Morner, N.-A., ed., Earth rheology, isostasy, and eustasy: New York, John Wiley, p. 449-463.

Newman, W. S., Cinquemani, L. J., Sperling, J. A., Marcus, L., and Pardi, R.R., 1987, Holocene neotectonics and the Ramapo fault zone sea-level anomaly--A study of varying marine transgression rates in the lower Hudson estuary, New York and New Jersey, *in* Nummedal, Dag, Pilkey, O.H., and Howard, J.D., eds., Sea-level fluctuation and coastal evolution: Tulsa, Oklahoma, Society of Economic Paleontologists and Mineralogists, Special Publication No. 41, p. 97-114.

Ovenshine, A.T., Lawson, D.E., and Bartsch-Winkler, S.R., 1976, The Placer River Silt--an intertidal deposit caused by the 1964 Alaska earthquake: U.S. Geological Survey Journal of Research, v. 4, p. 151-162.

Peterson, C. D., and Darienzo, M. E., 1991, Discrimination of climatic, oceanic and tectonic forcing of marsh burial events from Alsea Bay, Oregon, USA, *in* Rogers, A.M., Kockelman, W.J., Priest, George, and Walsh, T.J., eds., Earthquake hazards in the Pacific Northwest of the United States: U.S. Geological Survey Open-File Report 91-441C (Preliminary version of chapter in U.S. Geological Survey Professional Paper 1560), 53 p.

Plafker, George, 1972, Alaskan earthquake of 1964 and Chilean earthquake of 1960--Implications for arc tectonics: Journal of Geophysical Research, v. 77, p. 901-924.

Plassche, Orson van de, 1982, Sea-level change and water-level movements in the Netherlands during the Holocene: Mededelingen rijks geologische dienst, v. 36-1, 93 p.

Plassche, Orson van de, 1991, Late Holocene sea-level fluctuations on the shore of Connecticut inferred from transgressive and regressive overlap boundaries in salt-marsh deposits, *in* Gayes, P.T., Lewis, R.S., and Bokuniewicz, H.G., eds., Quaternary coastal evolution of southern New England: Journal of Coastal Research, special issue no. 11, p. 159-179.

Rampino, M.R., and Sanders, J.E., 1981, Episodic growth of Holocene tidal marshes in the northeastern United States--A possible indicator of eustatic sea-level fluctuations: Geology, v. 9, p. 63-67.

Shennan, Ian, 1986, Flandrian sea-level changes in the Fenland. II--Tendencies of sea-level movement, altitudinal changes, and local and regional factors: Journal of Quaternary Science, v. 1, p. 155-180.

Shennan, Ian, 1987, Global analysis and correlation of sea-level data, *in* Devoy, R.J.N., ed., Sea surface studies--A global view: London, Croom Helm, p. 198-230.

Shennan, Ian, 1989, Holocene sea-level changes and crustal movements in the North Sea region--An experiment with regional eustasy: *in* Scott, D.B., Pirazzoli, P.A., and Honig, C.A., eds., Late Quaternary sea-level correlation and applications: Dordrecht, The Netherlands, Kluwer Academic Publishers, p. 1-25.

Stevenson, J.C., Ward, L.G., and Kearney, M.S., 1986, Vertical accretion in marshes with varying rates of sea level rise, *in* Wolfe, D.A., ed., Estuarine variability: New York, Academic Press, p. 241-259.

Streif, Hansjorg, 1979, Cyclic formation of coastal deposits and their indications of vertical sea-level changes: Oceanis (France), v. 5, p. 303-306.

Streif, Hansjorg, 1987, Barrier islands, tidal flats, and coastal marshes resulting from a relative rise of sea level in East Frisia on the German North Sea coast, *in* van der Linden, W. J. M., Cloetingh, S. A. P. L., Kaasschieter, J. P. K., van de Graaff, W. J. E., Vandenberghe, J., and van der Gun, J. A. M., eds., Coastal lowlands: geology and geotechnology: Dordrecht, The Netherlands, Kluwer Academic Publishers, p. 213-223.

Tooley, M.J., ed., 1978, Sea-level changes in north-west England during the Flandrian Stage: Oxford, U.K., Clarendon Press, 205 p.

Valentine, D.W., 1992, Late Holocene stratigraphy as evidence for late Holocene paleoseismicity of the southern Cascadia subduction zone, Humboldt Bay, California: unpub. M.S. thesis, Dept. of Geology, Humboldt State University, Arcata, CA, 84 p.

Vick, G.S., 1988, Late Holocene paleoseismicity and relative sea level changes of the Mad River Slough, northern Humboldt Bay, California: unpub. M.S. thesis, Dept. of Geology, Humboldt State University, Arcata, CA, 84 p.

Comparison of Paleoseismic Geology of Subduction Zone Earthquakes in Alaska and Cascadia.

Gary A. Carver, Department of Geology,
Humboldt State University, Arcata, California 95521

Late Holocene geology along the Cascadia and eastern Aleutian-Alaskan subduction zones show many similarities which support the hypothesis that the Cascadia Subduction zone generates great subduction earthquakes. Coastal stratigraphy and geomorphology along both subduction zones include evidence of sudden changes in sea level which are interpreted to be coseismic, and gradual sea level changes attributed to interseismic deformation. In Alaska, coastal geology reflecting the 1964 earthquake provides a basis for comparison and calibration of the paleoseismic record.

Coastal stratigraphy in the fore-arc region that underwent coseismic subsidence in 1964, including Cook Inlet, most of the Kodiak Archipelago, and the Shelikof Straits contains evidence of repeated episodes of sudden submergence in the late Holocene. Alternating peat and mud sequences in bay and estuarine environments provides the best archive for this record. Although Prince William Sound and the northeast coast of Kodiak Island experienced coseismic uplift in 1964, late Holocene coastal geology reflects net submergence. Coastal geology of the eastern end of the subduction zone, the Yakataga segment, which did not rupture in 1964, includes flights of raised late Holocene terraces and broad intertidal wave-cut platforms which reflect both coseismic uplift and net emergence.

The late Holocene stratigraphy of salt marshes and tidal wetlands along the Washington and Oregon coast is similar to the stratigraphy in the Cook Inlet and Kodiak-Shelikof Straits region of Alaska and includes repeated submerged sequences of intertidal mud overlying salt marsh peats and forested wetland soils. Late Holocene coastal geology along the southern part of the Cascadia zone resembles the eastern Prince William sound and Yakataga segments of the Aleutian-Alaskan subduction zone. In northern California the late Holocene coastal geology shows strong influences of the coseismic growth of folds and thrusts in the accretionary margin. Raised late Holocene terraces and broad intertidal wave-cut platforms characterize this part of the coast except in the cores of several large synclines where submerged sequences of marine mud and wetland peats indicate coseismic subsidence and net submergence.

Some features of large shallow earthquakes along subduction zones and the recent crustal activities in the Tokai (Japan) region

Kiyoo Mogi

College of Industrial Technology, Nihon University

First, some features of large shallow earthquakes along subduction zones in the Pacific region are discussed. Data are mainly taken from Abe (1981).

Fig. 2 shows the space-time distributions of large shallow earthquakes of M 7.5 and larger in the northern part (A) and the southwestern part (B) of the circum-Pacific seismic belt which is shown in Fig. 1. Virtical axes indicate the distances measured from Vancouver and New Zealand along the seismic belts in (A) and (B), respectively. Horizontal axes indicate time. Alternation of active and quiet periods of these seismic belts is noticed, and changes in the seismic activity in the two regions complement each other.

The seismic belt in the northern Pacific region which is one of the most active subduction zone is discussed in more detail (Mogi, 1984). The top figure of Fig. 3 shows the M-T graph of great shallow earthquakes of Mw 8 and larger in this seismic belt. The bottom figure shows the distribution of focal regions of these great earthquakes. The period between 1950 and 1970 was a very active period.

Fig. 4 is another expression of the space-time distribution of these large shallow earthquakes. The distribution of focal regions

of these earthquakes along the seismic belt in 10-year intervals starting in 1920. It is very clear that the period between 1950 and 1970 was an active period.

These earthquakes in this active period can be devided into 4 groups that occurred near each other in time, as shown in Fig. 5. Fig. 6 shows the locations of earthquakes in these 4 groups. The numerals indicate the time of the occurrence of these earthquakes. It seems that each great earthquake led to the occurrence of another earthquake along the same plate boundary. This very long plate boundary from Alaska to northern Honshu was almost completely covered in a relatively short time. It may be probable that this caused a change in motive forve driving the plate motion. If there are such rhythmical changes in the plate motion, it might become possible to observe them using space technology in future (Mogi, 1984).

According to previous studies, a large shallow earthquake is sometimes preceded by a seismic quiescence. Fig. 7 shows the case of the 1973 Nemuro-hanto-oki earthquake of M 7.4 (Mw 7.8) as a typical example (Mogi, 1990). The focal region was noticeably quiet during the 12.5 years prior to the large earthquake.

There has been a great deal of debate concerning the mechanism of the seismic quiescence that precedes a large shallow earthquake. Fig. 8 gives what could be an important hint regarding this problem. In this figure, large shallow earthquakes of M 7.0 and larger along the subduction zone in the west coast of Central and South America (Mogi, 1986). The vertical axis is the distance measured from the

southern end of South America along the seismic belt shown in the left figure. The horizontal axis is time. It is noticed that the 1960 Chilean earthquake was preceded by 10 years of quiescence in a very large region extending 6,000km southward from Peru. Although the Chilean earthquake is the greatest earthquake this century, the length of the rupture zone is only 1,000km. This observed result suggests that the region where the 1960 Chilean earthquake occurred acted as a giant asperity, blocking the eastward movement of the oceanic plate. This result supports the explanation that seismic quiescence preceding an earthquake is due to the formation of a large asperities.

Fig. 9 shows the age of the ocean floor according to the Pitnam et.al.(1974). It can be seen that the seismic quiescent region before the Chilean earthquake forms a single block. This may support the above-mentioned explanation from the viewpoint of the asperity model.

The next topic is the recent crustal activities in the Tokai region. Along the Nankai-Suruga Trough, large low angle thrust type earthquakes have occurred repeatedly at regular intervals of 100 to 150 years (Ando, 1975). These earthquakes are caused by the subduction of the Philippine Sea plate beneath the Eurasian plate. In both the 1707 and 1854 earthquakes, the rupture zones extended over the whole region from the Nankai Trough to the Suruga Trough. In this century, however, the 1944 Tonankai and 1946 Nankaido earthquakes occurred along the Nankai Trough, but the Tokai region along the Suruga Trough remains unruptured (Ishibashi, 1976).

Therefore the Tokai region may be a seismic gap of the first kind, and may have a high potential as the site of the next large earthquake. However, since there are no records of a large shallow earthquake having occurred independently in this region, we must consider that there are problems in making this simple inference.

In this paper some recent changes in seismin activity and crustal deformation are discussed. Sometimes, before a major earthquake occurs, the focal region of the coming earthquake becomes guiet and simultaneously, the wide-ranging area surrounding this region tends to become active.

Fig. 10 shows epicentral distribution of shallow earthquakes of M 4.2 and larger for successive two periods (1950-1972) and (1973-1992). Data are taken from JMA reports. There was some activity before 1972 along the Suruga Trough and the Nankai Trough, but no earthquakes have occurred recently. This quiescence is continuing.

On the other hand, many moderate and large earthquakes have occurred in the surrounding area in the recent years. Fig. 11 shows the epicentral distribution of M 5.5 and larger in the same successive periods. A number of recent large earthquakes have occurred in the area surrounding the focal region of the anticipated Tokai earthquake. The top figure of Fig. 12 shows the M-T graph of earthquakes of M 5.5 and larger in the region shown in the left figure (A), and the bottom figure shows the space-time distribution of these earthquakes. These figures also show that the seismic activity in the surrounding region has increased in recent years.

Fig. 13 shows vertical movement of Omaezaki in relation to Kakegawa observed by leveling surveys by GSI (1991). Curve (A) is the original curve and Curve (B) is the corrected curve in which a seasonal variation was eliminated. The subsidence of the western coast of the Suruga Bay is steadily continuing. Fig. 14 is a summary of vertical movements of the western coast of the Suruga Bay including Omaezaki obtained by leveling surveys and tidal observations. It is noted that the rate of subsidence somewhat increased around 1974. Particularly, changes in the rate of subsidence and in seismicity pattern occurred simultaneously around 1974 and the state is continuing. Future changes of seismic activity and the crustal deformation in this area demand close attension. (Very recently the rate of subsidence seems to be decreasing.)

The possibility of earthquake prediction depends on whether short-term precursory phenomena are observed before the earthquake. Since precursory phenomena normally have a marked regional character, the type of phenomena that preceded the Tokai earthquake of 1854 may be expected before the next one. Unfortunately, there are no reliable data available from 1854. However, the 1944 Tonankai and the 1946 Nankaido earthquakes occurred adjacent to the Tokai region. They should provide valuable information. As shown in Fig.15, in both of these earthquakes, the trough side began to uplift a day or two before they occurred (Sato, 1977; Mogi, 1984/1985). Fig. 16 shows that marked anomalies were also observed in the wells and hot springs along the coast before the Nankaido

earthquake (Komukai, 1948). These changes began to occur one day - one week before the earthquake. If similar phenomena occur before the next Tokai earthquake, the changes may be sufficiently recorded by the present network.

Fig. 17 shows the distribution of observation stations for full-time monitoring of precursory phenomena of earthquakes in the Tokai region. As an example of results observed by this monitoring system, Fig.18 shows epicentral locations of shallow earthquakes in the recent three years in and around the Tokai region (JMA, 1992).

References

Abe, K., Magnitudes of large shallow earthquakes from 1904 to 1980, Phys. Earth Planet. Inter., 27, 72-92 (1981).

Ando, M., Source mechanisms and tectonic significance of historical earthquakes along the Nankai trough, Japan, Tectonophysics, 27, 119-140, 1975.

GSI (Geographical Survey Institute), Crustal movements in the Tokai district, Rep. Coord. Comm. Earthq. Predict., 46, 272-289, 1991.

Ishibashi, K., Re-examination of a great earthquake expected in the Tokai district : Possibility of the "Suruga Bay earthquake", Abstracts, Seism. Soc. Japan, 1976 No. 2, 30-34, 1976 (in Japanese).

JMA (Japan Meteorological Agency), personal comunication, 1992.

Kato, T.and K. Tsumura, Vertical land movement in Japan as deduced from tidal record, (1951-1978), Bull. Earthq. Res. Inst., Univ. Tokyo, 54, 559-628, 1979 (in Japanese).

Komukai, R., Report of the Nankaido Earthquake in the 21th Year of Showa, Earthquakes and Damages, Special Volume of Hydrographic Bulletin, Hydrographic Department of Japan, 12-52, 1948 (in Japanese).

Mogi, K., Successive occurrence of great shallow earthquakes along the northern Pacific seismic belt and the plate motion, abstracts, Seism. Soc. Japan, 1984 No. 1, p. 89, 1984 (in Japanese).

Mogi, K., Temporal variation of crustal deformation during the days preceding a thrust-type great earthquake -- the 1944 Tonankai earthquake of magnitude 8.1, Japan, Pageoph, 122, 765-780, 1984/1985.

Mogi, K., Global changes in seismic activities, Abstracts, Seism. Soc. Japan, 1986 No. 2, p. 126, 1986 (in Japanese).

Mogi, K., Seismicity before and after large shallow earthquakes around the Japanese islands, Tectonophysics, 175, 1-33, 1990.

Pitnam III, W.C., R.L.,Larson and E.M. Herron, Age of the ocean basins determined from magnetic anomaly lineations, Geol. Soc. Am. Map and Chart Series, MC-6, 1974.

Sato, H., Some precursors prior to recent great earthquakes along the Nankai trough, J. Phys. Earth, 25, Supple., S111-S121, 1977

U.S. Department of the Interior, Geological Survey, Preliminary Determination of Epicenters (PDE), (1981 - 1989).

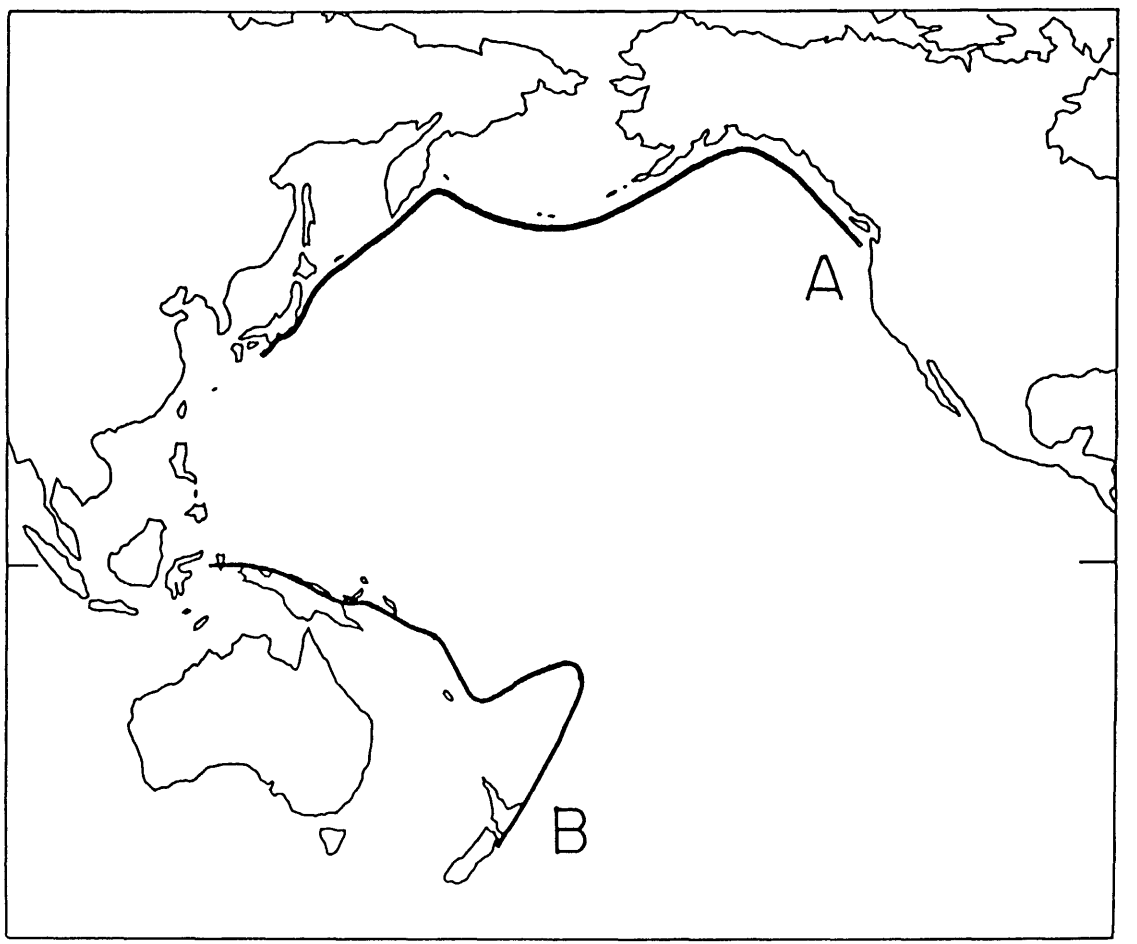

Fig. 1 Northern part (A) and southwestern part (B) of the circum-Pacific seismic belt.

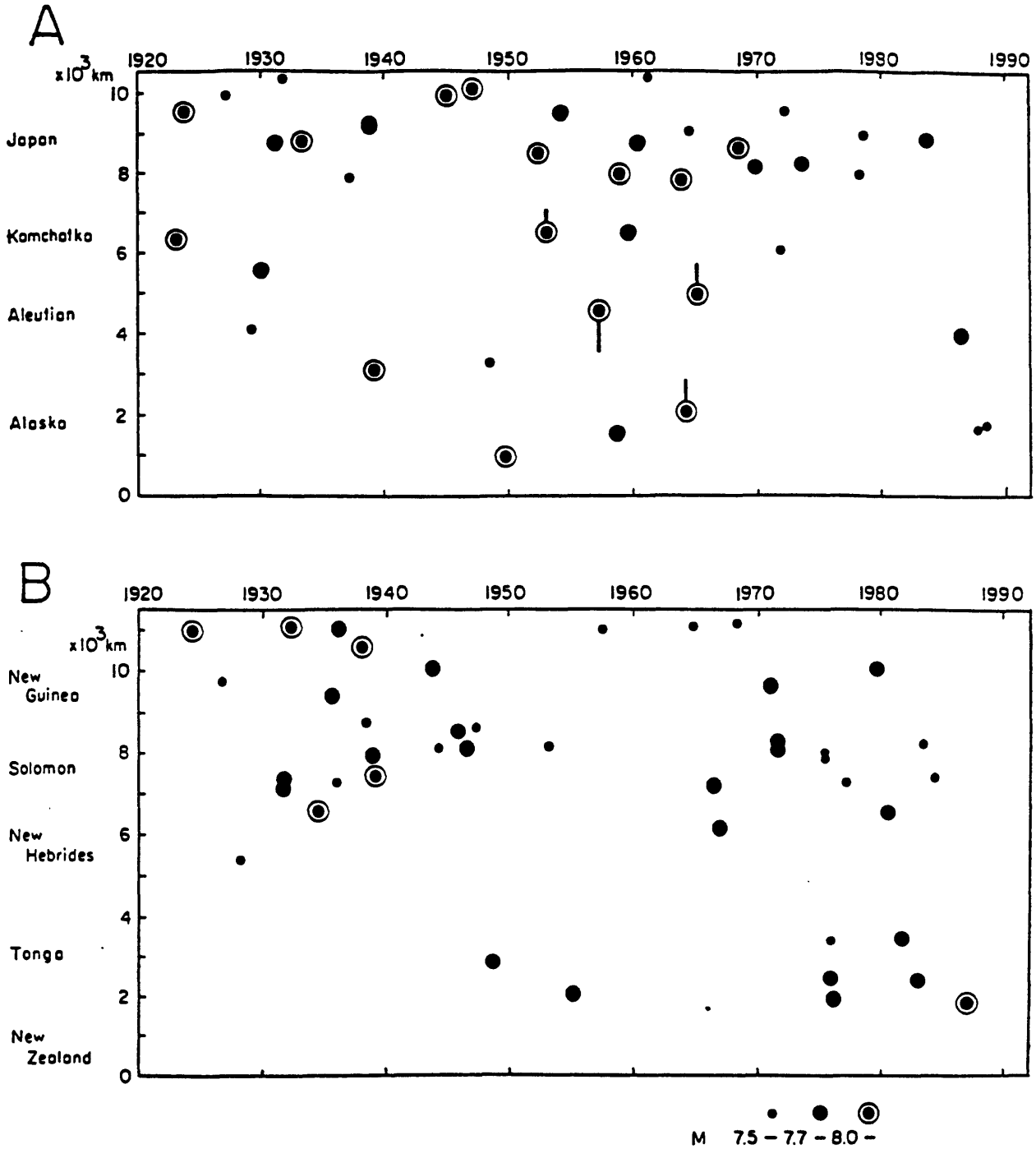

Fig. 2 Space-time distributions of large shallow earthquakes in the northern part (A) and southwestern part (B) of the circum Pacific seismic belt. Vertical axes indicate the distances measured from Vancouver and New Zealand in (A) and (B) respectively. Alternation of active and quiet periods of these seismic belts is noticed.

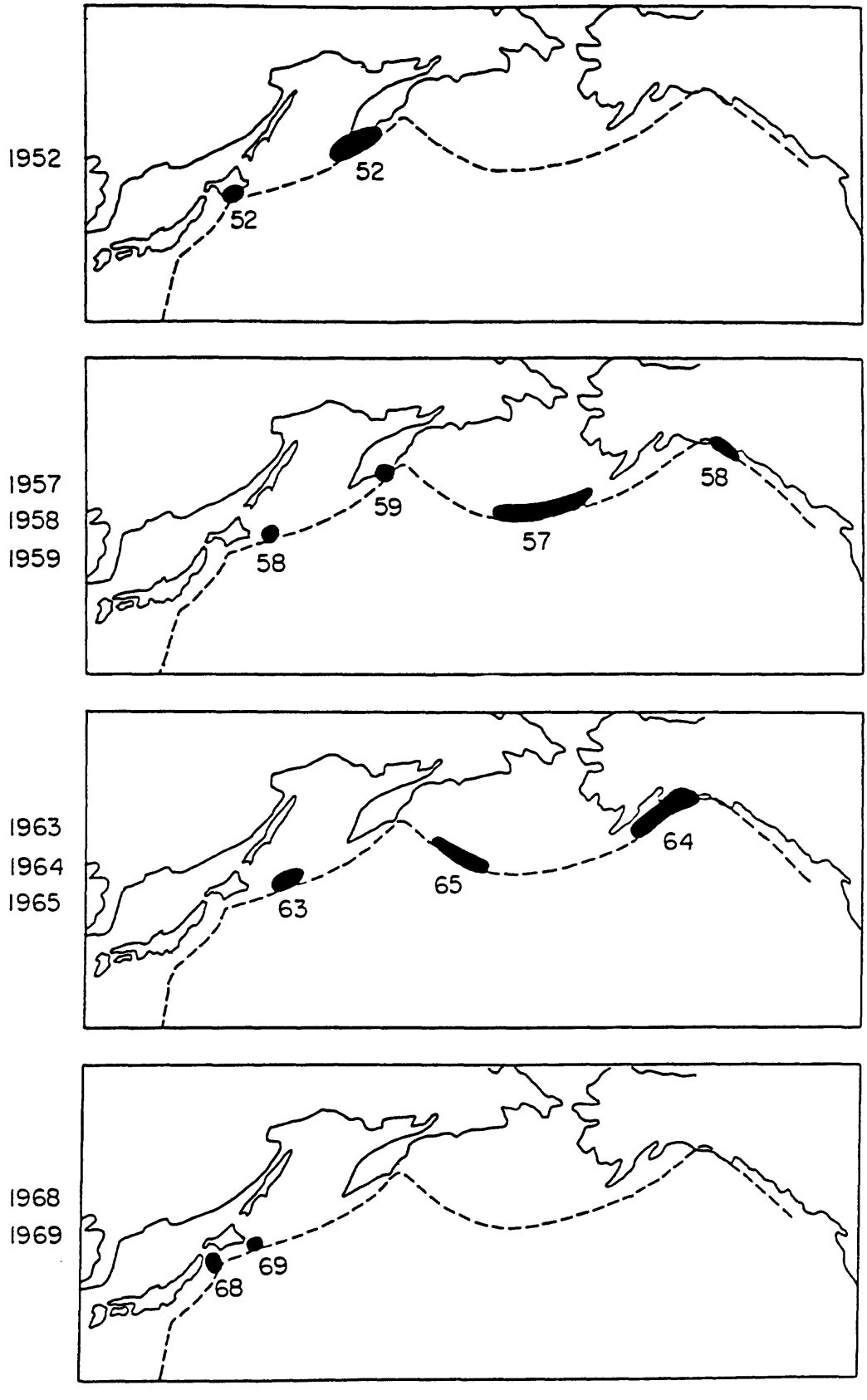

Fig. 6 Locations of great earthquakes of 4 groups which are labeled (1) to (4) in Fig. 5.

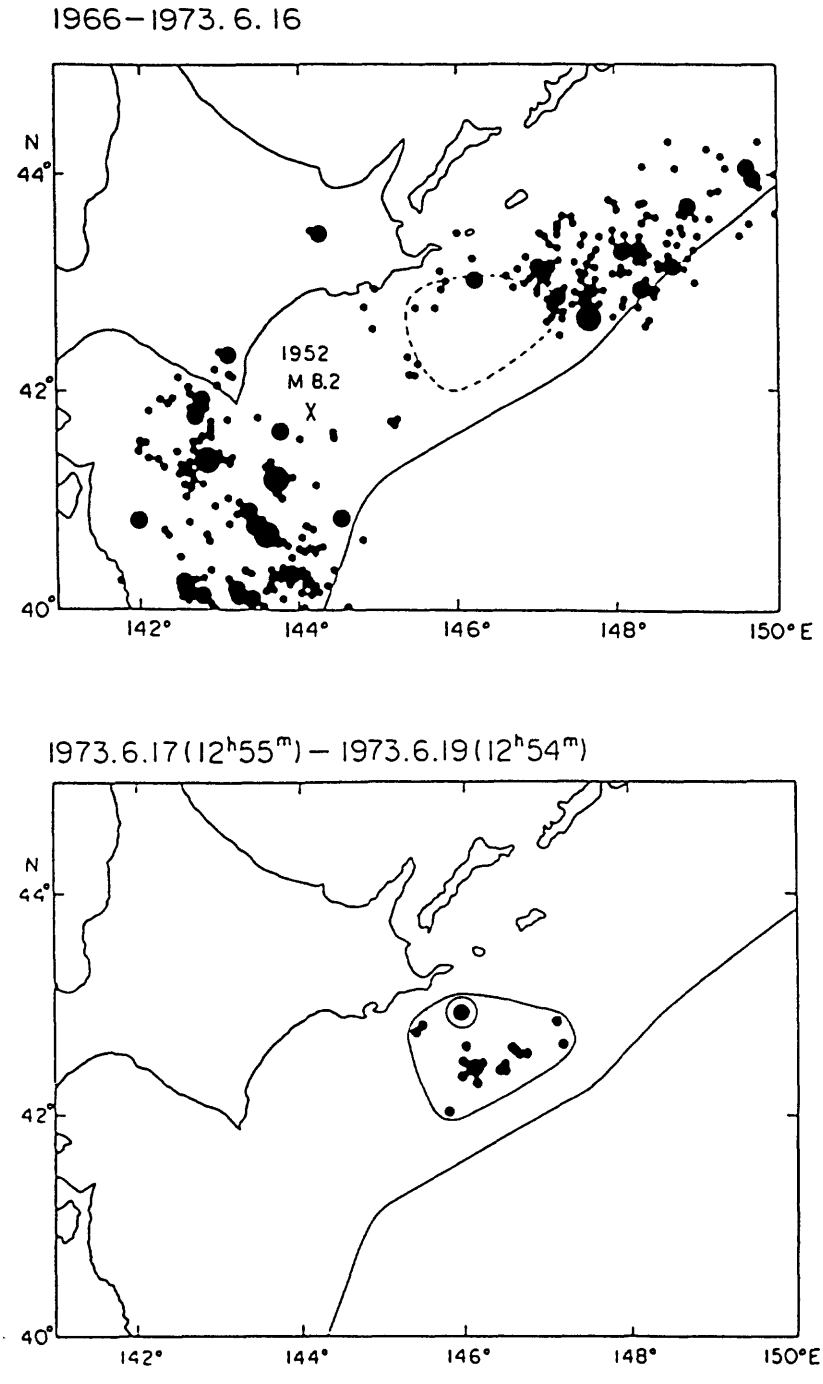

Fig. 7 Top: epicentral distributions of shallow earthquakes of M 5 and larger before the 1973 Nemuro-hanto-oki (Japan) earthquake (M 7.4, Mw 7.8). Bottom: the main shock and aftershocks over a 2-days period after the Nemuro-hanto-oki earthquake of June 17, 1973.

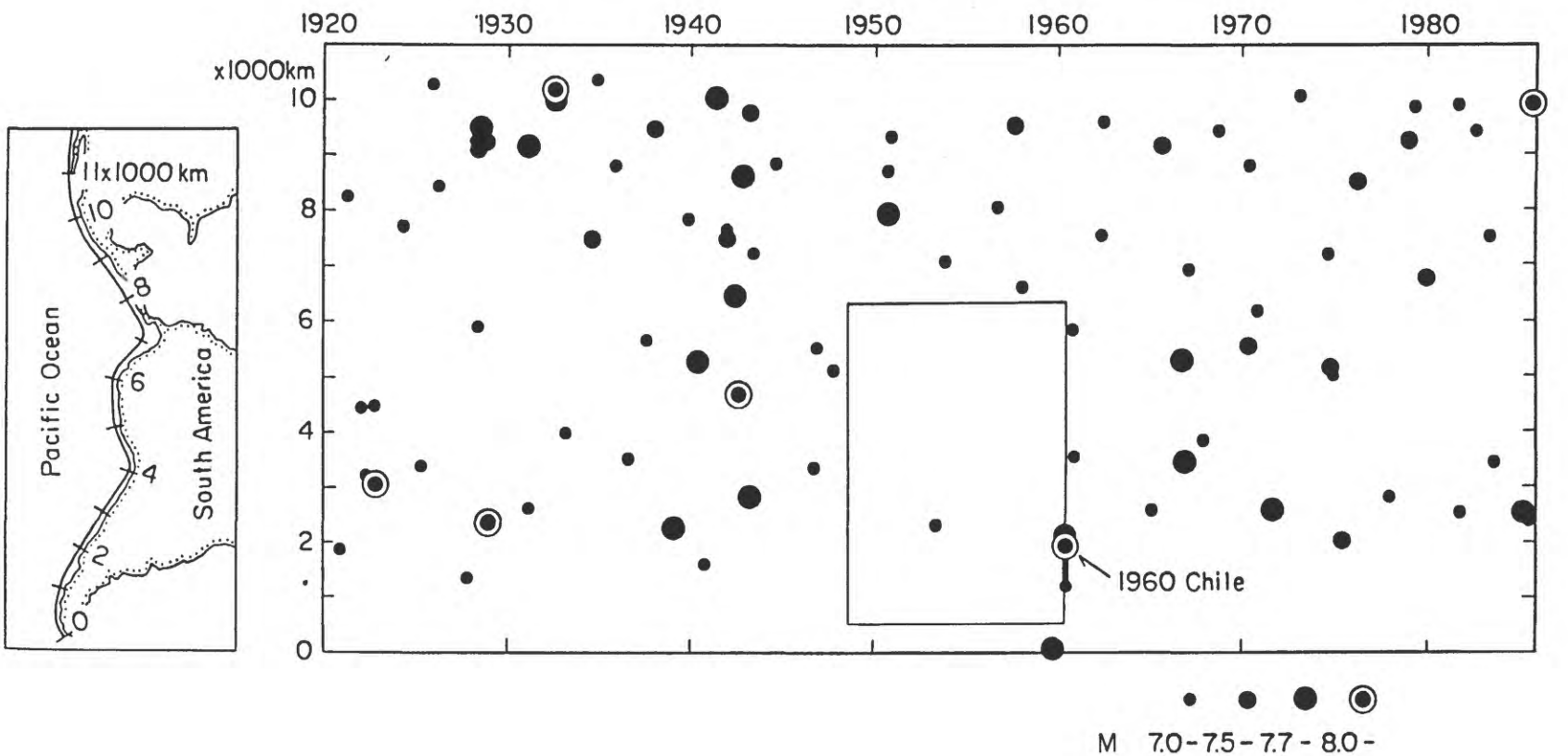

Fig. 8 Space-time distribution of large shallow earthquakes of M 7.0 and larger along the subduction zone in the west coast of Central and South America. The axis of abscissa is time and the ordinate is distance along the seismic belt shown in the left figure. The seismic quiescence in a wide area before the 1960 Chilean earthquake (Mw 9.5) is noted. Data are taken from Abe (1981) and PDE reports.

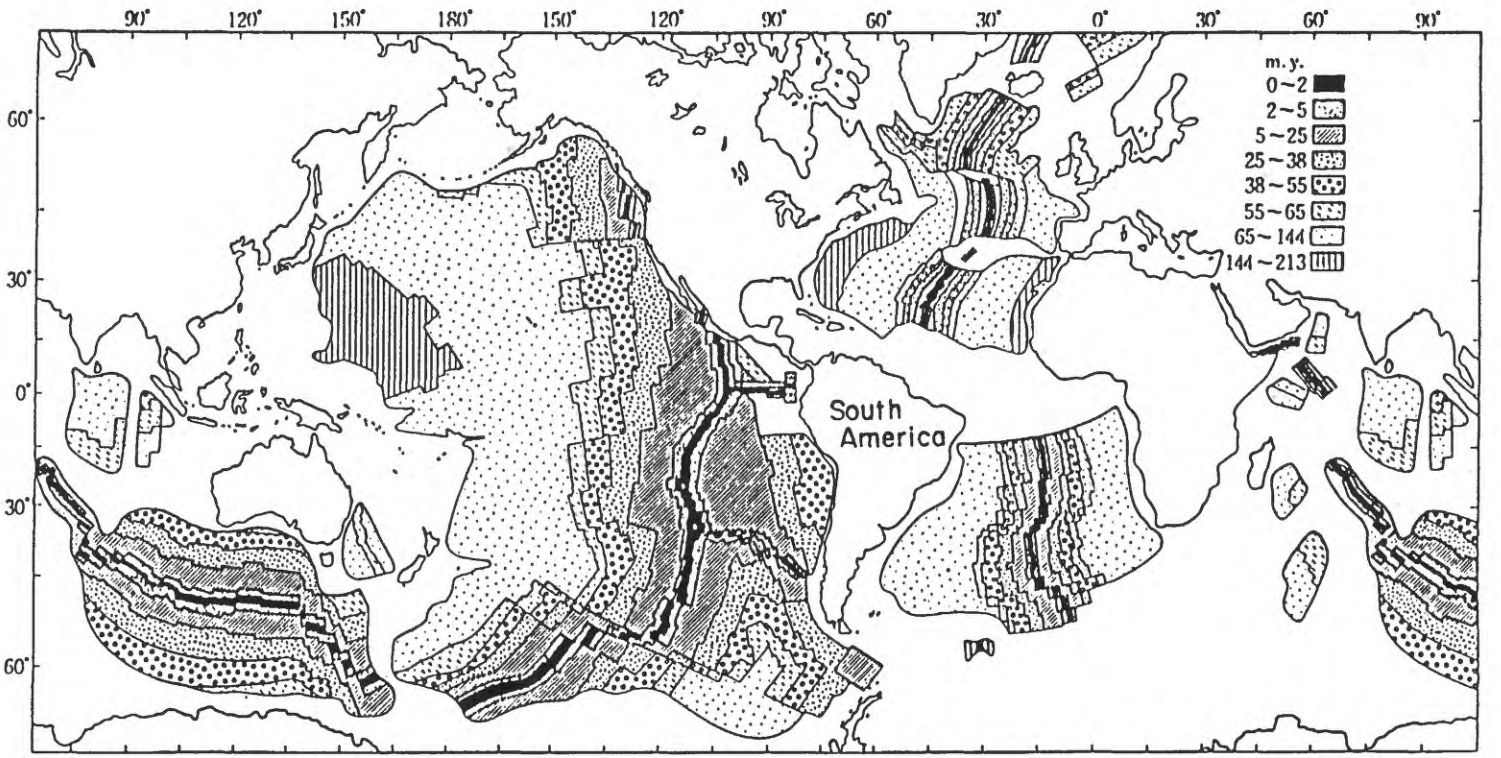

Fig. 9 Age of ocean floor. This suggest that the western coast of South America may be a single block. From Pitman et al. (1974).

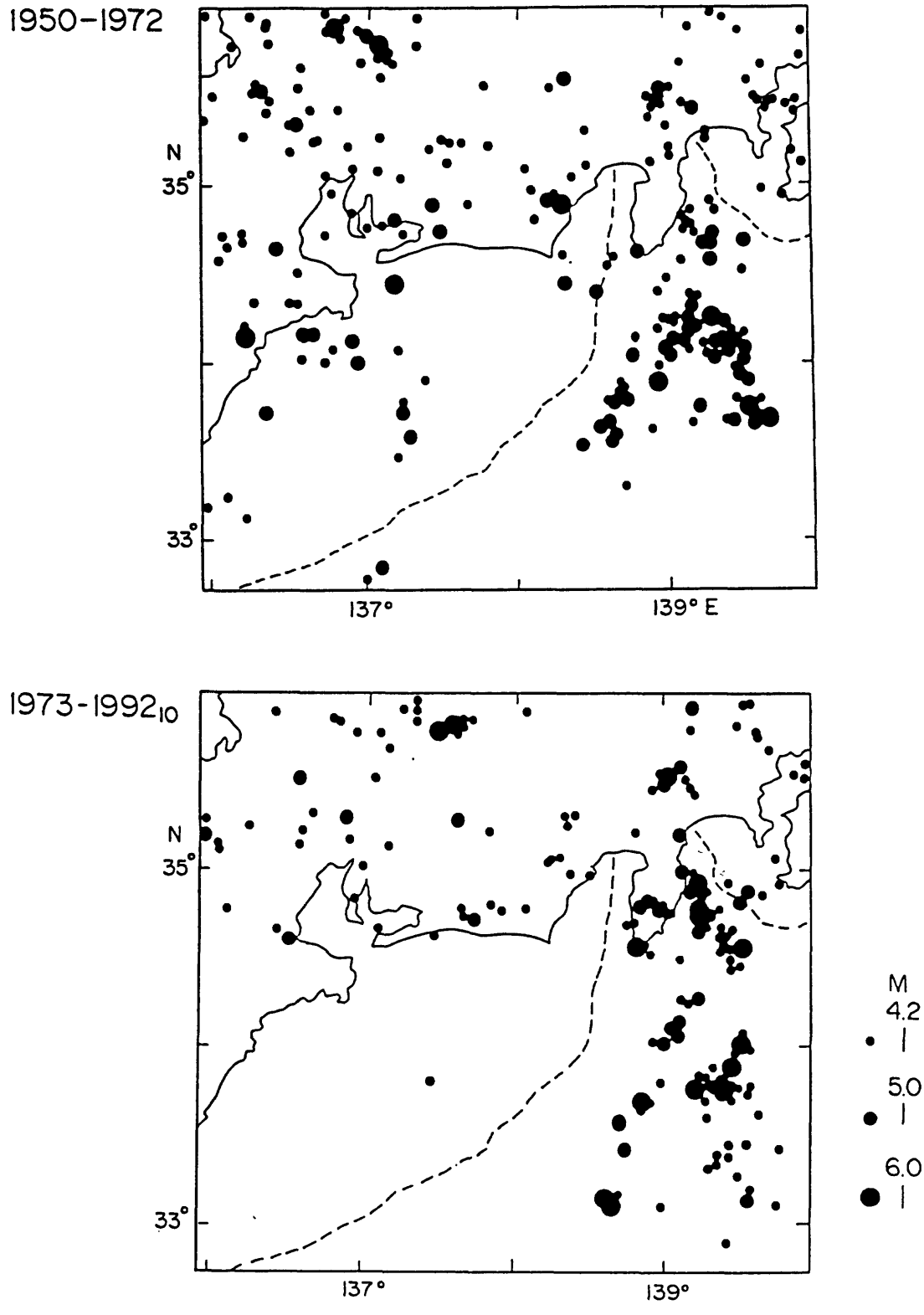

Fig. 10 Epicentral distributions of shallow earthquakes (less than 60km deep) of M 4.2 and larger that occurred in the Tokai region and the surrounding area for successive two periods (1950-1972) and (1973-1992$_{10}$). The region along the Suruga-Nankai Trough is quiet in recent years. Data are taken from JMA reports.

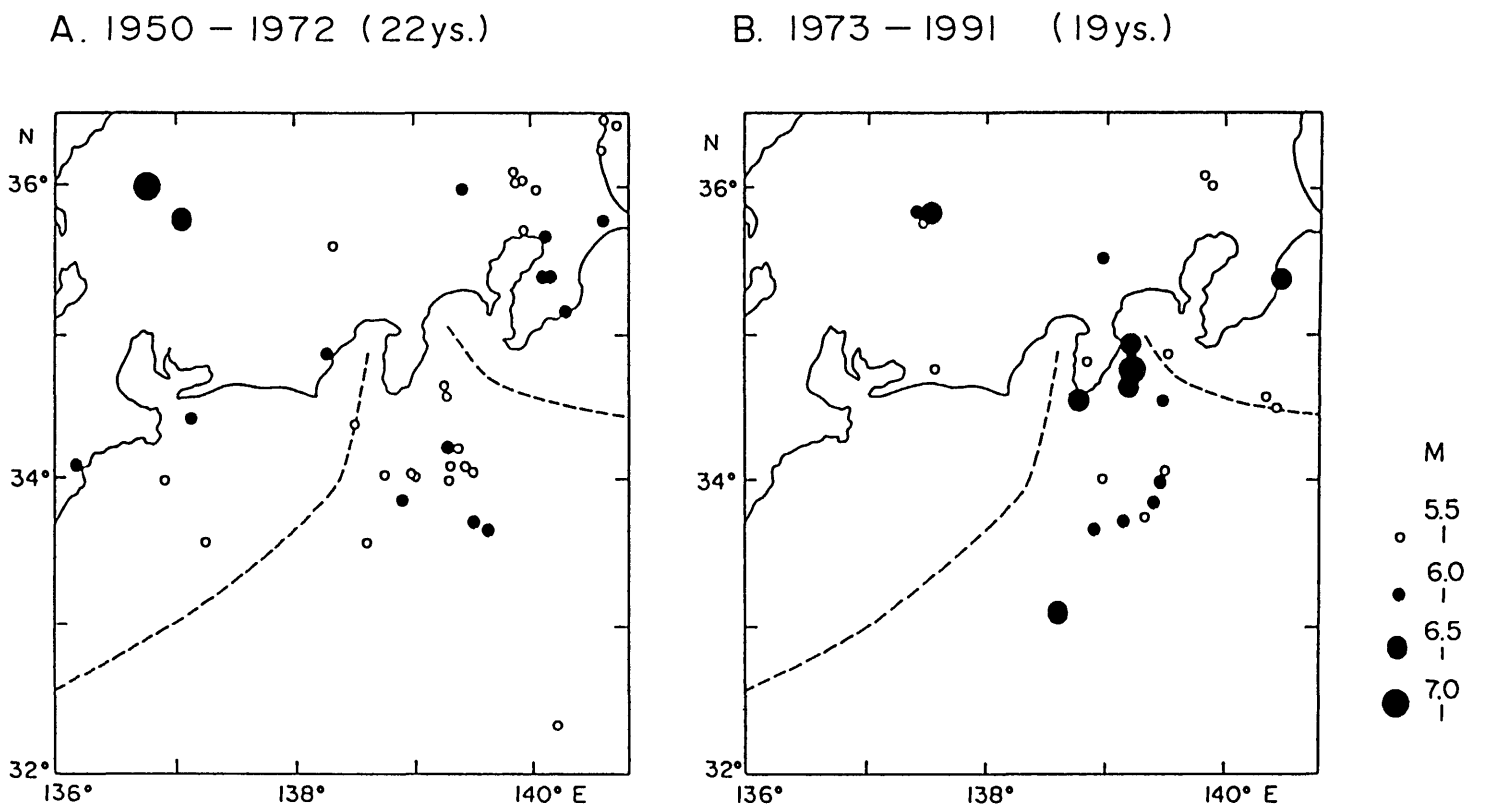

Fig. 11 Epicentral distributions of shallow earthquakes (less than 60km deep) of M 5.5 and larger during the same two periods as shown in Fig. 10. The surrounding region of the anticipated "Tokai earthquake" is active in recent years.

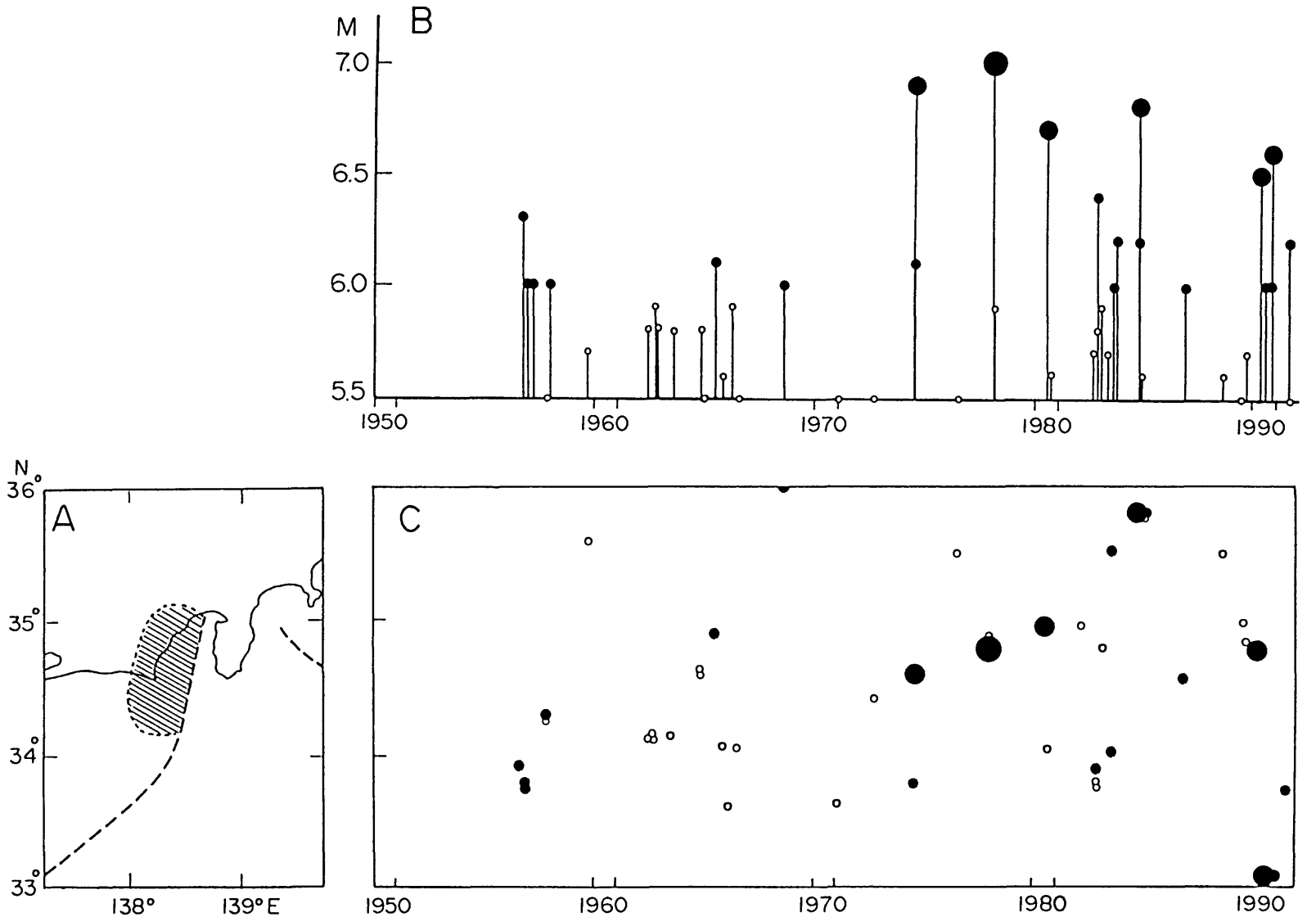

Fig. 12 B: M - T graph of shallow earthquakes (less than 60km) in the region shown in A. C: space-time distribution of these earthquakes. A significant change in seismic activity around 1974 is noted. Hatched area in A : the anticipaped "Tokai earthquake".

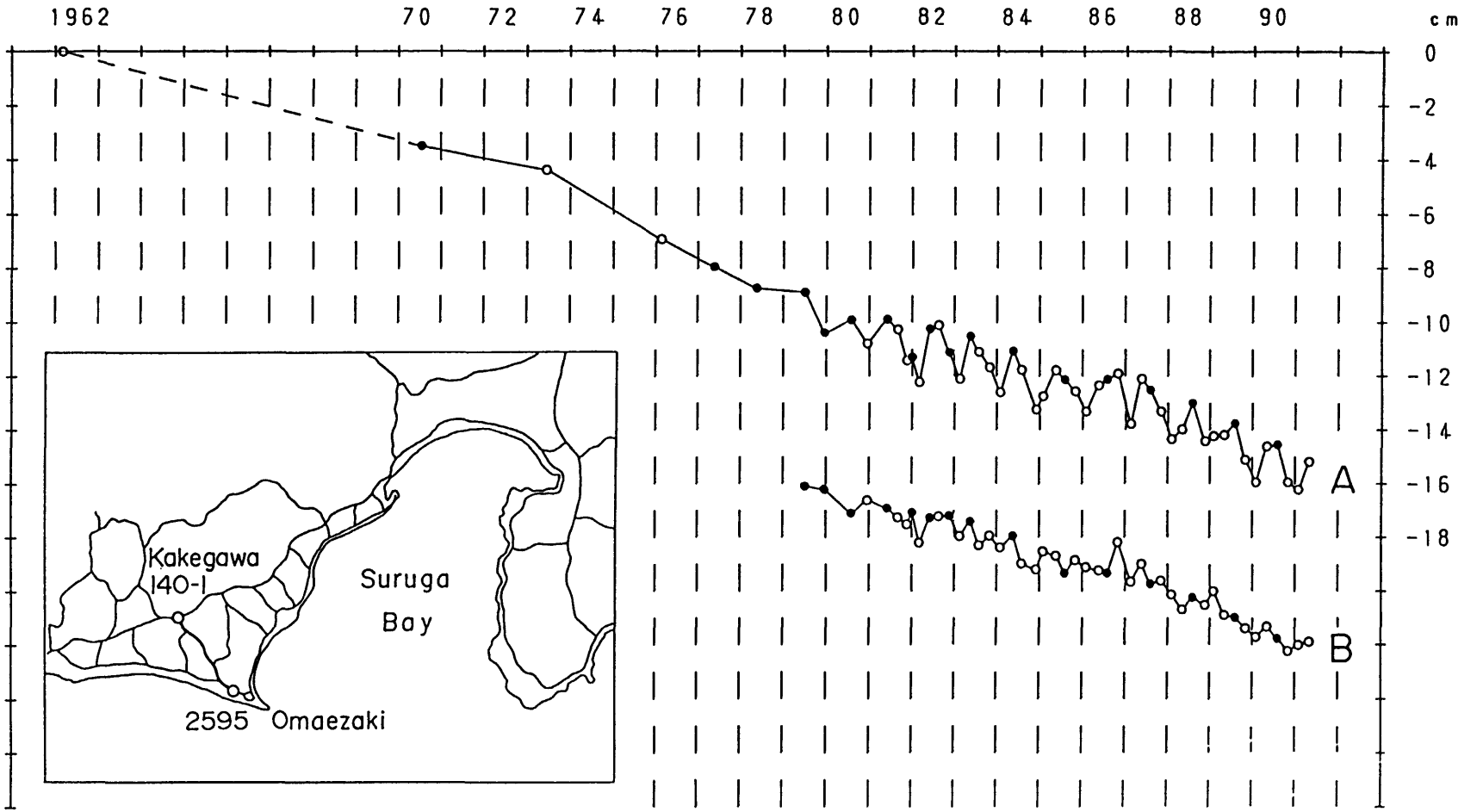

Fig. 13 Vertical movement of Omaezaki in relation to Kakegawa observed by leveling surveys. A: original curve; B: corrected curve in which a seasonal effect was eliminated. From GSI (1991).

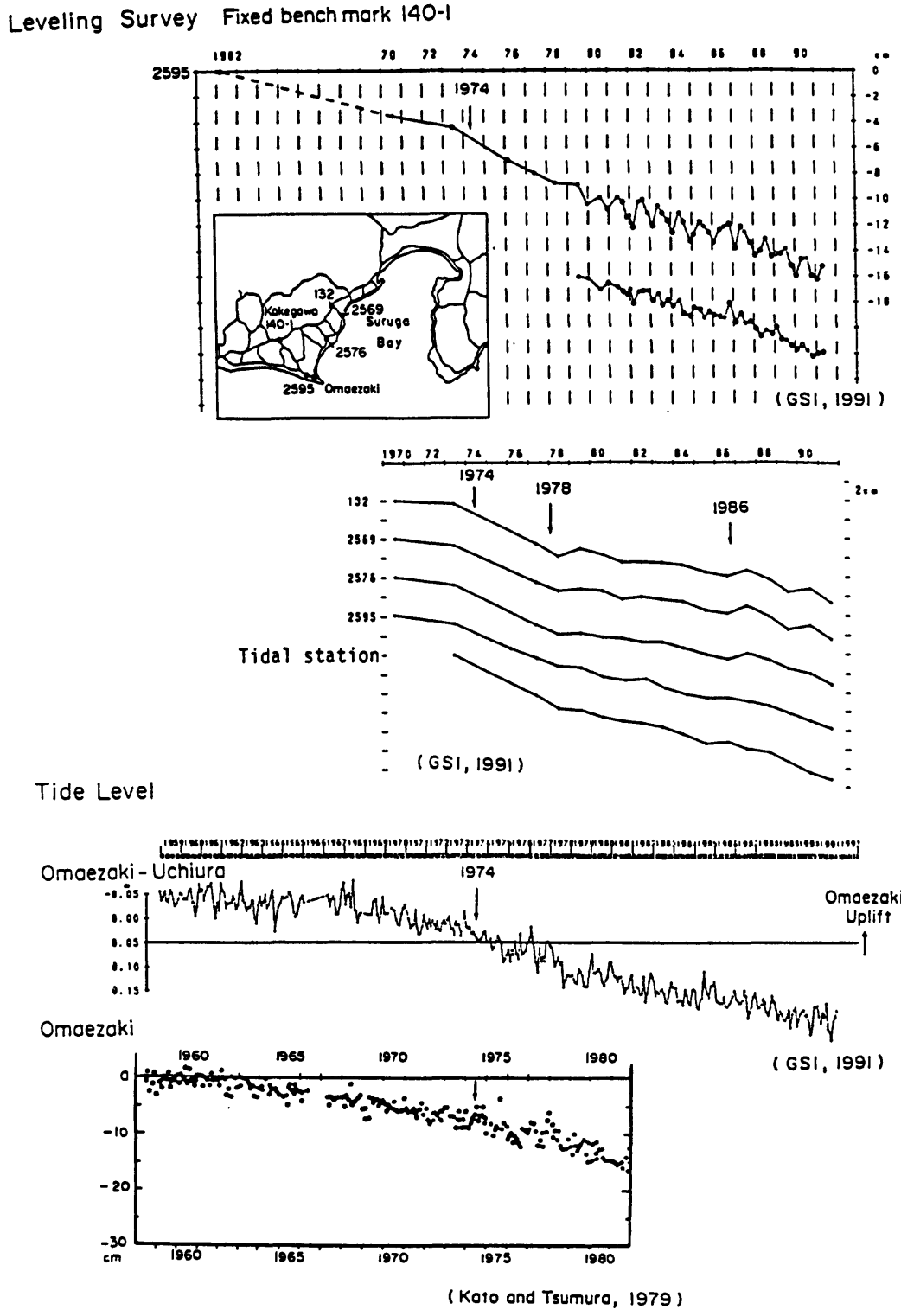

Fig. 14 Vertical movements of the western coast of the Suruga Bay including Omaezaki obtained by leveling surveys and tide level observations. (GSI, 1991; Kato and Tsumura, 1979). It is noted that the rate of subsidence increased around 1974.

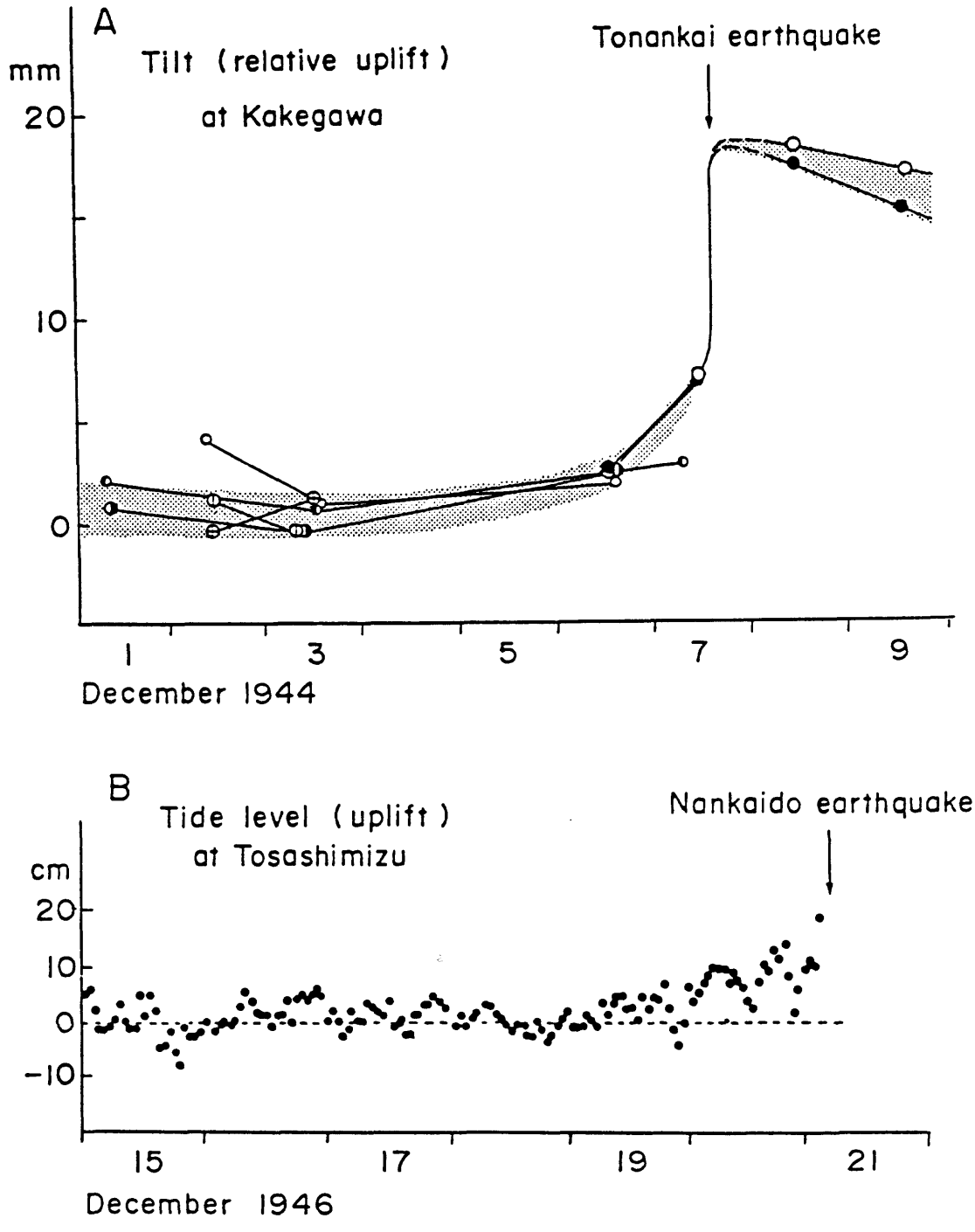

Fig. 15 Temporal variations of crustal deformation before the 1944 Tonankai earthquake (A) and the 1946 Nankaido earthquake (B) along the Nankai Trough. From Sato (1977); Mogi (1984/1985). Locations of Kakegawa and Tosashimizu are shown in Fig. 14 and 16, respectively.

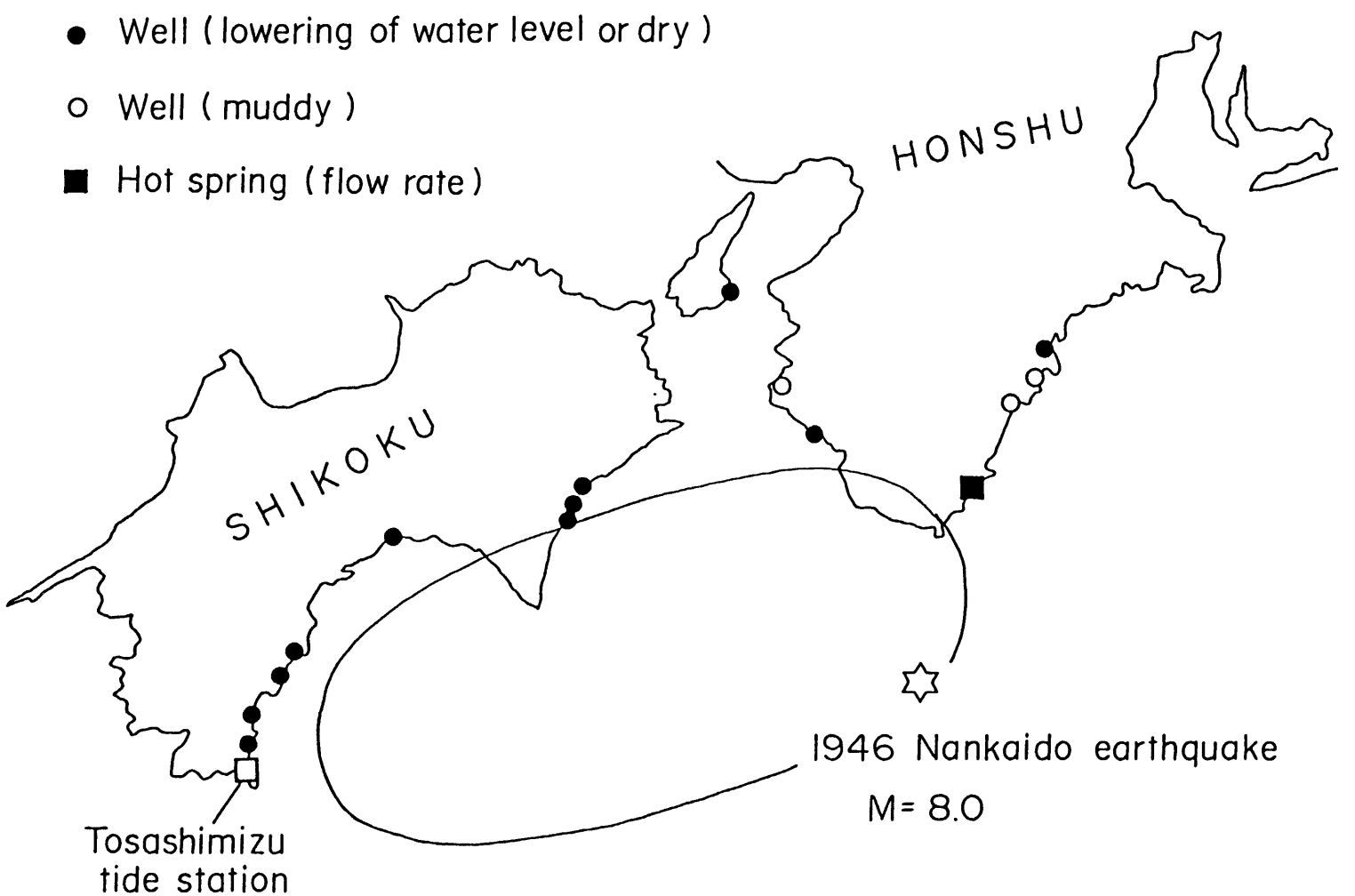

Fig. 16 Anomalous changes of ground water before the 1946 Nankaido earthquake of M 8.0. These changes began to occur one day - one week before the earthquake. Modified from Komukai (1948).

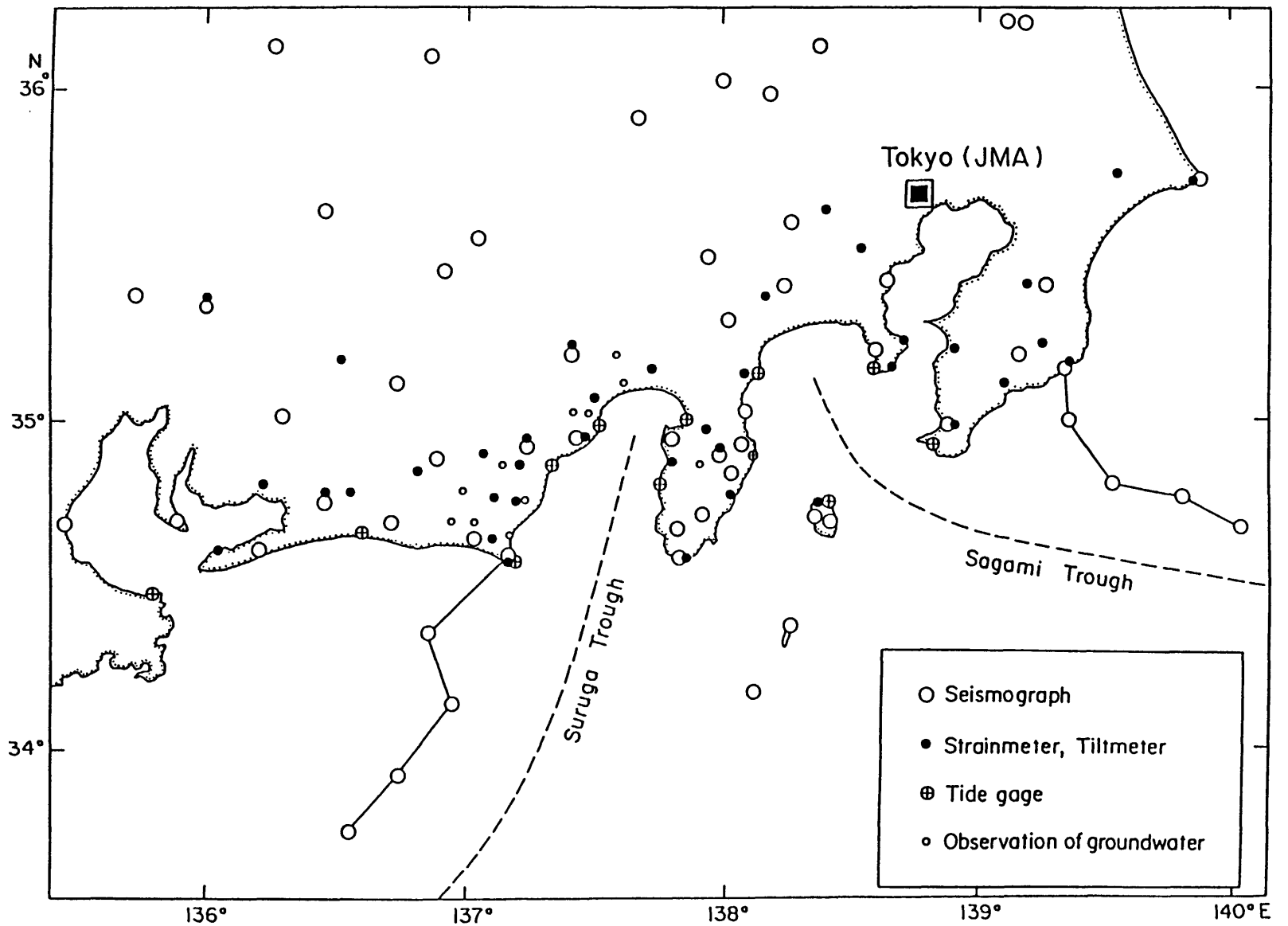

Fig. 17 Distribution of observation stations for full-time monitoring of precursory phenomena of earthquakes in the Tokai region. Data are telemetered to the center (JMA) at Tokyo.

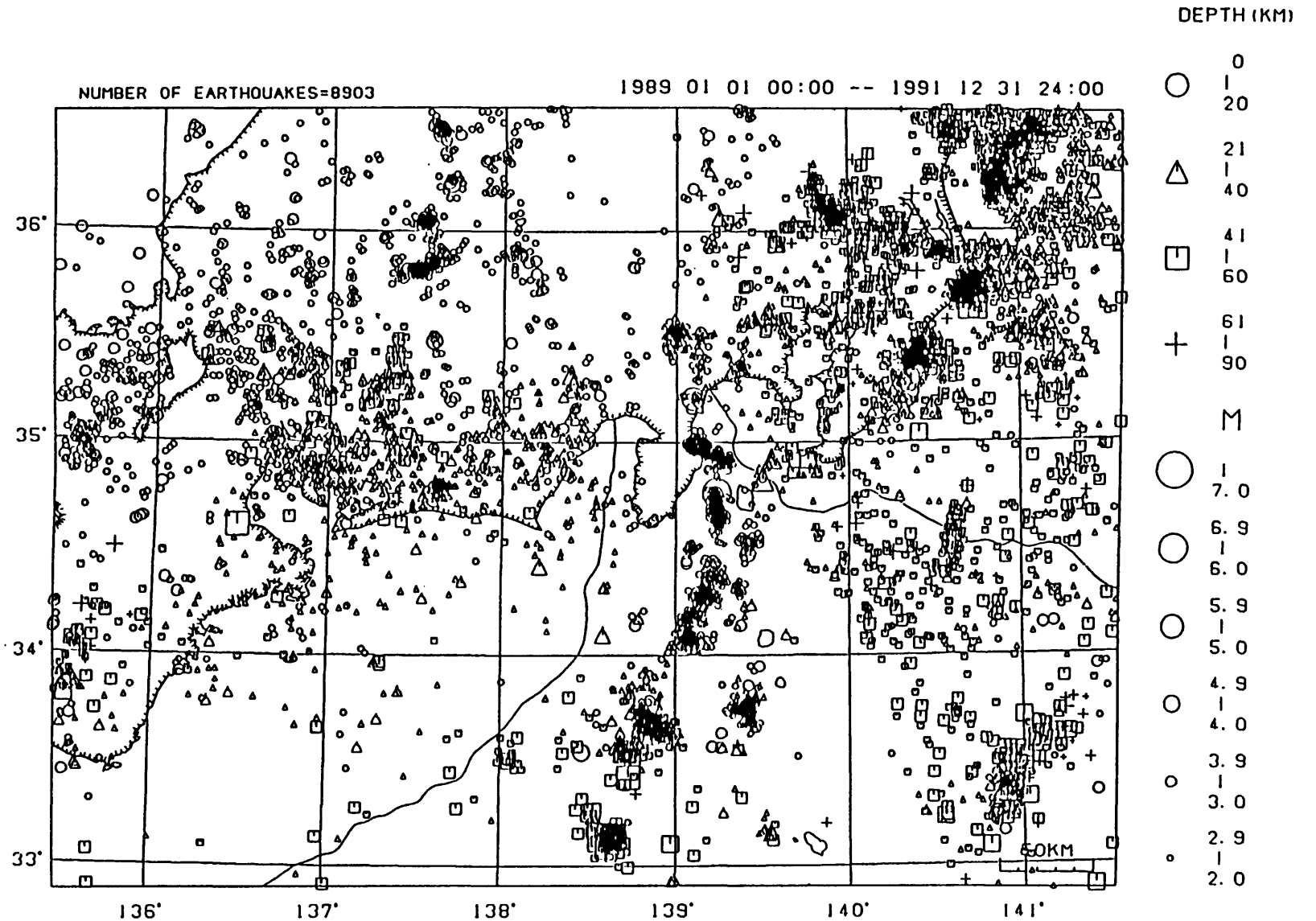

Fig. 18 Locations of recent earthquakes (1989-1991) observed by the seismic observation system in and around the Tokai region.

Comment on "Seismic Gap Hypothesis: Ten Years After" by Y.Y. Kagan and D.D. Jackson

Stuart P. Nishenko
National Earthquake Information Center, U.S. Geological Survey
Denver, Colorado

Lynn R. Sykes
Lamont-Doherty Geological Observatory and Department of Geological Sciences
Columbia University, Palisades, New York

Submitted to the Journal of Geophysical Research
August, 1992

Kagan and Jackson [K&J, 1991] recently published statistical tests of the seismic gap hypothesis, as presented by Kelleher, Sykes, and Oliver [KSO, 1973] and McCann, Nishenko, Sykes, and Krause [MNSK, 1979], stating that "the hypothesis of increased earthquake potential after a long quiet period can be rejected with a large confidence." Based on these test results, K&J concluded that the seismic gap hypothesis is invalid and propose a clustering model of earthquake occurrence as a replacement. If valid, this conclusion would have major implications for ongoing evaluations of seismic hazards, long-term earthquake prediction, and the physical basis for strain buildup and release in large earthquakes. In addition, this conclusion could dramatically change the rational for assigning priority to the study of certain faults and fault segments in populated areas as part of the U.S. National Earthquake Hazards Reduction Program and the International Decade of Natural Disaster Reduction. Given the societal and scientific importance of this issue, we feel that a closer examination and discussion of K&J's presentation is essential.

Upon examination we find that half of the earthquakes that K&J use to test the seismic gap hypothesis do not correspond to the selection criteria of MNSK. We conclude that K&J are evaluating a very different hypothesis than was originally presented by KSO and MNSK. In fact, K&J appear to be testing the hypothesis that the temporal duration of a gap can be used to anticipate *any* earthquake with $M \geq 7$. In contrast, the forecasts in KSO and MNSK were for a specific set of earthquakes that fulfilled certain criteria as to mechanism, type of plate boundary, and range of magnitudes. Our examination of a revised catalog indicates that elapsed time alone is not a powerful criteria for characterizing seismic potential in a system characterized by an order of magnitude or larger variation in recurrence time. Given the relatively small number of eligible events that have occurred during the interval 1973-1992, the hypothesis test does not yet have the power to adequately discriminate between alternative models at a high level of confidence.

Seismic Gaps, Seismic Potential, and Long-Term Probabilistic Earthquake Forecasts - A Historic Perspective

Since its introduction in 1965 by Fedotov, the seismic gap hypothesis has evolved as knowledge about earthquake history, pre-historic earthquakes, and the earthquake process has increased. Since there often is a tendency to confuse current concepts and

hypotheses with those of older studies, we review some of the salient points of the development of the seismic gap, seismic potential, and long-term probabilistic concepts.

The seismic gap hypothesis represents a simple application of the concept of a seismic cycle along a plate boundary - a period of steady-state loading and strain accumulation on a fault segment terminated by a sudden relaxation during an earthquake. As formulated in the 1960's and 70's, the seismic gap model is most closely aligned with Gilbert's [1909] idea of alternation - *"when a large amount of stored energy has been discharged in the production of a great earthquake....it would seem ...that the next event is more likely to occur at some other place"* and not rhythmic recurrence as K&J have indicated in their introduction. Both Fedotov [1965] and Mogi [1969] mapped the rupture zones of earthquakes with surface wave magnitudes (M_S) larger than 7.7 in the northwest Pacific using aftershocks, geodetic and tsunami data. They observed that aftershock zones of those events abutted and tended to fill in gaps where earthquakes of that type had not occurred for at least 30 to 100 years. Sykes [1971] showed how the theory of plate tectonics would favor seismic gaps as the most likely places for future large earthquakes along simple, well defined plate boundaries. He delineated three gaps with dimensions of greater than about 150 to 200 km for the Alaska-Aleutian subduction zone and the Fairweather transform fault. KSO built on these foundations and created a set of initial and supplemental criteria to define regions of special seismic potential. They recognized that certain seismic zones are probably permanently aseismic in terms of the occurrence of large earthquakes. Their initial criteria for the remaining areas, which they referred to as regions of special seismic potential, required that the segment in question be either a strike slip or thrust-type plate boundary that has not had a large or great earthquake in more than 30 years. The 30 year threshold was based on the shortest recurrence times observed in the circum-Pacific region *at that time*. The supplemental criteria took into account information about the historic record, whether the zone was near the end of a recurrence interval, or whether the zone was next in an apparent progression of earthquake activity along the plate boundary. The supplemental criteria also recognized that in regions with no record of large earthquakes, relative plate motion could be accommodated by either aseismic slip or small to moderate sized earthquakes.

KSO explicitly state (p. 2550) that each of the previous papers that they cited "*is restricted almost entirely to the largest class of earthquakes that occurred along the plate boundary under consideration.*" KSO used figures from some of those studies (e.g. Sykes [1971]) with attribution in their regional maps. They also noted regions where the largest known historic earthquakes were typically great ($M_S > 7.7$) events

(e.g., Kuriles, Alaska, South America) and other regions where the largest events to occur were usually major ($7.0 \leq M_S \leq 7.7$) earthquakes (e.g. Mexico and Central America). They used the term large earthquake to encompass both major and great earthquakes.

MNSK expanded upon the seismic potential concept by defining categories based on the amount of time elapsed ($T_{elapsed}$) since the last major or great event in any region, $T_{elapsed}<30$, $30 \leq T_{elapsed}<100$, and $T_{elapsed} \geq 100$ years (green, orange, and red colors on their Fig. 1), as well as recognizing three other types of regions with more equivocal hazard states. Both the 30 and 100 year cutoffs were arbitrarily chosen since the uncertainty in knowledge of recurrence periods was large at that time (p. 1086). They also recognized (p. 1086-1089) that since repeat times were poorly known for many areas around the circum-Pacific, some areas with relatively short repeat times (i.e. orange zones) would likely be more active during a given period of time than areas with long repeat times (i.e. red zones), which could be inactive for many more years to come. Nishenko and McCann [1981], in fact, noted that more large to great earthquakes had occurred in orange than in red zones in the interval 1978 to 1981. Inspection of Table 1 and the Note added in Proof in MNSK shows that for the 12 events in the interval 1968 to 1980, there were four times as many earthquakes in orange as in red areas. Most of the red areas, in fact, had ruptured previously in very great earthquakes, those of surface wave magnitude M_S, or moment magnitude $M_W > 8.5$, which we took then, as we do now, to be characterized by relatively long repeat times.

These observations and the publication of earthquake histories and more reliable repeat time estimates for areas in the circum-Pacific lead to the development in the 1980's of forecast models that explicitly included both recurrence, T_{ave}, and elapsed, $T_{elapsed}$, time information for individual fault segments, as well as estimates of magnitudes of events for those segments, information that we were well aware prior to 1981 represented serious shortcomings of the gap concept . Hence, concepts about earthquake recurrence and time-varying probabilistic assessment [see Lindh, 1983; Sykes and Nishenko, 1984; Nishenko, 1985], whether the recurrence of these large earthquakes is rhythmic (Gilbert, 1909), strictly periodic or quasi-periodic, time-predictable or slip-predictable were only addressed and applied to the seismic gap hypothesis within the last decade, following the publication of MNSK and Nishenko and McCann [1981]. Of those concepts, few if any seismologists or Quaternary geologists who study active faults think large earthquakes at a given place are strictly periodic.

The Seismic Gap Hypothesis

Clearly, if one wishes to test a particular realization or application of a hypothesis, it is necessary to adhere to the criteria developed at the time of publication of the hypothesis. The following sections we examine the hypothesis that is being tested by K&J, the data used for that test, and the inferences that can be drawn from those test results.

Elapsed Time Criteria

For the most part, K&J are testing the hypothesis that elapsed times of 30 and 100 years are good discriminants for ranking seismic potential. In other words, does the temporal duration of a gap have any value in anticipating a future event in that region? K&J state (p. 21425) this hypothesis (H_1) in terms of probability, P, as

$$P_{Red} > P_{Orange} > P_{Green} \qquad \text{(eqn. 1)}$$

Where red, orange, and green refer to the three categories of potential based on the 30 and 100 year elapsed times (i.e., red:$T_{elapsed} \geq 100$ years, orange: $30 \leq T_{elapsed} < 100$ years, and green: $T_{elapsed} < 30$ years) . This hypothesis can also be written as

$$P_{(E \mid T_{elapsed} \geq 100)} > P_{(E \mid 30 \leq T_{elapsed} < 100)} > P_{(E \mid T_{elapsed} < 30)} \qquad \text{(eqn. 2)}$$

or the probability for an earthquake (E) is conditional on the amount of time elapsed, $T_{elapsed}$, since the last earthquake in a particular gap The null hypothesis (H_O) is that all 3 categories have the same likelihood or probability (i.e., $P_{Red}=P_{Orange}=P_{Green}$).

Earthquakes Chosen For Analysis

In addition to the elapsed-time component discussed above, the seismic gap hypothesis of MNSK specifically addresses the types of earthquakes to be considered (p. 1086-87). These criteria identify shallow(<40 km), large (M>7) earthquakes along simple plate boundaries (convergent or transform). The catalog of 56 events of M_S or $M_W \geq 7.0$ from January 1973 to April 1988 that K&J have presented for testing (their Table 1) contains a number of events that were explicitly excluded by MNSK in their list of 12 assumptions and limitations. Data selection based on hypocentral or focal mechanism information does not negate the the worth of the seismic gap hypothesis, as K&J have stated (p. 21422), but rather serves to identify exactly what earthquakes should be included in the hypothesis test. Neither KSO or MNSK proposed a generic model for earthquake occurrence. By appealing to objectivity, K&J have allowed *all*

earthquakes with M≥7 to be considered in their hypothesis test. This has significantly changed the hypothesis to be tested from one that addresses a specific set of interplate earthquakes to one that addresses *all* earthquakes above a certain magnitude threshold, regardless of location and mechanism.

Location Criteria

In the name of objectivity, K&J have also introduced a considerable amount of noise into their test by using only the largest-scale (about 1:70,000,000) summary map in MNSK without verifying their assessments of location and seismic potential using the numerous regional maps in MNSK. This noise only affects K&J's portrayal or application of the gap hypothesis, and not the actual hypothesis itself. K&J attempt to use that map and two similar ones by KSO to locate earthquake rupture zones for events as small as magnitude 7.0 with respect to the designated classes of seismic potential as defined by KSO and MNSK. The length along strike of the rupture zone of an earthquake of M_S or M_W 7.0 is about 40 km. Locating it on the colored map of MNSK with an accuracy of half that dimension, 20 km, or better requires making measurements on the colored map to 0.3 mm or better.

KSO [1973] recognized *the dangers in interpreting these maps literally* and warned their readers not to use the least detailed (large scale) maps (their Figs. 1 and 2) in their paper for more than an overview, but rather to use the appropriate detailed figures in the paper for each region. This warning was ignored by K&J. For example K&J incorrectly assess the 1979 Colombia (M_W 8.2) earthquake as being half in an orange and half in a green area. Had they consulted the more detailed maps of South America in KSO and MNSK, it would have been evident that the 1979 great earthquake, in fact, fell in the remaining portion of the rupture zone of the 1906 Colombia-Ecuador M_W 8.8 earthquake that had not reruptured in the 1942 (M_S 7.9) and 1958 (M_S 7.8) shocks. Aftershocks of the 1979 shock nearly filled that remaining gap, and rupture in 1979 progressed from its epicenter at the southwestern end of the gap to the northeast [Kanamori and McNally, 1982]. Kanamori and McNally [1982] also modelled the Rayleigh wave spectra to obtain the rupture dimension along strike for the 1979 earthquake; Beck and Ruff [1984] modeled seismic moment release, and Herd et al. [1981] describe uplift along the coast.

The selection criteria specified that intraplate events were to be excluded from consideration. Yet K&J included events which involved strike-slip motion along the north side of the Aleutian arc (#9), well to the north of the plate boundary, and intraplate reverse faulting near the axis of the Peru-Chile trench (#28), well to the west

of the plate boundary. Several of the smaller events in their table involved a predominance of either high-angle reverse faulting or strike-slip faulting in zones that had previously ruptured in much larger interplate thrust events. The most glaring error is the assignment of a potential category to the major Costa Rican earthquake of April 22, 1991 (Table 4 of K&J), which did not occur along the Cocos-Caribbean plate boundary, but on a different tectonic feature, the North Panama fold and thrust belt, a region never discussed by either KSO or MNSK. As a further example of the oversimplified use of these large scale maps, the Taiwan and New Britain regions were portrayed with a two-color code (red and orange) to schematically indicate that the region is extremely active for large shocks with repeat times of generally less than 30 years (MNSK p. 1137). Yet K&J disregarded this description and have literally included each bar in these schematically coded areas in their indexing and hypothesis testing.

Magnitude Criteria

K&J state that the seismic gap concept is often interpreted to apply only to "plate boundary rupturing" or "gap-filling" events, which may be larger in some zones than in others. They go on to state that neither KSO nor MNSK define clearly what would qualify as such an event for each plate boundary segment. K&J, however, then test the end member concept that is farthest in its definition from being a gap-filling earthquake, i.e. the occurrence of *any* event of $M_S \geq 7.0$ in one of the three zones of seismic potential defined by MNSK (i.e., those zones colored red, orange, and green). K&J are correct that KSO and MNSK did not explicitly state what size or magnitude event would constitute a success or failure of the hypothesis for each zone. However, KSO and MNSK were well aware, and stated (KSO, p. 2547; MNSK, p.1094) that the maximum size of plate-rupturing events differs considerably both along and among active plate boundaries. They and previous workers on seismic gaps noted that for some plate boundaries the largest ruptures in the past have been truly great earthquakes, (i.e., $M_W > 9$) while other plate boundaries have experienced only events in the $7 \leq M_W \leq 8$ range. The choice of M 7 as a threshold in 1979 was motivated, in part, by the recognition that the error in mapping aftershock zones was comparable in size to the rupture zone of an event near magnitude 7.

A careful reading on MNSK indicates that they did convey a qualitative sense of what size event would constitute a success or failure of their assignments of seismic potential. For example, in their Figure 8 MNSK regarded the 1971 Chilean earthquake of M_W 7.8 as filling the northern third of the gap which last ruptured in the great (M_W 8.5) Chilean shock of 1906. They designated the remainder of the 1906 Chilean

rupture zone as a region of the next to highest potential (orange color) and the 1971 rupture zone as having a low potential (green color). Both KSO and MNSK regarded the 1942 (M_S 7.9) and 1958 (M_S 7.8) shocks as partially filling (about 40%) of the rupture zone of the great (M_W 8.8) Colombia-Ecuador earthquake of 1906. Likewise, they also designated the remainder of the 1906 zone as having a high potential (orange). That remaining segment ruptured in 1979, several months after the publication of MNSK, in an event of M_S 7.7. Thus, a fairly typical pattern of several fault segments along an active plate boundary breaking in a single great event followed a cycle later by those segments rupturing in individual large to great earthquakes was clearly recognized by KSO and MNSK. Hence, they regarded an earthquake as either gap filling or partially gap filling if its rupture length was approximately 25% or more of the length of the rupture zone of the previous great event and if it was large enough to break the entire downdip width of the plate interface that is capable of rupturing seismically.

MNSK also state in their criteria that "*large shocks are assumed to rupture the plate boundary from 0 to 40 km in depth*" (P. 1087, #8), and that a "*common assumption often made in in analysis of seismic gaps is that large shocks rupture the entire plate boundary in depth*" (p. 1085). Scholz [1990], Pacheco et al.[1992], and Pacheco and Sykes [1992] classified earthquakes as being either large or small by whether or not they rupture the entire downdip width of the seismogenic zone (that area of major faults that is capable of nucleating earthquakes). As illustrated in Fig. 1, small earthquakes have no bounds in length along strike, L, or downdip width, W. Large earthquakes have no limits in L but their downdip width is bounded by the extent of brittle material, that is, from the earth's surface to the onset of ductile deformation at depth. Pacheco and Sykes [1992] assembled a new catalogue of worldwide shallow (depth < 70 km) earthquakes of $M_S \geq 7.0$. They and Pacheco et al. [1992] examined the slope (b value) of the frequency-magnitude relationship for sub-sets of that catalogue. They concluded that the b value changes from about 1.0 to 1.5 for interplate thrust events at subduction zones at M_S 7.5 and in a similar way for earthquakes along transform faults at a much smaller magnitude, M_S 5.9. They propose that the change in slope marks the transition from small to large earthquakes. The transition occurs at a larger magnitude for shallow thrust events at subduction zones since W is much greater there (50 to 200 km) than it is for nearly vertical transform faults where W is about 10 km. Most of the events examined by K&J (their Table 1) occurred in the vicinity of subduction zones. Thus, the transition from small to large rupture should occur for most of their events near M_S 7.5.

Revised Hypothesis Test

Application of the selection criteria of MNSK to Table 1 of K&J significantly reduces the number of events (to 52% of the original catalog for the period 1973 to 1988, and to 45% of the original catalog for the period 1979 to 1988) we consider eligible for testing the seismic gap hypothesis as originally stated in 1979 . Our revised catalog is presented in Table 1. The ineligible events (and the reasons for our rejection) are listed in Table 2. Even then, roughly half of the remaining earthquakes in Table 1 are events with magnitudes M_S<7.5. It is likely that most, and perhaps all, of the events smaller than M_S 7.5 did not break the entire downdip width of the plate interface, a fundamental assumption about events that KSO and MNSK considered to be gap-filling or partly-gap filling earthquakes. Thus, K&J's analysis is biased towards small earthquakes whereas most papers on seismic gaps and zones of seismic potential have focused on larger events. Accordingly, we have subdivided Table 1 into events with M_S <7.5 and $M_S \geq 7.5$. Of course, the delineation of a change in b value and the naming of events in this way as either small or large postdates the publication of KSO and MNSK. Nevertheless, we believe that the context of those two papers is clearly that of events that rupture the entire downdip width of the seismogenic zone and not that of smaller events that do not.

K&J test the differences between all earthquakes of $M_S \geq 7$ in the Red and Green and the Red and Orange categories of earthquake potential (i.e., $P_{Red} > P_{Green}$ and $P_{Red} > P_{Orange}$), and assert that seismic activity in the Green and Orange zones is indistinguishable (i.e., $P_{Orange} = P_{Green}$). Using the revised catalog in Table 1, we first test those eligible earthquakes with $M_S \geq 7.5$. In Table 1.I there are 1 Red, 8 Orange, and 6 Green earthquakes for the interval 1973 to 1988. For the shorter time interval, 1979 to 1988, there are no Red events, 4 Orange, and 3 Green earthquakes. This latter score differs from the K&J score of 1 Red, 2.5 Orange, and 5.5 Green earthquakes for this same time interval (1979-1988) and illustrates the effects of the selection criteria previously discussed. Inspection of Table 1.I indicates that during the last 16 years there have clearly been more Orange than Red earthquakes, confirming the initial observation that was made over a decade ago by Nishenko and McCann [1981]. For both time intervals, 1973-1988 and 1979-1988, we find that there are similar numbers of Orange and Green earthquakes. Hence, for earthquakes with $M_S \geq 7.5$, the difference between the Orange and Green or Red + Orange and Green categories is not significant enough to warrant rejection of the null hypothesis ($P_{Orange}=P_{Green}$).

Examination of earthquakes between M_S 7.0 and 7.5 (Table 1.II) during the same intervals 1973-1988 and 1979-1988, indicates that there were no Red, 6 Orange, and 9 Green; and no Red, 6 Orange, and 5 Green events, respectively. Again, there is no significant difference between the Orange and Green categories. Not surprisingly, combining Tables 1.I and 1.II for all eligible earthquakes of $M_S \geq 7.0$ yields the same conclusion.

Both K&J and the preceding discussion have tested specific applications of the gap concept by KSO and MNSK and shown that there is no significant difference between the Orange and Green categories of seismic potential as defined in 1979. In many cases, information for specific plate-boundary segments is sparse; hence uncertainties in those estimates are also large and should be subject to modification as more information becomes available. Inspection of Table 1 in K&J indicates that some of the "failures" of the gap hypothesis (as stated in 1979) occurred in areas with relatively poorly defined segmentation and rupture histories. For example, events in 1977 (M_S 7.6, not listed in K&J), 1979 (#19) and 1984 (#36) all occurred in the vicinity of the 1966 M_S 7.7 Solomon Islands earthquake.. While this entire region had been colored green by MNSK, analysis by Wesnousky et al. (1986) indicates that these subsequent events ruptured adjacent, non-overlapping segments of the plate boundary which had probably not ruptured in large or great earthquakes since the 1920's and 30's (Nishenko, 1991). Similarly, the 1980 M_S 7.7 Santa Cruz Islands (#23) earthquake was judged by Tajima et al. (1990) to represent the rupture of an asperity that acted as a barrier to the 1966 M_S 7.9 earthquake, even though the 1-day aftershock zone suggests rupture propagation into the 1966 zone. These examples represent improvements in the resolution and definition of earthquake rupture zones in this region. Application of the same methodology in light of these post-MNSK studies would result in different scores for the same $M_S \geq 7.5$ earthquakes in Table 1.I (i.e., 11 Orange and 3 Green events during the interval 1973-1988). These revised scores would be significant to reject the null hypothesis at the 0.02 significance level. The above example illustrates the dramatic effect that just 4 earthquakes have on the test results. Given the small number of earthquakes that have occurred in the 16 year interval 1973 to 1988, the hypothesis test does not yet have enough power to distinguish between alternative models.

Conclusions and Discussion

Both K&J and this study have examined the seismic gap hypothesis, as proposed by KSO and MNSK, and have come to significantly different conclusions. The

conceptual differences between our two studies is summarized by the magnitude-time matrix shown in Figure 2. KSO, MNSK and K&J have examined the utility of using elapsed time, $T_{elapsed}$, as the sole criteria for characterizing seismic potential. By virtue of the magnitude threshold and data selected to evaluate the gap hypothesis, K&J have altered the hypothesis from one that applies this criteria to a specific group of earthquakes to one that includes *any* event equal to or larger than M_S 7. In contrast, KSO and MNSK addressed the largest events that were associated with a particular simple plate boundary. These two hypotheses occupy different positions in Figure 2. K&J contend that the rejection of their version of the gap hypothesis implies that a clustering model of earthquake occurrence is a better model than one based on quasi-periodic earthquake recurrence. The elapsed time component of the seismic gap hypothesis, however, does not explicitly include any statement about recurrence time, T_{ave}, which occupies a different column in Figure 2. Hence, we fail to see how rejection of one element by K&J supports their conclusion about another element in Figure 2. Our examination of the revised seismicity catalog indicates that elapsed time alone is not a powerful criteria for characterizing seismic potential in a system characterized by an order of magnitude or larger variation in recurrence time.

The seismic gap and seismic potential hypotheses, put forth in 1973 and 1979, were intended to be working hypotheses that would be tested, modified, or discarded if necessary. Following the publication of MNSK and Nishenko and McCann (1981), we have gone on to include, what we believe, are refinements that improve long-term forecasts, by including information about the rates of plate motion, average repeat time, and estimates of earthquake size in a probabilistic manner for specific segments of relatively simple, major plate boundaries. While the criticisms of K&J focus upon papers published 13 and 19 years ago, it is clear from their article that they have fundamental disagreements with work published since then by Lindh [1983], Sykes and Nishenko [1984], Nishenko and Jacob [1990] and the Working Group on California Earthquake Probabilities [1988, 1990] that utilize information on repeat times of large characteristic earthquakes for segments of very active faults to calculate probabilities of rupture during the next one to a few decades. These more recent forecasts belong to a different matrix element in Figure 2, and the results from the tests discused here have little bearing on these other elements. An evaluation of the methodology used in these more recent models will be published in the near future (Nishenko and Perkins, manuscript in preparation, 1992).

In hindsight, some of the "failures" of the seismic gap hypothesis could have been avoided given better definition of earthquake rupture zones (e.g. the 1966, 1977, 1979,

and 1984 Solomon Islands events) at the time the potential estimates were formulated and published. In other areas, clear examples of failures do exist. These include cases where the repeat time was less than 30 years (the 1986 M_W 8.0 Central Aleutians event [#50] occurred in the vicinity of the epicenter of the great 1957 M_W 8.6 earthquake, as did the 1975 M_W 7.6 Southern Chile event (#10) which occurred near the epicenter of the giant M_W 9.5 1960 earthquake), and zones with complex modes of rupture, whereby shallow portions of the plate interface have ruptured independently of deeper portions (e.g., 1978 M_W 7.5 Kurile [#13] event ruptured the area updip of the 1958 M_W 8.4 earthquake, and perhaps the 1985 M_W 7.5 Michoacan aftershock [#45] which ruptured updip of the 1979 M_W 7.5 Petatlan event [UNAM, 1986]).

Both K&J and this comment have demonstrated the necessity for the clear definition of the seismic gap (or any) hypothesis to avoid later misinterpretation and misunderstanding. Definitions of what constitutes an earthquake prediction require a specification of magnitude, location, and time interval (e.g., Wallace et al., 1984). Explicit definitions of expected location or plate boundary segmentation, expected recurrence time, magnitude, and mechanism (and their associated uncertainties) also need to be established for probabilistic earthquake forecasts. In other words, future forecasts need to anticipate the type of statistical testing that K&J have attempted with the KSO and MNSK models. Recent forecasts by the Working Group on California Earthquake Probabilities [1988, 1990] and Nishenko and Jacob (1991) for the Queen Charlotte-Alaska-Aleutian seismic zone fulfill many of these requirements.

Both the Working Group (1990) and Savage (1991) constructed hypothesis tests of the forecast estimates for the 1989 Loma Prieta, California earthquake using previously published recurrence time estimates and their uncertainties. For forecasts involving many seismic zones, such as the entire circum-Pacific region, some specification of the time period the forecast addresses should be included with the individual forecast parameters. This verification interval may or may not be coincident with the exposure windows commonly stated for conditional probability estimates (e.g. a 0.67 probability in the next 30 years) K&J used 16 years of data to test the gap hypothesis and admit that the sample sizes were too small in the critical cases to reach any significant conclusions. Both KSO and MNSK recognized that long time intervals, on the order of decades, would be needed to properly test the seismic gap hypothesis. During the time interval under discussion, there have been no events with $M_W > 8.2$ in the areas under consideration. In fact, the last 20 years have been one of relatively low overall seismic moment release (see Figure 3). None of the interplate events that have occurred are even remotely comparable in size to the truly great events of 1952, 1957,

1960, 1964, and 1965. The record of generally higher moment release during the last 90 years indicates, however, that the period of low moment release during the last 20 years is unlikely to continue in the decades ahead. We expect that truly great earthquakes will occur again and that the sites of past events of that type that have not ruptured in that way for more than a century are likely locations for these future events.

While there has always been an awareness of "clustering" associated with the occurrence of major and great earthquakes, the gap hypothesis intentionally focused on other aspects of earthquake occurrence along simple plate boundaries. In many cases, large shocks following great earthquakes represent new breakage in areas adjacent to, but different from, the zones that broke in the preceding mainshock. In some cases, closely spaced events in space and time represent progressions of activity along plate boundaries . Clear examples include the 1957, 1964, and 1965 sequence along the Alaska- Aleutian plate boundary, where 2400 km of plate boundary broke within 9 years, a small fraction of the time between similar sized events along any particular segment. Likewise, several segments of the North Anatolian fault ruptured in a relatively short amount of time, 1939-1943 [Richter, 1958]. Fedotov [1965], Mogi [1969], Varnes [1989], and Sykes and Jaume [1990] report increases in seismicity in advance of a number of large and great earthquakes. Ultimately, a physical model that takes into account contributions from both large and small, interplate and intraplate seismicity throughout the entire seismic cycle along plate boundaries is necessary to better describe seismic hazards along simple plate boundaries.

ACKNOWLEDGEMENTS

We thank Drs. J. Beavan, J. Dewey, R. Masse, D. Perkins, and C. Scholz for stimulating discussion and for critically reviewing this manuscript. This work was supported by the U.S. Geological Survey (Nishenko) and NSF grant EAR-91044158 (Sykes). Lamont-Doherty Geological Observatory Contribution 0000000.

REFERENCES

Beck, S.L. and L.J. Ruff, The rupture process of the great 1979 Colombia earthquake: evidence for the asperity model, *J. Geophys. Res., 89*, 9281-9291.

Fedotov, S.A., Regularities of the distribution of strong earthquakes in Kamchatka, the Kurile Islands and northeastern Japan (in Russian), *Tr. Inst. Fiz. Zemli Akad. Nauk SSSR, 36,* 66, 1965.

Gilbert, G.K., Earthquake forecasts, *Science, 29,* 121-138, 1909

Herd, D. G., T.L. Youd, H. Meyer, J. L. Arango, W.J. Person and C. Mendoza, The great Tumaco, Colombia earthquake of 12 December 1979, *Science, 211,* 441-445, 1981.

Kagan, Y.Y. and D.D. Jackson, Seismic gap hypothesis: Ten years after, *J. Geophys. Res., 96,* 21,419-21,431, 1991.

Kanamori, H. and K.C. McNally, Variable rupture mode of the subduction zone along the Ecuador-Colombia coast, *Bull. Seismol. Soc. Am., 72,* 1241-1253, 1982.

Kelleher, J., L.R. Sykes and J. Oliver, Possible criteria for predicting earthquake locations and their application to major plate boundaries of the Pacific and the Caribbean, *J. Geophys. Res., 78,* 2547-2585, 1973.

Lindh, A.G., Preliminary assessment of long-term probabilities for large earthquakes along selected fault segments of the San Andreas fault system in California, *U.S. Geol. Surv., Open File Rep.,* 83-63, 1-15, 1983.

McCann, W.R., S.P. Nishenko, L.R. Sykes and J. Krause, Seismic gaps and plate tectonics: Seismic potential for major boundaries, *Pageoph, 117,* 1082-1147, 1979.

Mogi, K., Some features of recent seismic activity in and near Japan, 2, Activity before and after great earthquakes, *Bull. Earthquake Res. Inst. Tokyo Univ., 47*, 395, 1969.

Nishenko, S.P., Seismic potential for large and great interplate earthquakes along the Chilean and southern Peruvian margins of South America: A quantitative reappraisal, *J. Geophys. Res., 90*, 3589-3615. 1985.

Nishenko, S.P. and K.H. Jacob, Seismic potential of the Queen Charlotte-Alaska-Aleutian seismic zone, *J. Geophys. Res., 95*, 2511-2532, 1990.

Nishenko, S.P. and W.R. McCann, 1981, Seismic potential for the worlds major plate boundaries: 1981, in, D.W. Simpson and P.G. Richards, eds., Earthquake Prediction, An International Review, Maurice Ewing Series 4, p. 20- 28, American Geophysical Union, Wash., D.C.

Pacheco, J.F. and L.R. Sykes, Seismic moment catalog of large, shallow earthquakes, 1900 to 1989, *Bull. Seismol. Soc. Am., 82*, 1306-1349, 1992.

Pacheco, J.F., C.H. Scholz and L.R. Sykes, Changes in frequency-size relationship from small to large earthquakes, *Nature, 355*, 71-73, 1992.

Richter, C.F., Elementary Seismology, W.H. Freeman and CO., San Fransisco, 768 pp., 1958.

Savage, J.C., Criticism of some forecasts of the National Earthquake Prediction Evaluation Council, *Bull. Seismol. Soc. Am., 81*, 862-881, 1991.

Scholz, C., The Mechanics of Earthquakes and Faulting, *Cambridge University Press, New York*, 439 p., 1990.

Sykes, L.R., Aftershock zones of great earthquakes, seismicity gaps, and earthquake prediction for Alaska and the Aleutians, *J. Geophys. Res., 76*, 8021- 8041, 1971.

Sykes, L.R. and S. Jaum'e, Seismic activity on neighboring faults as a long-term precursor to large earthquakes in the San Francisco Bay area, *Nature, 348*, 595-599, 1990.

Sykes, L.R. and S.P. Nishenko, Probabilities of occurrence of large plate rupturing earthquakes for the San Andreas, San Jacinto, and Imperial Faults, California, 1983-2003, *J. Geophys. Res., 89*, 5905-5927, 1984.

Tajima, , F., L.J. Ruff, H. Kanamori, J. Zhang, and K. Mogi, Earthquake processes and subduction regime in the Santa Cruz Islands region, *Phys. Earth Planet. Inter., 61*, 269-290, 1990.

UNAM Seismology Group, The September 1985 Michoacan earthquakes: aftershock distribution and history of rupture, *Geophysical Research Letters, 13*, 573-576, 1986.

Varnes, D., Predicting earthquakes by analyzing accelerating precursory seismic activity, *Pageoph, 130*, 661-686, 1989.

Wallace, R.E., J.F. Davis, and K.C. McNally, Terms for expressing earthquake potential, prediction, and probability, *Bull. Seismol. Soc. Am., 74*, 1819-1825, 1984

Wesnousky, S., L. Astiz, and H. Kanamori, Earthquake multiplets in the southeastern Solomon Islands, *Phys. Earth Planet. Inter., 44*, 304-318, 1986.

Working Group on California Earthquake Probabilities, Probabilities of large earthquakes occurring in California on the San Andreas fault, *U.S. Geological Survey , Open File Report 88-398, 1-62,* 1988.

Working Group on California Earthquake Probabilities, Probabilities of large earthquakes in the San Francisco Bay region, California, *U.S. Geological Survey Circular, 1053, 1-51,* 1990.

FIGURE CAPTIONS

Figure 1. Two types of earthquakes; small and large. *L* is rupture length, along strike of the fault, *W*, is the down-dip width of rupture The transition between small and large earthquakes occurs at M_S 5.9 for transform faults and M_S 7.5 for subduction zones [from Pacheco, Scholz, and Sykes, 1992].

Figure 2 Magnitude-Time matrix. K&J - Kagan and Jackson [1991]; KSO - Kelleher, Sykes, and Oliver [1973] ; MNSK - McCann, Nishenko, Sykes, and Krause [1979]; N&J - Nishenko and Jacob [1991]; WGCEP - Working Group on California Earthquake Probabilities [1988, 1990]

Figure 3. Logarithm of seismic moment (M_O) in N-m as a function of time on a global basis from 1900 to 1989. The curve was smoothed with a three year running average. Note that the period 1973-1989 is one of relatively low overall seismic moment release in the circum-Pacific region [after Pacheco and Sykes, 1992]

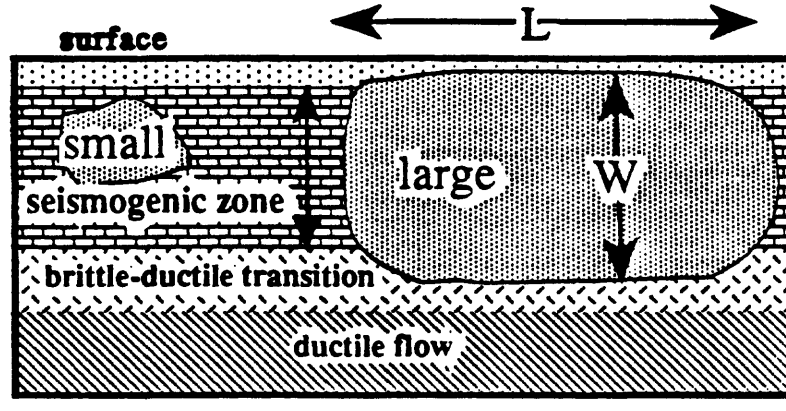
surface
L
small
seismogenic zone
large
W
brittle-ductile transition
ductile flow

FIGURE 1

	Telapsed	Telapsed/Tave
all M_S > 7.0	K&J	
"Characteristic" magnitudes	KSO MNSK	WGCEP N&J

Magnitude-Time Matrix

Figure 2.

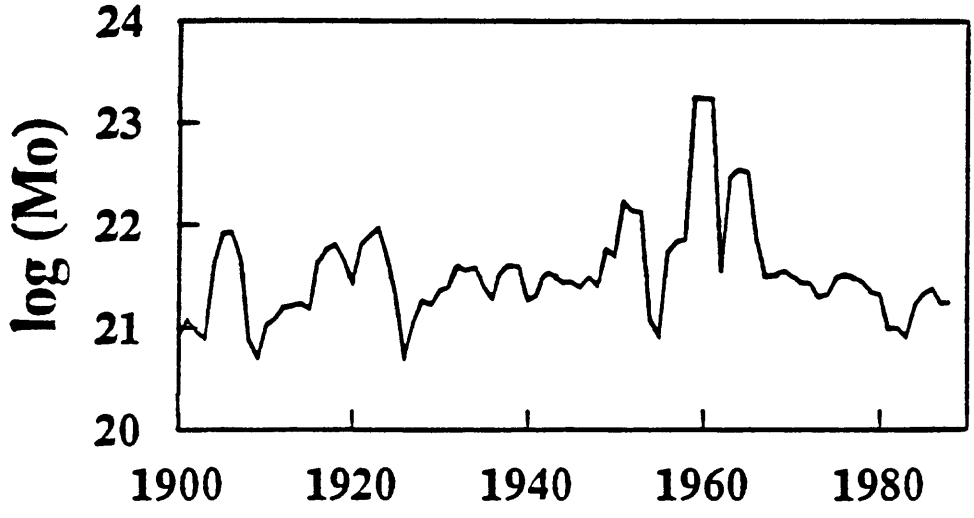
log (Mo)
24
23
22
21
20
1900
1920
1940
1960
1980

TABLE 1
ELIGIBLE EARTHQUAKES
I. Earthquakes with $M_S \geq 7.5$

K&J #	DATE	M_S [1]	M_W [2]	K&J [3]	N&S [4]
1	1/30/73	7.5	7.6	(R)	[O]
3	6/17/73	7.7	7.8	(G)	[O]
6	10/3/74	7.6	7.9-8.0	(R)	[R]
10	5/10/75	7.7	7.6	(G)	[G]
*	4/21/77		7.5		[G]
13	3/24/78	7.6	7.5	(G)	[G]
14	6/12/78	7.7	7.6	(R)	[O]
16	11/29/78	7.7	7.5-7.7	(G/R)	[O]
18	3/14/79	7.6	7.5	G/R, G	O
20	12/12/79	7.7	8.1-8.2	R, G/O	O
23	7/17/80	7.9	7.7-7.8	-, G	G
36	2/7/84	7.5	7.5-7.6	-, G	G
40	3/3/85	7.8	7.6-8.0	R, O	O
44	9/19/85	8.1	7.9-8.1	R, O	O
50	5/7/86	7.7	7.9-8.0	G, G	G

TABLE 1 (con't)
ELIGIBLE EARTHQUAKES
II. Earthquakes with $7.0 \leq M_S < 7.5$

K&J #	DATE	M_S[1]	M_W[2]	K&J[3]	N&S[4]
2	2/28/73	7.2	7.0	(G)	[G]
5	8/18/74	7.1	---	(G)	[G]
11	1/21/76 †	7.0	7.0	(G)	[G]
15	8/23/78	7.0	---	(G)	G
17	2/28/79	7.1	7.3-7.5	R,-	O
19	10/23/79	7.1	---	-, G	O
21	2/23/80	7.0	---	G, G	G
25	1/30/81	7.0	7.0	G, G	G
29	10/25/81	7.3	7.2-7.3	R,O	O
30	12/26/81	7.1	7.0	-, G	G
32	6/7/82	7.0	---	G,G	O
33	8/5/82	7.1	---	-, G	G
34	4/3/83	7.3	7.4	G, O	O
35	10/4/83	7.3	7.6	G, O	O
43	7/3/85	7.2	7.2	-, O	G

NOTES:

1. M_S values from K&J, Table 1.
2. M_W values computed from seismic moments in Pacheco and Sykes [1992]. No entry indicates that either the revised M_S or M_W value is below 7.0.
3. Seismic potential assignments by K&J. Pre-1979 potential assignments attributed to KSO are either high (R) or low (G) and shown in parentheses. Post-1979 evaluations are attributed to both KSO (if available) and MNSK, respectively. The three stage classification of MNSK is based on the time elapsed, $T_{elapsed}$, since the last large earthquake - R ($T_{elapsed} \geq 100$ years), O ($30 \leq T_{elapsed} < 100$ years), and G ($T_{elapsed} < 30$ years).
4. Seismic potential assignments by this study using only the 3 stage classification of MNSK. Pre-1979 evaluations indicated by brackets. All seismic potential evaluations were updated as of the time of the earthquakes listed above.

ADDITIONAL NOTES:

* Not listed in K&J, Table 1
†. Unknown focal mechanism

TABLE 2
INELIGIBLE EARTHQUAKES
Earthquakes not suitable for hypothesis testing according to selection criteria of McCann et al. [1979]

K&J #	DATE	M_S[1]	M_W[2]	NOTES
4	6/24/73	7.1	7.3	1
7	10/8/74	7.5	6.9	2
8	11/9/74	7.2	7.0	1
9	2/2/75	7.6	7.1	2
12	3/23/78	7.5	7.5	1
22	7/8/80	7.5	7.5	1
24	10/25/80	7.2	7.5	3
26	7/6/81	7.0	7.5	2
27	7/15/81	7.0	7.1	2
28	10/16/81	7.2	7.1	2
31	1/11/82	7.1	7.1	3
37	3/24/84	7.0	7.1	3
38	11/17/84	7.2	7.1	3
39	12/28/84	7.0	6.7	2
41	4/9/85	7.2	7.1-7.2	1
42	5/10/85	7.1	7.2	2
45	9/21/85	7.6	7.3-7.7	1
46	11/28/85	7.0	6.9	2
47	11/28/85	7.1	7.0	2
48	12/21/85	7.3	7.1	2
49	4/30/86	7.0	6.9	1
51	11/14/86	7.8	7.3	4
52	2/8/87	7.4	7.1-7.3	2
53	3/5/87	7.3	7.5	5
54	10/16/87	7.4	7.3	3
55	2/24/88	7.0	7.2	3
56	4/12/88	7.0	7.1	3

1. M_S values from K&J, Table 1.
2. M_W values computed from seismic moments in Pacheco and Sykes [1992].

REASONS FOR REJECTION:

1. Foreshock or aftershock
2. Intraplate, strike slip, or normal faulting mechanism
3. High-angle reverse faulting
4. Multibranched zone of deformation
5. Occurred in zone with incomplete historic record

Recurrence History of Great Subduction Zone Earthquakes along the Sagami and Suruga-Nankai Troughs, Japan, and its Tectonic Implication

Katsuhiko ISHIBASHI

International Institute of Seismology and Earthquake Engineering
1 Tatehara, Tsukuba, 305 Japan

Abstract:— The Sagami and Suruga-Nankai troughs south off central and southwest Japan are the northernmost subduction boundary of the Philippine Sea plate. I summarize the recurrence history of great subduction zone earthquakes along these troughs based on the latest studies and discuss significant tectonic factors affecting it.

I conclude that along the northwestern part of the Sagami trough the recurrence pattern is simple in that great Kanto earthquakes repeat every 200 - 300 years releasing almost all crustal strains accumulated by the relative plate motion with the rate of 3 - 4 cm/y (i.e., seismic coupling ~ 100 %). The latest and the second latest events occurred in 1923 and 1703. The 1293 and the 878 disastrous earthquakes are strongly suspected to be older examples. Furthermore, we cannot deny the possibility that unknown Kanto earthquakes took place in the 15th and 11th centuries.

The southeastern part of the Sagami trough may be aseismic due to the nearness to the triple junction and a presumable plate mechanical boundary developed near the east coast of the Kanto district. The 1605 earthquake is doubtful and the 1953 earthquake was not a subduction zone event but a tear faulting within the subducted Pacific slab.

The space-time distribution of great Tokai and Nankai earthquakes along the Suruga-Nankai trough has turned out more regular than before by the progress of historical seismology. The regularity suggests that here also the recurrence pattern is basically as simple as that along the Sagami trough. However, I infer that the Suruga-Nankai trough is not a simple subduction boundary because of the eastward movement of southwest Japan as a part of microplate and that the relative plate motion is accommodated partly by inland active faults together with the trough. In particular, the Median Tectonic Line, an interarc transcurrent fault, seems important. An irregularity in the recurrence of the Tokai and Nankai earthquakes demonstrated by the 1605 great tsunami earthquake was probably caused by the 1586 inland great earthquake and the 1596 rupture of the Median Tectonic Line.

STRONG GROUND MOTION PREDICTION FOR CASCADIA SUBDUCTION EARTHQUAKES

Paul Somerville
Woodward-Clyde Consultants, 566 El Dorado Street, Pasadena, CA 91101

Subduction Earthquakes. The shallow dip and near-shore location of the potentially seismogenic plate interface of the Cascadia subduction zone make it geometrically analogous to the Sagami trough near Tokyo, the Nankai and Hyuganada troughs in southwest Japan, and subduction zones in North, Central and South America. The magnitude 8 Michoacan, Mexico and Valparaiso, Chile earthquakes in 1985 provided strong motion recordings close to large subduction earthquakes that are very relevant to the prediction of strong ground motion in the Cascadia subduction zone. These recordings were used to refine empirical strong motion attenuation relations, and to test seismologically-based ground motion models that were subsequently applied to the Cascadia subduction zone. The various ground motion prediction models are in reasonable agreement, suggesting that there is a fairly good basis for predicting strong ground motions from large subduction earthquakes, at least on rock and for frequencies above about 1 Hz. However, the ground motions from the recent Petrolia, California earthquake of April 25, which appears to be a subduction earthquake (the first known Cascadia subduction earthquake in historical time) are larger than those predicted by most attenuation relations. The ground motions from subduction earthquakes are expected to be somewhat larger than those for crustal earthquakes of the same magnitude and distance. Additional uncertainties in the prediction of strong ground motions on rock sites in the Puget Sound and Portland regions are due to uncertainties in the location and downdip extend of the seismogenic part of the plate interface, and in the distribution of slip as a function of depth on the plate interface.

Wadati-Benioff Earthquakes. The largest strong motion recordings in the Puget Sound region are from the magnitude 6 3/4 1949 and 1965 Olympia and Seattle earthquakes which both occurred in the Wadati-Benioff zone. These recordings have been used to check empirical strong motion attenuation relations and to test seismologically-based ground motion models. The recordings appear to have been strongly influenced by site response, and have larger motions at periods longer than 1 second than predicted by most models. The motions are expected to be significantly stronger than those for crustal earthquakes of the same magnitude and closest distance. The ground motions from magnitude 8 subduction earthquakes are expected to be about twice as large as those recorded during these two events at periods shorter than 1 second, and more than twice as large at longer periods.

Site Response. In recent years, information on the shallow velocity structure in the Portland and Puget Sound regions has been gathered for use in estimating site response, and recordings from explosions and earthquakes have been used to empirically estimate site amplification factors. These shallow velocity models and recorded data are probably relevant for estimating site response at high frequencies. Modeling studies have been done that take into account the focussing effects of topography on the contact between bedrock and sediments in the Puget Trough from motions arriving almost vertically from below. However, these studies have not considered the possible effects of trapping of waves in basin structures.

Basin Response. Both the Puget Sound and Portland regions are potentially subject to the effects of trapping of waves in basin structures. The Puget Trough has unconsolidated sediments as thick as 1,000 meters, and the Tualatin and Portland Basins have sedimentary rocks overlying the Columbia basalt at depths as much as 300 meters. The large velocity contrasts in these structures may be very effective in trapping seismic energy at periods of about one second and longer. These effects are expected to be important both for subduction earthquakes and for crustal earthquakes in which the motions enter the basins through their margins. For crustal earthquakes, there is evidence of basin response in the intensity pattern observed in the Puget Sound region from the 1981 Elk Lake earthquake. Subduction earthquakes have large spectral amplitudes at long periods, and the potential amplification of these large long period motions by basin response has important implications for the safety of structures such as bridges and highrise buildings. These effects are not included in conventional site response analyses using 1-D velocity models, because waves arriving from below cannot become trapped in such structures. Modeling of strong motion recordings from the 1971 San Fernando, 1987 Whittier Narrows, and 1989 Loma Prieta earthquakes using 2-D and 3-D velocity models indicates the importance of considering the role of laterally varying structure in amplifying strong ground motions.

Abrupt Uplift Within the Past 1700 Years at Southern Puget Sound, Washington

Robert C. Bucknam, Eileen Hemphill-Haley, Estella B. Leopold

Shorelines rose as much as 7 meters along southern Puget Sound and Hood Canal between 500 and 1700 years ago. Evidence for this uplift consists of elevated wave-cut shore platforms near Seattle and emerged, peat-covered tidal flats as much as 60 kilometers to the southwest. The uplift was too rapid for waves to leave intermediate shorelines on even the best preserved platform. The tidal flats also emerged abruptly; they changed into freshwater swamps and meadows without first becoming tidal marshes. Where uplift was greatest, it adjoined an inferred fault that crosses Puget Sound at Seattle and it probably accompanied reverse slip on that fault 1000 to 1100 years ago. The uplift and probable fault slip show that the crust of the North America plate contains potential sources of damaging earthquakes in the Puget Sound region.

Western Washington State has at least three dissimilar sources of earthquakes that could damage metropolitan areas near Puget Sound. The best documented of these sources, the interior of the subducted Juan de Fuca plate, has released several 20th-century earthquakes of magnitude (M) 6 or 7 from depths of 50 to 60 km beneath Puget Sound (*1*). A second source, the offshore part of the boundary between the Juan de Fuca and North America plates, lacks historical seismicity but may produce infrequent earthquakes as large as M = 8 or 9 (*2–4*). In this report we present evidence for a third source—historically quiescent faults within the North America plate. We propose that one or more large earthquakes on such faults account for uplift that occurred in the southern Puget Sound region between 500 and 1700 years ago. Accompanying reports present evidence that one of these earthquakes generated a tsunami (*5*) and may also account for landslides (*6*), rock avalanches (*7*), and turbidity currents (*8*) (Fig. 1).

The most conspicuous evidence for earthquake-induced uplift at Puget Sound is a raised wave-cut platform at Restoration Point (*9*), the easternmost part of a peninsula 5 km west of Seattle (Fig. 1). The raised platform extends discontinuously along the coast nearly 3 km to the northwest and 7 km to the west of the peninsula (*10*). The peninsula is fringed by the raised platform (Fig. 2), which is expressed as a seaward sloping, nearly planar bedrock surface as much as 7 m above high tide (*11*). Organic-rich sand 20 to 40 cm thick overlies much of the platform, which is cut on steeply dipping Tertiary siltstone and sandstone. Much thicker deposits of sand and gravel cover the platform 2.5 km northwest of Restoration Point; these deposits contain shallow-water marine mollusk shells in growth position (*12*).

The raised platform at Restoration Point, which resembles the adjacent modern platform at sea level, records about 7 m of uplift. Erosion at the seaward edge of the raised platform has produced a low bedrock scarp as much as 3 m high. High tide coincides approximately with the foot of the scarp. The corresponding part of the raised platform lies 7 m higher. Because the type of rock and exposure to waves are similar on the modern and raised platforms, we assume that the landward edge of the raised platform similarly formed at about the level of high tide, in which case the net uplift is 7 m (*13*).

The nearly planar form of the raised platform indicates that it was uplifted suddenly. Low linear ribs of the most resistant of the Tertiary beds can be traced from the modern platform onto and across the raised platform. Postuplift weathering has subdued these features on the raised platform, but

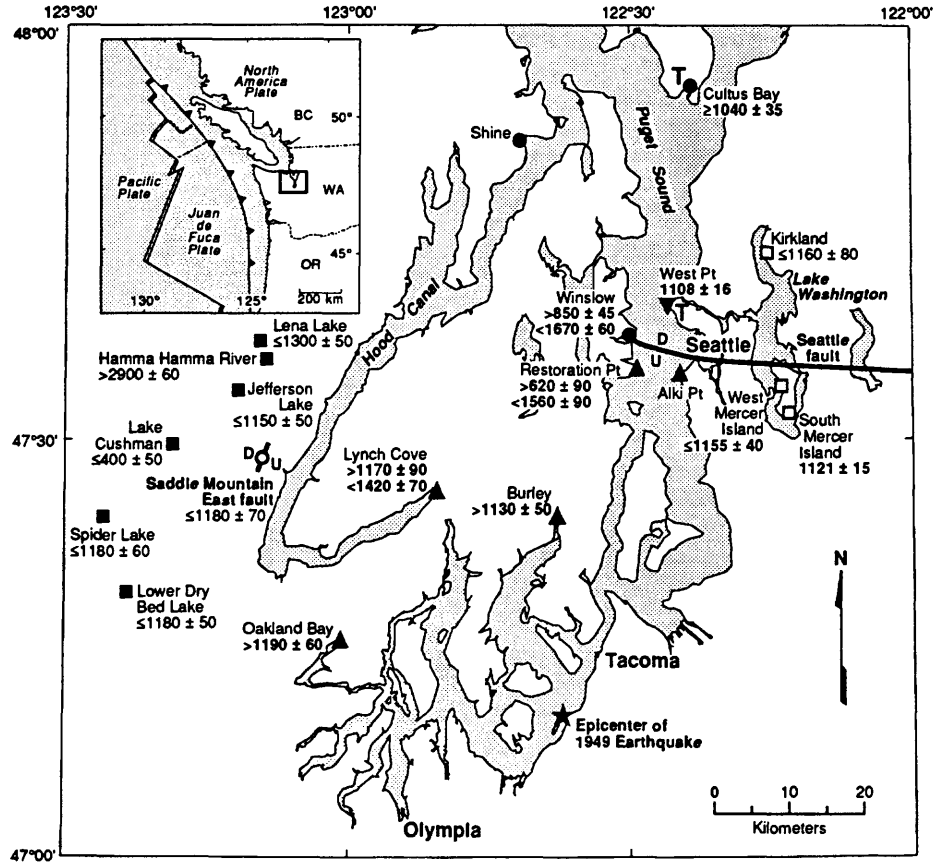

Fig. 1. Location and radiocarbon age of features bearing on seismic events in the Puget Sound region of Washington between 500 and 1700 years ago. Features: uplifted tidal flat or wave-cut marine platform (this paper) (▲); subsided tidal marsh or swamp (*5*) (▼); tidal-marsh deposit showing little or no abrupt change in level in past 2000 years (Cultus Bay, Winslow) (*5*) or in past 3000 years (Shine) (*26*) (●), probable tsunami deposit (*5*) (T); rock avalanche (*7*) (■); landslide (*6*) (□); ponds impounded along fault scarp (*6, 24*) (○). Radiocarbon ages in ^{14}C years before A.D. 1950, with 1 standard error quoted by laboratory; ages shown in boldface were adjusted for measured $^{13}C/^{12}C$ ratio. Age of feature relative to average age of dated material: identical within 10 years (no prefix); older (≥) or younger (≤) by as much as decades; older (>) or younger (<) by as much as centuries. Where multiple limiting ages are available, only the youngest limiting maximum or oldest limiting minimum ages are shown. Ages are not shown for landslides distinctly older than 900 to 1300 years at Lake Washington. Relative movement on fault: U, up; D, down.

R. C. Bucknam, U.S. Geological Survey, Mail Stop 966, Box 25046, Denver, CO 80225.
E. Hemphill-Haley, U.S. Geological Survey, Mail Stop 999, 345 Middlefield Road, Menlo Park, CA 94025
E. B. Leopold, Department of Botany, KB-15, University of Washington, Seattle, WA 98195.

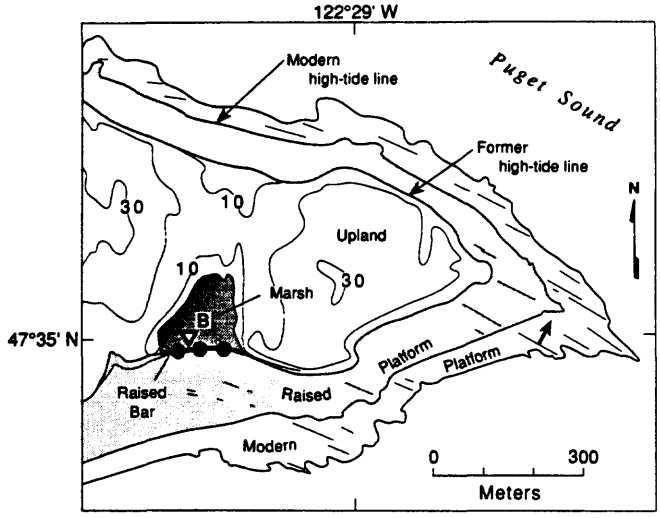

Fig. 2. Map of Restoration Point, showing relative elevation contours (in meters); datum is approximate mean sea level. Fine straight lines are bedrock ribs of resistant sedimentary rock that dip steeply in direction shown by arrow. Inverted triangle at B is location of the columnar section shown in Fig. 3B.

ribs with as little as 20 to 30 cm of relief are conspicuous. This preservation suggests that slow uplift would have left recognizable patterns of intermediate shoreline features on the uplifted surface, such as bars of beach gravel or small erosional scarps. In a careful search we found no such features, with one doubtful exception (*14*). This lack of intermediate shorelines is inconsistent with slow (aseismic) uplift, which would have taken at least a decade at the highest known aseismic uplift rates (*15*). Therefore, we suspect that the uplift accompanied an earthquake.

Radiocarbon ages show that the abrupt uplift occurred between 500 and 1700 years ago. A concentrate of humus from the basal 4 cm of the organic sand that overlies the bedrock of the raised platform gave a minimum time for the uplift of 500 to 800 years ago (620 ± 90 ^{14}C yr B.P.) [*16*, *17*]. Beach gravel and tidal flat mud, now 6 to 7 m above high tide, underlie a small marsh in the isthmus west of the peninsula (Fig. 2). Rounded fragments of detrital charcoal from the uplifted tidal flat mud (Fig. 3B) gave a maximum time for the uplift of 1300 to 1700 years ago (1560 ± 90 ^{14}C yr B.P.).

A marine platform also stands a few meters above high tide at Alki Point in Seattle, 5 km east of Restoration Point. Although that platform is mostly obscured by houses and roads, a recent excavation exposed a planar sand-covered bedrock surface 4 m above present high tide. Uplift of this surface was greater than 4 m because the landward edge of the platform was not exposed in the excavation.

Deposits at a small marsh at Winslow (Fig. 1), just 5 km north of Restoration Point, give evidence that the amount of vertical displacement was quite variable locally. The marsh at Winslow is underlain by peat that was deposited during the past several thousand years (Fig. 3A), that is, including the time of the uplift at Restoration Point. Diatom assemblages from mud directly beneath the peat indicate that the site was a freshwater bog or swamp 1600 to 2100 years ago. Peat about 30 cm higher in the section (1400 to 1700 years ago) contains diatoms characteristic of freshwater bogs or swamps but tolerant of slightly brackish water. The peat also contains a few fossil diatoms characteristic of brackish to marine environments. They presumably were blown or washed into the peat; thus, the site was near marine water and may have been only slightly above the level of the highest tides. Tidal marine water inundated the site more frequently by 700 to 900 years ago as shown by radiocarbon-dated leaf bases of *Triglochin maritimum*, a common plant of brackish and saltwater tidal marshes in Washington (*18*).

The deposits at the Winslow marsh lack clear-cut evidence of an abrupt change in relative sea level in the past 2000 years. If the Winslow marsh changed level at the time of the uplift at Restoration Point, it probably subsided as shown by the change from mostly freshwater wetland to tidal marsh. Such subsidence could have accompanied the uplift at Restoration Point, as inferred for a site 9 km to the northeast at West Point (*5*). Alternatively, the tidal marsh at Winslow could have originated from a gradual rise in relative sea level.

In any case, the lack of uplift at Winslow implies that the amount of vertical displacement was variable—at least 7 m over the 5 km between Restoration Point and Winslow. A similar difference exists to the east between Alki Point (uplift >4 m) and West Point [subsidence ≥ 1 m (*5*)]. Both Restoration Point and Alki Point are on the south side of the Seattle fault [Fig. 1; (*19*)], a major east-trending structure that has been inferred from depth-to-bedrock data (*10*), gravity anomalies (*12*), and seismic reflection profiles (*20*). The long-term sense of offset inferred on this fault is south side up. The coincidence of the pattern of vertical displacement in the marshes and terraces with the same sense of late Cenozoic displacement on a major fault nearby suggests that the uplift occurred in conjunction with slip on the Seattle fault. Because no surface rupture is apparent, fault slip at depth may have been accommodated by folding or warping at and near the surface.

Large uplift south of the Seattle fault and small subsidence north of the fault suggests that reverse slip occurred on a south-dipping fault, rather than normal slip on a north-dipping fault. For dipping normal faults, subsidence is large and uplift is small. The ratio of subsidence to uplift suggests that dip of the fault is less than about 70° (*21*).

Our radiocarbon ages only broadly limit the time of this fault slip and associated uplift to between 500 and 1700 years ago. A narrower range between 1000 and 1100 years ago is suggested by radiocarbon dating and tree-ring correlation of tsunami and landslide deposits near Seattle, provided that these deposits are coeval with the uplift (*5*).

There is also evidence for uplift between 1000 and 1500 years ago at the heads of three bays in southwest Puget Sound and Hood Canal, 30 to 55 km southwest of Restoration Point. The strongest case for uplift in these other areas comes from Lynch Cove, at the landward end of Hood Canal (Fig. 1). We also found evidence of uplift at Oakland Bay, 25 km southwest of Lynch Cove, and at Burley, 15 km southeast of Lynch Cove (Fig. 1).

Tidal flat sediment overlain by freshwater peat provides the evidence of abrupt uplift at Lynch Cove. Fossil diatoms (Fig. 3C) show that the sediment accumulated below high tide, on a tidal flat. By contrast, woody roots, diatoms, and seeds of plants characteristic of moist upland meadows and freshwater marshes show that the overlying peat formed above the highest tides. The sharp contact at the base of the peat and the lack of intervening salt-marsh deposits suggests that the change from tidal flat to upland meadows and marshes was abrupt (*22*). A rise in relative sea level subsequent to the uplift allowed high tides to submerge the upland meadows and marshes many centuries later, as shown by salt marsh peat that overlies the freshwater peat.

Relief of the former tidal flat beneath the peat shows that the uplift at Lynch Cove exceeded 2 m. The former tidal flat surface buried beneath the peat descends gently toward the central part of the cove. Before uplift, the highest point on the former tidal flat was below high tide, and after uplift the lowest point on that surface beneath the freshwater peat was above high

tide. The relief between these two points is at least 2 m.

The oldest age determined thus far for the lowermost several centimeters of the peat at Lynch Cove is 900 to 1300 years (1170 ± 90 ^{14}C yr B.P.), which is a minimum for the time of the uplift. Upland shrubs had become established on the surface by 800 to 1100 years ago (1050 ± 70 ^{14}C yr B.P.) as shown by the age of a woody root in growth position in the sediment beneath the peat (Fig. 3). A well-rounded detrital fragment of wood from the sediment beneath the peat gave an age of 1300 to 1500 years (1420 ± 70 ^{14}C yr B.P.), which is a maximum for the time of uplift.

As at Lynch Cove, peat containing abundant wood overlies mud at Oakland Bay and Burley, and roots of woody shrubs are also present locally in the uppermost several decimeters of the mud at both sites. Radiocarbon ages of the lowermost few centimeters of the peat at Oakland Bay and Burley are similar to those at Lynch Cove—1190 ± 60 ^{14}C yr B.P. at Oakland Bay and 1130 ± 50 ^{14}C yr B.P. at Burley (*23*). Also, as at Lynch Cove, a rise in relative sea level since the uplift has resulted in the formation of salt-marsh deposits on the freshwater peat at both sites.

Uplift of tidal flats in the Lynch Cove–Oakland Bay areas, uplift adjacent to the Seattle fault, and formation of an 8-m-high fault scarp along the Saddle Mountain East fault [Fig. 1; (*24*)] probably reflect slip on several faults in the crust of the North America plate. The slip may have occurred either as a series of events closely spaced in time (up to several centuries apart) or as synchronous coordinated events. We implicate more than the Seattle fault because uplift of the Lynch Cove–Oakland Bay area appears too distant (35 to 60 km from the Seattle fault) and too large (locally at least 2 m) to be solely the result of slip on that fault. Alternative, but less likely, origins for uplift in Puget Sound are earthquakes within the subducting Juan de Fuca plate or at the boundary between the Juan de Fuca and North America plates. Earthquakes in the subducted plate are unlikely sources of widespread uplift, as judged from the lack of recognized uplift from a M = 7.1 earthquake in the Juan de Fuca plate deep under southern Puget Sound (epicenter in Fig. 1). However, we cannot rule out coeval slip on faults in the North America plate and on the Juan de Fuca plate boundary because ^{14}C ages for the uplift resemble ages for abrupt subsidence and unusual ground-water eruption along the Pacific coast of Washington (*4*).

The size of the smallest earthquake compatible with the uplift between Seattle and Oakland Bay can be estimated by comparison of the uplift produced by the magnitude 7.3 earthquake of 1980 near El Asnam, Algeria, with that at Puget Sound. The El Asnam earthquake produced 5 m of uplift along a high-angle reverse fault (*25*), comparable to the amount of abrupt uplift near the Seattle fault. We conclude that faults in the North America plate can produce damaging earthquakes, probably of magnitude 7 or larger, in the Puget Sound region.

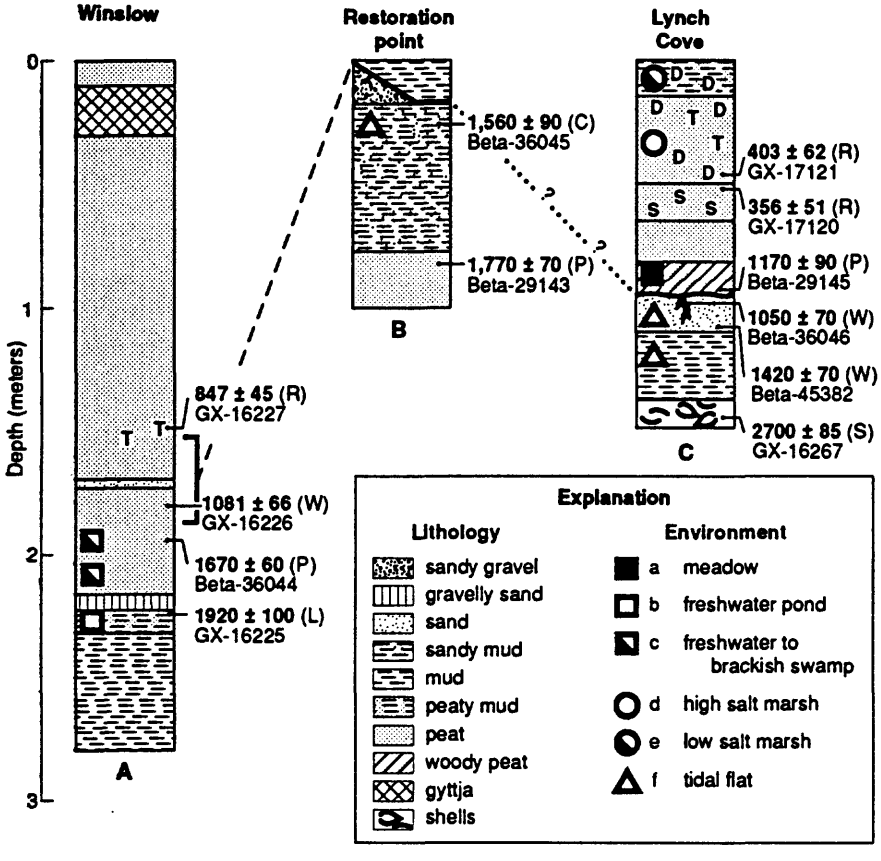

Fig. 3. Generalized composite columnar sections at uplift sites in central and southern Puget Sound region. (**A**) Winslow, (**B**) Restoration Point, and (**C**) Lynch Cove. Dashed line between sections shows inferred correlation of uplift event (shown by heavy line in sections), dotted and queried where uncertain, and time interval of Restoration Point uplift at Winslow site within bracketed interval on (A). (C) represents the stratigraphy in the seaward part of the Lynch Cove marsh. Radiocarbon ages on right side of columns are conventional radiocarbon ages (*17*), corresponding analytical laboratory numbers, and abbreviations for material dated: C, charcoal; L, leaf; P, peat; R, rhizome or leaf base; S, marine shell; W, wood. Abbreviations in explanation: a to e, representative diatom species for environments (*27*): a (A), *Fragilaria virescens*, b, *Navicula radiosa*; c, low salt marsh, *Gyrosigma eximium*; d, *Pinnularia lagerstedtii*; e (B), *Gyrosigma balticum*; and (C), *Dimeregramma minor*. Representative plant species for environment from fossil seeds: f (C), *Vaccinium* sp. or *Gaultheria* sp., and *Urtica* sp. Fossil rhizomes and inferred environments (*18*): D, *Distichlis spicata*; T, *Triglochin maritimum* (high salt marsh); S, *Scirpus acutus* (freshwater to brackish marsh).

REFERENCES AND NOTES

1. R. S. Ludwin, C. S Weaver, R S. Crosson, in *Neotectonics of North America*, D B. Slemmons, E. R. Engdahl, M. D. Zoback, D D. Blackwell, Eds. (Geological Society of America, Boulder, CO, 1991), pp. 77–98.
2. T. H. Heaton and S. H. Hartzell, *Science* **236**, 162 (1987).
3. B. F. Atwater, *ibid.*, p 942.
4. T. H. Heaton and S. H. Hartzell, *J. Geophys Res.* **97**, 1901 (1992).
5. B. F. Atwater and A. L. Moore, *Science* **258**, 1614 (1992).
6. G. C. Jacoby, P. L. Williams, B. M. Buckley, *ibid.*, p. 1621.
7. R. L Schuster, R. L. Logan, P. T. Pringle. *ibid.*, p 1620.
8. R. E. Karlin and S. E. B. Abella, *ibid.*, p. 1617.
9. H. H. Waldron, *U.S. Geol. Surv. Geol. Quadr. Map GQ-706* (1967).
10. J. C. Yount, G. R. Dembroff, G. M. Barats, *U.S. Geol. Surv. Misc. Field Stud. Map MF-1692* (1985).
11. We use high tide as an equivalent of mean higher high water.
12. H. D. Gower, J. C. Yount, R. S. Crosson, *U.S Geol. Surv. Misc. Invest Map I-1613* (1985).
13. The abrupt uplift could have differed by several meters from 7 m because of subsequent uplift, subsidence, or regional rise in sea level of 1 to 2 m
14. Faint lineations of unknown origin parallel the coast on the southeast part of the raised platform. They lack relief and are defined by variations in the tone of grass on the platform during the dry season.
15. At vertical uplift rates on the high end of those that have been observed for tectonic uplift (for example, 70 mm/yr) [A. R. Nelson and W. F Manley, in *Impacts of Tectonics on Quaternary Coastal Evolution*, Y. Ota, A. R. Nelson, K. Berryman, Eds.

(*Quat. Int.* **15/16**, special issue, 1992), p. 61], aseismic uplift of Restoration Point would have required 100 years. Even at the highest known rates of uplift of about 200 to 800 mm/yr, which have only been observed on the flanks of active volcanoes [K. R. Lajoie, in *Active Tectonics: Impact on Society* (National Academy Press, Washington, DC, 1986), pp. 95–124], 7 m of uplift would have required at least a decade.

16. This age is likely much younger than the time of uplift due to continual addition of young organic material to the soil profile [J. A. Matthews, *Geogr. Ann.* **62A**, 185 (1980)].
17. Ages in parentheses are conventional radiocarbon ages in ^{14}C years before A.D. 1950, corrected for the measured $^{13}C/^{12}C$ ratio, with 1 standard deviation in the age quoted by the laboratory. These ages were converted to 1σ tree-ring calibrated age ranges [M. Stuiver and P. J. Reimer, *Radiocarbon* **28**, 1022 (1986)] with the use of an estimated laboratory error multiplier of 2 and are reported in the text as "years ago" relative to A.D. 1990. The humus concentrate was calibrated with a range of 300 years for the carbon in the sample. For marine shells we used a reservoir correction of 800 ± 25 years [S. W. Robinson and G. Thompson, *Syesis* **14**, 45 (1981)].
18. F. Weinmann, M. Boule, K. Brunner, J. Malek, V. Yoshino, *Wetland Plants of the Pacific Northwest* (*Final Report*, U.S. Army Corps of Engineers, Seattle, 1984).
19. J. C. Yount and M. L. Holmes, *Geol. Soc. Am. Abstr. Progr.* **24**, 93 (1992).
20. J. C. Yount and H. D. Gower, *U.S. Geol. Surv. Open-File Rep. 91-147* (1991).
21. L. Mansinha and D. E. Smylie, *Seismol. Soc. Am. Bull* **61**, 1433 (1977).
22. Over most of the area at Lynch Cove a layer of very fine-grained, well-sorted sand, commonly 10 to 20 cm thick, caps the section of tidal flat mud that underlies the peat. Locally, the sand wedges out and the peat lies directly on mud. Both the sand and the mud contain diatoms characteristic of tidal flats.
23. Laboratory numbers Beta-46730 and Beta-49176, respectively.
24. J. R. Wilson, M. J. Bartholomew, R. J. Carson, *Geology* **7**, 235 (1979).
25. J. C. Ruegg, M. Kasser, A. Tarantola, J. C. Lepine, B. Chouikrat, *Seismol. Soc. Am. Bull* **72**, 2227 (1982). The geodetic data also showed 0.8 m of subsidence of the downthrown block. Ruegg *et al.* found that the observed displacements imply that there was 8 m of slip on a fault about 35 km long that extended from the surface to a depth of 12 km at dips between 54° and 70°.
26. M. Eronen, T. Kankainen, M. Tsukada, *Quat. Res.* **27**, 147 (1987).
27. E. Hemphill-Haley, thesis, University of California, Santa Cruz, CA (1992). H. Germain, *Flore des Diatomées Eaux Douces et Saumâtres* (Boubée, Paris, 1981), p. 72; N. Foged, *Bibliotheca Phycologica* (Cramer, Vaduz, 1981), Band 3, p. 123.
28. We thank B. Atwater, T. Barnhard, B. Benson, and J. Suhy for their help with this study, and property owners who generously provided access to critical sites on their land. P. Bierman reported the Alki Point excavation. The manuscript was improved by reviews by B. Atwater, A. Nelson, K. Berryman, and C. Weaver.

24 July 1992; accepted 22 October 1992

The Work of the Coastal Movements Data Center

Shouichi Matsumura
Geographical Survey Institute
Tsukuba, Ibaraki, 305, Japan

In Japan, the sea level is monitored at throughout the country by several government agencies and there are over 500 such sites. In many countries sea level observation is only provisional, but in Japan, high quality observations have been carried out for a long time at a number of tide stations. This is because 1) there is a regular need to determine the datum level for repeated leveling and hydrographical surveying due to deformation of the ground caused by frequent earthquakes, 2) it is necessary to keep records of tsunami (tidal waves caused by earthquakes) and recurring high tides, 3) it is also necessary to constantly collect data on tidal constants and variations in sea conditions to assist forecasting tides for fishing, shipping and other marine activities, and 4) as the coastal areas have a high population density and civil engineering works are carried out extensively, it is necessary to determine the datum level for each area.

In Japan, modern geodetic surveys were undertaken 100 years ago throughout the country, and thereafter country wide surveys were repeated to understand, as described above, not only the large crustal movements accompanying earthquakes and the steady crustal movements under normal conditions, but also the precursory crustal movements immediately before an earthquake. From such historical background, the observation of crustal movements plays a very great role in predicting earthquakes in Japan. In particular, distinct crustal movements in littoral areas are often seen in Japan whose Pacific coasts are very close to the subduction zone or the trenches. Hence it is important to have a thorough grasp of such crustal movements.

In order to gather the tide data obtained by the various organizations and thus facilitate analysis of the crustal movements in the coastal region, the organizations cooperated and established a Coastal Movements Data Center with the Geographical Survey Institute as the secretariat in 1965. The operation of the Center is briefly described in Reference 1.

As stated previously, there are more than 500 tide stations in Japan, but 117 were registered with the Center as of November 1992(Fig. 1). Details are given in Table 1.

Geographical Survey Institute	25 stations
Japan Meteorological Agency	54 stations
Hydrographic Department	28 stations
Earthquake Research Institute	1 station
Others	9 stations

Table 1 Tide stations registered in the Coastal Movements Data Center

The requirements for registration of a tide station are not expressly provided, but in principle they are as follows.

1) Data is successively acquired, arranged and managed orderly.
2) The tide station should be made of concrete on a bedrock or other firm foundation.
3) The tide gauge should have a highly reliable, simple structure and be specifically a float type (Fig. 2).
4) Levelling at the tide station is determined via measurement from the bench mark.

The Coastal Movement Data Center is continuously searching for tide stations satisfying these requirements. Every year two or three stations are added, subject to the approval of the relevant organizations. Data from the tide stations is transmitted partly by telecommunication lines but mostly by mail to the Center, which then arranges them into the following documents as a service to users.

1) Distribution Map of Tide Stations of the Coastal Movements Data Center
2) Monthly Report on the Coastal Movements Data Center
3) Annual Report on the Coastal Movements Data Center
4) Tables and Graphs of Annual Mean Sea Level along the Japanese Coast (issued every five years)
5) List of Tide Stations in Japan (issued every 10 years)
6) Report on Connecting Leveling to Tide Bench Marks

Some examples of crustal movements shown by the data of the Center are given below.

(Example 1)

Excluding non-crustal movements as far as possible from the data throughout the country, the levels from 1951 to 1981 were calculated. The results are shown in Fig. 3. The figure also shows numerically the result of the national leveling carried out from 1962 to 1968 and the crustal movements calculated from the data of the leveling from 1975 to 1982. The tide data and leveling data show a generally good correlation, but there is a difference in the southwestern part of Japan.

(Example 2)

Fig. 4 shows vertical ground movements determined by leveling for the Tokai District, where the "Tokai Earthquake" is anticipated. It can be seen that due to the sliding of the Philippine Sea plate, the area from Omaezaki to Yaizu is subsiding at the rate of 4~5mm a year. Fig. 5 shows the differences in sea level at tide stations in this area. Subsidence at Omaezaki and Yaizu is readily apparent when compared to Uchiura and Maisaka. Differences in sea level allow real time observation over leveling, so to facilitate prediction of the "Tokai Earthquake", the tide data of the area is transmitted to the Coastal Movements Data Center by telecommunication line and monitored there.

(Example 3)

Differences in sea level at Ito, Izu Peninsula, and Aburatsubo are shown in Fig. 6. In the eastern part of the Izu Peninsula, swarm earthquakes have occurred every years since 1978, and in June 1989, a small submarine eruption occurred to the east of Ito City. The only activity thereafter was small swarm earthquakes in August and December 1991. As shown in Fig. 6, the level in the general area of Ito City rose significantly between 1978 to 1989, remaining thereafter in line with declining earthquake activity.

(Example 4)

In March 1982, an earthquake of M 7.1 at a depth of 40km occurred off the coast of Urakawa, Hokkaido. Immediately before the earthquake, a leveling survey carried out quite by chance indicated the possibility of a precursory rising phenomenon occurring around Urakawa (Fig. 7). Differences in sea level at Urakawa and Muroran (Fig. 8) also supported this conclusion.

(Example 5) In Kyushu, a comparison of leveling surveys conducted between 1975-1978 and 1981-1983 indicates subsidence in the northern part and rising in the southern part (Fig. 9), but those conducted between 1981-1983 and 1987-1990 conversely indicate rising in the north and subsidence in the south. The question of whether this was an indication of actual crustal movement or a misinterpretation due to measurement error created some debate. Data for differences in sea levels in the district (Fig. 10) supports the former view.

The Coastal Movements Data Center operates smoothly through good cooperation between the various organizations, and from the experience acquired so far, the results of analysis of the crustal movements using the data from the Center have proved to be highly reliable. As a result, the Center is regarded as playing an important role in clarifying coastal movements from an academic point of view. Furthermore, the information it provides is expected to be instrumental in predicting the "Tokai Earthquake", just as it was shown to be of use at the time of the submarine volcano eruption east of Ito City.

(Reference 1)

The Operation of the Center

(Object)
1. The Coastal Movements Data Center referred to detects crustal movements from data records of government tide and arranges the data in a standard form and publishes it for practical use in predicting earthquakes.

(Projects)
2. To implement this objective, the Center is working on the following projects; Preparing a distribution map of tide stations registered with the Center Arranging the monthly mean tide levels of the tide stations registered with the Center and publishing monthly and annual reports of tide levels Arranging the results of observation of the tide levels in the past for a substantial period and publishing them.
Performing other necessary projects for the operation of the Center.

(Commission)
3. To ensure smooth operation of the projects, the Center has an operation committee consisting of experienced personnel from the relevant government agencies, and the Director General of the Geographical Survey Institute commissions them.

(Terms of Office)
4. The term of office of each committee member is two years, and when a vacancy occurs, the term of office of the member filling the vacancy is the remaining period of the predecessor.

(General Meeting)
5. The Center holds a general meeting or meetings once or more a year for deliberation of matters concerning the running of the Center.

(Administration)
6. Administration of the Center is undertaken by the Geographical Survey Institute of the Ministry of Construction.

(Supplementary Provision)
This procedure applies from July 12, 1977.

(Reference 1)

The Operation of the Center

(Object)
1. The Coastal Movements Data Center referred to detects crustal movements from data records of government tide and arranges the data in a standard form and publishes it for practical use in predicting earthquakes.

(Projects)
2. To implement this objective, the Center is working on the following projects; Preparing a distribution map of tide stations registered with the Center Arranging the monthly mean tide levels of the tide stations registered with the Center and publishing monthly and annual reports of tide levels Arranging the results of observation of the tide levels in the past for a substantial period and publishing them.
Performing other necessary projects for the operation of the Center.

(Commission)
3. To ensure smooth operation of the projects, the Center has an operation committee consisting of experienced personnel from the relevant government agencies, and the Director General of the Geographical Survey Institute commissions them.

(Terms of Office)
4. The term of office of each committee member is two years, and when a vacancy occurs, the term of office of the member filling the vacancy is the remaining period of the predecessor.

(General Meeting)
5. The Center holds a general meeting or meetings once or more a year for deliberation of matters concerning the running of the Center.

(Administration)
6. Administration of the Center is undertaken by the Geographical Survey Institute of the Ministry of Construction.

(Supplementary Provision)
This procedure applies from July 12, 1977.

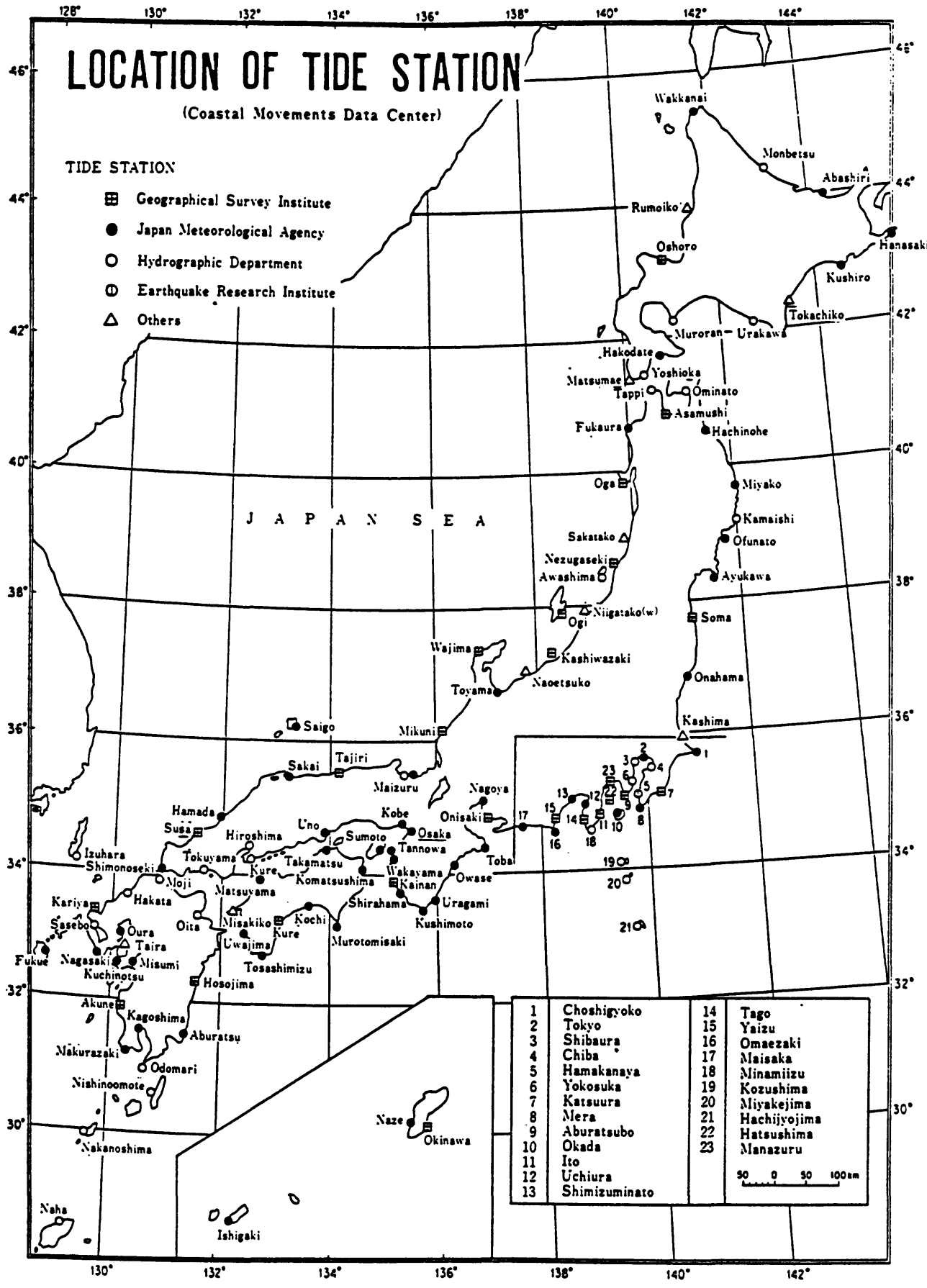

Fig. 1 Location of Tide Station

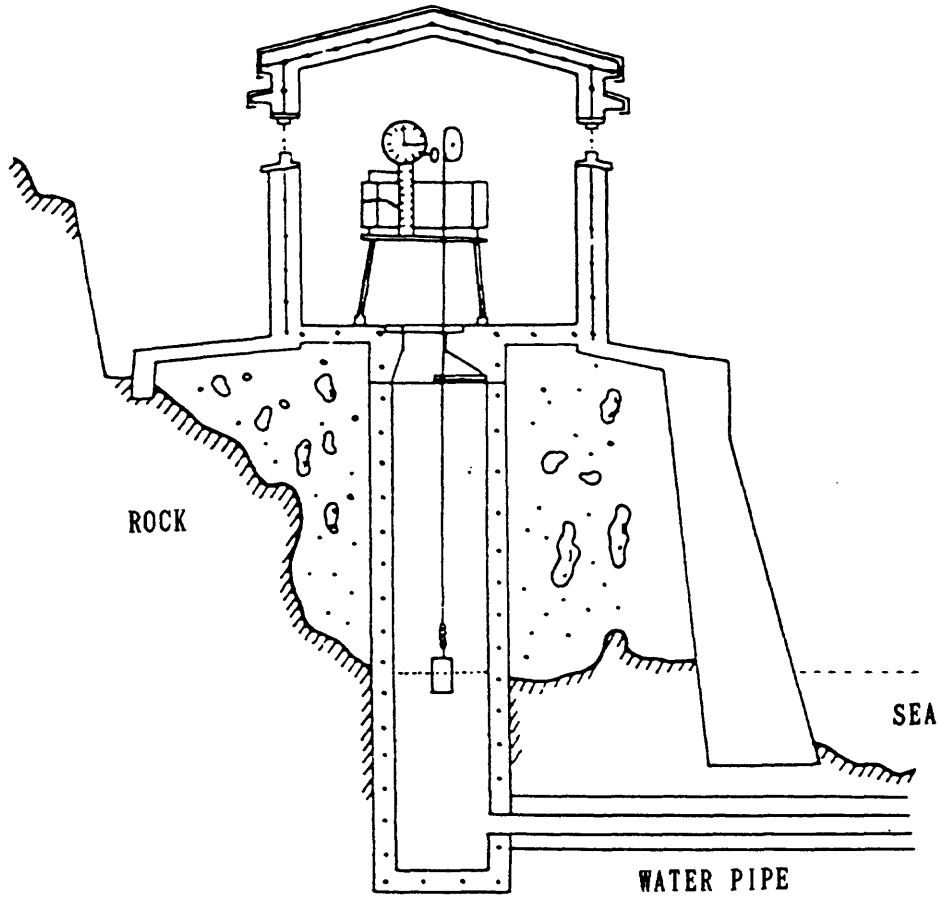

Fig. 2 Tide Station

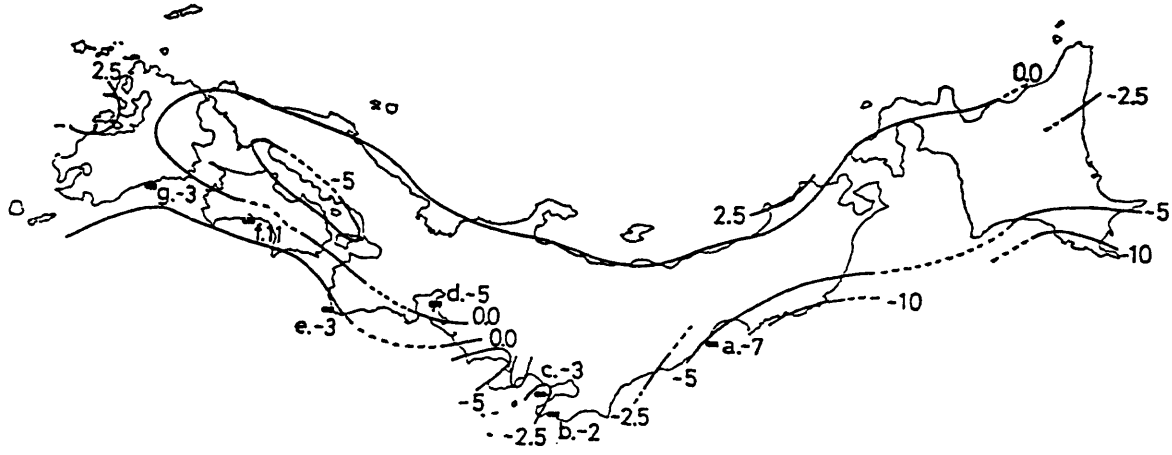

Fig. 3 Vertical crustal movements as deduced from tidal records and releveling

Vertical crustal movements along the coast of the pacific ocean obtained from releveling are shown at seven tide stations, a. Soma, b. Katsuura, c. Aburatsubo, d. Onisaki, e. Kushimoto, f. Kure and g. Hosojima.

Unit: mm/year.

(After Nakahori [1985], reformation from Kato[1983] by Nakahori)

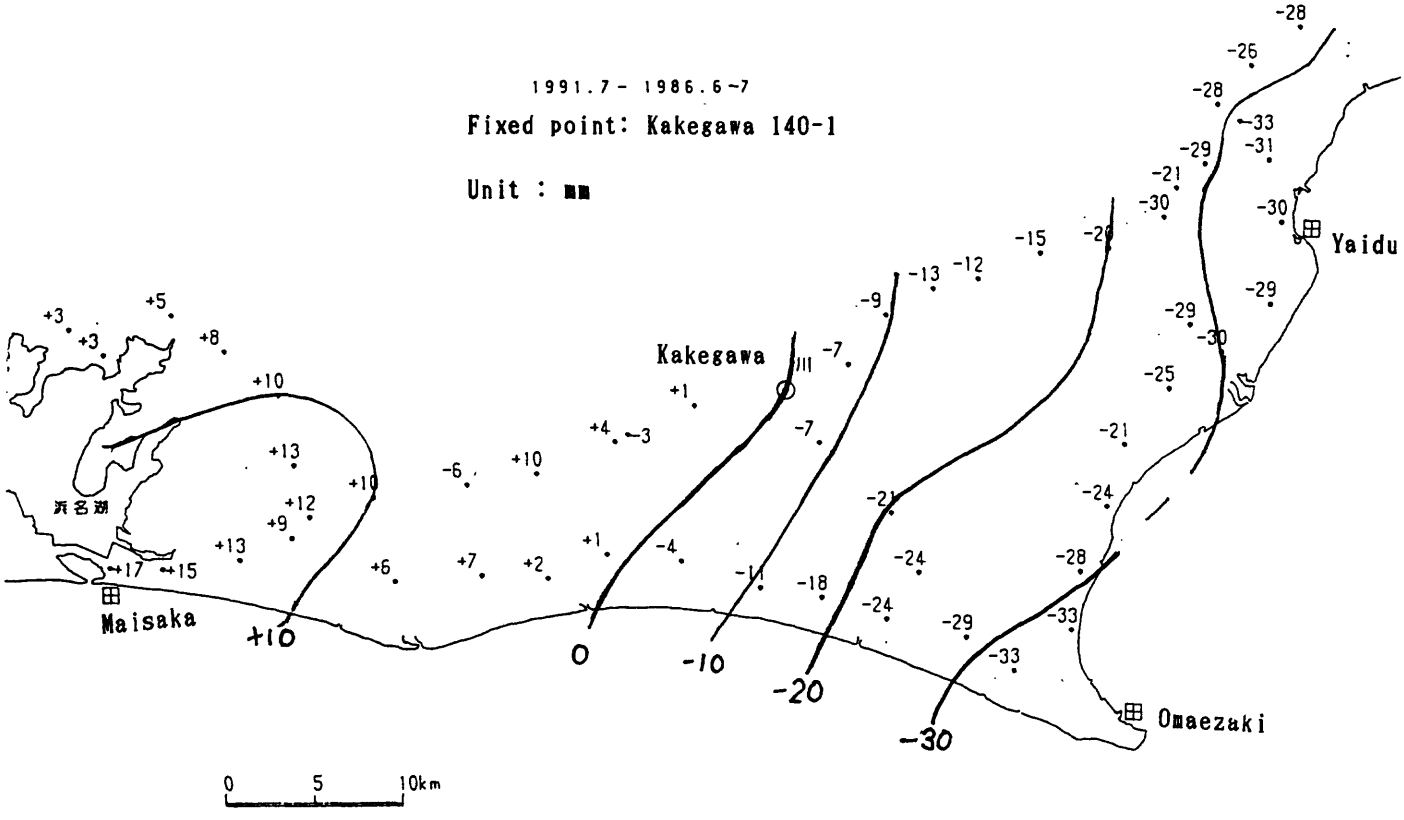

Fig. 4 Vertical crustal movements in the Tokai district in 1991 July - 1986 July,
(Geographical Survey Institute[1992])

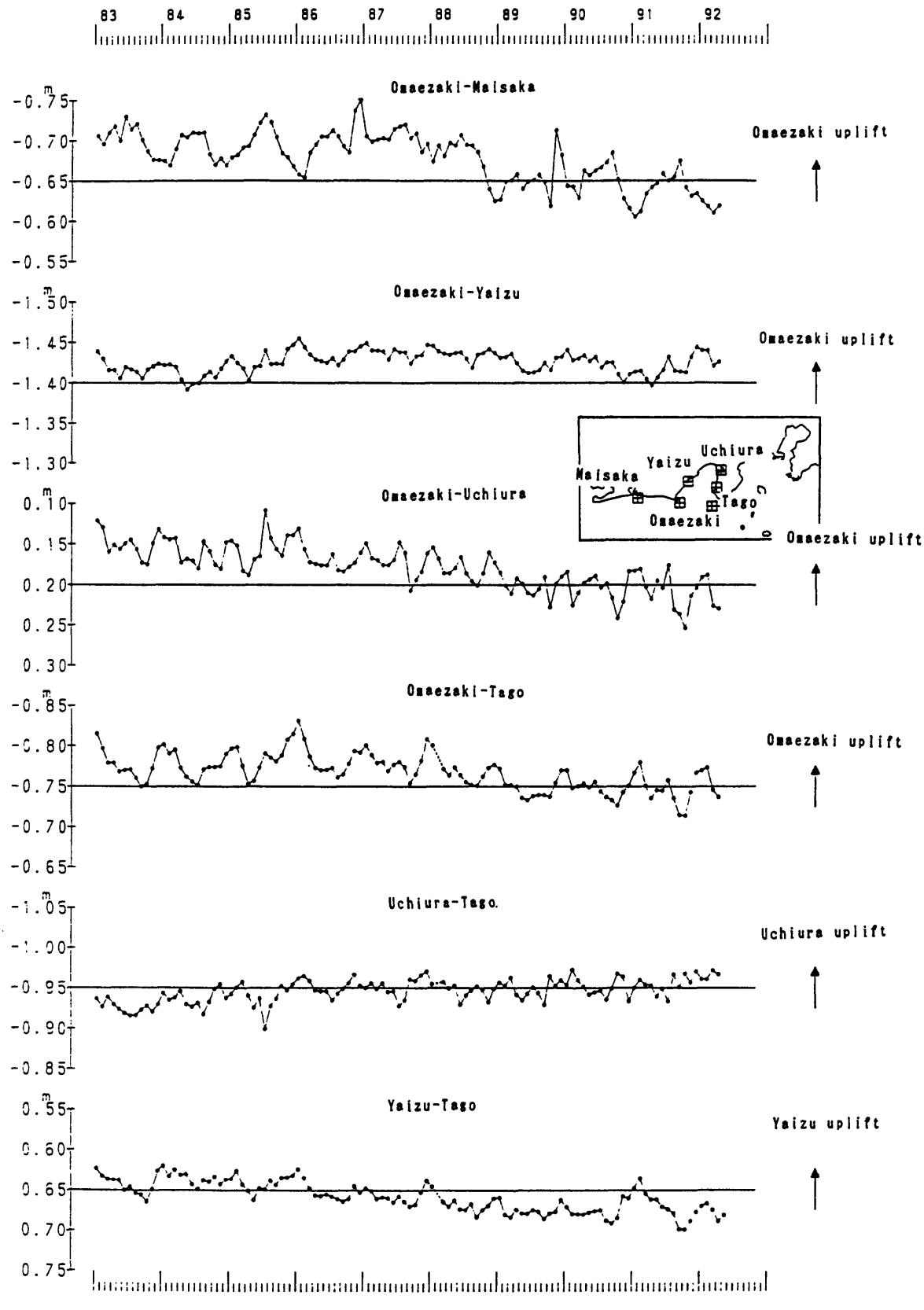

Fig. 5 Differences in monthly mean sea levels of tide station pairs in the Tokai district
(Reformation from Coastal movements data center[1991])

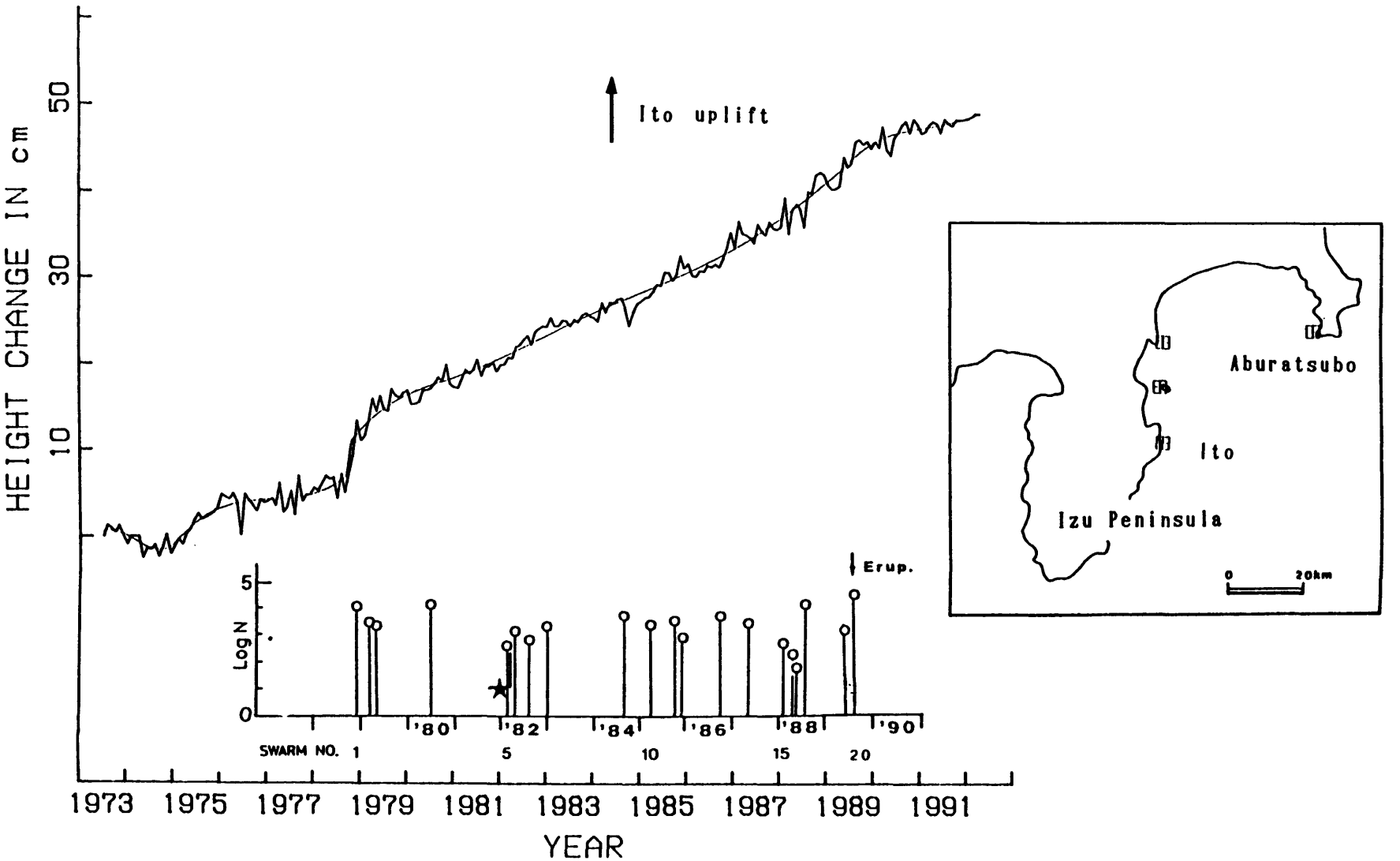

Fig. 6 Differences in monthly mean sea levels between the Ito and the Aburatsubo tide stations

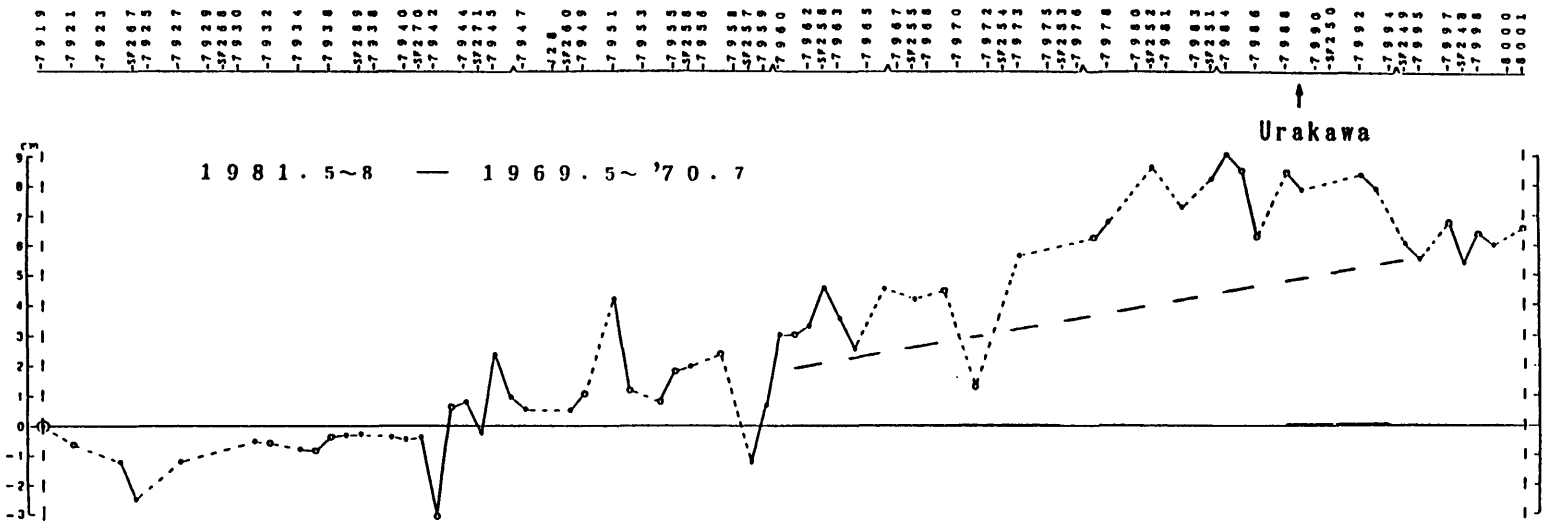

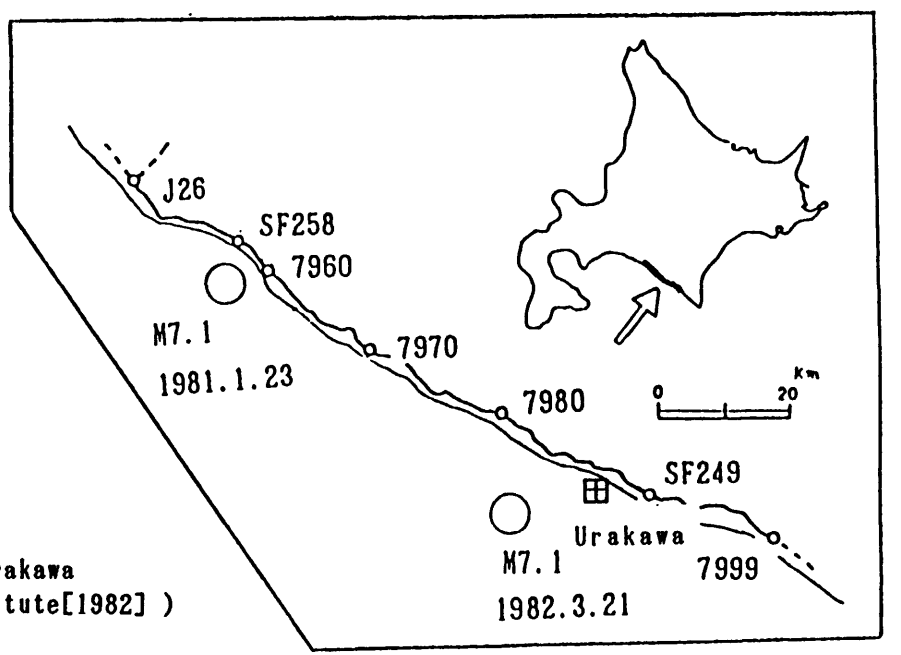

Fig. 7 Vertical crustal movements around Urakawa
(Geographical Survey Institute[1982])

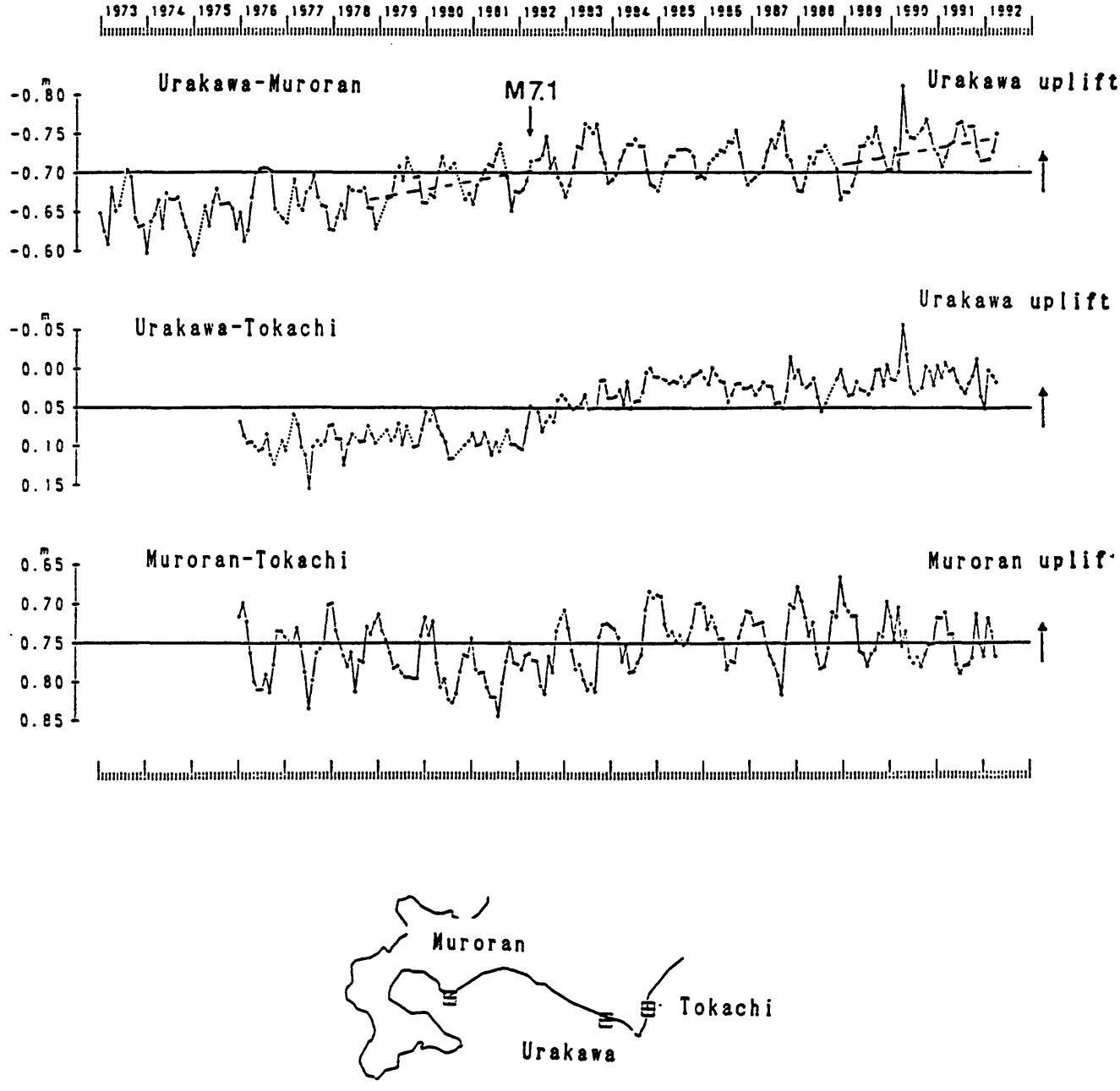

Fig. 8 Differences in monthly mean sea levels among the Urakawa, the Muroran, and the Tokachi-ko tide stations

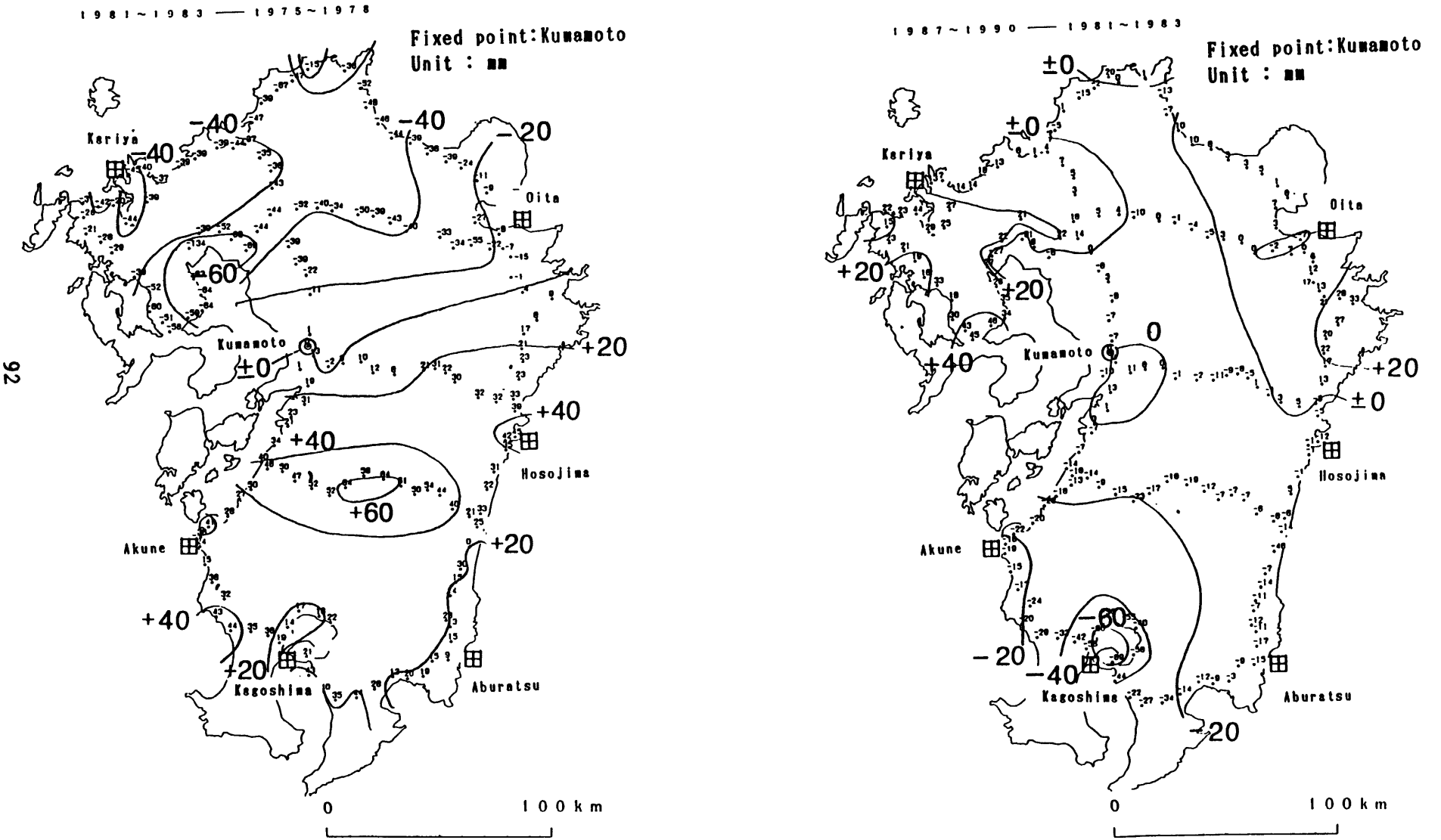

Fig. 9 Vertical crustal movements in the Kyushu district

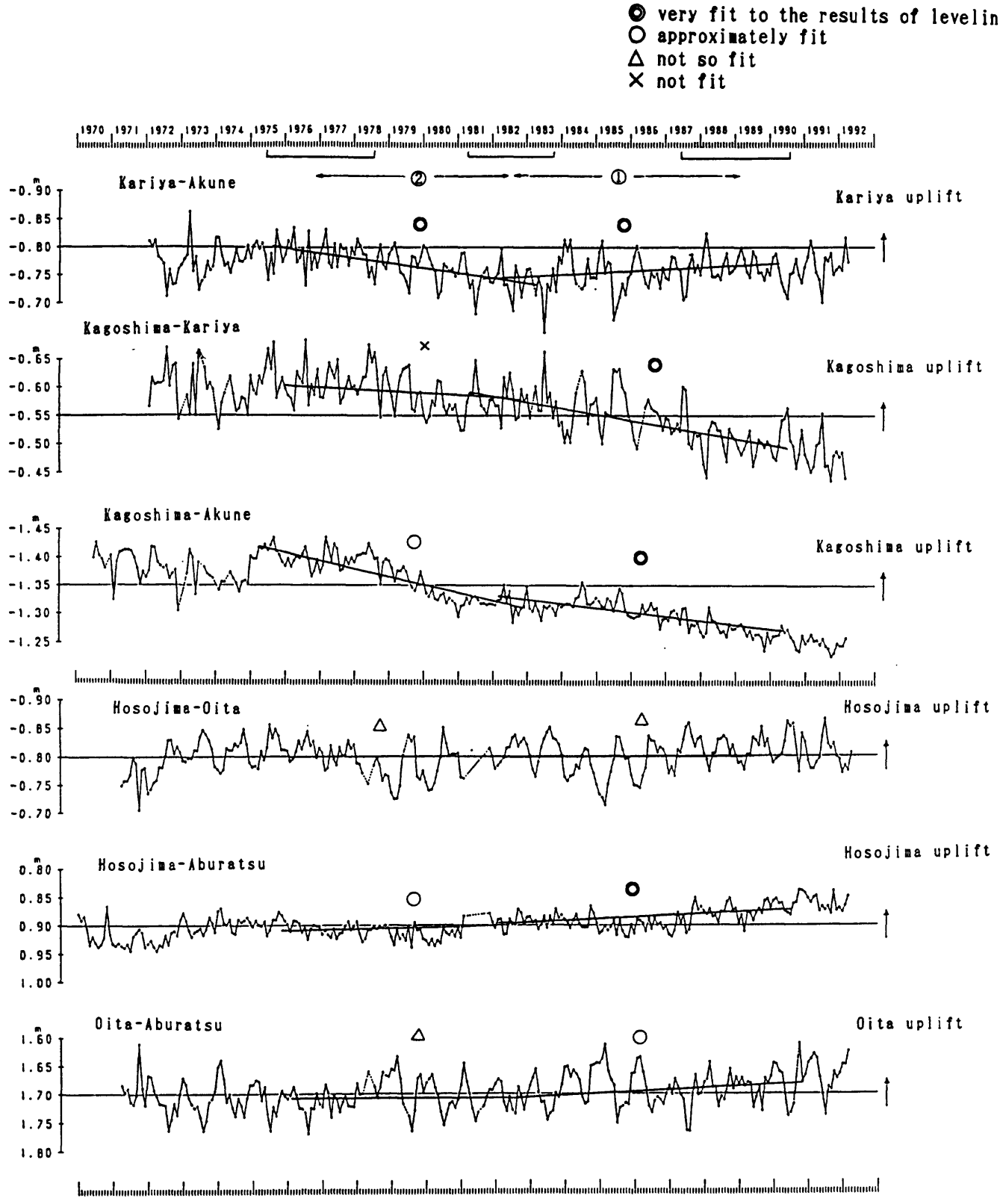

Fig. 10 Differences in monthly mean sea levels of tide station pairs in the Kyushu district
(Coastal movements data center[1991])

Seismicity, Stress Orientation and Configuration of the Aleutian Megathrust in the Vicinity of the Great 1964 Alaska Earthquake

C.D. Stephens, R.A. Page, J.C. Lahr, K.A. Fogleman, T.M. Brocher, M.A. Fisher, and E.L. Geist (U.S. Geological Survey, Menlo Park, CA 94025)

The great 1964 Alaska earthquake ruptured the Pacific-North American plate boundary along the northern end of the Aleutian megathrust (Figure 1) where tectonic interaction between the two plates is complicated by ongoing subduction and accretion of the Yakutat terrane (for example, Plafker, 1987). Since at least the early 1970's, when the USGS established a seismograph network surrounding the epicentral area in Prince William Sound, the megathrust has been nearly aseismic. Because of this quiescence there is little direct evidence to constrain the geometry of the megathrust. However, by combining well-contrained hypocenters and focal mechanisms in the Prince William Sound region with the results of seismic profiling, we are able to relate the megathrust to the interface between the overlying North American plate and the underthrusting Yakutat terrane, which has been transported on the Pacific plate and subducted beneath the continent.

Seismic reflection and refraction profiling in the Prince William Sound region of southern Alaska (Brocher and others, 1991) reveals an extensive, gently landward-dipping mid-crustal reflector defining the top of a layer with a P-wave velocity of about 6.9 km/sec (Figure 2). This layer lies well above the subducted oceanic crust and Moho of the Pacific plate, and its apparent eastward continuation has led to the interpretation that it represents subducted lower crustal rocks of the Yakutat terrane (Brocher and others, 1991; Griscom and Sauer, 1990). Hypocenters of recent, well-recorded earthquakes, when relocated with a velocity model based on the seismic refraction profiling, tend to be concentrated at or just below this mid-crustal reflector (Figure 3) rather than within the underlying Pacific plate. Furthermore, focal mechanisms determined from regionally-recorded P-wave polarities show a remarkably consistent pattern in this depth range, where T-axes tend to be subhorizontal and oriented west-east to northwest-southeast (Figure 4). Both the distribution of seismicity and the orientation of T-axes appear to be continuous with the deeper, more steeply inclined Wadati-Benioff zone seismicity west and north of Prince William Sound (for example, Page and others, 1989), where the least-compressive principal stress axis inferred from the focal mechanisms aligns with the downdip direction of the seismic zone.

Evidence that the west- to northwest-directed extensional stress found in the subducted plate beneath Prince William Sound may extend seaward of the trench comes from the northwestward orientation of T-axes determined for the sequence of two magnitude 7-class earthquakes in the northern Gulf of Alaska in 1987-88 (Lahr and others, 1988).

Our conclusion that the megathrust beneath Prince William Sound lies at the top of the subducted lower crustal rocks of the Yakutat terrane has several important implications. One is that the giant asperity at the northern end of the 1964 rupture zone, which released most of the seismic moment in the earthquake (Ruff and Kanamori 1983; Kikuchi and Fukao, 1987), is linked to the presence of the subducted Yakutat terrane. The anomalous plate thickness produced by welding lower crustal rocks of the Yakutat terrane to the top of the Pacific oceanic lithosphere may increase bending resistance or buoyancy, thus causing the subducting plate to follow a relatively flat trajectory. This geometry would result in a broad contact zone between the plates, as is reflected in the aftershock zone of the 1964 earthquake (Figure 5). In addition, the eastward limit of rupture during the 1964 earthquake may have been structurally controlled. Both the early aftershock activity and moment release from the 1964 earthquake die off rapidly near the longitude of Kayak Island (Figure 5) where the mid-crustal reflector ramps upward significantly (Figure 6). If the megathrust is marked by the mid-crustal reflector, then this upwarping in the configuration of the megathrust may have impeded further rupture to the east.

References

Algermissen, S.T., W.A. Rinehart, R.W. Sherburne, and W.H. Dillinger, Jr., 1972, Preshocks and aftershocks, in, The Great Alaska Earthquake of 1964: Seismology and Geodesy, pp. 313-364, National Academy of Sciences, Washington, D.C.

Bayer, K.C., R.E. Mattick, G. Plafker, and T.R. Bruns, 1978, Refraction studies between Icy Bay and Kayak Island, eastern Gulf of Alaska, U.S. Geological Survey Journal of Research, v. 6, pp. 625-636.

Brocher, T.M., M.J. Moses, M.A. Fisher, C.D. Stephens, and E.L. Geist, 1991, Images of the plate boundary beneath southern Alaska, in, Continental Lithosphere: Deep seismic reflections, AGU Monograph, Geodynamic Series, v. 22, pp. 241-246.

Davies, J., L. Sykes, L. House, and K. Jacob, 1981, Shumagin seismic gap, Alaska Peninsula;

History of great earthquakes, tectonic setting, and evidence for high seismic potential, Journal of Geophysical Research, v. 86., pp. 3821-3855.

Demets, C., R.C. Gordon, D.F. Argus, and S. Stein, 1990, Current plate motions, Geophysical Journal International, v. 101, pp. 425-478.

Griscom A., and P.E. Sauer, 1990, Interpretation of magnetic maps of the northern Gulf of Alaska, with emphasis on the slope magnetic anomaly, U.S. Geological Survey Open-File Report 90-348, 18 p.

Kikuchi, M., and Y. Fukao, 1987, Inversion of long-period P-waves from great earthquakes along subduction zones, Tectonophysics, v. 144, pp. 231-247.

Lahr, J.C., R.A. Page, C.D. Stephens, and D.H. Christensen, 1988, Unusual earthquakes in the Gulf of Alaska and Framentation of the Pacific Plate, Geophysical Research Letters, v. 15, n. 13, p. 1483-1486.

Page, R.A., C.D. Stephens, and J.C. Lahr, 1989, Seismicity of the Wrangell and Aleutian Wadati-Benioff zones and the North American Plate along the Trans-Alaska Crustal Transect, Chugach Mountains and Copper River Basin, southern Alaska, Journal of Geophysical Research, v. 94, pp. 16,059-16082.

Plafker, G., 1987, Regional geology and petroleum potential of the northern Gulf of Alaska continental margin, in D.W. Scholl, A. Grantz, and J.G. Vedder, eds., Geology and resource potential of the continental margin of western North America and adjacent ocean basins.- Beaufort Sea to Baja California, Earth Science Series, v. 6, pp. 229-268, Circum-Pacific Council for Energy and Mineral Resources, Houston, Texas.

Reasenberg, P. and D. Oppenheimer, 1985, FPFIT, FPPLOT, and FPPAGE: Fortran computer programs for calculating and displaying earthquake fault-plane solutions, U.S. Geol. Surv. Open-File Report 85-739, 109 p.

Ruff, L. and H. Kanamori, 1983. The rupture process and asperity distribution of three great earthquakes from long-period diffracted P-waves, Physics of the Earth and Planetary Interiors, v. 31, pp. 202-230.

Schwab, W.C., T.R. Bruns, and R. von Huene, 1980, Maps showing structural interpretations of magnetic lineaments in the northern Gulf of Alaska, U.S. Geological Survey Misc. Field Studies Map, MF-1245, scale 1:500,000.

Figure Captions

Figure 1. Map of tectonostratigraphic terranes (light dashed and solid lines; Yakutat terrane is highlighted by stippled pattern) in the northern Gulf of Alaska (after Plafker, 1987), and aftershock zone (slanted shading) of the great 1964 Alaska earthquake (after Davies and others, 1981). Sedimentary upper crustal rocks of the Yakutat terrane are being deformed in a fold and thrust belt that extends between the Kayak Island and Pamplona zones. The Slope Magnetic Anomaly (after Schwab and others, 1980) is inferred to mark southern extent of basaltic lower crustal rocks of the Yakutat terrane east of about 148° W longitude; note that the extension of the anomaly for more than 100 km west of the Kayak Island zone suggests that lower crustal rocks of the Yakutat terrane have been subducted at least this far. Stars indicate epicenters of 1964 earthquake and two recent large shocks in the northern Gulf of Alaska (Lahr and others, 1988). Plate motion vector from Demets and others (1990). Location of schematic cross section in Figure 6 is indicated by heavy solid line. PWS - Prince William Sound; FF - Fairweather fault.

Figure 2. Map of depth contours (heavy lines, in km) at top of mid-crustal layer with P-wave velocity of 6.9 km/s. Contours were interpolated from seismic velocity structures derived from deep reflection/refraction profiles of the Trans-Alaska Crustal Transect program (thin solid lines) and from shallow marine seismic profiles of Bayer and others (1978; thin dashed lines). Slope Magnetic Anomaly marks southern extent of basaltic lower crustal rocks of the Yakutat terrane. A and A' are endpoints of the vertical seismic reflection profile shown in Figure 3. Star indicates epicenter of 1964 earthquake. Contours of water depth are in meters.

Figure 3. Selected, well-recorded earthquakes located within 20 km of the section A-A' along the PWS line (Figure 2) are shown in relation to the vertical seismic reflection data. The megathrust is inferred to coincide with the top of the reflective layer indicated by arrows. Earthquakes occurred between July 1985 and May 1989 when the regional seismograph network was augmented by several local stations. Hypocenters were determined using a velocity model based on seismic refraction profiling. Event selection criteria include having at least one recording station within 15 km epicentral distance.

Figure 4. Orientation of T-axes for higher-quality focal mechanisms of 779 earthquakes. Unit-

length axes are projected onto horizontal (*top*) and vertical (*bottom*) planes, so that shorter line segments correspond axes nearly perpendicular to the planes. Focal mechanisms were determined using initial P-wave polarites and a modified version of the computer program FPFIT (Reasenberg and Oppenheimer, 1985), and were selected on the basis of having the 90% confidence regions for both the P- and T- axes cover less than 20% of the focal sphere. Line B-B' (*top*) shows the orientation of cross section (*bottom*), which is approximately perpendicular to the downdip direction of the Wadati-Benioff seismic zone in the subducting plate. CI - Cook Inlet, PWS - Prince William Sound.

Figure 5. Map showing the first five days of aftershocks from the 1964 Alaska earthquake (modified from Algermissen and others, 1972; symbol key at lower right), and the distribution of seismic moment release (large filled circles) during the mainshock (modified from Kikuchi and Fukao, 1987); seismic moment is distributed over a uniformly-spaced grid of points covering the rupture surface, and circle size is proportional to the moment released at each point. Slope Magnetic Anomaly marks southern extent of lower crustal rocks of Yakutat terrane. Note that near Prince William Sound (PWS) the downdip width of the rupture zone inferred from the distribution of aftershocks is at least 150 km, and that both the number of aftershocks and seismic moment release decline sharply about 50 km west of Kayak Island.

Figure 6. Schematic west-east cross section near Kayak Island showing configuration of a magnetic mass that may correspond to basaltic, lower crustal rock of the Yakutat terrane (modified from Griscom and Sauer, 1990). This body is inferred to coincide with a regional, mid-crustal layer that has a P-wave velocity of about 6.9 km/s and produces strong arrivals on both seismic reflection and refraction profiles. The megathrust is inferred to lie at the top of this layer. Note the upward ramping in the mid-crustal layer near Kayak Island that is also evident in the contours of Figure 2.

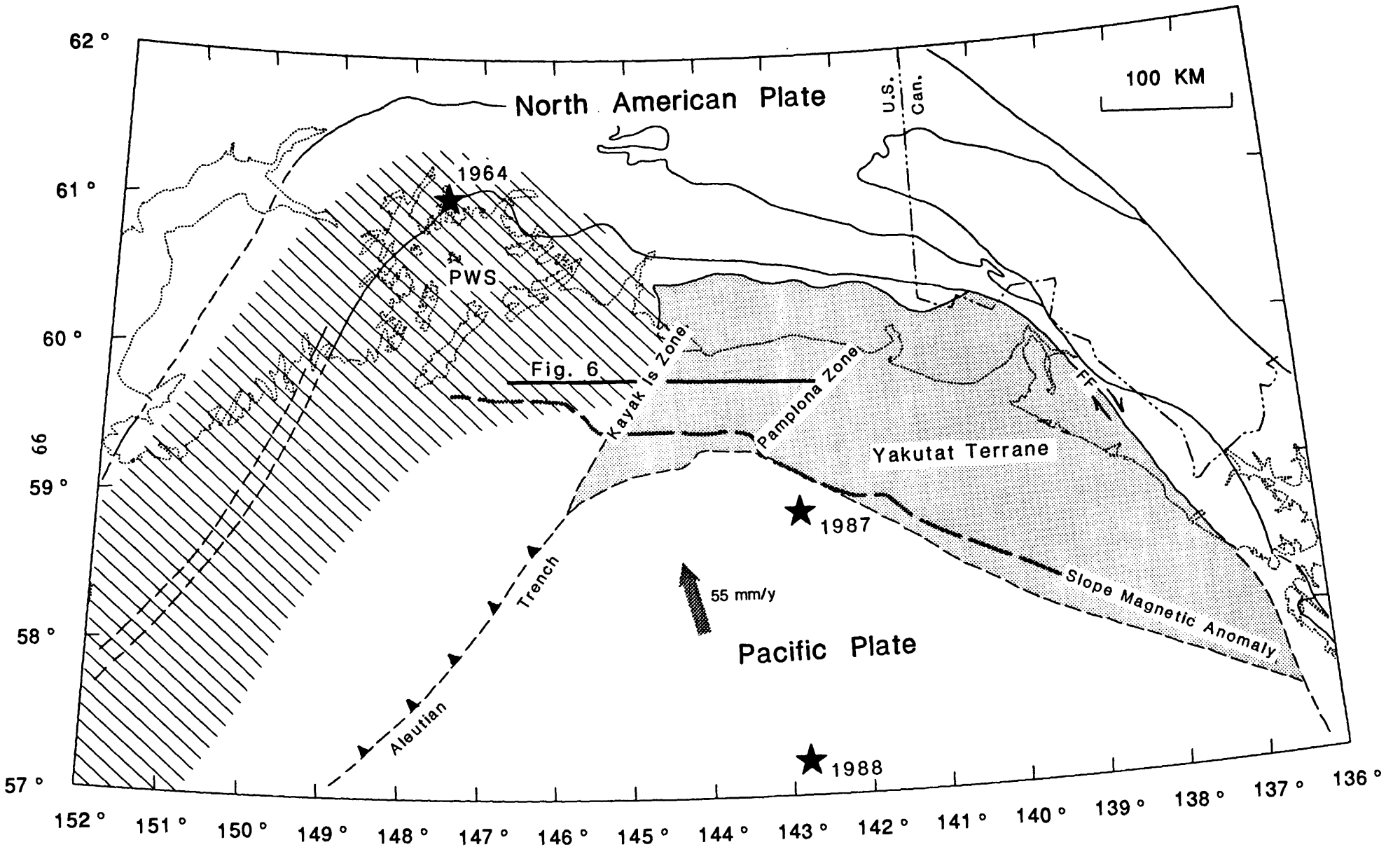
62 °
61 °
60 °
59 °
58 °
57 °
152 °
151 °
150 °
149 °
148 °
147 °
146 °
145 °
144 °
143 °
142 °
141 °
140 °
139 °
138 °
137 °
136 °
66
North American Plate
U.S.
Can.
100 KM
1964
PWS
Fig. 6
Kayak Is Zone
Pamplona Zone
FF
Yakutat Terrane
1987
55 mm/y
Pacific Plate
Slope Magnetic Anomaly
Trench
Aleutian
1988

FIGURE 1

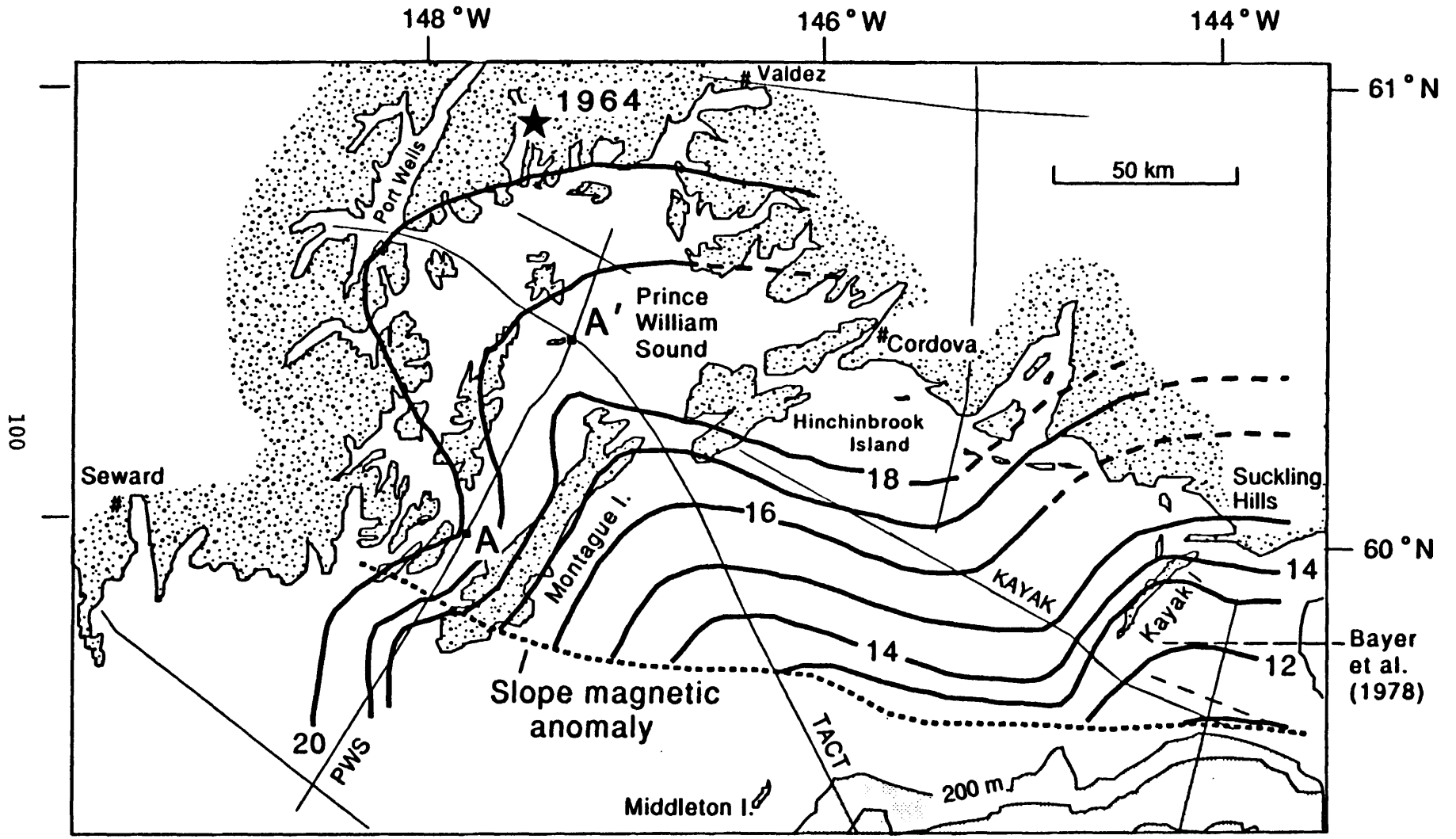
148 °W
146 °W
144 °W
61 °N
60 °N
100
Valdez
1964
Port Wells
50 km
A'
Prince
William
Sound
Cordova
Hinchinbrook
Island
Seward
A
Montague I.
18
16
14
14
12
20
Suckling
Hills
KAYAK
Kayak
Bayer
et al.
(1978)
Slope magnetic
anomaly
PWS
TACT
200 m
Middleton I.

FIGURE 2

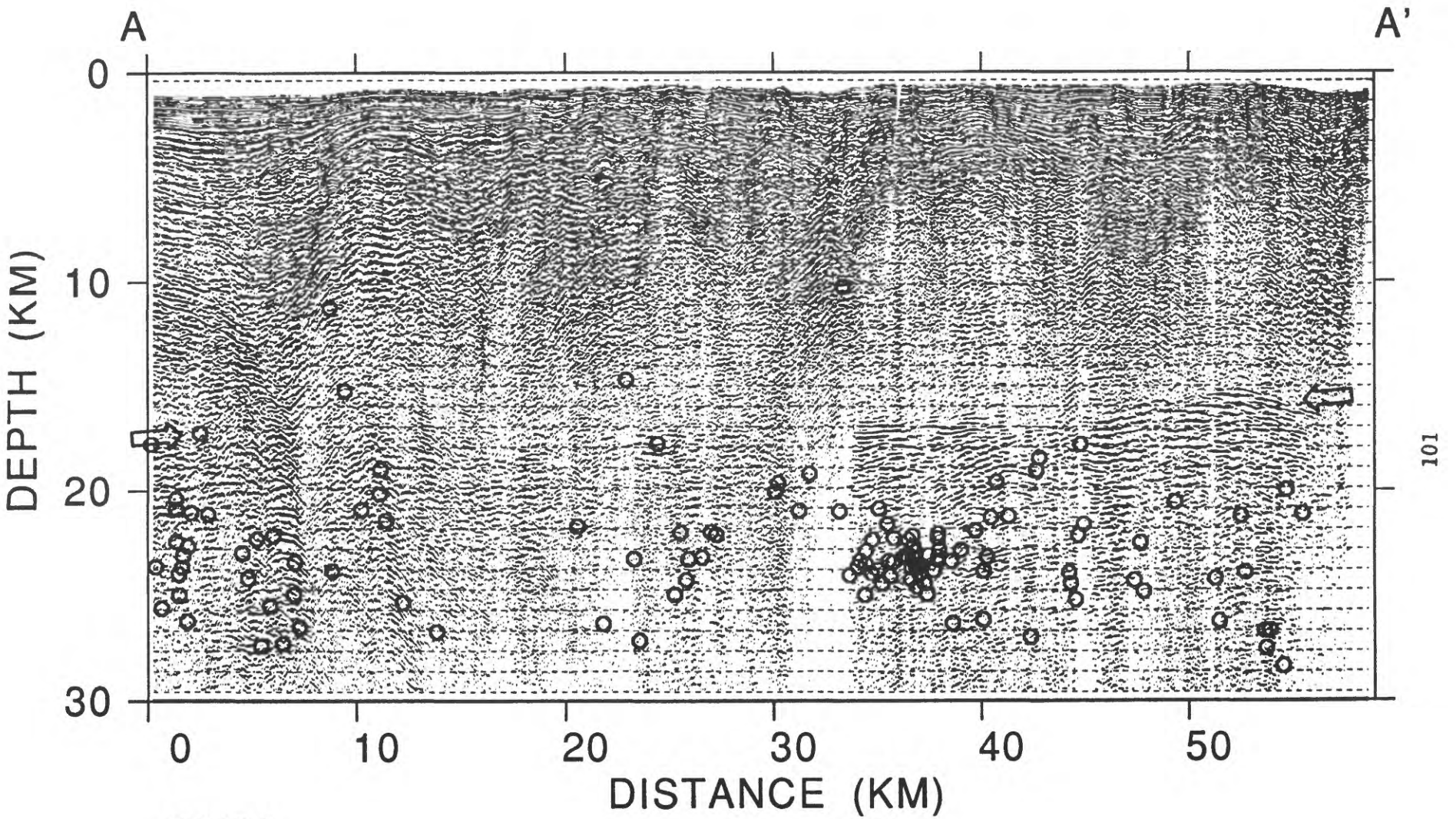

FIGURE 3

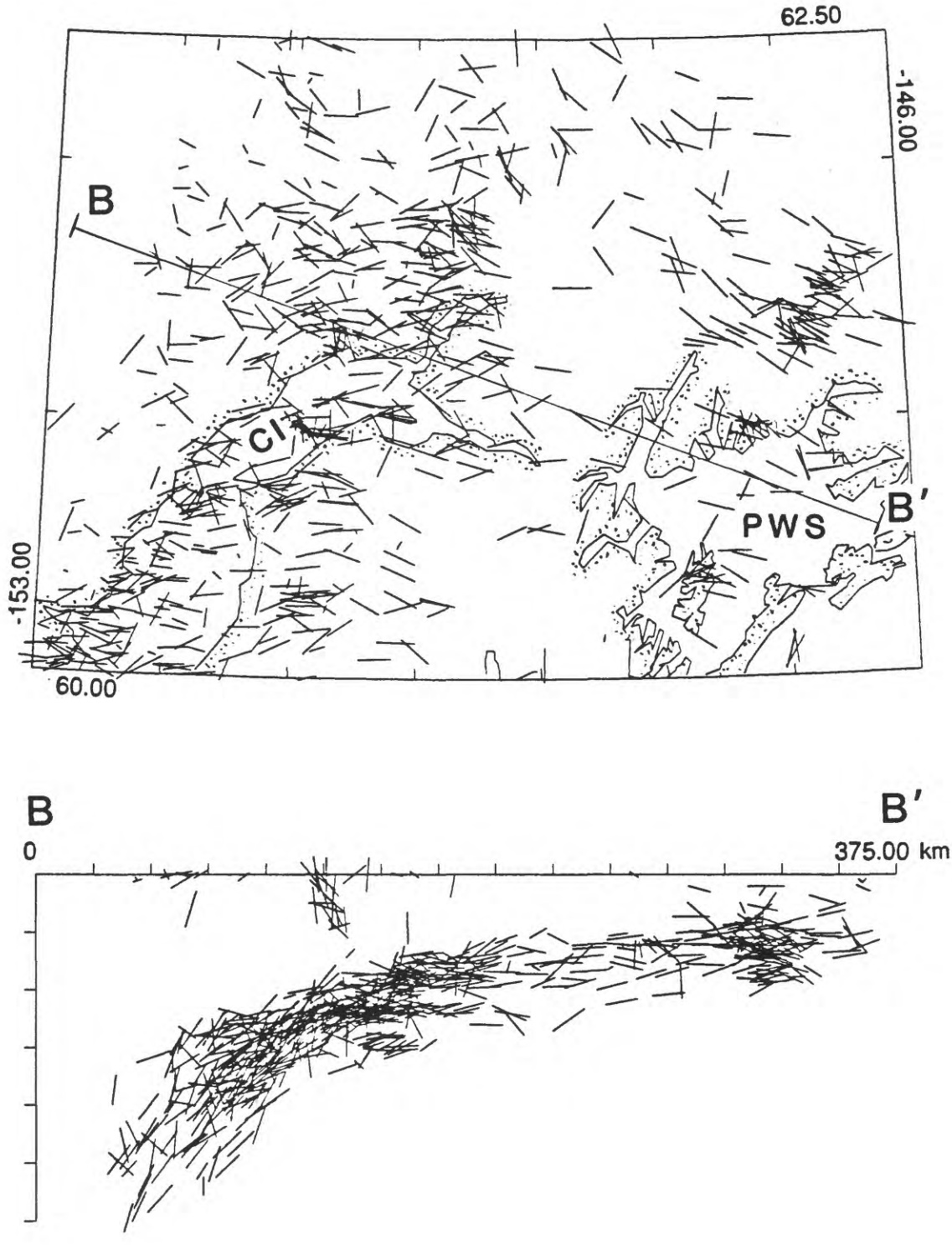

FIGURE 4

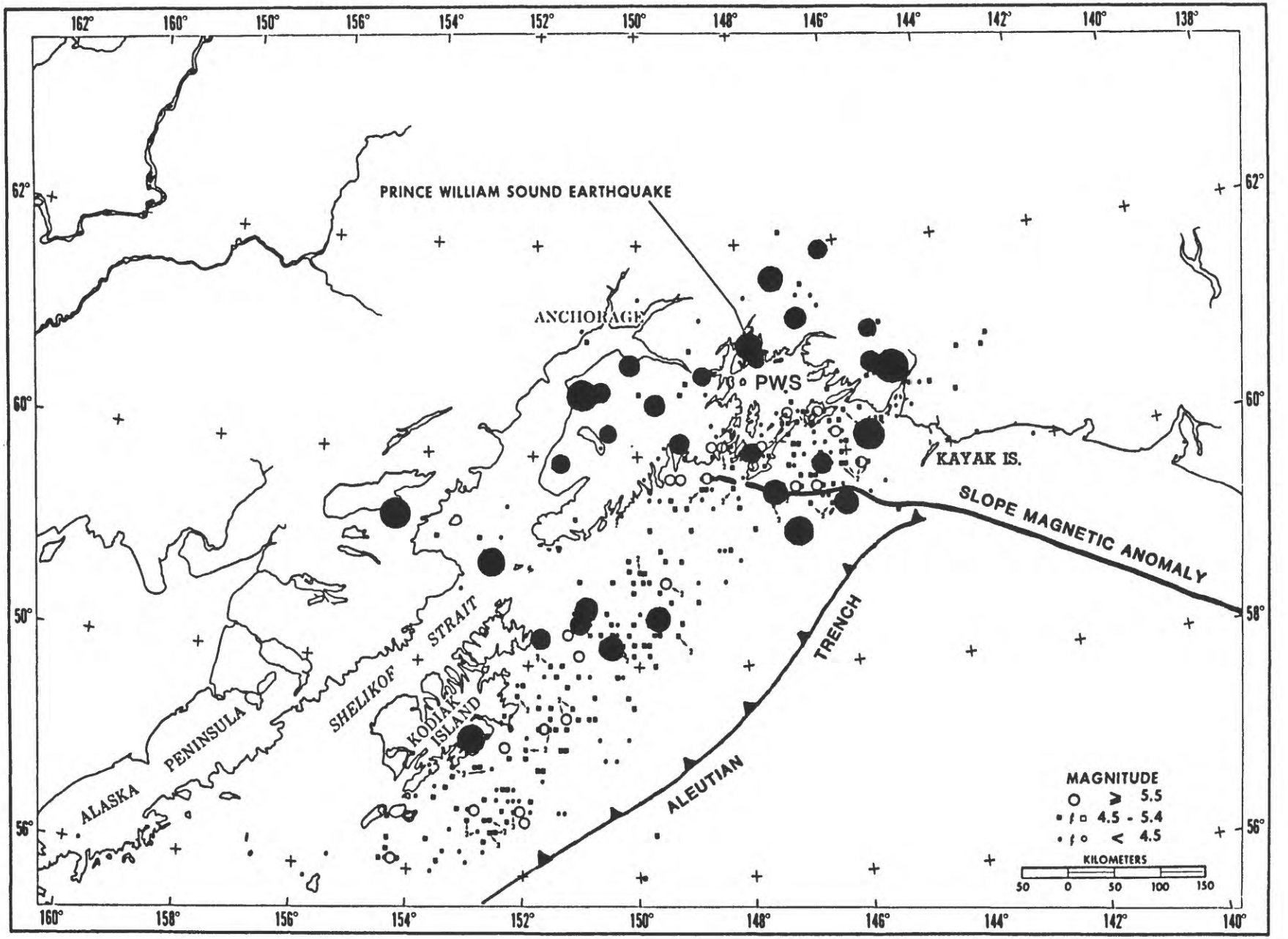
PRINCE WILLIAM SOUND EARTHQUAKE
ANCHORAGE
PWS
KAYAK IS.
SLOPE MAGNETIC ANOMALY
TRENCH
ALEUTIAN
SHELIKOF STRAIT
KODIAK ISLAND
ALASKA PENINSULA
MAGNITUDE
≥ 5.5
4.5 - 5.4
< 4.5
KILOMETERS
50 0 50 100 150
162° 160° 150° 156° 154° 152° 150° 148° 146° 144° 142° 140° 138°
62° 60° 58° 56°
160° 158° 156° 154° 152° 150° 148° 146° 144° 142° 140°

FIGURE 5

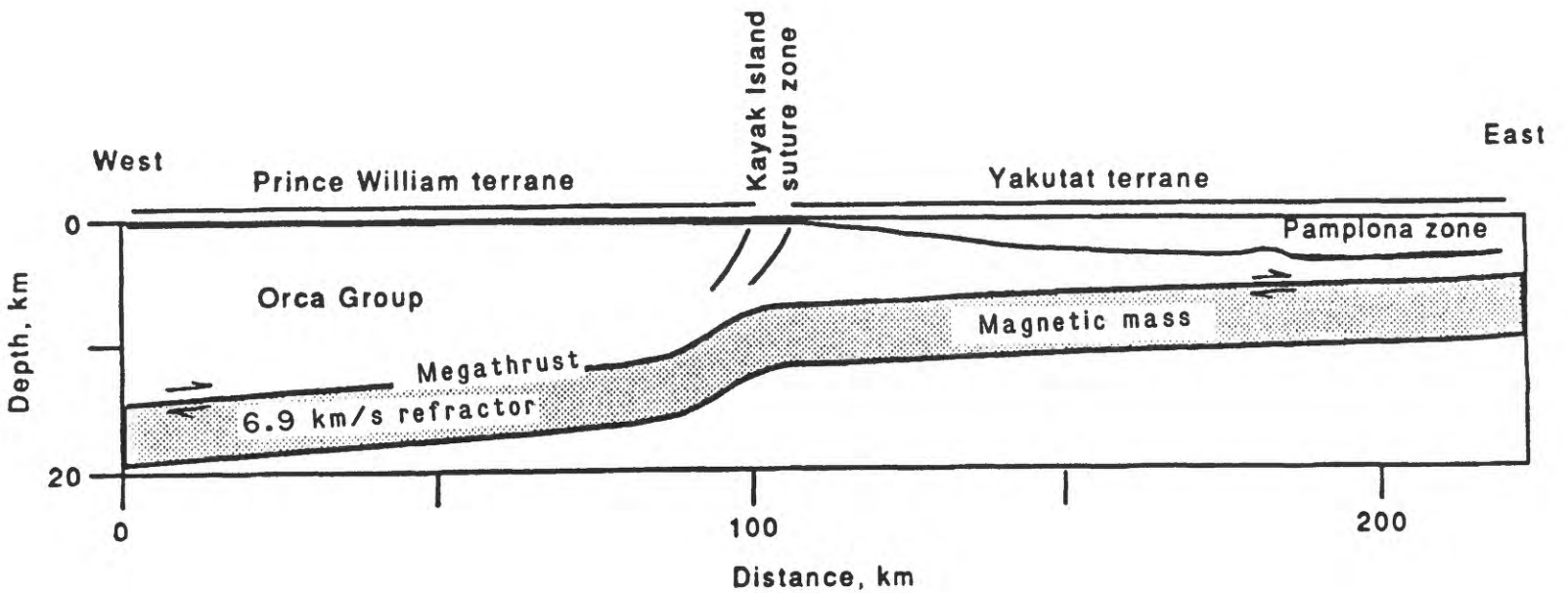
West
Prince William terrane
Kayak Island suture zone
Yakutat terrane
East
Pamplona zone
Orca Group
Magnetic mass
Megathrust
6.9 km/s refractor
Depth, km
0
20
0
100
200
Distance, km

Figure 6

Regional Seismic Network Recording and Analysis Under Technological Change

Steve Malone
Geophysics Program, University of Washington
Seattle, WA 98195 U.S.A.

The basic goals of a regional (or national) seismic network have changed little over the years; record and process seismic data for research, educational and public information uses. Recent technological improvements mean that these goals can be met using more and higher quality data and more quickly. The challenge to the network operator is to take advantage of new technology where it is cost effective without getting bogged down in development and implementation projects. How this is done is dependent on the size and purpose of the network. Seismic networks can be broken down roughly by area covered and number of stations into four categories (Table 1). In each of these categories recent technological changes are effecting the quantity and quality of seismic data gathered and the processing and analysis of those data.

TABLE 1. SEISMIC NETWORKS (Examples)

International Networks
- IRIS GSN - Global
- MedNet - Southern Europe, northern Africa
- POISIDON - Japan, eastern Pacific
- ORFEUS - Europe
- ISC - International coordination

National Networks
- US National Seismic Network
- JMA National Network
- Canadian National Seismic Network

Regional Networks (25-500 stations)
- USGS (CalNet, Hawaii, Southern Great Basin ...)
- Other Federal agencies (DOE, USBR...)
- University run (Washington, Utah, Nevada, Alaska....)
- State run (CDMG in California..)

Local Networks (<25 stations)
- University run (VPI, Boston College, MIT,....)
- State run (Idaho, Kansas....
- Private run (Usually near major power plants or dams)

Recent technology changes effecting seismic networks fall into three general categories:

1. New broad-band sensors and high resolution data loggers.
2. Rapid evolution of computer size and speed.
3. Local and wide-area computer network standardization and proliferation.

Improvements in sensor and data-logger technologies have largely effected the international and national networks, though even for most of these networks 20 year old technology is the backbone of the systems. Recent computer innovations and low prices have primarily effected the regional and local networks such that virtually all such networks are recorded digitally even if the telemetry from station to recording computer is still analog. Recent improvements in wide-area digital communications is just starting to make an impact on seismic networks. Two examples are the satellite telemetry used by the US National Seismic Network and the distributed *GOPHER* system of the IRIS GSN rapid data

retrieval system. An example of the integration of this latter system in a conventional regional network is currently taking place at the University of Washington which operates the *Washington Regional Seismograph Network* (WRSN).

The WRSN is a typical medium to large sized US seismic network largely made up of field equipment from the 1960s and 1970s and recording technology of the early 1980s. Most seismic data is telemetered via telephone, microwave, or radio voice grade circuits in analog form from single component field sites to the central recording site in Seattle (Figure 1). Here it is digitized at 100 samples per second per channel and processed automatically for event detection and preliminary location parameters. Routine manual analyses of these data are done using computer graphics displays within a few days of recording to determine location, size, and focal mechanism parameters for each detected earthquake. Reduced data and earthquake catalogs are provided immediately to other researchers and the public through a variety of means including electronic mail, FAXes and a computer bulletin board.

With the recent availability of high quality sensors and data-loggers the challenge is to rapidly integrate data from these new instruments with the older analog telemetry data. This is done easily by using the *GOPHER* dial-up system developed for the IRIS GSN (Figure 2). This system, as it runs at the IRIS Data Management Center (DMC), takes as input preliminary location information about world-wide earthquakes from the USGS National Earthquake Information Center (NEIC). P-wave arrival times for an earthquake are computed for each of the GSN stations around the world with dial-up capability. *GOPHER* then "goes for" the data by telephoning each station and down-loading selected time wave-form segments to the main DMC machine. The actual telephone calls are placed by several different computers around the world interconnected by the InterNet, a global computer network using a standardized, non-proprietary protocol (Figure 3). Data for each event is kept in a simple and popular format (SAC) at the IRIS DMC (and other data centers) and a menu driven user interface is provided on an open login account so anyone can access the data.

One of the IRIS remote *GOPHER* machines is located at the University of Washington, on the same local computer network as the machines used to record and process data from the WRSN. This local *GOPHER* receives requests from the IRIS DMC to dial-up US GSN stations and retrieved data for earthquakes of international interest; however, it also receives requests from a WRSN computer to retrieve data for events of local interest from both GSN stations and similar stations operated as part of the WRSN. A few modern high-quality stations are being added to the WRSN to improved the data quality for local earthquakes. Because continuous telemtry of three-component high-dynamic range data is not cost effective data from these stations are recovered using dial-up telephone calls by the *GOPHER* system only for events detected by the conventional analog regional network.

Several other regional seismic networks, including two in California, and one in Japan are using the *GOPHER* system to access data from their own high quality stations as well as the GSN set of stations and are using their own analog networks rather than alerts from the NEIC to trigger data retrieval. The integration of this *GOPHER* acquired data with the older, lower quality data is still under development. Combining wave-form data of differing types and from different networks is a problem plagued by multiple formats, different computer operating systems, and lack of motivation. One hope for the future is to have all data, from both the new high-quality stations as well as the older single-component stations in a standard format so that all data from different networks can be merged together and analyzed as a single data set.

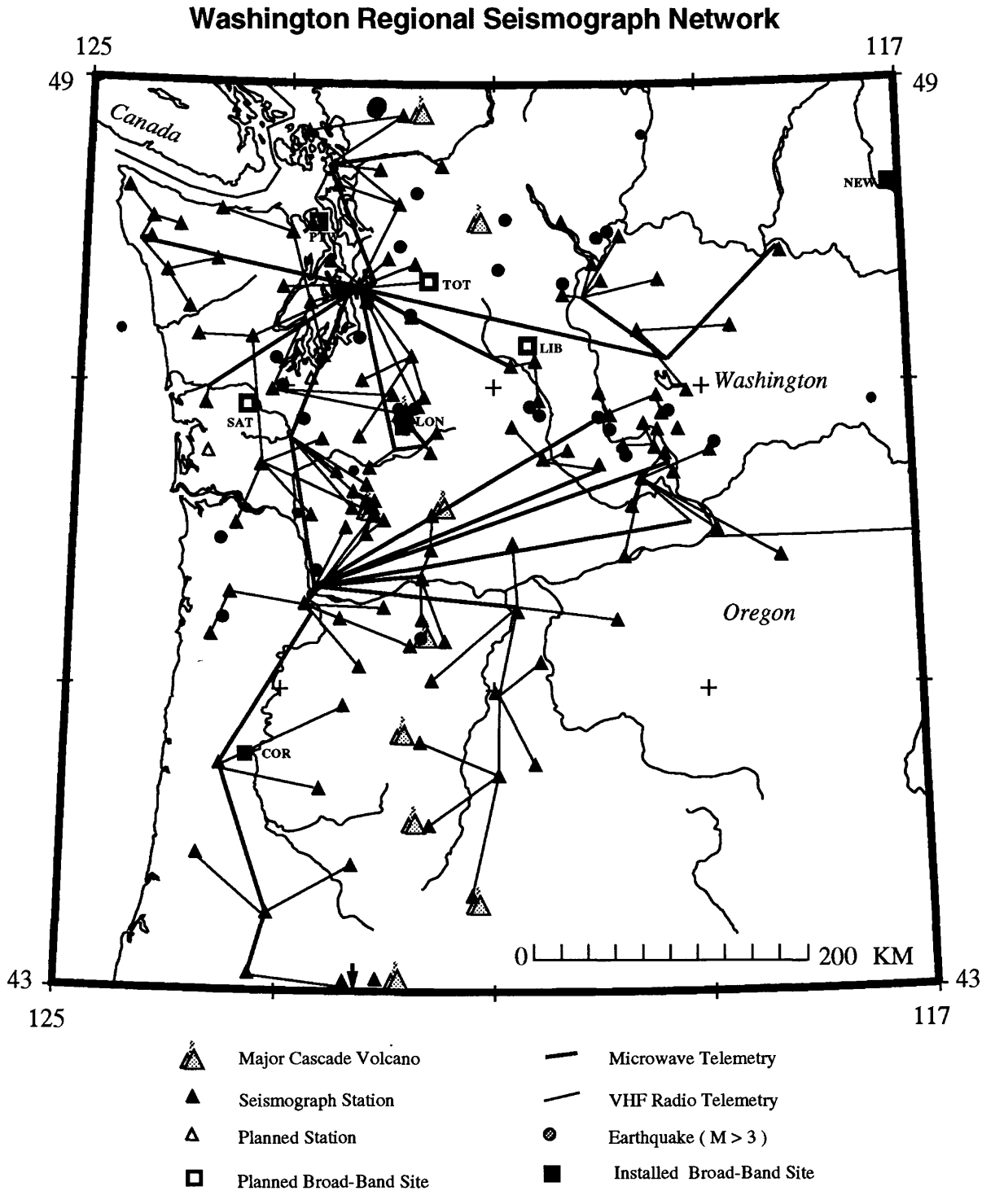

FIGURE 1. Washington Regional Seismograph Network showing conventional short-period telemetry stations (triangles), new high-quality stations (squares), and recent larger (M>3) earthquakes (circles).

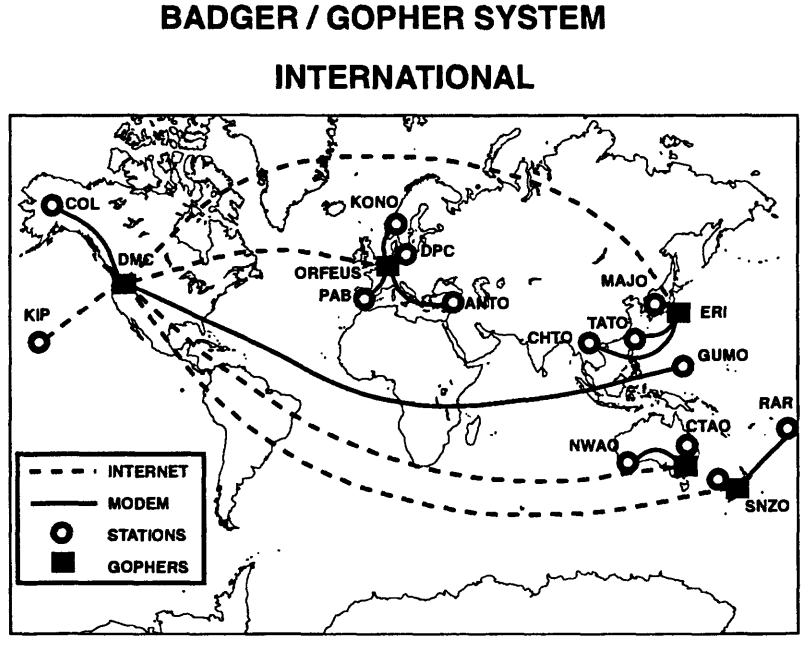

FIGURE 2. World map showing the IRIS GOPHER stations and machines used to call them as controlled by the BADGER system at the DMC. There are seven additional stations in the US called by the domestic GOPHER system located at the University of Washington and California Institute of Technology.

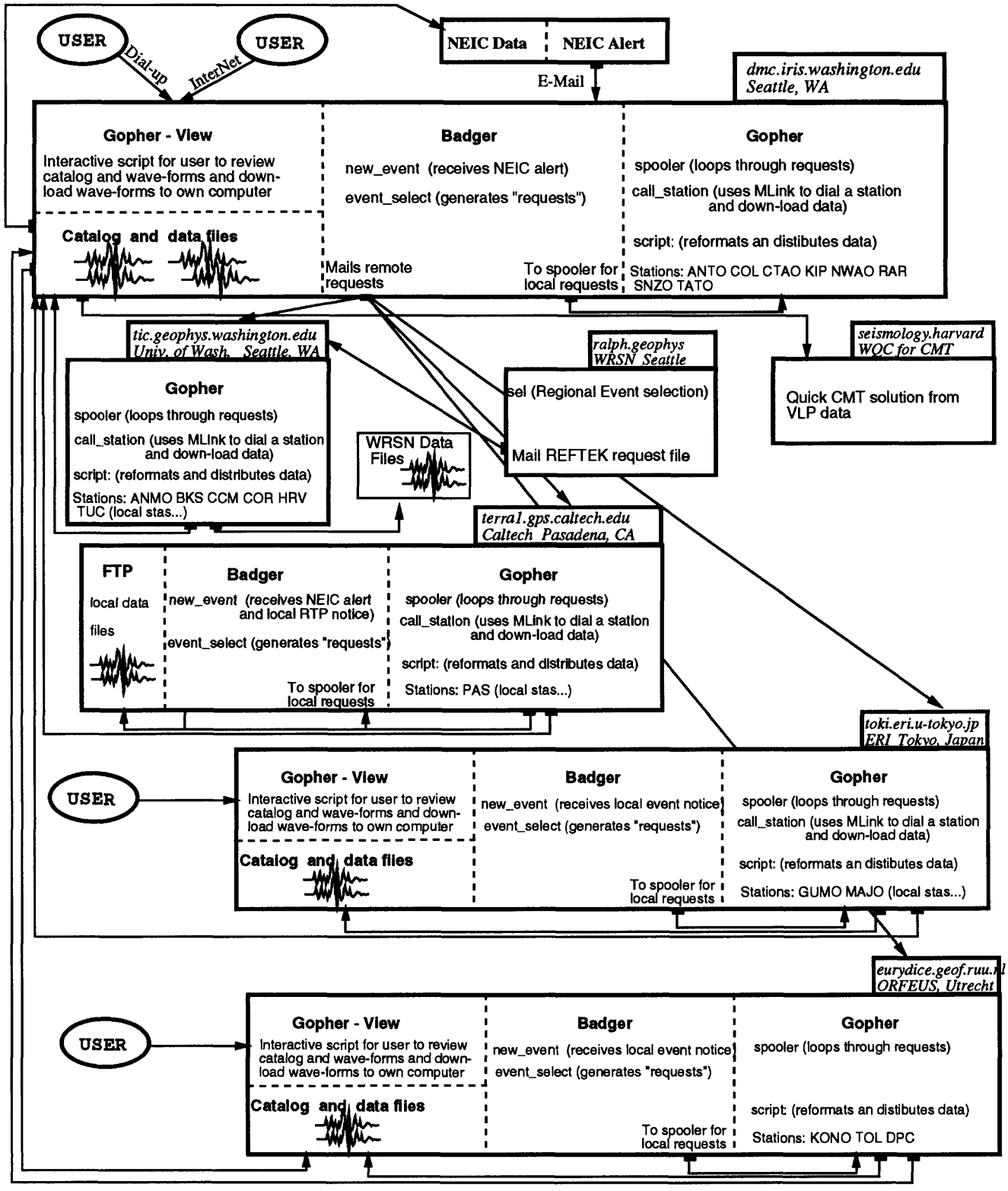

FIGURE 3. Block diagram of current Badger/Gopher system as it is run for IRIS.

The plan for intensified observational facilities for prediction research of earthquakes occurring in the Tokyo metropolitan area

Kazuo Hamada

NIED:National Research Institute for Earth Science and Disaster Prevention
Tsukuba-shi, 305 Japan

The plan consists of one 3000-m deep borehole station, twelve 2000-m borehole stations, six cable-type OBSs, and twelve GPS stations. All the borehole stations have a three-component set of seismometers and a two-component set of tiltmeters.

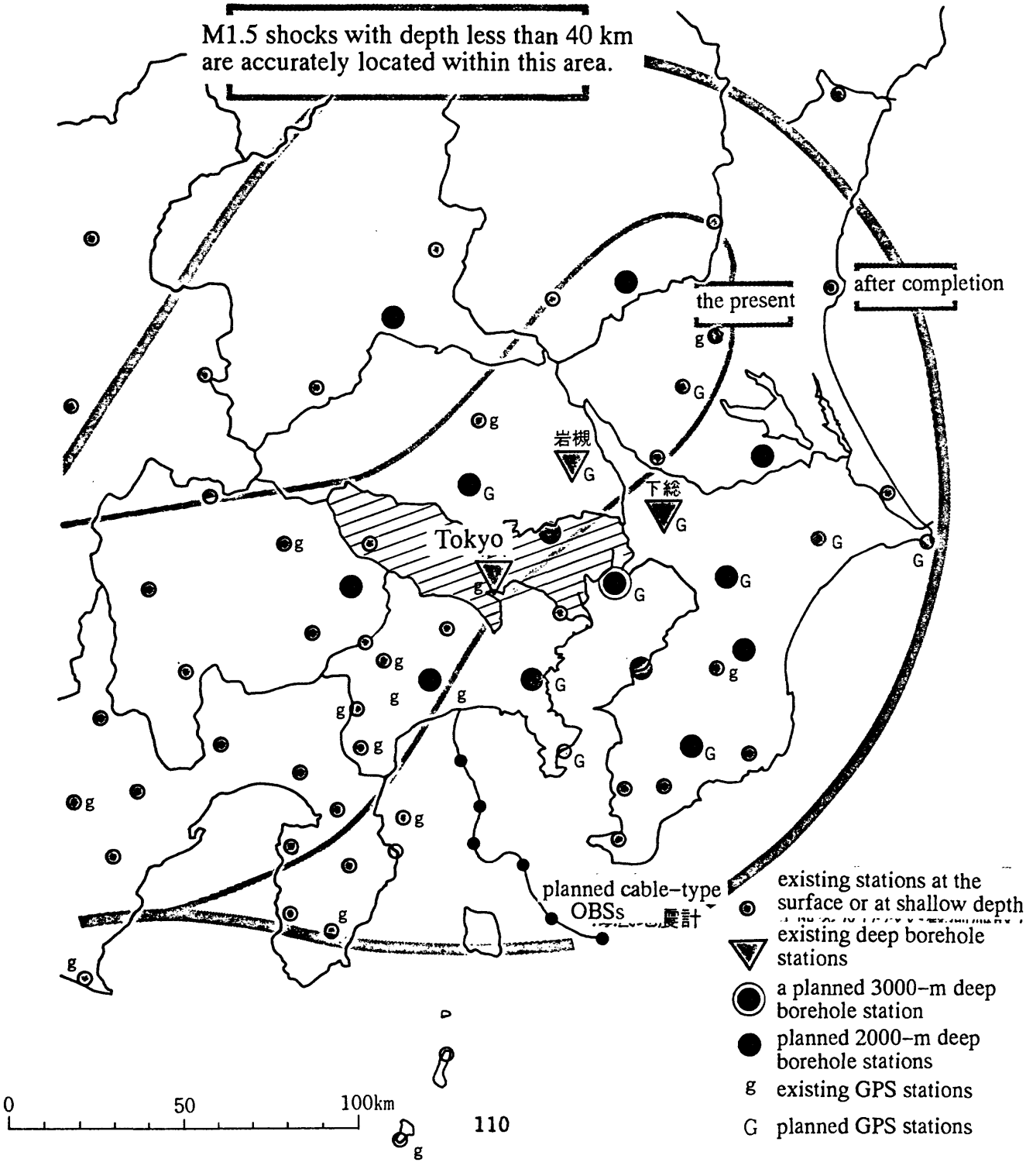

PROBING THE ACTIVE SUBDUCTION ZONE OF THE PACIFIC NW, USA

W.D. Mooney, J. Luetgert, and E. Criley (all at: U.S. Geological Survey, 345 Middlefield Rd., MS977, Menlo Park, CA 94025)
K. Miller, J. Gridley and G.R. Keller (University of Texas-El Paso)
A. Tréhu and J. Nabelek (Oregon State University, Corvallis, OR)
N.I. Christensen (Purdue University, West Lafayette, IN)

Despite the importance of the Pacific Northwest as a natural laboratory of active tectonic processes, and of seismic and volcanic hazards, only a limited amount of deep seismic profiling has been conducted in this region. We began to address this deficiency in September, 1991, with a major active seismic field program (Figure 1) consisting of three seismic refraction/wide angle reflection profiles located (1) on the east flank of the Puget Sound Basin of Washington (N-S profile); (2) on the west flank of the Willamette Lowland of Oregon (N-S profile); and (3) across the central Oregon Coast Ranges and up to the foothills of the Cascades Range (E-W profile).

Several scientific objectives have been targeted in this work:

- Determination of the relationships between seismicity and structure - What is the relationship between forearc seismicity and crustal and upper mantle structure? Are there structural boundaries/offsets that have not yet revealed themselves in the seismicity?
- Determination of the structure of sedimentary basins west of the Cascades, such as the Chehalis Basin. How have these basins evolved as accretion has continued to the west?
- What has been the role of tectonic and magmatic underplating in building the continental crust? How much crust has been added by these processes?
- What is the crustal thickness and composition of the Coast Range and does it vary across strike? Is the crustal structure of the Coast Range purely a product of accretionary processes and/or later tectonic events?
- What is the nature of the eastern boundary of the Coast Range? Does it possibly influence the localization of Cascade volcanoes?

During the field project a total of 10 large bore-hole shots, ranging in size from 900 to 1800 kg, were recorded by a large complement of seismographs, including: 200 Seismic Group Recorders (SGRs), 185 PRS-1s, 18 PRS-4s, 30 6-channel REFTEKS, 120 FM-Cassette recorders, and two 96-channel seismic reflection spreads. These profiles provide more than 330 km of deep seismic data, which defines the crustal and upper mantle structure in unprecedented detail.

Preliminary data interpretation indicates a crustal thickness of ~43 km beneath the profile in Washington State (Figure 2). We have identified a 20-km-thick high-velocity lower-crustal layer that may have been thickened by mafic intrusions. In the upper crust, several fault-bounded basins are clearly outlined by first-arrival traveltime data.

The N-S seismic profile in Oregon indicates a substantially thicker crust (more than 30 km) than appears in many previous geophysical interpretations. The average crustal velocity is high (6.8 km/s or greater), and is indicative of substantial amounts of mafic rocks in the deep crust, in agreement with the positive Bouguer gravity anomaly. Strong wide-angle reflections from depths of 40+ km may be from the subducting Juan de Fuca plate. The crustal seismic velocities determined from the 1991 Oregon seismic refraction data are in excellent agreement with laboratory velocity measurements made at high pressure on rock samples collected in the Coast Ranges.

These data provide excellent velocity and structural control for the crust and upper mantle in the fore-arc and Cascades region and provide constraints on the interpretation of gravity, aeromagnetic, magnetotelluric, seismic reflection, and seismicity data. The resultant structural framework is essential

to the accurate evaluation of mechanisms for crustal earthquakes and will substantially improve our ability to locate and evaluate earthquakes recorded by the existing earthquake net.

References:

Luetgert, J.H., Mooney, W.D., E. Criley, G.R. Keller, J. Gridley, K. Miller, A. Tréhu, J. Nabelek, S.B. Smithson, C. Humphreys, N.I. Christensen, R. Clowes, and I. Asudeh, 1991. Crustal Architecture of the Pacific NW: The 1991 Seismic Field Experiment, EOS, 72:44:323.

Luetgert, J.H., Mooney, W.D., E. Criley, G.R. Keller, J. Gridley, K. Miller, A. Tréhu, J. Nabelek, S.B. Smithson, C. Humphreys, N.I. Christensen, R. Clowes, and I. Asudeh, 1992. Crustal velocity structure of the Pacific NW: The 1991 Seismic refraction/wide-angle reflection experiment, GSA Abst. with Programs, 24:5:66.

Mooney, W.D., J.Luetgert, E. Criley, G.R. Keller, J. Gridley, K. Miller, A. Tréhu, J. Nabelek, S.B. Smithson, C. Humphreys, N.I. Christensen, R. Clowes, and I. Asudeh, 1991. The 1991 Pacific Northwest Seismic Field Experiment, EOS, 72:44:326.

Tréhu, A. M., J.N. Nabelek, S. Azevedo, T.M. Brocher, J. Luetgert, W.D. Mooney, I. Asudeh, R. Clowes, G.R. Keller, K. Miller, and Y. Nakamura, 1992. Crustal Structure of the Cascadia Subduction Zone Beneath Western Oregon, GSA Abst. with Programs, 24:5:66.

Holbrook, W.S., W.D. Mooney, and N.I. Christensen, 1992. Seismic velocities in the lower continental crust. In: D.M. Fountain, ed., The Lower Continental Crust. Elsevier, Amsterdam, 1-30.

Luetgert, J.H., 1992. Interactive two-dimensional seismic raytracing for the Macintosh™. U.S.G.S. Open File Report 92-356.

Mooney, W.D. and R. Meissner, 1992. Multi-genetic origin of crustal reflectivity: a review of seismic reflection profiling of the continental lower crust and Moho. In: D.M. Fountain, ed., The Lower Continental Crust. Elsevier, Amsterdam, 31-52.

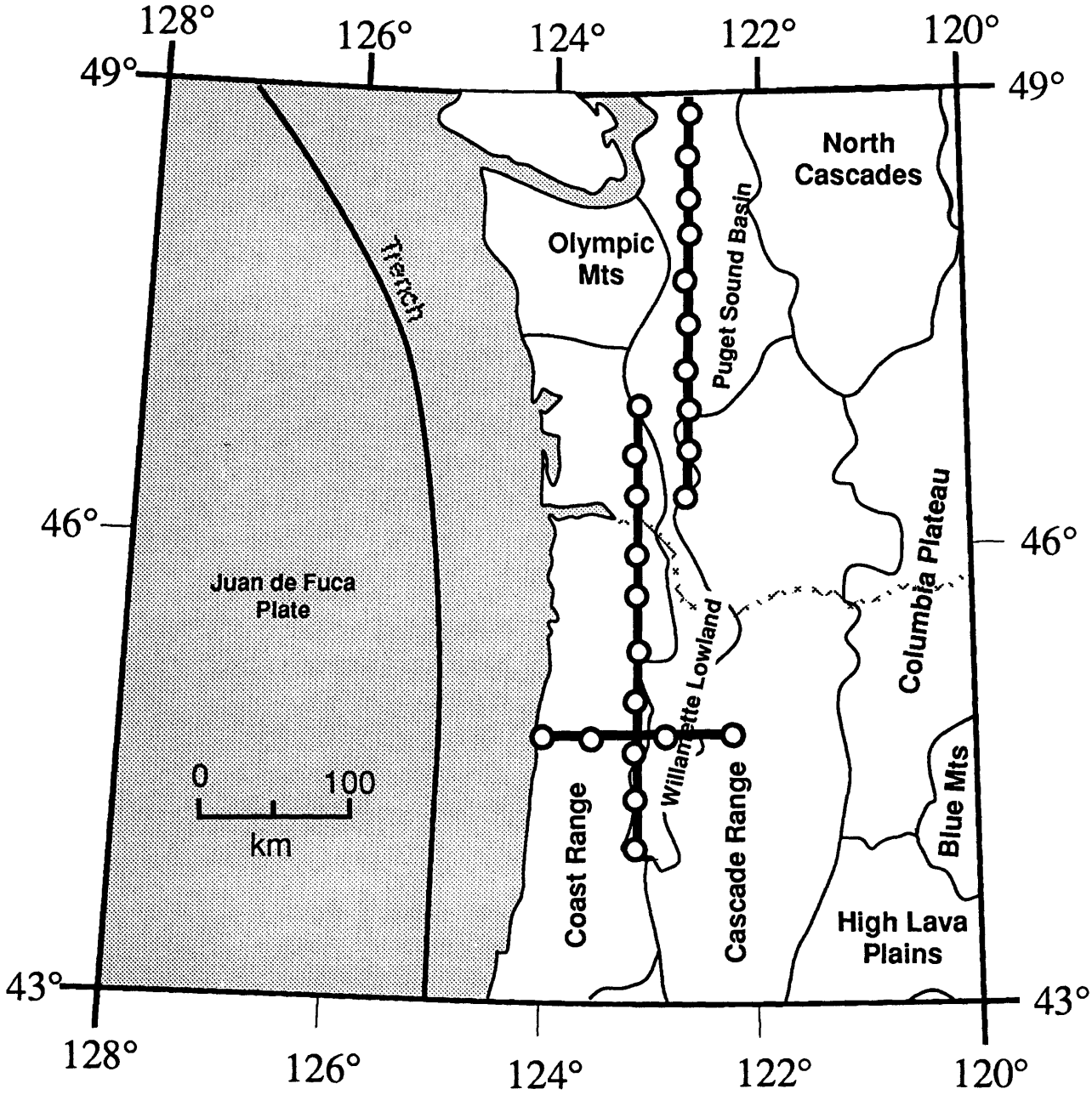

Figure 1. Location of 1991 seismic refraction profiles in Washington and Oregon.

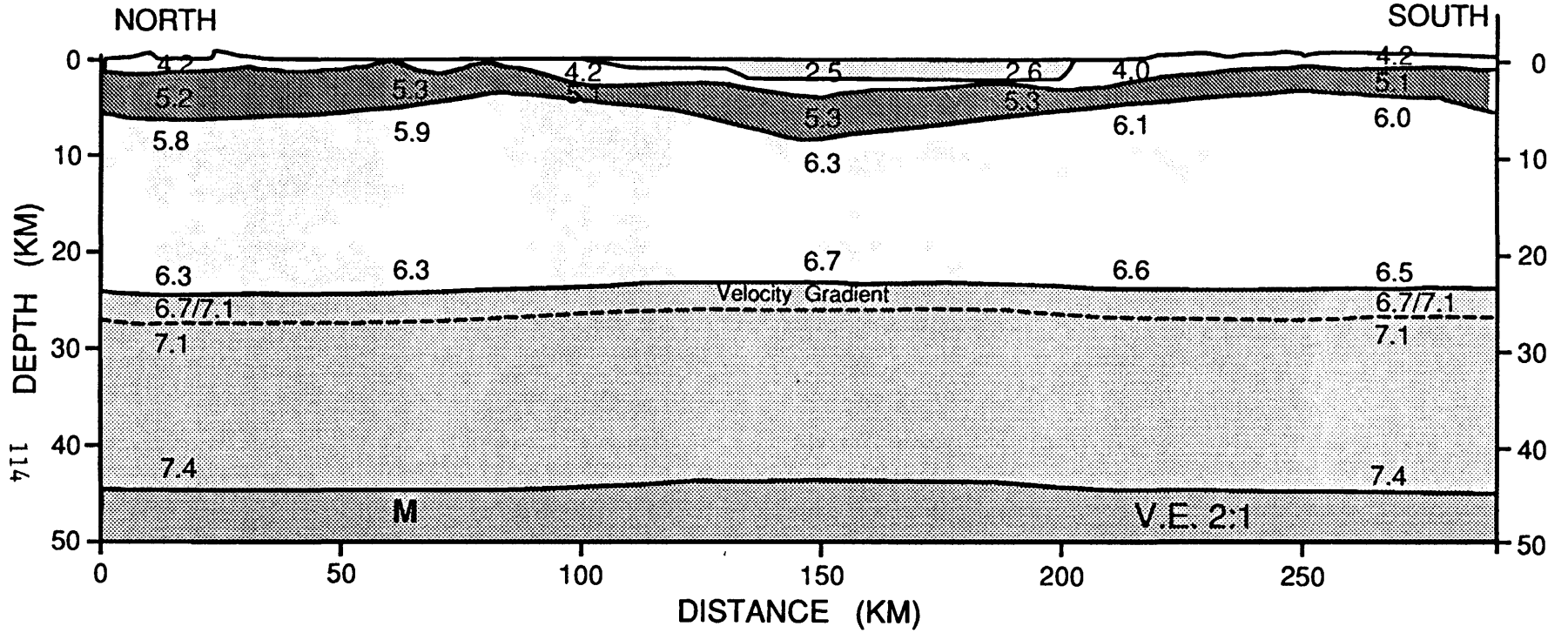

Figure 2. Preliminary crustal model derived from 1991 profile in Washington State.

Cascadia Subduction Zone: Large Scale Structure Studies

R. S. Crosson (Geophysics Program, University of Washington, Seattle, WA 98195; 206-542-8020)

Our current understanding of Cascadia subduction zone structure stems largely from diverse seismic observations. Critical seismic velocity structure of the subducted slab comes from marine refraction and reflection measurements, and shallow subduction zone structure is constrained by onshore/offshore active experiments. Reference continental seismic velocity structure comes from refraction measurements and inversion of earthquake arrival time data, with newer refraction/reflection results emerging. Beneath western Washington, the slab is active seismically while exhibiting only weak seismicity to the north beneath British Columbia and to the south beneath Oregon. Thus, seismicity give us a restricted, although information rich, window on subduction zone structure.

Independent and complementary interpretations of slab structure have been made from receiver function analysis at selected continental sites along the subduction zone. These, combined with seismicity, give us the clearest picture of an upwarp in the slab beneath the Olympic - central Puget Sound region. The upwarp accommodates plate deformation required by present trench geometry, and provides a rational mechanism for the Olympic uplift. Beneath the Olympic - central Puget Sound region, the slab dips about 10° to the east or east northeast. Steeper dips of 15-20° are typical at the same distance from the trench to the north and south. Independent evidence from the observation of anomalous P phases suggests that the subducted oceanic crust acts as a low velocity waveguide where the slab lies beneath the continental Moho. Most intraslab earthquakes appear to originate within the subducted oceanic "upper mantle" region.

Slab structure deeper than 80-100 km is most readily imaged by teleseismic tomography. Recent work by VanDecar has shown that the slab steepens to a 50° dip angle beneath Washington, but that the deep slab signature decreases from southern Washington southward to Oregon, leading to speculation of slab tearing possibly resulting from changes in subduction kinematics.

Results of Recent Geodetic VLBI Experiments by the Communications Research Laboratory

By

T. Yoshino, F. Takahashi, H. Kunimori
(Communications Research Laboratory, 4-2-1, Nukui-kita, Koganei, TOKYO 184, JAPAN)

Y. Koyama, K. Heki
(Kashima Space Research Center, 893-1, Hirai, Kashima, IBARAKI 314, JAPAN)

J. Amagai
(Science and Technology Agency, 2-2-1, Kasumigaseki, Chiyoda, TOKYO 100, JAPAN)

T. Kondo
(Hiraiso Solar Terrestrial Research Center, 3601 Isozaki, Nakaminato, IBARAKI 311-12, JAPAN)

and

S. Matsuzaka, M. Tobita, S. Matsumura, M. Murakami
(Geographical Survey Institute, 1 Kitasato, Tsukuba, IBARAKI 305, JAPAN)

ABSTRACT

In this paper, we describe the results from recent geodetic experiments organized by the Communications Research Laboratory (CRL) using Very Long Baseline Interferometry (VLBI).

A VLBI station on Minamitorishima (Marcus Island) located on the only Japanese island on the Pacific plate, has been operated since 1989 for the geodetic VLBI experiments with Kashima station and a Chinese station located near Shanghai. Position of the Minamitorishima station was first determined in 1989. VLBI experiments have been conducted every year since. The Minamitorishima-Kashima baseline is found to be getting shorter by about 7.7 cm/year, which is significantly smaller than the value predicted by the geological plate motion model assuming these station fixed on the Pacific and the Eurasian plates respectively. This difference is explained partly by a displacement of Kashima station with respect to the Eurasian plate due to the east-west contraction of the Northeastern Japan, and partly by an excess velocity of the Pacific plate around the Minamitorishima caused by the episodicity of the plate convergence at the Japan Trench.

Baseline length change with the Shanghai VLBI station suggests that this station is moving east-southeastward by about 1 cm/year with respect to the stable interior of the Eurasian plate. This may be the first space geodetic evidence that the collision of the Indian continent to the Eurasian plate is causing large scale eastward extrusions of several blocks in the Eastern Asia.

CRL has been conducting domestic geodetic VLBI experiments in collaboration with the Geographical Survey Institute (GSI), e.g. JEG (Japanese Experiment for Geodesy) series which started as single baseline experiments between Kashima and the GSI's Tsukuba VLBI station which is about 50 km west of Kashima. Geodetic VLBI experiments were conducted using this baseline more than ten times from 1984 to 1991. There has been no significant changes in this baseline vector so far and this baseline is now used as a 'standard' VLBI baseline for research and development purposes.

Since 1992, two new stations were added to form a new VLBI network surrounding the Tokyo metropolitan area. Bi-monthly VLBI experiments are done on this network to understand the crustal deformation in the area which is important to make earthquake predictions in this area possible.

1. Western Pacific VLBI experiments

1.1 Introduction

The Western Pacific VLBI Network (WPVN, Fig.1) was constructed by the Communications Research Laboratory (CRL) to study relative movements of the tectonic plates in and around Japan by repeated geodetic VLBI observations among the stations located on these plates. The network consists of Kashima station (34 m new multi-frequency antenna and older 26 m antenna) on the Japanese mainland (normally considered to reside on the Eurasian plate), Minamitorishima station on the Pacific plate (the only Japanese island on this plate) and Minamidaito station on the Philippine Sea plate. Shanghai VLBI station operated by Shanghai Observatory, the Chinese Academy of Sciences also takes part in the observation regularly. The Minamitorishima VLBI station was newly installed as a fixed station with a 10 m antenna on the island in 1988 (Hama & Amagai, 1990). WPVN has been regularly operated every year since 1989 and the baseline length changes between Kashima, Shanghai and Minamitorishima stations are estimated with an accuracy better than 1 cm/year. In this chapter, we briefly describe WPVN experiments and discuss about the geodynamic implications of the obtained baseline length changes. The motion of the Minamidaito station is not discussed in this paper because of small number of experiments.

1.2 Experiments

New K-4 (Hama et al., 1990; Kiuchi et al., 1990) terminals developed by CRL, were utilized in some domestic VLBI experiments instead of Mark-III (Clark et al., 1985) and K3 (Kawaguchi et al., 1982) VLBI data acquisition terminals because it is compact, reliable and easy to operate. A compact frequency standard system consisting of a highly stable crystal oscillator and a Cesium-beam clock (Kiuchi et al., 1989) was used at the Minamitorishima station instead of a conventional hydrogen

maser. This frequency standard requires shorter integration time (typically 120 seconds) at a data processing so that we may not lose the signal coherence during the integration period and to obtain maximum signal-to-noise ratios. Taking account of the time necessary to attain tape synchronization in the correlation processing, 196 seconds period was chosen as the actual observation time. This relatively short integration time means that we have to choose stronger radio sources in the observation schedules.

In the first geodetic VLBI experiment by WPVN conducted in 1989, local radio interference was found to affect seriously in the S-Band data at Minamitorishima station. From the next experiment, the observation frequencies were shifted to avoid such interferences. In 1990, in addition to the regular stations, namely Kashima, Shanghai and Minamitorishima, the Fairbanks VLBI station joined one of the experiments. In 1991, in order to get more precision in geodetic results, continuous 168 hour (7 days) VLBI experiments were conducted between Kashima and Minamitorishima stations. The Shanghai stations took part in two 24-hour portions of this long observing session. In 1992, VLBI experiments were done twice using Kashima, Minamitorishima and Shanghai stations.

1.3 Data Analysis

In the baseline analysis, we used only the group delay data. Our data analyses are based on the following two software systems. The first one is the CALC (ver.6) developed by the Goddard Space Flight Center (GSFC). It is used for the calculation of the partial derivatives and the theoretical delays. The other one is our own software system called Acos Software System (ASS), which is used for the least-squares parameter estimation. Data analyses are performed independently for individual observing sessions. Cable delay corrections are applied to all the observed delay data. Ionospheric delay corrections are done by forming an ionosphere-free linear combination of the delays in two observing frequencies (X and S bands). Clock offsets were modeled as polynomials of time and breaks were inserted where necessary. Dry components of tropospheric delays are removed beforehand using the Saastamoinen model (Saastamoinen, 1972) to calculate the zenith delays and the CFA2.2 mapping function (Davis et al., 1985) to convert them to the line-of-sight directions. This mapping function is also used when we estimate the wet components of tropospheric zenith delays. They were modeled as continuously changing values with new changing rates estimated every six hours. An a-priori constraint of 50 psec/sec was applied as the changing rate differences between adjacent intervals (Heki, 1990).

To estimate the station coordinates, the position of Kashima is fixed because it is well determined in the terrestrial reference frame. In some of the experiments, the older 26 m antenna in Kashima was used instead of the main 34 m antenna. In these cases, the obtained baseline vectors were converted to those with 34 m antenna using the baseline vector between these two antennas which had been independently determined by VLBI experiments (Koyama et al., 1991).

1.4 Geodetic results

Baseline length changes between Kashima, Shanghai and Minamitorishima stations are shown in Fig.2(a-c). In addition to WPVN experiments, Kashima and Shanghai have been regularly participating in

international VLBI experiments called PPM-S (Pacific Plate Motion - South) where Fairbanks (Alaska, USA), Kauai (Hawaii, USA) and Tidbinbilla (Canberra, Australia) are participated. Baseline length obtained in these experiments (Ma et al., 1992) are also included to analyze the Kashima-Shanghai baseline vector change.

Heki & Yoshino (1990) gives two different predictions for the baseline length changes for these stations. The first estimate is based on the assumption that the Shanghai and Kashima stations are fixed on the Eurasian plate and that the Minamitorishima station is fixed on the Pacific plate. The first predicted baseline length changes are-9.0 cm/yr (Kashima-Minamitorishima), -9.6 cm/yr (Shanghai-Minamitorishima) and 0.0 cm/yr (Kashima-Shanghai). We used NUVEL1 model (DeMets et al., 1990) as the plate motion model. The second prediction takes account of the displacement of the Kashima station with respect to the Eurasian plate due to the east-west contraction of the Northeast Japan (Heki et al., 1990). This contraction is thought to be caused by the compressional stress fields applied by the subducting Pacific plate. In the second prediction, changing rates of the baseline length are -6.8 cm/yr (Kashima-Minamitorishima), and -2.2 cm/yr (Kashima-Shanghai). In both of these predictions, Shanghai and Minamitorishima stations are assumed to be fixed on the Eurasian and Pacific plates respectively. We test the validity of this assumption in the following section.

1.4.1 Movement of Shanghai

Observed baseline length change between Kashima and Shanghai is -2.90 +/- 0.26 cm/yr. This supports our assumption that the Kashima station is moving west-northwestward with respect to the stable interior of the Eurasian plate. However, the observed rate is significantly (at 95 % confidence level) larger than the predicted one (-2.2 cm/yr). Because the movement of Kashima station is based on the actual measurements by VLBI (i.e., no assumption was made on its movement), this is considered to be due to the movement of Shanghai station with respect to the Eurasian plate. In order to clarify the movement vector of Shanghai, we studied the baseline length changes between Shanghai and other stations in the PPM-S VLBI network, which consists of Fairbanks (Alaska, North American plate), Kauai (Hawaii, Pacific plate) and Tidbinbilla (Canberra, Australian plate). These baselines have been measured since 1988.

According to NUVEL1, the baseline length change between Shanghai and Fairbanks is -0.3 cm/yr while the observed change was -0.79 +/-0.24 cm/yr. This is slightly smaller than the prediction but the difference is not significant. Baseline length change in Shanghai-Fairbanks and Shanghai-Kauai are observed to be -8.00 +/- 0.27 cm/yr and -6.06 +/- 0.33 cm/yr respectively. NUVEL1 predicts them to be -7.29 cm/yr and -5.31 cm/yr respectively. Hence the differences between them are significant (> two sigmas). These differences suggest that the Shanghai station is moving east-southeastward with respect to the stable interior of the Eurasian plate.

We can estimate the horizontal movement of a station using baseline length change assuming that the difference between predicted and observed changes are due to the movement of this station with respect to the plate on which the station is supposed to reside. In this case, horizontal velocity of Shanghai with respect to the Eurasian plate is estimated to be 9.4 mm/yr toward N102E (depicted as 'observed-1' in

Fig.3). This is also found to be significantly (at the 99% confidence level) different from zero.

Ma et al. (1992) gives the velocities of all the VLBI stations in the world obtained by a combined parameter estimation using all the geodetic VLBI data. Because VLBI can only determine the 'relative' positions, there is, however, a rotational and translational freedom in these vectors. We estimated three rotations about geocentric x,y and z axes so that the velocities of some of these stations best coincide with those predicted by no-net-rotation NUVEL1 (nnr-NUVEL1) model (Argus & Gordon, 1991). We selected Kauai, Fairbanks, Wettzell(Germany) and Onsala (Sweden) stations to obtain the rotation values. They all lie in the stable interior of the plate and their velocities are very well determined by frequent VLBI observations. Then by applying the obtained rotation for all the stations, we got the velocity vector of each station in the nnr-NUVEL1 frame. Then by comparing these vectors with those calculated from nnr-NUVEL1, we get displacement vectors of the stations with respect to the plate to which the station is supposed to belong. It is shown in Fig.4 as 'observed-2'. It is well coincident with 'observed-1'.

Molnar & Tapponnier (1975) suggested that the northward movement of the Indian plate after its collision about 40 Ma ago with the Asian continent is partly compensated by the eastward extrusion of several continental blocks. Recently Armijo et al. (1989) analysed the displacement rate of major strike-slip faults in the Central Asia and proposed the instantaneous movement parameters (Euler pole position and rotation rate) of one of the blocks (North Tibet block) which is being extruded. We tentatively assume that this North Tibet block and the South China block to which Shanghai belong move as a single block. This assumption may not be appropriate because there is a reverse fault system (Lungmen Shan Faults) between these blocks which may make the eastward movement of the South China block smaller. However, this assumption would give us the maximum estimate of the eastward movement of the Shanghai station. The 'expected' vector in Fig.3 shows the calculated velocity assuming the south China block rotates about the same Euler pole as the north Tibet block. It is about 1.2 cm/year in the direction of N100E (Fig.3). The observed vectors are slightly shorter but in the same direction as the expected vector. This strongly suggests that the observed movement of Shanghai station is explained by the eastward extrusion of the South China block associated with the collision between the Indian and the Asian continents.

1.4.2 Movement of Minamitorishima

Fig.2a and 2c show the length change of the Kashima-Minamitorishima and Shanghai-Minamitorishima baselines. The former baseline length is changing at a rate of -76.7 +/- 4.4 mm/yr. This is larger than the predicted value of -6.8 cm/yr (Heki & Yoshino, 1990), which is the rate predicted by fixing Minamitorishima on the Pacific plate and introducing the velocity of Kashima in Heki et al. (1990). The difference is slightly larger than the two sigma uncertainty. The changing rate of the latter baseline length is -118.7 +/- 6.7 mm/yr. This is larger than -9.6 cm/yr (Heki & Yoshino, 1990), predicted by fixing Minamitorishima and Shanghai on the Pacific and Eurasian plates respectively. If we assume the movement of the Shanghai station estimated in the previous section, the prediction is -10.5 cm/yr but about one centimeter per year excess

shortening still remains. These may suggest that this part of the Pacific plate is moving faster by about one tenth than NUVEL1 model predicts.

Minamitorishima is about 1000 km from the nearest plate boundary. Heki et al. (1992) showed that episodic movements at the plate boundaries triggers the inward propagation of the velocity 'pulses' into the plate interiors. This process results in the gradual change of the purely episodic ground movements near the boundaries to the purely continuous movements in the interiors. In the area at a medium distance from the boundaries, this model predicts the alternation of the acceleration and slowing down of the plate motions with the period of episodic plate movements at the boundaries. Now we assume 100 km for the lithospheric thickness, 200km for the asthenospheric thickness and 5 x 10E19 poise for the asthenospheric viscosity. Then the irregularity of the plate speed amounts up to plus minus 10 percent of the average velocity (Fig.5), that is, the excess speed of 1 cm/yr of the Pacific plate around Minamitorishima is physically possible. Observed baseline length changes are still not accurate enough and it is still premature to make a decisive conclusion, these experiments may lead us to a better understanding of the physical property of the plates and the subduction process at trenches.

2. Domestic VLBI experiments

2.1 Introduction

CRL and Geographic Survey Institute (GSI) of Japan have carried out a series of geodetic VLBI experiments called JEG (Japanese Experiments for Geodesy) on the 55 km baseline between Kashima VLBI station and a 5 m transportable VLBI station at Tsukuba, about 50 km west of Kashima (Fig.6). This baseline is relatively short and is suitable for intercomparisons with other techniques such as the conventional ground survey results (Imae, 1991) and Global Positioning System (GPS). Both of the station are located in the southern part of the Ibaraki Prefecture, which is considered to be one of the stable regions with little local crustal deformations in Japan (Fujii et al., 1985). Due to these points, this baseline is used for the research and development in Japanese geodetic VLBI as a Japanese 'standard baseline'.

In fact, this baseline has been used to test some innovative VLBI techniques. The compact frequency standard composed of a crystal oscillator and a Cesium-beam clock (Kiuchi et al., 1989) used in the Minamitorishima VLBI station was first tested using this baseline. A wave front clock (Kiuchi & Kondo, 1991) technique was also tested in this baseline.

This baseline have been measured once or twice a year since 1984. In 1992, two more VLBI stations, namely Koganei station with 3m antenna at the CRL, about 30 km west of the central part of Tokyo and the station with 2.4m antenna at Kanozan (Mt. Kano) in Boso Peninsula were added to the original JEG experiment to extend a local VLBI network, which is called the Metropolitan Diamond Cross (MDX) network (Fig.6). MDX experiments were carried out three times in 1992 without Kanozan station. Bi-monthly MDX VLBI experiments are conducted since 1993. In addition to the establishment of the standard baseline, the MDX experiments have another aim to reveal crustal deformation around the

Tokyo metropolitan area where a large earthquake is anticipated in the near future.

2.2 Experiments

We have performed series of JEG experiments thirteen times from 1984 to 1991. K-3 data acquisition systems (Kawaguchi et al., 1982) and hydrogen maser frequency standards were used at both stations. In the first experiment (JEG-1), we determined delays only for 47 observations because the correlated flux density of some radio sources had been overestimated. The observation schedule was improved from the second experiment by including stronger radio sources such as 3C84 and 3C273B. Although they are not point sources, they are not resolved with such a short distance radio interferometer.

2.3 Data Analysis

In the data analysis, tropospheric delays were corrected in the same way as the WPVN experiments except that the zenith tropospheric delays were estimated as the difference from a reference station (i.e., zenith delays of one of the stations was fixed to zero) since the elevation differences are not large enough to enable separation of the tropospheric delays among the stations. Ionospheric delays were not corrected because the baseline length is considered short enough to assume ionospheric conditions for individual stations identical. Station positions, radio source positions and earth orientation parameters were kept consistent throughout the experiments by adopting values in Ma et al. (1989) whenever possible.

2.4 Geodetic results

The estimated positions of the Tsukuba station with respect to Kashima are shown in Fig. 7a. Root mean square dispersion of the estimated position around their mean position is better than one centimeter in the horizontal plane but as large as a few centimeters in the vertical axis due to the lack of the enough number of low elevation observations (Heki, 1990). Fig.7a also indicates that both the error ellipsoids and their dispersion are smaller in winter. This is thought to imply relatively dry tropospheric conditions in this region, where the daily mean vapor pressure fluctuation is usually around 5 mbar in winter while they are from 20 to 30 mbar in summer (Japan Meteorological Agency, person. comm.). Using the Chi-square statistical test at 95 % confidence level, there are no systematic changes in the estimated Kashima-Tsukuba baseline vectors. Fig. 7b shows the estimated positions of the Koganei station newly added when JEG experiments evolved into the MDX experiments. Station position repeatabilities are not so good as the Tsukuba station because of the small antenna aperture but this will be overcome by further innovating the VLBI data acquisition terminals such as wider-bandwidth receiving and data recording systems.

Acknowledgments

We are grateful to all the staff at Kashima Space Research Center, Shanghai Observatory, GSI station in Tsukuba and other VLBI stations for the observations they performed and for their helpful

suggestions. We also thank to the staff in the Japanese Maritime Self-Defense Agency and the Japan Meteorological Agency to their help for the experiment in Minamitorishima station.

References

Amagai,J., H. Kiuchi, and N. Kawaguchi, Short baseline experiments using the highly transportable VLBI station, IEEE Trans. Instrum. Meas., 38, 672-675, 1989.

Argus, D. F. and R. G. Gordon, No-net-rotation model of current plate velocities incorporating plate motion model NUVEL-1, Geophys. Res. Lett., 18, 2039-2042, 1991.

Armijo, R., P. Tapponnier and H. Tonglin, Late Cenozoic rightlateral strike-slip faulting in Southern Tibet, J. Geophys. Res., 94, 2787-2838, 1989.

Clark,T.A., B. E. Corey, J. L. Davis, G. Elgered, T.A. Herring, H. Hinteregger, C. A. Knight, J. I. Levine, G. Lundqvist, C. Ma, E. F. Nesman, R. B. Phillips, A. E. E. Rogers, B. O. Ronnang, J. W. Ryan, B. R. Schupler, D. B. Shaffer, I. I. Shapiro, N. R. Vandenberg, J. C. Webber and A. R. Whitney, Precision geodesy using the Mark-III Very-Long-Baseline Interferometer system, IEEE Trans. Geosci. Remote Sensing, GE-23, 438-449, 1985.

Davis,J.L., T. A. Herring, I. I. Shapiro, A. E. E. Rogers and G. Elgered, Geodesy by radio interferometry : Effects of atmos- pheric modeling errors on estimates of baseline length, Radio Sci., 20, 1593-1607, 1985.

DeMets, C. R. G. Gordon, D. F. Argus and S. Stein, Current plate motions, Geophys. J. Int. 101, 425-478, 1990.

Fujii, Y., K. Miyashita and Y. Kitazawa, Crustal deformation and seismicity in and around Ibaraki, The Earth Monthly, 7, 79-84, 1985 (in Japanese).

Hama,S. and J. Amagai, 10m antenna for Minamitorishima (MARCUS) Isl., Rev. Commun. Res. Lab., 36, 61-64, 1990 (in Japanese with English abstract)

Hama,S., H. Kiuchi and J. Amagai, The K-4 high density data recorder, Rev. Commun. Res. Lab., 36, 91-95, 1990 (in Japanese with English abstract).

Heki,K., Three approaches to improve the estimation accuracies of the vertical VLBI station positions, J. Geod. Soc. Japan, 36, 143-154, 1990.

Heki, K. and T. Yoshino, Purposes of the development of Western Pacific VLBI Network, Rev. Comm. Res. Lab., 36, 15-22, 1990 (in Japanese with English abstract).

Heki, K., Y. Takahashi and T. Kondo, Contraction of northeastern Japan: evidence from horizontal displacement of a Japanese station in global very long baseline interferometry networks, Tectonophysics, 181, 113-122, 1990.

Heki, K., G. R. Foulger, B.R. Julian and C.-H. Jahn, Plate dynamics near divergent boundaries : geophysical implications of post-tectonic crustal deformation in NE Iceland, J. Geophys. Res., 1992 (submitted).

Imae, M., Domestic VLBI experiments at the Commucications Research Laboratory, J. Commun. Res. Lab., 1991.

Kawaguchi,N., Y. Sugimoto, H. Kuroiwa, T. Kondo, S. Hama, J. Amagai, T. Morikawa and M. Imae, The K-3 hardware system being developed in Japan and its capability, NOAA Technical Report NOS 95 NGS 24, Proceeding of Symposium No.5, 163, 1982.

Kiuchi,H., J. Amagai and Y. Abe, A new VLBI data acquisition system, K-4, Rev. Commun. Res. Lab., 36, 79-90, 1990 (in Japanese with English abstract).

Kiuchi,H., J. Amagai and N. Kawaguchi, A highly stable crystal oscillator applied to geodetic VLBI, J. Commun. Res. Lab., 36, 107-124, 1989.

Kiuchi,H. and T. Kondo, International VLBI experiment using wave front clock technic, J. Commun. Res.Lab., 1991.

Koyama,Y., J. Amagai and H. Kiuchi, Precise position determination of new VLBI station at Kashima, J. Commun. Res. Lab., 1991.

Ma,C., J.W.Ryan and D. Caprette, Crustal Dynamics Project Data Analysis - 1988, NASA Technical Memorandum 100723, 1989.

Ma,C., J.W.Ryan and D. Caprette, Crustal Dynamics Project Data Analysis - 1991, NASA Technical Memorandum 104552, 1992.

Molnar, P. and P. Tapponnier, Cenozoic tectonics of Asia: Effectsof a continental collision, Science, 189, 419-426, 1975.

Saastamoinen, J., Atmospheric correction for the troposphere and stratosphere in radio ranging of satellites, in the Use of Artificial Satellites for Geodesy, Geophys. Monogr. Ser., 15, edited by S.W.Henriksen et al., 247-251, AGU, Washington D.C., 1972.

Figure Captions

Fig. 1
Stations in the Western Pacific VLBI Network (WPVN) and plate boundaries around Japan. In this paper, results of geodetic VLBI experiments are discussed among Kashima, Shanghai and Minamitorishima stations.

Fig. 2
Baseline length changes (a) between Kashima and Minamitorishima, (b) Kashima-Shanghai and (c) Shanghai and Minamitorishima.

Fig. 3
Movement of the North Tibet block with respect to the stable interior of the Eurasian plate. This is based on the Euler pole of the block obtained by Armijo et al. (1989) by analyzing the slip rate of the major strike-slip faults such as Altyn-Tagh Fault. Movement of the South China block was obtained assuming that this and the North Tibet block behave as a large single block. The movement of the South China block is thought to be slightly smaller due to the reverse fault system (Lungmen Shan Fault system) separating these two blocks.

Fig. 4
Velocity vectors of the Shanghai VLBI station with respect to the (stable interior of the) Eurasian plate. The first observed vector is estimated using the baseline length changes with Kashima, Fairbanks (Alaska), Kauai (Hawaii) and Cambella (Australia) VLBI stations. The second observed vector is obtained by rotating the velocity vectors of world-wide VLBI stations (Ma et al., 1992) so that they best coincide with no-net-rotation NUVEL1 (Argus and Gordon, 1991). The predicted vector is obtained by assuming the Shanghai station fixed on the 'North Tibet' block in Armijo et al. (1989).

Fig. 5
Fluctuation of the plate velocity of a oceanic plate near the subduction zone. The plate is assumed to move in a purely episodic manner at the subduction zone and these movements propagate into the plate interior to form a purely continuous movement there (Heki et al., 1992). Thickness of the overlying plate and the underlying asthenosphere were assumed to be 100 km and 200 km respectively and we used 5 x 10E19 poise for the asthenospheric viscosity. Episodic movements are supposed to occur every century as earthquakes with slips of 10 meters. Plate velocity during 100 years after an episodic movement shows larger fluctuations for a point closer to the boundary. Fluctuation is about +/- 10 % for a point 1000 km apart from the boundary. This suggests the excess velocity of about 1 cm/yr at Minamitorishima physically possible.

Fig. 6
Metropolitan Diamond Cross (MDX) VLBI network started in 1992 to monitor the crustal deformation around the Tokyo area. Kashima-Tsukuba baseline has been frequently measured since 1984 to establish a 'standard baseline' which could be used for research and development purposes.

Fig. 7
Estimated positions of (a)Tsukuba and (b)Koganei VLBI stations projected onto horizontal and vertical planes. Error ellipses indicate one-sigma formal errors. It is clear that the coordinate repeatability is better in winter due to the relatively dry atmospheric condition.

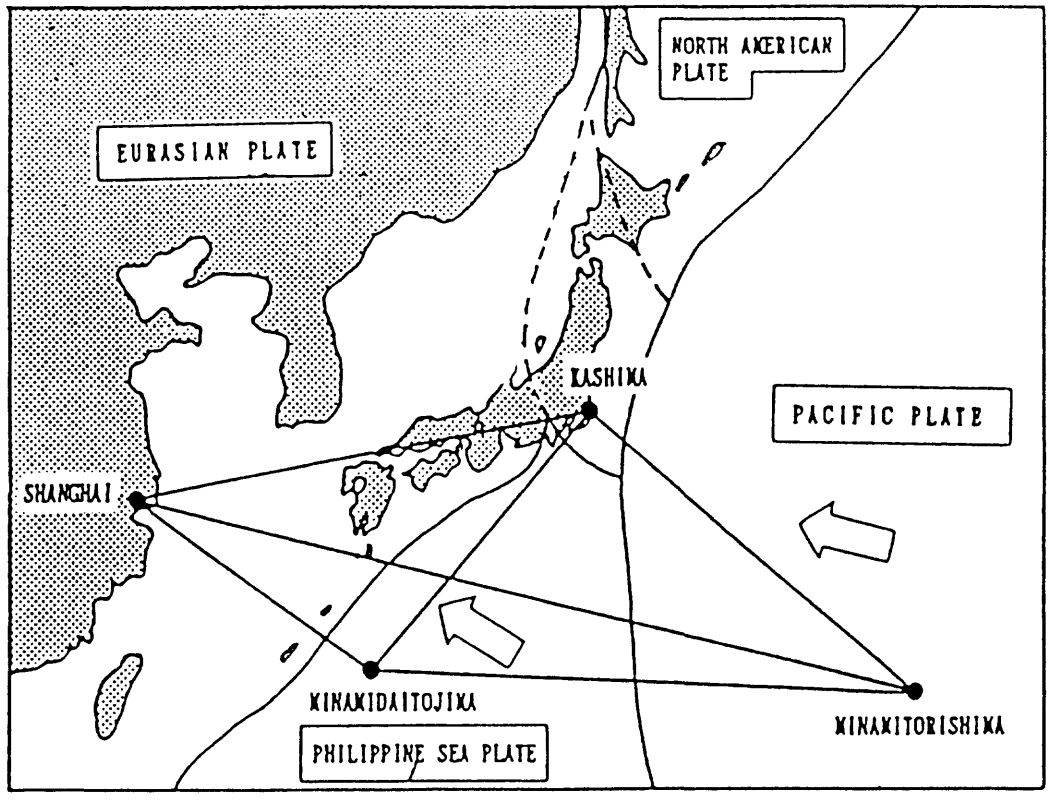
NORTH AMERICAN PLATE
EURASIAN PLATE
KASHIMA
PACIFIC PLATE
SHANGHAI
MINAMIDAITOJIMA
MINAMITORISHIMA
PHILIPPINE SEA PLATE

Fig.1

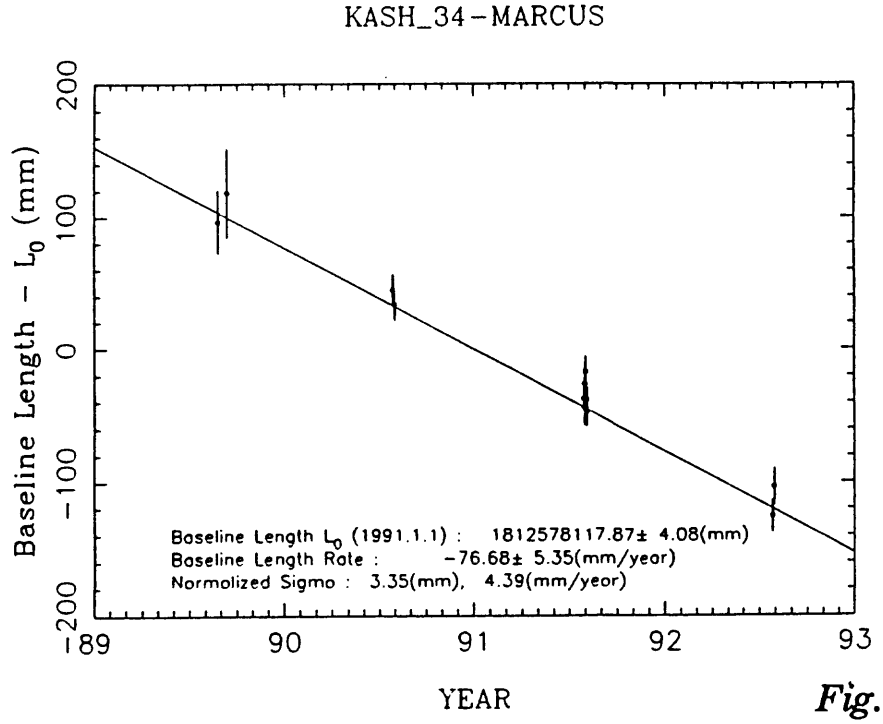
KASH_34-MARCUS
Baseline Length - L_0 (mm)
200
100
0
-100
-200
89
90
91
92
93
YEAR
Baseline Length L_0 (1991.1.1) : 1812578117.87± 4.08(mm)
Baseline Length Rate : -76.68± 5.35(mm/year)
Normolized Sigmo : 3.35(mm), 4.39(mm/yeor)

Fig.2a

KASHIMA - SESHAN25

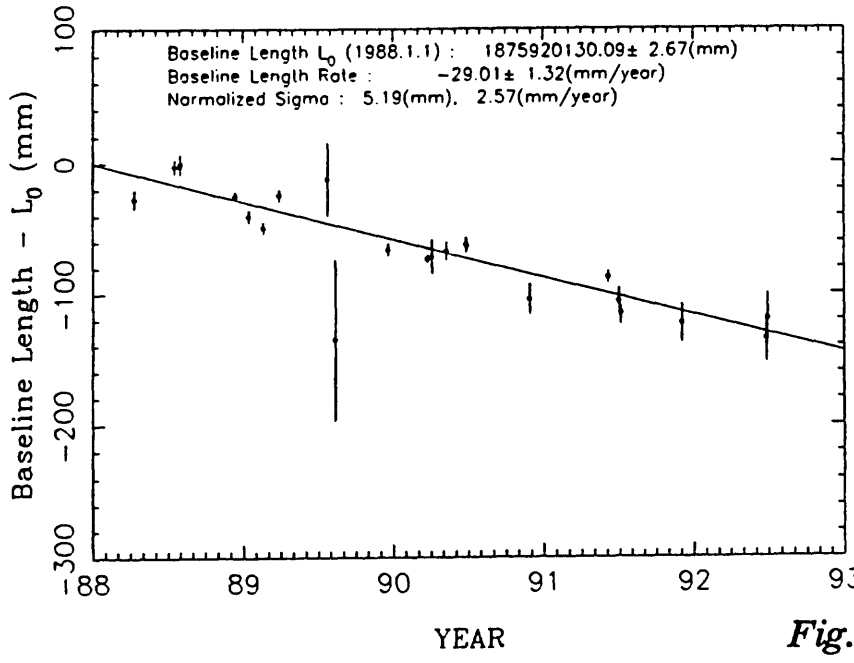

Fig.2b

SESHAN-MARCUS

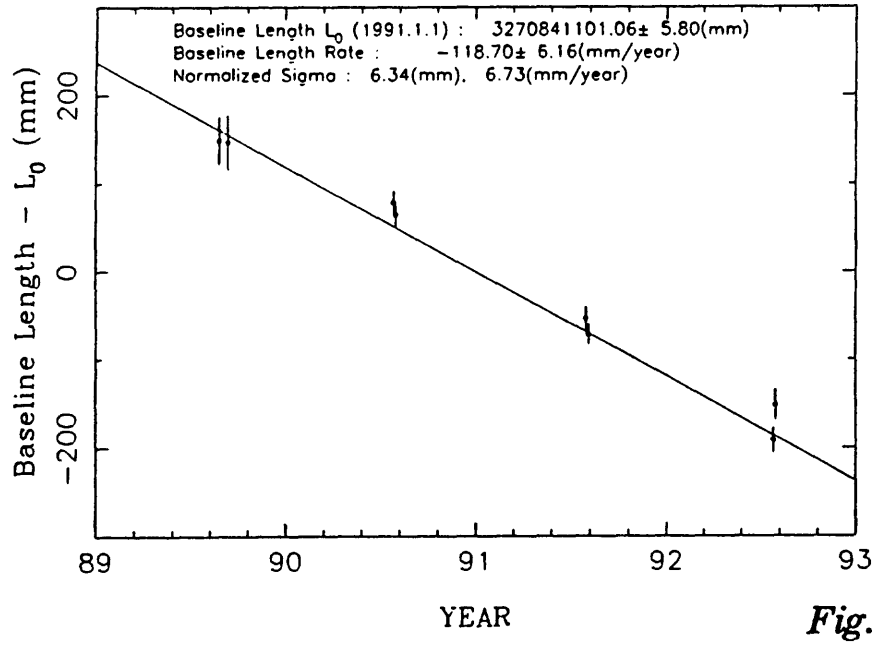

Fig.2c

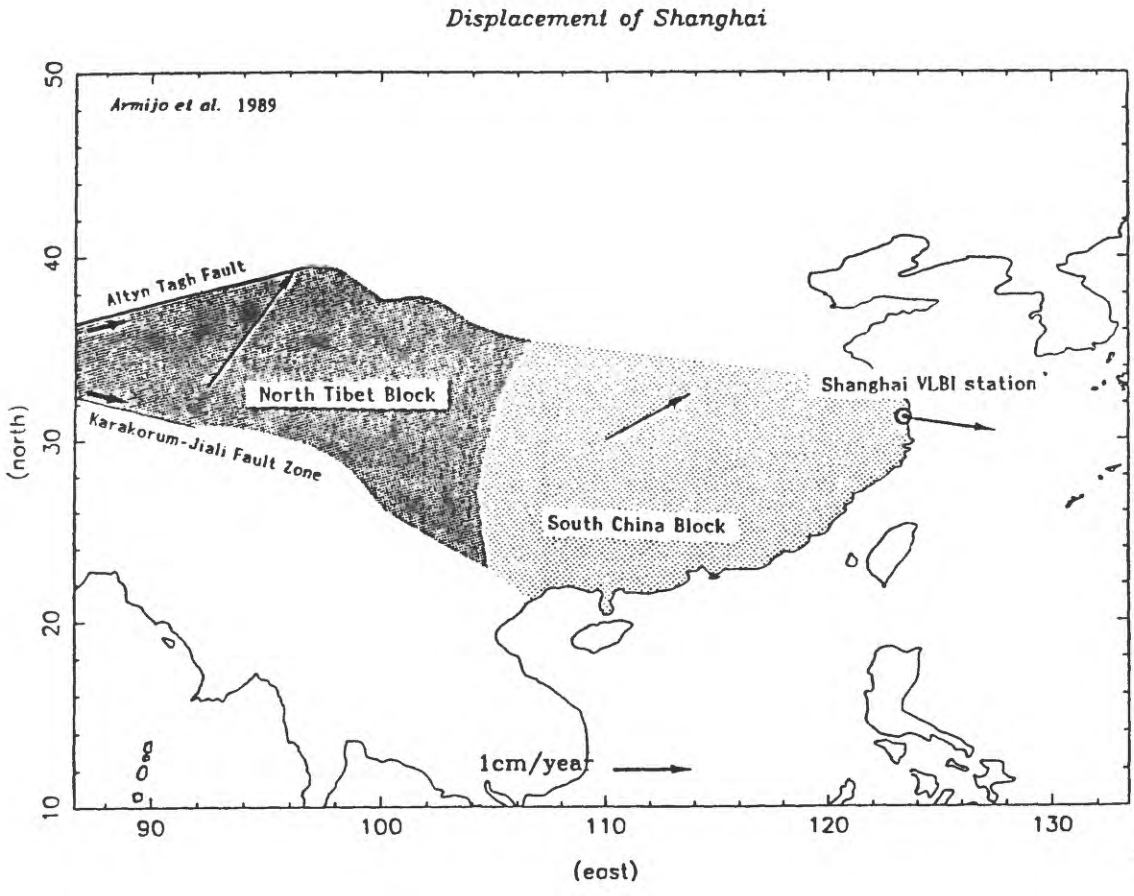
Displacement of Shanghai
Armijo et al. 1989
Altyn Tagh Fault
North Tibet Block
Karakorum-Jiali Fault Zone
South China Block
Shanghai VLBI station
1cm/year
(north)
(east)
10
20
30
40
50
90
100
110
120
130

Fig.3

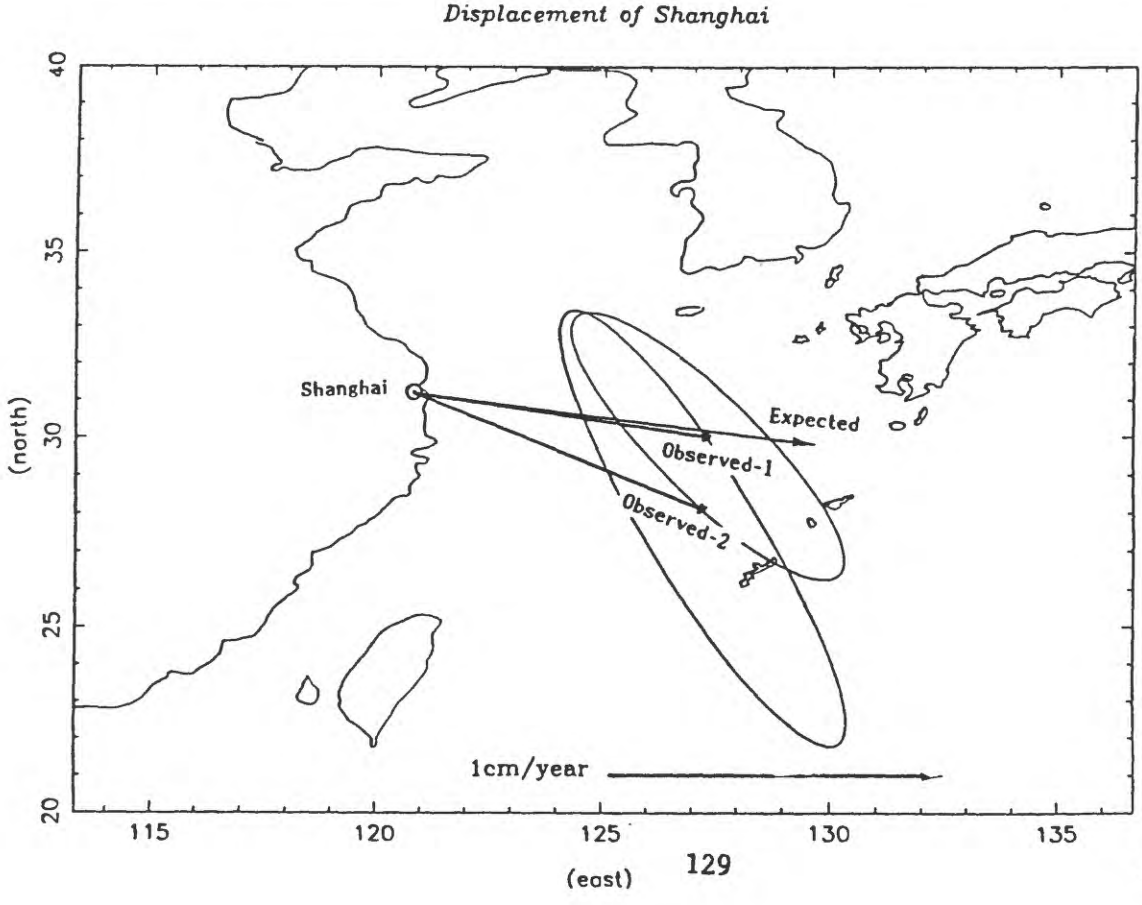
Displacement of Shanghai
Shanghai
Expected
Observed-1
Observed-2
1cm/year
(north)
(east)
20
25
30
35
40
115
120
125
130
135

Fig.4

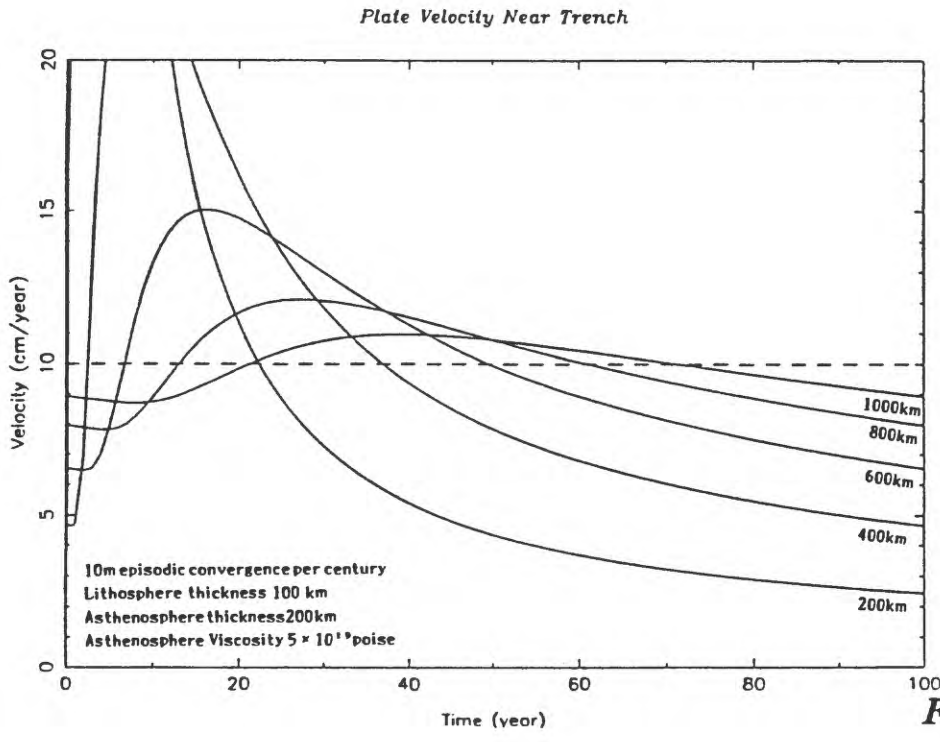
Plate Velocity Near Trench
Velocity (cm/year)
Time (year)
0
5
10
15
20
0
20
40
60
80
100
1000km
800km
600km
400km
200km
10m episodic convergence per century
Lithosphere thickness 100 km
Asthenosphere thickness200km
Asthenosphere Viscosity 5 × 10²⁰poise

Fig.5

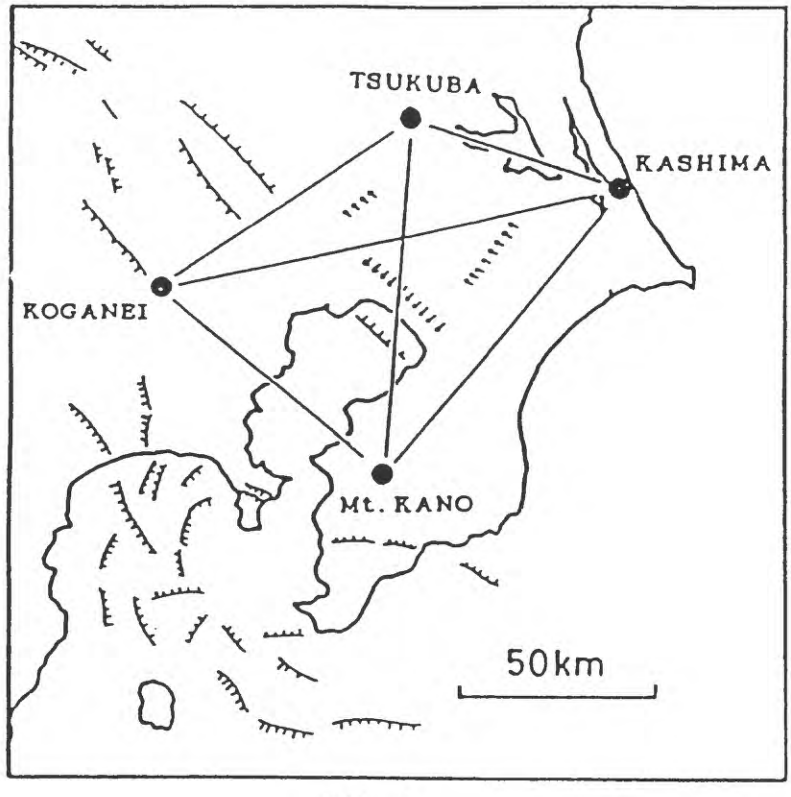
TSUKUBA
KASHIMA
KOGANEI
Mt. KANO
50km

Fig.6

RELATIVE POSITION OF TSUKUBA

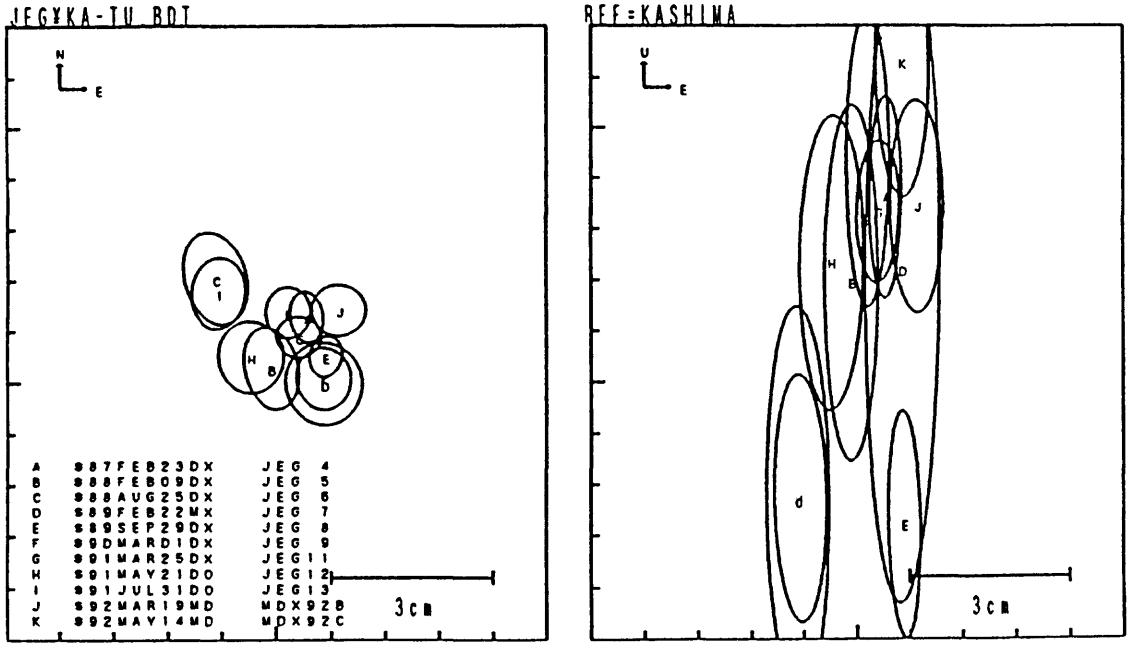

* Ellipses are representing 1 σ error

Fig. 7a

RELATIVE POSITION OF KOKUBUNJ

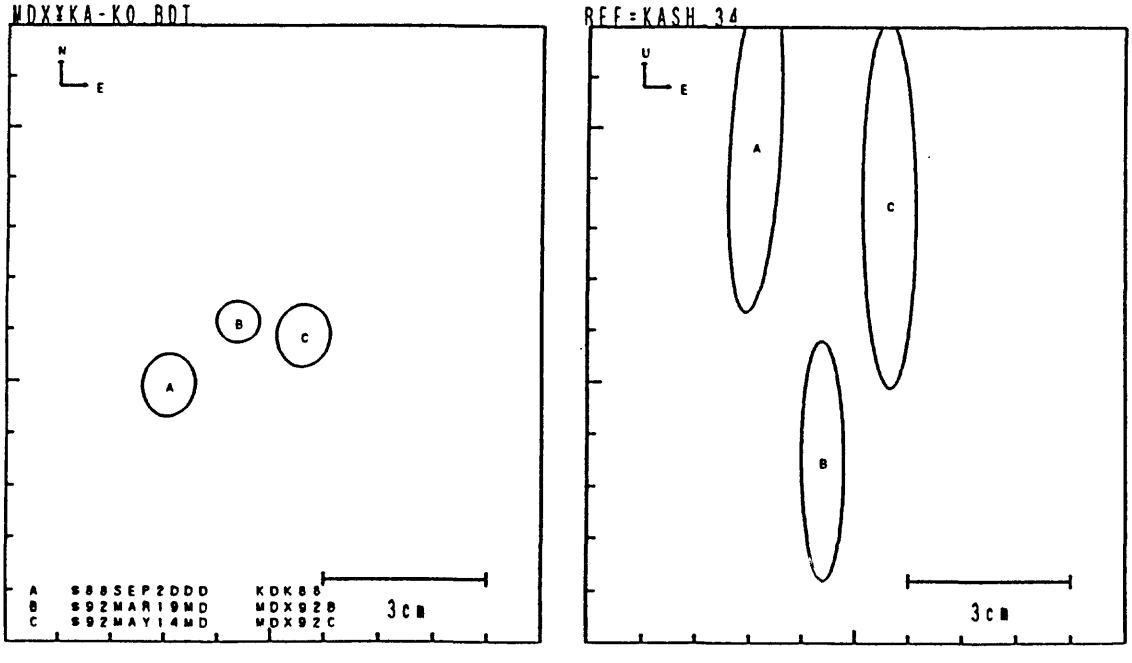

* Ellipses are representing 1 σ error

Fig. 7b

Submitted to the 8th Joint Meeting of the UJNR Earthquake Prediction Technology, Seattle, November 1992

New Bathymetric Survey and Processing System based on Sea Beam 2000

Akira ASADA and Shigeru KATO

Hydrographic Department, Japan Maritime Safety Agency
Tsukiji 5-3-1, Chuo-ku, Tokyo 104 Japan

Abstract

The Hydrographic Department, Japan Maritime Safety Agency has installed a most advanced bathymetric surveying system, called Sea Beam 2000 on the newly built survey vessel Meiyo in October 1990, with the close cooperation of SeaBeam Instruments Inc.

The present Sea Beam 2000 has become to have a good capability of 120 deg. swath width and side scan image output of the deep sea floor by combining interferometric technology since February 1992. By adopting the interferometric technology, the resolving performance of bottom reflection wave and the reliability of the multibeam depth measurement are improved remarkably.

During the stage of the designing and developing of the project to built a new Meiyo, a new integrated navigation system and a new data processing system for the Sea Beam 2000 were contributed. For example, the computer program which eliminates 1 or more percent of abnormal data by automatically identifying abnormalities based on the continuity of the topographic feature was very useful.

As the Sea Beam 2000 records additionally intensity data of 121 beams, a intensity map by using a digital color photograph printer was made after the corrections of angle and position of the beam intensity data. Furthermore, we also made a 3-dimensional map by using with depth data. The color 3-dimensional intensity map is useful to examine the detail tectonic landform of the sea floor, such as fissure, fault escarpment and fold structure.

Introduction

Large Earthquakes around Japan have been occurred along the plate convergent boundary. First priority area for the earthquake prediction project of Japan is the large earthquakes zone occurred along the convergent boundary of plates. However, the basic data have not yet been prepared such as topographic map and the distribution of active faults because of the difficulty of the seabottom survey.

Detail relief of the sea floor is very important information in order to examine the tectonic structure concern with earthquake mechanism. Because tectonic landform which is the evidence of the crustal movement accompany with the big earthquakes can easy be preserved on the sea floor rather than land topography.

The Hydrographic Department of Japan Maritime Safety Agency has been taking charge of fundamental seabottom bathymetric survey and earth crustal survey by the method of seismic profiling (Kato, 1987). During the carrying forward the scheme, some technical evolution has been experienced in the field of the sea floor survey methods.

This paper described the outline of a new technology of the sea floor survey and the trial of the practical use expected for earthquake prediction research along convergent boundaries of plates.

New surveying and processing system

Installation of the multi beam sounding survey system 'Sea Beam' was a revolutionary event in the fields seabottom survey in 1983 (Asada and Nakanishi, 1986). Detail bathymetry map along the trench and trough surveyed by the system revealed many remarkable fault escarpments and the structure of accretionary prism (Kato, 1991). Meandering canyon along the Sagami Trough was the most surprising submarine topography (Asada, 1986).

On the other hand, acoustic backscattering measurement method for deep sea floor such as Grolia, Seamark II or IZANAGI(Yamamoto et al.,1992) was also remarkable progress. Side scan image map is very useful due to its detail texture of sea floor surface for trace the faults and fracture. However, these side scan sonars have to be towed a large equipment and cannot obtain the accurate water depth.

The Hydrographic Department has installed a most advanced bathymetric surveying system, called Sea Beam 2000 on the newly built survey vessel Meiyo in October 1990, with the close cooperation of Sea Beam Instruments Inc.

The present Sea Beam 2000 has become to have a good capability of 120 deg. swath width and side scan image output of the deep sea floor by combining interferometric technology since February 1992 (Asada,1992). Figure 1 shows the beam pattern of the Sea Beam 2000. Both accurate water depths and acoustic backscattaring image map can be obtain by the system. By adopting the interferometric technology, the resolving performance of bottom reflection wave and the reliability of the multibeam depth measurement are improved remarkably.

As the Sea Beam 2000 records additionally intensity data of 121 beams, a intensity map by using a digital color photograph printer was made after the corrections of angle and position of the beam intensity data. Furthermore, 3-dimensional map by using with depth data was also made.

Both accurate water depths and acoustic backscattaring image map can be obtain by the system. Because of released from the towing work the survey operation becomes easily.

Trial of the practical application

1) Practical survey off Izu Peninsula and tectonic setting of the survey area

Practical survey of the new survey system conducted by the survey vessel Meiyo which installed the Sea Beam 2000 system in March 1992.

The survey area located in the northern border of Philippine Sea plate across the Eastern Izu Tectonic Line(EITL). Figure 2 shows the location of the survey area and with bathymetry. EITL was supposed one of the important tectonic line in the plate boundary zone.

Compression of N-S direction is prominent in the survey area (Ukawa, 1991) under the influence of movement of Philippine Sea plate. Major topographical features such as Hyotanse and Zenisu Ridge elongates with NE to SW direction which ran parallel to EITL. An earthquake fault named Irozaki Fault appeared at the associated with 1974 Izu-hanto oki Earthquake. The fault is located the southernmost of Izu Peninsula which run with NW-SE direction.

2) Minor topography analysis

Figure 3 shows the bathymetric chart off Izu Peninsula processed by the meshed Sea Beam 2000 depth data. It is easy to understand that the Izu Spur elongated from the Izu Peninsula is nonsymmerty with both slopes, and Drainage of the Iro Canyon is restricted by tectonic structure.

Figure 4 shows a post processing intensity map of the same area. Bright area which is the strong reflection area is supposed the rock outcrop or rough sea floor. Dark color area which is the weak reflection area is supposed the mud and fine sediment covered sea floor. Figure 5 shows the 3-dimennsional intensity map and Figure 6 shows the interpretation map of the sea floor texture based on the bathymetric and intensity maps.

Several tectonic and sedimentological characteristics of the survey area examined by the bathymetric and intensity maps are as follows;

a) Tectonic lineament with NE-SW direction along the EITL is not recognized. It means the EITL in the area is not active.

b) In the Izu Spur and Iro Canyon Area tectonic lineaments (L1 -L7 in Figure 6) with the direction of NNE-SSW are dominant.

c) Some tectonic lineaments with NW-SE direction (L8-L10) are recognized. The direction is parallel to the Irozaki fault. L8 is the remarkable tectonic lineament with some meter displacement which is not extract from the bathymetric chart. It is possible that L8 is an earthquake fault appeared at the Izuhanto oki eathquake.

d) Small drainage system is developed the southeastern slope of the Izu Spur and the southern area of Hyotanse.

e) A canyon floor with bright color caused by deepening (V1) and a meandering canyon with dark color axial line (V2) can be detected easily.

Conclusion

The characteristics of the new bathymetric survey and processing system are as follows;
1) Onboard operation becomes easily and efficiently rather than side scan sonar for deep waters.
2) It is easy to grasp the traces of the recent crustal movement from the intensity image.
3) It is useful for the tectonic and sedimentological detail analysis combined bathymetry and intensity image.

Reference

Asada, A. (1986) 3-D image processing of Sea Beam Bathymetric data- as applied from the Sagami Trough to the Izu-Ogasawara Trench. Rep. Hydrographic Dep., 21, 113-133.

Asada, A. (1992) Sea Beam 2000: Bathymetric surveying with interferometry. Sea Technology, 33, 6, 10-15.

Asada, A. and A. Nakanishi (1986) Contour processing of Sea Beam Bathymetric Data. Rep. Hydrographic Dep., 21, 89-112.

Kato, S. (1987) Seabottom survey for earthquake prediction by the Hydrographic Department of Japan. Proceeding of Earthquake Prediction Research (1987), 45-49.

Kato, S. (1991) A geomorphological study on the classification and evolution of trenches around Japan. Rep. Hydrograhic Dep., 27, 1-57.

Ukawa, M. (1991) Collision and fan-shaped compressional stress pattern around the Izu block at the northern edge of the Philippine Sea plate, J. Geophys. Res., 96, 713-728.

Yamamoto, F., E. Tokuyama, K. Yorimitsu and A. Taira (1989) Oceanfloor imaging System -IZANAGI-. J. Japan Soc. Marine Surveys Technology, 1, 45-54.

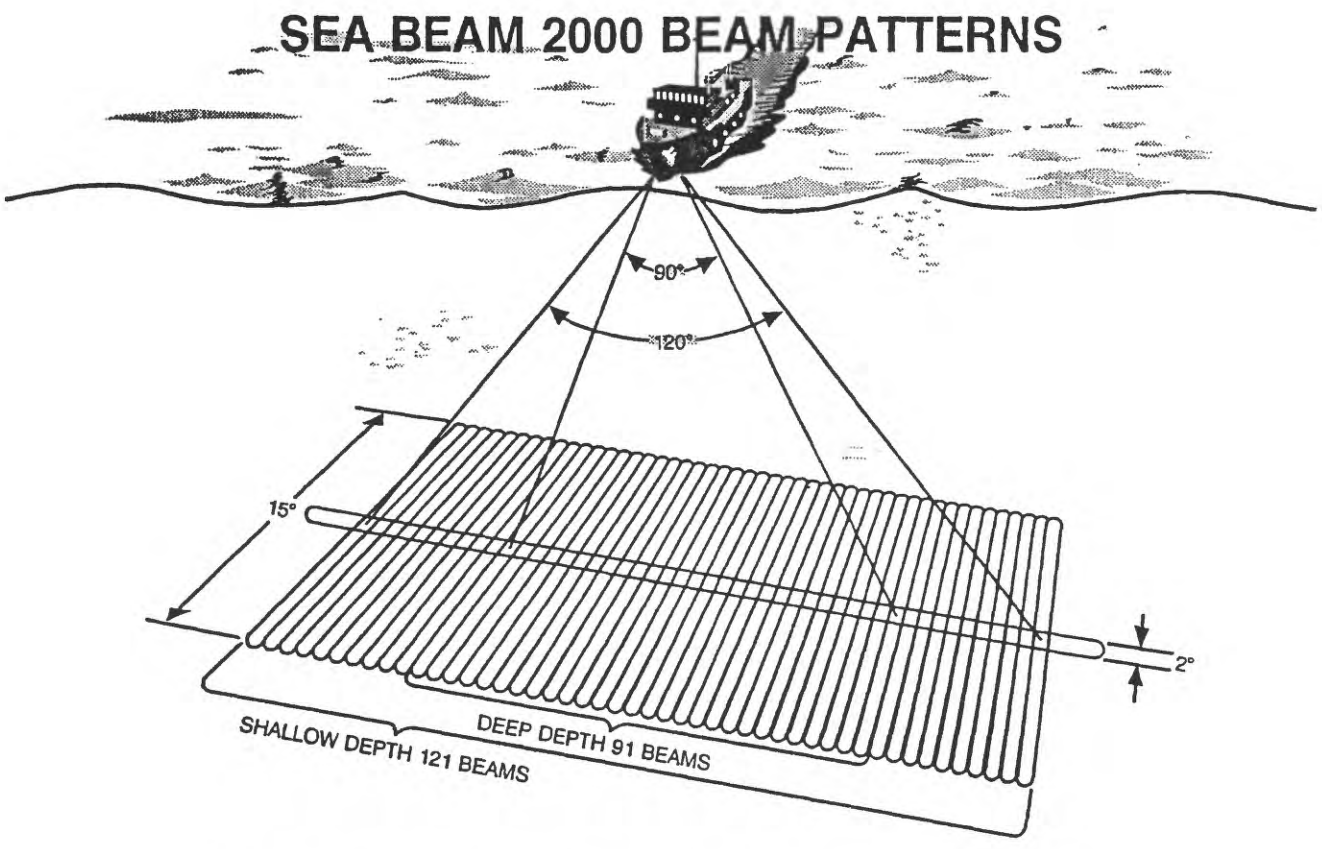

Figure 1 Beam pattern of the Sea Beam 2000

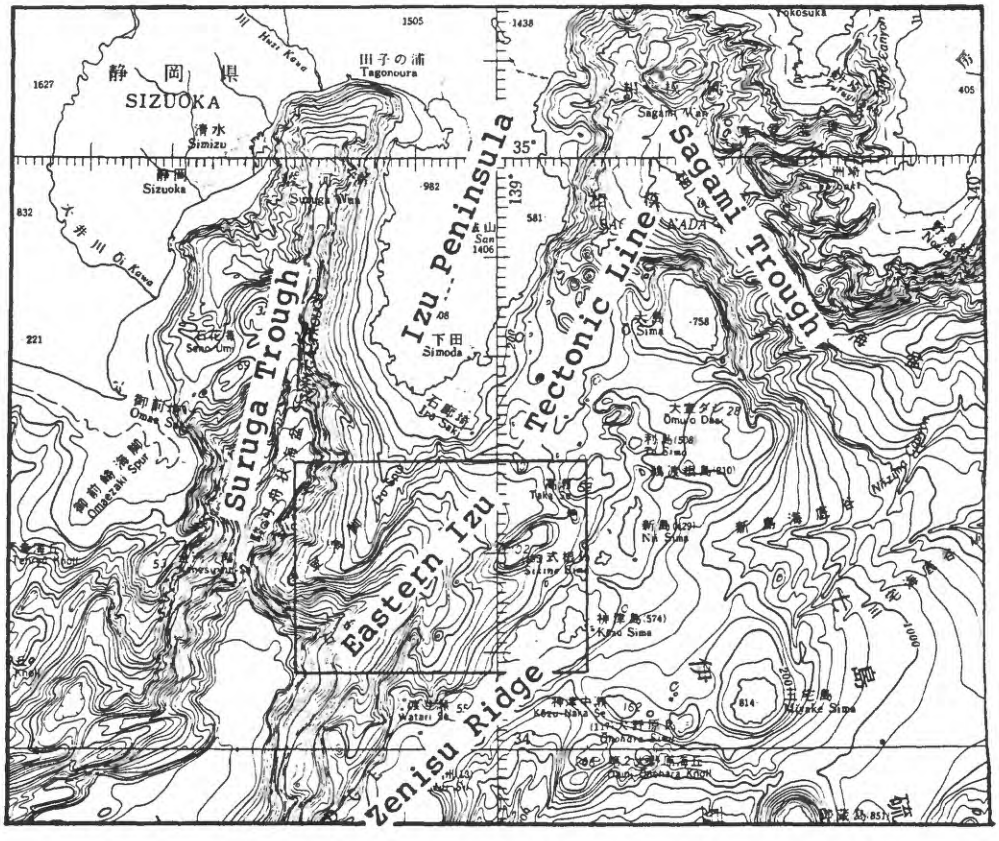

Figure 2 Bathymetric map around Izu Peninsula. Box shows the survey area.

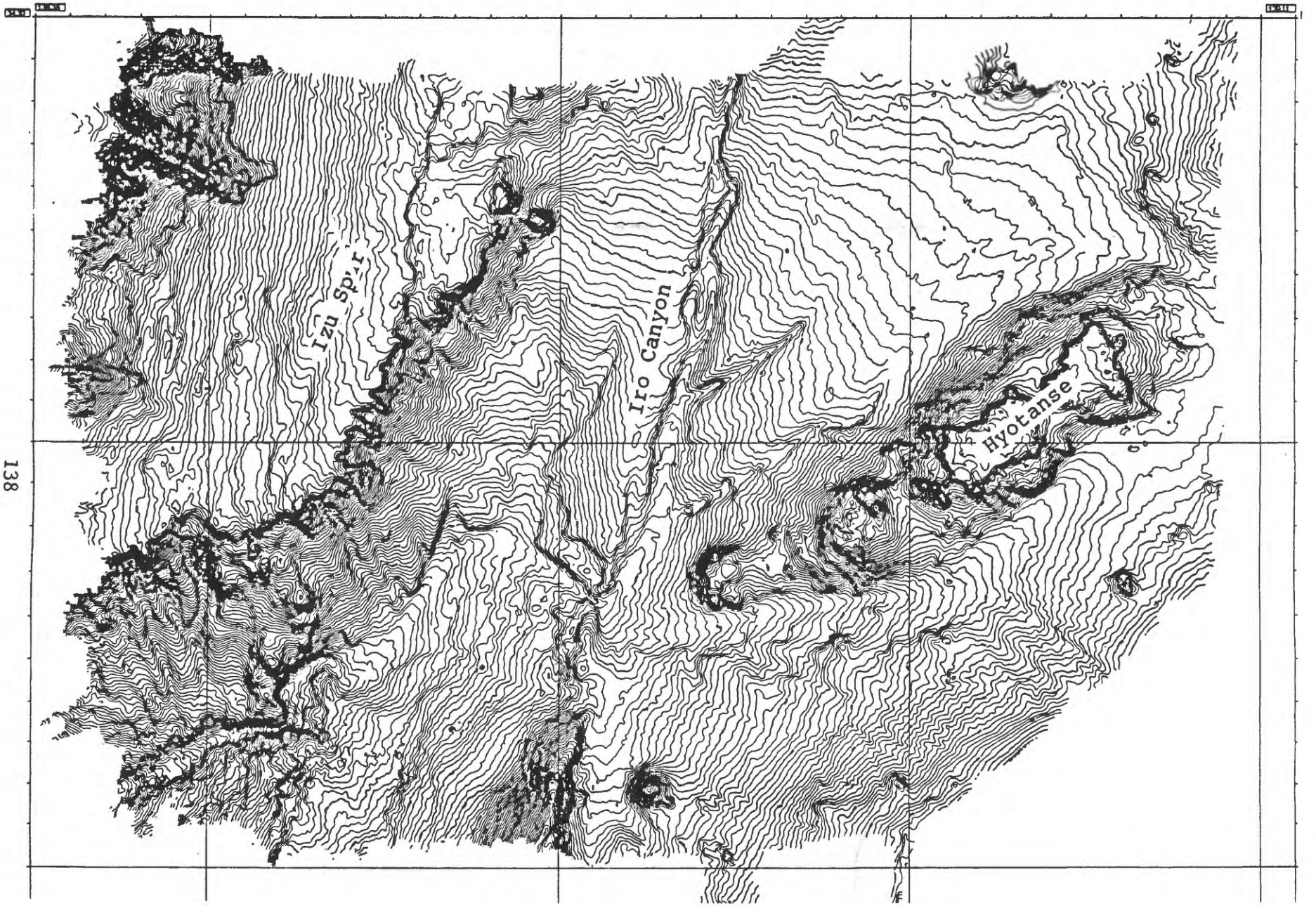

Figure 3 Bathymetric map of the survey area.

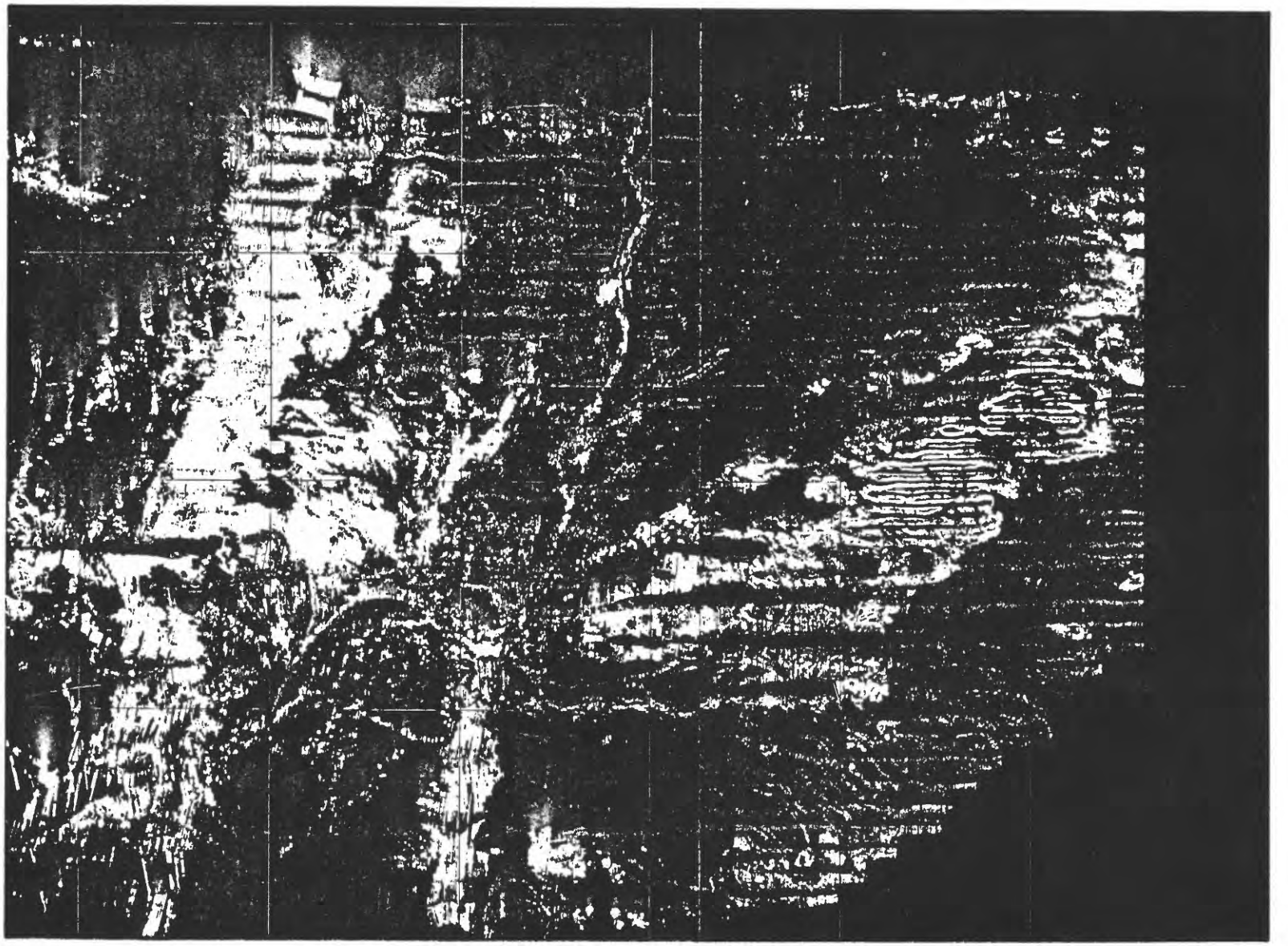

Figure 4 Beam intensity image map processed by using 121 beam intensity of Sea Beam 2000 off Izu Peninsula.

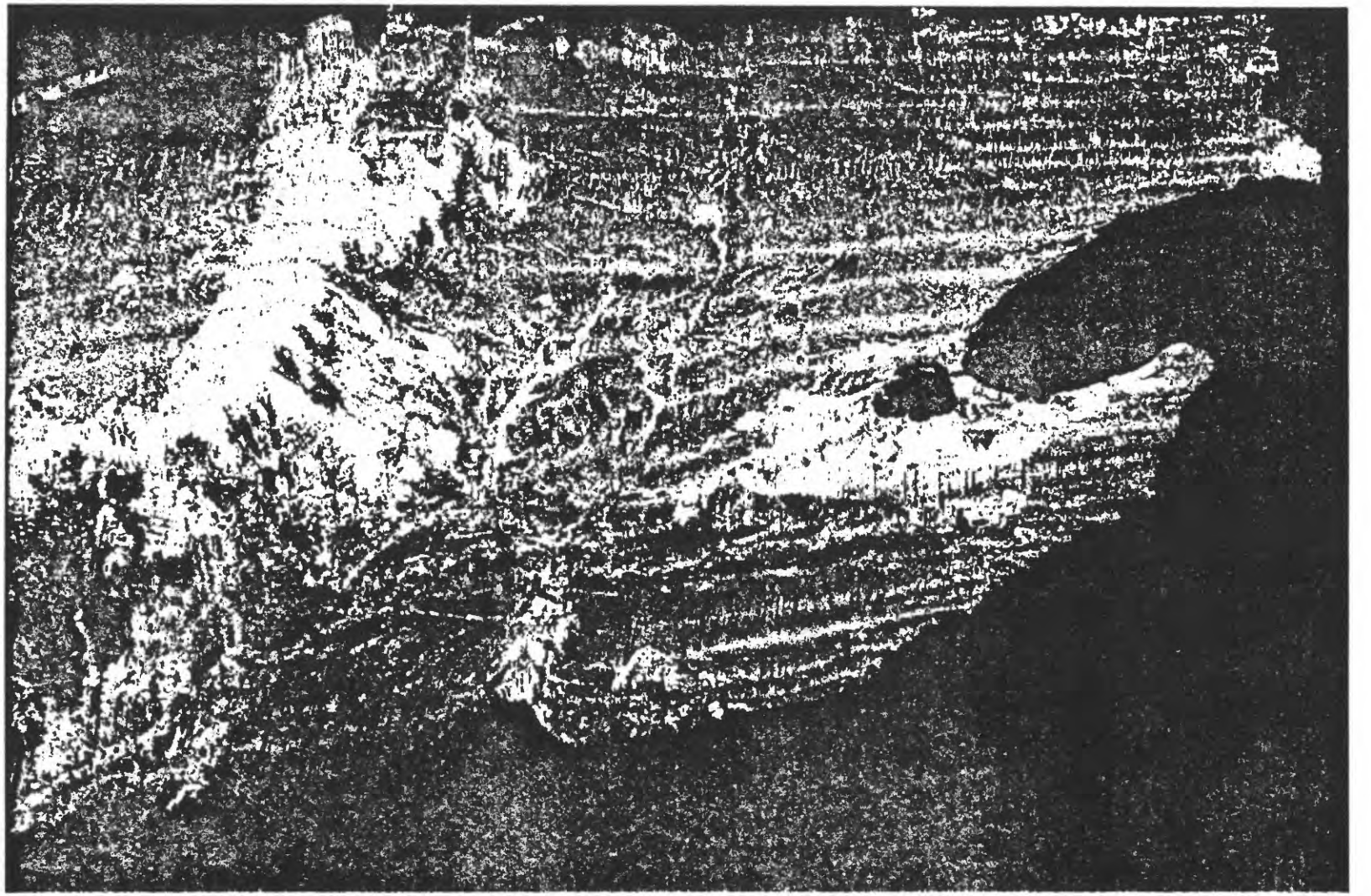

Figure 5 3-dimmensional intensity map of the survey area.

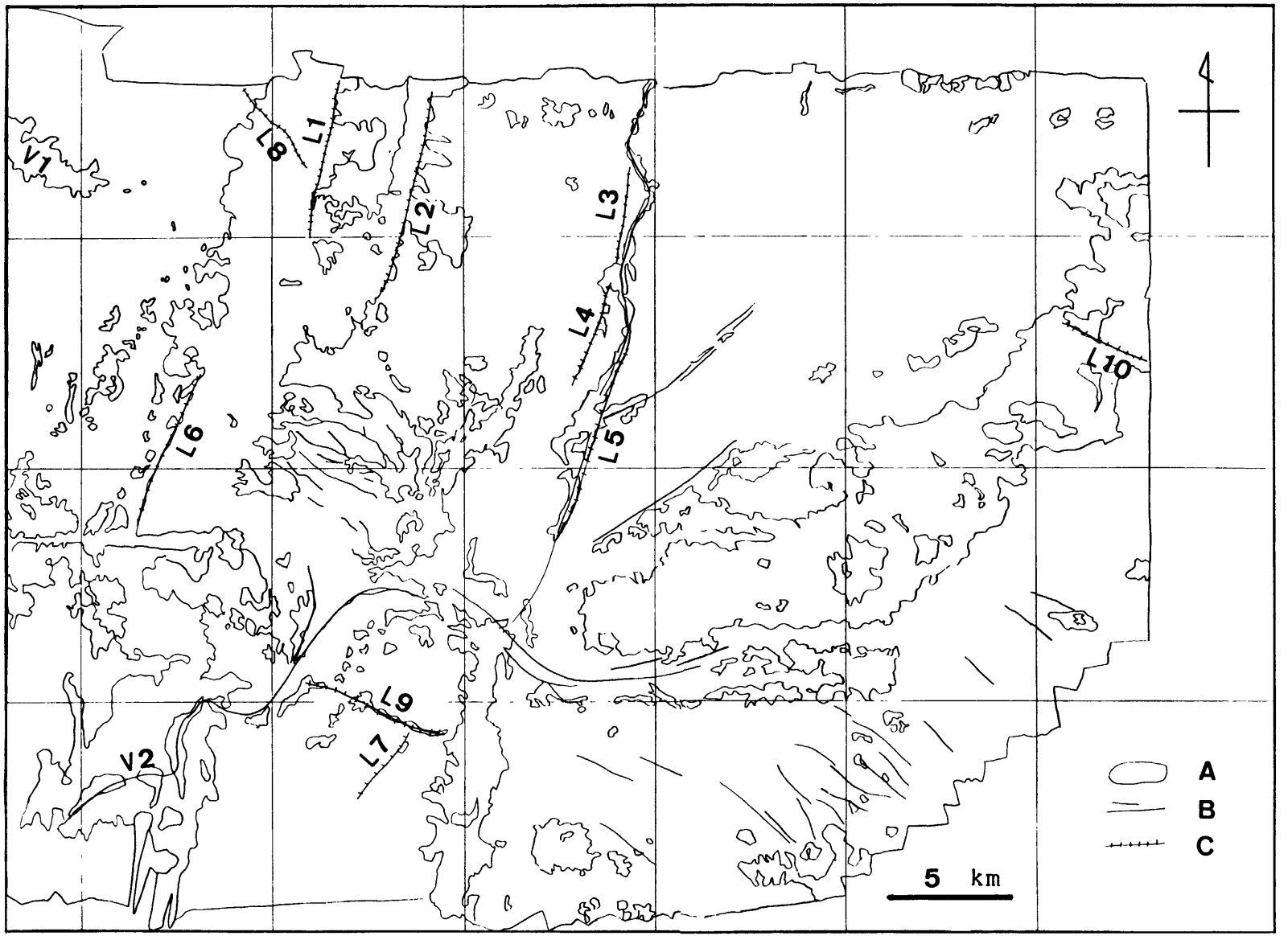

Figure 6 Sea floor texture and lineament map based on the bathymetric and intensity maps.
A; Bright area supposed rock outcroped or rough sea floor, B; Drainage Lineament, C; Tectonic linearment.

Statistics of earthquake precursors in Japan in the 20 years preceeding the end of 1990

Kazuo Hamada

NIED:National Research Institute for Earth Science and Disaster Prevent
Tsukuba-shi, 305 Japan

The national program of earthquake prediction in Japan was launched in 1965 with financial support from the government. Since then earthquake prediction related work: surveys, observations, and research in the fields of seismology, geodesy, geo-electromagnetism, geo-chemistry, and geology have been progressing step by step.

The present author has been systematically observing precursors to earthquakes and has carried out analysis to determine experimental regularities, particularly for the 20 years preceeding the end of 1990. The author presents here: 1) characteristic features of precursors from the statistical viewpoint, and 2) examples of multiple precursors to several earthquakes.

Generally speaking earthquake precursors are not defined in the strictest sense. When anomalies are found in seismic or geodetic observations and these anomalies are thought to have a causal relation to the following earthquake, such anomalies are reported as possible precursors. There is no complete evidence for such anomalies in most of the cases. However, at the same time there is no complete evidence to deny that they are precursors either. In order to avoid complication the author uses the word "precursor" for a possible precursor. The degree of a precursor's validity depends on each case.

The table below lists the number of precursors to earthquakes with $5.0 \leq M$ within the space time domain including the Japanese mainland. The table also includes the proportion of the number of earthquakes associated with precursors to the number of all earthquakes (B/C) and the rate of the number of precursors to the number of earthquakes associated with them (A/B). The table displays very advantageous, convenient statistics; larger earthquakes have a tendency to be accompanied by more precursors and the rate of the number of precursor-associated earthquakes to all earthquakes increases significantly with magnitude. Approximately 80% of earthquakes are accompanied by precursors for the magnitude range $7.0 \leq M \leq 8.0$, while it is only 8% for the magnitude range $5.0 \leq M \leq 6.0$. An average number of precursors is 6.9 for earthquakes with $7.0 \leq M \leq 8.0$, while it is only 1.7 for earthquakes with $5.0 \leq M \leq 6.0$.

All the earthquakes were selected in the space domain:29.3°-45.7°N,
128.0°-147.0°E, and depth<90 km, which includes the Japanese mainland.
A:The number of precursors.
B:The number of earthquakes associated with the precursors.
C:The number of all earthquakes within that time period and magnitude range.
A/B:Ratio A to B. B/C:Ratio B to C.

		5≤M<6	6≤M<7	7≤M<8
Period:	A:	123	103	76
1971-90	B:	71	32	11
	C:	928	99	14
	A/B:	1.7	3.2	6.9
	B/C:	8%	32%	79%

Several examples of multiple precursors of the following earthquakes will be demonstrated.

Name	Y.M.D.	Lat.	Long.	Dep.	M	The number of precursors
Off Nemuro Peninsula	1973 06 17	42.967	145.950	40	7.4	9
Near Izu-Oshima Is.	1978 01 14	34.767	139.250	0	7.0	23
Off Miyagi Prefecture	1978 06 12	38.150	142.167	40	7.4	12
Off Ibaraki Prefecture	1982 07 23	36.183	141.950	30	7.0	9
Off Akita Prefecture	1983 05 26	40.350	139.083	14	7.7	8

fn:ujnr3

A CONSTITUTIVE LAW FOR RATE OF EARTHQUAKE PRODUCTION AND ITS APPLICATION TO EARTHQUAKE CLUSTERING

James H. Dieterich
U. S. Geological Survey
Menlo Park, California

ABSTRACT

Seismicity is modeled as a sequence of earthquake nucleation events in which the distribution of initial conditions over the population of nucleation sources and stressing history control the timing of earthquakes. The model is implemented using solutions for nucleation of unstable fault slip on faults with experimentally derived rate- and state-dependent fault properties. This yields a general state-variable constitutive formulation for rate of earthquake production resulting from an applied stressing history. To illustrate and test the model some characteristics of seismicity following a stress step have been explored. It is proposed that various features of earthquake clustering arise from sensitivity of nucleation times to the stress changes induced by prior earthquakes. The model gives the characteristic Omori aftershock decay law and assigns physical interpretation to aftershock parameters. Earthquake data appear to support a model prediction that aftershock duration, defined as the time for rates to return to the background seismicity rate, is proportional to mainshock recurrence time. Observed spatial and temporal clustering of earthquake pairs arise as a consequence of the spatial dependence of stress changes of the first event of the pair and time-dependent nucleation. Applications of the constitutive formulation are not restricted to the simple stress step models investigated here. It may be applied to stressing histories of arbitrary complexity. The apparent success at modeling clustering phenomena suggest the possibility of using the formulation to estimate short- to intermediate-term earthquake probabilities following occurrence of other earthquakes and for inversion of temporal variations of earthquake rates for changes in driving stress.

INTRODUCTION

Change of the rate of production of earthquakes is a readily observed and characteristic feature of earthquake occurrence. Physical causes of temporal variations of seismic activity remain poorly understood. However, various characteristics of earthquake activity indicate a connection between alteration of stress and earthquake rates. Significant geologic events which modify stress state are often associated with pronounced changes of the rate of production of earthquakes. Examples, include aftershocks following large earthquakes, earthquake swarms associated with magma intrusion processes and systematic variation of background seismicity through the stressing cycle of great earthquakes [for example, *Ellsworth and others*; 1981]. Also, changes of effective stress related to impoundment of reservoirs and fluid injection into deep wells are well-known to alter seismicity. Finally, at distances generally not associated with aftershocks, *Reasenberg and Simpson* [1992] have reported correlations between small stress changes calculated for the 1989 Loma Prieta, California earthquake and small changes in the rates of production of background seismicity.

This paper presents a general approach for obtaining rate of earthquake production resulting from some stressing history. The concept is implemented for faults with rate- and state-dependent constitutive properties which are derived from laboratory fault slip experiments. Previously, some effects of stress perturbations on rate of earthquake occurrence and earthquake probability have been simulated for faults with these properties [*Dieterich*, 1986; 1987, 1988b]. Those previous applications employed numerical simulations or limited closed-form solutions. The following presents a general constitutive formulation for rate of earthquake production on faults with rate- and state-dependent friction. The formulation is amenable to exact solution for simple stressing perturbations and by straight-forward numerical implementation it may be applied to stressing histories of arbitrary complexity. To illustrate and test the model some applications to earthquake aftershocks and earthquake clustering are presented.

Table 1 lists symbols used in this study and equation numbers where the symbols first

appear.

MODEL

General formulation. In the following discussion the term 'earthquake nucleation' is used to describe the processes and interactions that lead to the initiation of an earthquake instability at some specific place and time. Nucleation is assumed to occur over a restricted region which is referred to as a nucleation source. The essential concept of the analysis is the treatment of a seismically active volume of the earth as having a population of sources that nucleate successive earthquakes to produce observed seismicity. The objective is to find the time at which each source in the population initiates an earthquake by following the evolution of conditions on the sources when subjected to some stressing history.

To implement this proposition requires a specific model of the earthquake nucleation process. The general formulation scheme developed in equations (1) through (4) can be employed for any model of the earthquake nucleation process. Constitutive properties and system interactions that provide a mechanism for the onset of unstable fault slip must be specified giving the time t at which a particular source nucleates an earthquake from initial conditions and stressing history:

$$t = F(C, \tau(t)) \ , \tag{1}$$

where C represents initial conditions and $\tau(t)$ is some general stressing history. For example, in a model with instantaneous nucleation at a stress threshold, C might be expressed as the initial stress relative to the stress threshold. In this work, which is implemented for a model of time-dependent nucleation, C is the initial slip speed on the nucleation source.

Changes of stress state within the volume containing the population of nucleation sources may arise from external processes and possibly from earthquakes occurring within the volume. As used here, stressing history may also include changes of effective normal

stress brought about by pore pressure changes. The volume is assumed to be sufficiently small such that all sources experience the same changes of stress although conditions, which include initial stress state, will vary over the population of sources.

The work employs the convention of redefining C at the start of every time step in situations where time stepping is employed to follow the evolution of conditions. In general, the distribution of initial conditions at the start of a time increment will be determined by the prior stressing history and the prior distribution. Consequently, a distribution of initial conditions under some reference stressing history is first constructed. In setting up the reference distribution it is assumed that a constant steady-state seismicity rate r develops under a condition of stressing at the constant reference rate, $\dot{\tau}_r$. Hence,

$$t = n / r \tag{2}$$

where n is the sequence number of the earthquake source and indicates the nth source in the distribution. Although strictly regular seismicity is assumed for construction of the reference distribution, the constant rate r may be interpreted as a statistical measure of expected rate of earthquake production for some magnitude interval (*i.e.* Poisson model of occurrence). This appears to be the simplest assumption to make for defining the distribution. Alternate assumptions to (2) might be to specify a non-steady distribution of earthquakes over time, based for example, on models of stress heterogeneity or variation of seismic potential through the cycle of great earthquakes. For the specific implementation developed below, use of steady-state rate appears to be adequate, at least over time intervals that are small compared to the mean recurrence time of major crustal earthquakes.

Equating (2) with the specific solution of (1) for the constant stressing rate $\dot{\tau}_r$, gives the distribution of initial conditions that yields the constant reference seismicity rate

$$C = G\,(n, r, \dot{\tau}_r) \quad . \tag{3}$$

Substituting the distribution of initial conditions into the general solution of (1) gives the distribution of earthquake times for the general stressing history

$$t = F\left(G\left(n, r, \dot{\tau}_r\right), \tau(t)\right) . \qquad (4)$$

Because stressing histories may be rather complicated, involving stress jumps and irregular fluctuations, practical applications may require numerical treatment – for example, by time-marching, using steps composed of simple stressing functions. In order to update initial conditions for each time step, such applications require determination of the change of C at the sources, arising from the stressing history and the nucleation process.

As formulated, this approach does not predict magnitude of the earthquakes, but because it yields rate of production of earthquakes in response to a stressing history, it can be combined with magnitude-frequency relations or may be used with stochastic models that employ seismicity rate.

Implementation using rate- and state-dependent friction. Using solutions for the nucleation of slip instabilities on faults with rate- and state-dependent fault strength [*Dieterich*, 1992] the procedure just presented is followed to obtain a specific formulation for rate of earthquake production. In Appendix A derivations for the nucleation process on have been generalized somewhat from *Dieterich* [1992]. Appendix B derives the distributions of initial conditions and earthquake times corresponding to equations (3) and (4) respectively. Based on these results Appendix B further obtains a general formulation for rate of earthquake production. Results of those derivations are summarized below.

The rate- and state-dependent representation of fault constitutive properties provides a framework to quantify somewhat complicated experimental observations of fault properties and to unify concepts of dynamic/static friction, earthquake fracture energy, displacement weakening, time-dependent healing, slip history dependence and slip speed dependence [*Dieterich*, 1979a; 1981; *Ruina*, 1983]. In addition to representing observed transient and steady-state velocity dependencies during stable sliding, this constitutive relation has been applied to model the spontaneous time-dependent onset of unstable slip in laboratory experiments [*Dieterich*, 1979b; 1981; *Ruina*, 1983; *Rice and Gu*, 1983; *Weeks and Tullis*, 1985 *Blanpied and Tullis*, 1986; *Okubo and Dieterich*, 1986; *Tullis and Weeks*,

1986;], fault creep [*Scholz*, 1988], earthquake afterslip [*Marone and others*, 1991] and the earthquake cycle along plate boundaries [*Tse and Rice*, 1986; *Stuart*, 1988].

Several essentially equivalent rate- and state-dependent fault constitutive representations have been discussed in the literature. A simplified form used by *Ruina* [1983], based on *Dieterich* [1979a; 1981] and generalized for multiple state variables [*Rice and Gu*, 1983] may be written as

$$\tau = \sigma \left[\mu_o + A \ln\left(\frac{\dot{\delta}}{\dot{\delta}^*}\right) + B_1 \ln\left(\frac{\theta_1}{\theta^*_1}\right) + B_2 \ln\left(\frac{\theta_2}{\theta^*_2}\right) + \ldots \right] , \qquad (5)$$

where τ and σ are shear and normal stress respectively, $\dot{\delta}$ is slip speed, θ_i are state variables. Parameters μ_0, A and B_i are experimentally determined coefficients. The terms with asterisks are normalizing constants.

Applications to problems in nature have generally employed only one state variable. Simulations of some laboratory experiments has been improved by use of two state variables [*Ruina*, 1983; *Weeks and Tullis*, 1985; *Tullis and Weeks*, 1986]. Because little complexity is added, derivation of solutions for the nucleation process (Appendix A) and derivations pertaining to earthquake rates with populations of sources (Appendix B) retain the use of multiple state variables.

From experimental observations, state is inferred to depend on sliding and normal stress history. This study employs

$$d\theta_i = \left[\frac{1}{\dot{\delta}} - \frac{\theta_i}{D_{c_i}}\right] d\delta - \left[\frac{\alpha_i \theta_i}{B_i \sigma}\right] d\sigma \quad , \qquad (6)$$

for evolution of state by displacement, δ and normal stress, σ. In (6) D_{c_i} is a characteristic displacement and α_i is a parameter governing normal stress dependence of θ_i. At steady state (σ=constant, $d\theta/dt$=0) $\theta_{ss} = D_c / \dot{\delta}$. When not at steady-state, θ evolves toward θ_{ss}. The displacement dependence of (6) is that proposed by *Ruina*

[1983] and the normal stress dependence is from *Linker and Dieterich* [1992]. An alternate representation of displacement-dependence of θ, used in several studies [*e. g.*, *Tse and Rice*, 1986; *Tullis and Weeks*, 1986] does not permit the simple derivations employed here, but numerical simulations of the nucleation process gives comparable results for the time dependence of earthquake nucleation for both evolution laws [*Dieterich*, 1992].

The nucleation process on faults with rate and state-dependent constitutive properties is characterized by an interval of self-driven accelerating slip that precedes instability. Over a range of stresses the logarithm of the time to instability is found increase with decreasing stress. Appendix A derives solutions for a simplified representation of the source that have been shown to be in excellent agreement with results of detailed numerical simulations. Simulations of faults with heterogeneous properties show a) the zone of most rapid acceleration tends to shrink to a characteristic fault length l_c (Appendix A, equation A2) as the time of instability approaches and b) nucleation sources of length l_c develop spontaneously in regions where the shear stress relative to the sliding resistance averaged over l_c is higher than the surroundings. In the context of the current model the population of sources is postulated to arise from heterogeneity of fault conditions.

In general slip speed is determined by the independent variables θ, τ, σ. It is shown in Appendix A that in an accelerating slip patch θ is determined by slip. Under this condition the dependence of the time to instability on initial conditions is fully specified by the initial slip speed, $\dot{\delta}_0$ of the patch (Appendix A, equation A7). Slip speeds remain very small until a short time prior to the onset of instability. Hence, the interval of premonitory slip may be quite long.

Following the procedure described above the distribution of initial slip speeds from Appendix B is

$$\dot{\delta}(n) = \frac{1}{H\sigma\gamma\left[exp\left(\frac{\dot{\tau}_r n}{A\sigma r}\right) - 1\right]} \quad , \quad \text{where } H = \frac{B}{D_c} - \frac{k}{\sigma} \quad , \tag{7}$$

k is the effective fault patch stiffness and γ is a state variable that evolves with time and stressing history. The term H does not appear again in the formulation. For the initial reference distribution corresponding to (3), γ takes the value

$$\gamma = \frac{1}{\dot{\tau}_r} \quad . \tag{8}$$

Because slip speed increases as the nucleation process develops, the distribution of slip speeds evolves with time. Appendix B shows that the distribution retains the form of (7), independent of subsequent stressing history, but γ evolves with stressing history as described by

$$d\gamma = \frac{1}{A\,\sigma}\left[dt - \gamma d\tau + \gamma\left(\frac{\tau}{\sigma} - \alpha\right) d\sigma \right], \tag{9}$$

where $\alpha=\alpha_1+\alpha_2+$ .. for applications involving multiple state variables. Recall that σ is taken to be effective normal stress, hence (9) may be employed to model effects of pore-fluid pressure changes on seismicity rates.

For positive shear stressing rates with $\dot{\sigma}=0$, equation (9) has the property that γ seeks the steady-state value,

$$\gamma_{ss} = 1 / \dot{\tau} \quad , \tag{10}$$

with the characteristic relaxation time of $(A\sigma/\dot{\tau})$.

The distribution of earthquake times is obtained by substituting the distribution of initial conditions into the solutions for time to instability. In turn, seismicity rate, R is obtained by differentiating the distribution of times giving the general result

$$R = \frac{r}{\dot{\gamma}\,\dot{\tau}_r}, \qquad (11)$$

where r is the steady-state seismicity rate at the reference shear stressing rate $\dot{\tau}_r$. From (10) and (11) it is seen that at steady state the ratio of seismicity rates (R/r) is simply ($\dot{\tau}/\dot{\tau}_r$). Rate R may be interpreted as a statistical representation of expected rate of earthquake production for some magnitude interval.

Equations (9) and (11) are a principal result of this study and represent a state-dependent constitutive formulation for rate of earthquake production.

Some useful non-steady-state solutions of (9) are given in Appendix B. These include evolution of γ with time under constant stress, linear change of shear stress with time and change of shear stress with the logarithm of time (equations B7, B17 and B21, respectively) and evolution of γ for step of shear and normal stress (equation B11).

Figure 1 plots the slip speed distribution of equation (9) against instability time. Also shown is the effect of a stress step on the distribution as given by (B11).

Effects of simple stressing perturbations on seismicity rate may be obtained by substituting solutions of (9) into (11) assuming the seismicity is initially at steady state ($\gamma_0 = 1/\dot{\tau}_r$). For simulation of complex stressing histories a straightforward procedure to implement consists of breaking the stressing history into time steps of constant shear stressing rate and stress steps (of τ and σ) and successively applying the appropriate solutions to follow the evolution of γ from increment to increment. Seismicity during a time step is then obtained by substituting the result for evolution of γ with time (B7 or B17) into (11) and using as γ_0 the value of γ previously obtained for the start of the increment. Alternatively, numerical solutions of (9) may be obtained.

Parameter values. To implement the model fault constitutive parameters A and α which appear in (9) and (11) must be specified. From laboratory observations coefficient A generally has values in the range 0.005 to 0.012 for various temperature and pressure conditions. Under hydrothermal conditions, it appears that somewhat larger values (A~0.02) may be appropriate [*Blanpied and others*, 1991, *Blanpied, personal*

communication]. Numerical examples in the following use A=0.01. Experimental determination of α is presently limited to a single study [*Linker and Dieterich*, 1992] which obtained $\alpha = 0.23$ and established generally that $0 \leq \alpha \leq$ *steady-state friction.*

APPLICATION TO EARTHQUAKE CLUSTERING

Seismicity rate following a stress step. To illustrate and test the model some characteristics of rate of earthquake production following a stress step have been explored. It is proposed that several types of clustered earthquake phenomena represent a perturbation of background seismicity resulting from the change of stress state caused by previous earthquakes.

In the interest of simplicity the stress step induced by a previous earthquake on the surrounding region is represented as a positive step in shear stress, $\Delta\tau$, with normal stress held constant. The solution of (9) for a stress step (B11) shows that a decrease of effective normal stress σ produces the same qualitative effect as an increase of shear stress in that both decrease γ and lead to higher rates of earthquake production. Subsequent evolution of γ is independent of prior processes that caused γ to change. Hence, time-dependent features described below that result from a positive step of shear stress would also arise from negative steps of normal stress. The following applications further assume constant $\dot{\tau}$ following a stress step and steady-state seismicity rate, r, before the step (*i.e.* $\gamma_0 = 1 / \dot{\tau}_r$).

Under these assumptions, simple expressions may be obtained for seismicity rate. First, equation (B11) is employed to evolve γ through the stress step to obtain γ immediately after the step. This becomes γ_0 in (B7) or (B17) which then give the evolution of γ for the subsequent time interval where stressing rate is assumed constant. Finally, the expressions for γ resulting from these operations are substituted into (11) to yield seismicity rate as a function of time after the stress step:

$$R = \frac{r\dot{\tau}/\dot{\tau}_r}{\left[\frac{\dot{\tau}}{\dot{\tau}_r} exp\left(\frac{-\Delta\tau}{A\sigma}\right) - 1\right] exp\left[\frac{-t}{t_a}\right] + 1}, \quad \dot{\tau} \neq 0, \tag{12}$$

and

$$R = \frac{r}{exp\left(\frac{-\Delta\tau}{A\sigma}\right) + t\,\dot{\tau}_r/A\sigma}, \quad \dot{\tau} = 0 \tag{13}$$

where, $\dot{\tau}_r$ and $\dot{\tau}$ are the stressing rate prior to and following the step, respectively, t is set to zero at the time of the stress step and

$$t_a = \frac{A\sigma}{\dot{\tau}} \tag{14}$$

is the characteristic relaxation time for the perturbation of earthquake rate. Note that for $\Delta\tau$=0, and $\dot{\tau} \neq \dot{\tau}_r$ (12) gives the time-dependent change of seismicity for a change of stressing rate from $\dot{\tau}_r$ to $\dot{\tau}$. Figure 1 illustrates the effect of a stress step on the distribution of slip speeds and its effect on the distribution of nucleation times.

Origin of aftershocks. It is proposed that aftershocks are caused by the step-like change of stress that occurs at the time of mainshock. Two general observations support this hypothesis. First, aftershocks often cluster in those areas near a mainshock rupture where stress changes favor aftershock fault slip, including zones off the principal fault plane [*e.g., Stein and Lisowoski*, 1983]. Second, sudden jumps of stress from causes unrelated to fault slip also stimulate aftershock-like bursts of seismicity followed by the $1/t$ decay characteristic of aftershock sequences. An example of the latter are aftershock-like bursts of seismic activity on the south flank of Kilauea volcano following dike intrusion

events [*Dvorak and Tanigawa*, 1985].

Equations (12) and (13) are plotted in Figure 2. Note that equation (13) has the form of Omori's law for aftershock decay:

$$R = \frac{a}{b+t} \quad . \tag{15}$$

Similarly equation (12) gives Omori's law for $t / t_a < 1$, but seismicity rate merges to the steady-state background rate for $t / t_a > 1$. This characteristic of (12) makes it a somewhat preferable representation of aftershock decay for many applications.

The agreement of this model with Omori's law permits assignment of physical interpretations to aftershock parameters. From (13) and (15):

$$a = \left(\frac{A\sigma}{\dot{\tau}_r}\right) r ,$$

$$b = \left(\frac{A\sigma}{\dot{\tau}_r}\right) exp\left(\frac{-\Delta\tau}{A\sigma}\right) = \left(\frac{A\sigma}{\dot{\tau}_r}\right)\left(\frac{r}{R_0}\right) , \tag{16}$$

where R_0 is the initial seismicity rate following the step at t=0. If stressing rate is the same before and after the mainshock ($\dot{\tau}_r = \dot{\tau}$) then from (14) $(A\sigma) / \dot{\tau}_r = t_a$ and

$$a = r\, t_a \ , \quad b = t_a exp\left(\frac{-\Delta\tau}{A\sigma}\right) = t_a\left(\frac{r}{R_0}\right) . \tag{17}$$

As shown in Figure 2 , normalized seismicity rates, R/r for different stress steps all decay along the same $1/t$ asymptote. The characteristic time t_e for the rate to merge with the $1/t$ asymptote is obtained by solving for the intersection of R_0 with the asymptote formed by setting $\Delta\tau = \infty$ in (13) giving

$$t_e = \frac{A\sigma}{\dot{\tau}_r} \exp\left(\frac{-\Delta\tau}{A\sigma}\right) = b \ . \qquad (18)$$

See Figure 2 for graphical interpretation of t_e.

Aftershock duration. Aftershock duration is defined here as t_a, the characteristic time (equation 16) for aftershocks to return to the background seismicity rate. From (14) t_a is independent of the magnitude of the stress step, but depends upon stressing rate. Assuming stressing rate can be approximated as the stress change on the mainshock rupture, $\Delta\tau_e$, divided by mean earthquake recurrence time, t_r, gives

$$t_a = \frac{A\sigma}{\dot{\tau}} = t_r \frac{A\sigma}{-\Delta\tau_e} \ . \qquad (19)$$

The negative sign in (19) arises because stress decreases on the earthquake rupture surface. A similar result is given by *Dieterich* [1988b]. Equation (19) constitutes a specific prediction of this model. In this prediction, earthquake magnitude does not explicitly affect aftershock duration, but will enter indirectly if t_r is a function of magnitude. As a test of this predicted dependence of aftershock duration on recurrence time, some preliminary data for t_a and t_r have been assembled. Data sources and methods of parameter estimation are summarized in Table 2. Figure 3 plots the data and the predicted relationships between recurrence time and aftershock duration. These results, though quite preliminary and having large scatter appear consistent with the prediction of (19) and suggest that more systematic study of aftershock duration may be warranted.

Spatial effects due to non-uniform stress changes. Because aftershock rate depends on the magnitude of the stress step, systematic spatial variations of the magnitude of the stress change will result in systematic spatial variation of seismicity in the vicinity of a previous earthquake. The following gives a simplified representation stress change from slip on a planar surface in a homogeneous elastic media which should be common to all earthquakes:

$$\Delta\tau = -\Delta\tau_e \left[\left(1 - \frac{c^3}{x^3} \right)^{-1/2} - 1 \right] , x > c \ , \qquad (20)$$

where c is crack radius and x is radial distance from the center of the crack. This approximation does not represent azimuthal dependencies of shear stress, but it does incorporate both the square root stress singularity at the crack tip and the stress fall-off by $1/x^3$ at larger distances which are characteristic of cracks in an elastic medium. Equation (20) is employed to illustrate general characteristics of seismicity resulting from a non-uniform stress change in the vicinity of an earthquake rupture. Other stress components and stresses at locations not lying on the projection of the mainshock fault surface will show comparable distance effects. However, application of the model to specific aftershock patterns would of course require detailed computation of the entire stress field.

Substitution of (20) into (12) gives seismicity rate as a function of time and distance following a uniform stress change $\Delta\tau_e$, on a circular crack:

$$R = \frac{r \dot{\tau} / \dot{\tau}_r}{\left(\frac{\dot{\tau}}{\dot{\tau}_r} exp\left[\left(\frac{\Delta\tau_e}{A\sigma} \right) \left(\left\{ 1 - \frac{c^3}{x^3} \right\}^{-1/2} - 1 \right) \right] - 1 \right) exp\left[\frac{-t}{t_a} \right] + 1} , x > c \ , \dot{\tau} \neq 0 \ . \qquad (21)$$

Using (19), the term $\Delta\tau_e / A\sigma$ appearing in (21) may be replaced by $-t_r/t_a$. Figure, 4 plots rate as a function of distance at different times using (21).

The net seismicity rate originating from a finite region surrounding a mainshock is obtained by numerically integrating (21) over a region of interest assuming background rate r is the same everywhere in that region (Figure 5). For a finite region it is found that earthquake rate R decays by $(1/t)^p$, where p=~0.8. This is in contrast to the decay by $1/t$ arising at any point or for finite regions where the stress change is uniform. The

decrease of decay rate derives from the dependence of t_e on magnitude of the stress step. At time t, some regions will be at $t < t_e$ (rate approaches constant rate asymptote) while other regions will be at $t > t_e$ (rate decays along the $1/t$ asymptote).

Figure 5 also illustrates a potential source of bias that can arise in estimation of aftershock parameters such as t_a where the parameters vary in space. Estimates of aftershock duration may be seriously underestimated if regions with little or no increase in earthquake rate are included in the aftershock count. For example, in Figure 5 the cumulative rate over the region from x/c=1.001 to x/c = 8 also shows an interval of decay with p~0.8, but has an apparent aftershock duration that is much less than the actual aftershock duration.

Aftershock zones characteristically expand with time [*Tajima and Kanamori*, 1985; *Wesson*, 1987]. Apparent spread of an aftershock zone in the present model arises from the non-uniform stress change of the mainshock. Substituting the expression for $\Delta\tau$ of (20) into (18) yields

$$t_e = t_a exp\left[\frac{\Delta\tau_e}{A\sigma}\left(\left\{1 - \frac{c^3}{x_e^3}\right\}^{-1/2} - 1\right)\right], x > c, \qquad (22)$$

where the result of (19) may be used to replace the $(\Delta\tau_e/\sigma A)$ term. Recall that t_e is the characteristic time aftershock rate begins to merge with the $1/t$ asymptote. At distance $\leq x_e$ normalized rates R/r begin to approach the same $1/t$ asymptote. Along the asymptote the normalized seismicity rate is independent of the original stress change. However, at $x > x_e$, the normalized rates are smaller and scale by $\exp(\Delta\tau/A\sigma)$, where $\Delta\tau$ decreases with distance. Hence, x_e in (22) marks the location of the apparent edge of the aftershock zone at time t_e. As $x_e \rightarrow \infty$, $t_e \rightarrow t_a$, and aftershocks merge with the background rate.

The position of x_e at successive time steps is indicated in the example of Figure 4. Figure 6 plots x_e against t_e from (22). The expansion curves of Figure 6 appear to be consistent with the aftershock observations of *Tajima and Kanamori* [1985] and *Wesson* [1987] for values of (t_r/t_a) in the range 10 to 50 which are suggested by the data of Figure

3. The predicted smooth expansion of the aftershock region shown in figure 6 assumes both idealized stress changes of (20) and that parameters r, A and σ do not vary with location. Less systematic propagation of aftershock zones will occur if the restrictions of these assumptions are relaxed.

Non-constant stressing following an earthquake. Figure 7 illustrates seismicity for a sequence of stress steps representing a hypothetical stressing history consisting of a mainshock followed by two large aftershocks. This example assumes uniform stress changes over the region of interest and is computed using (B17) and (B11) to follow the evolution of γ through the several loading ramps and steps, respectively. Following each stress step, t is set to zero and the value of γ at the end of the stress step becomes γ_0 for the next loading ramp. Note, that the calculated seismicity rate, when plotted against the logarithm of the time following the mainshock, appears to show that the duration of secondary aftershock sequences scale by the time following the mainshock. Note also that the effect of secondary aftershocks is to increase the slope of the aftershock decay. Both effects are artifacts of plotting the entire sequence against logarithm of time after the mainshock. If rates are plotted against logarithm of time following each later stress step, the slope of the decay following the step again gives p=1 with characteristic time of decay t_a.

In general, non-constant stressing history following an earthquake stress step may alter aftershock decay rates. Figure 8 gives earthquake rate for a stressing history consisting of an initial stress step at t=0 followed by stressing that varies with the logarithm of time. Evolution of γ was found by first applying equation (B11) for a stress step then applying equation (B21) for stressing by logarithm of time. This example provides an approximation of effects that would arise from creep processes that add to or relax an earthquake stress step. If stress increases with the logarithm of time, the slope of the aftershock decay again gives p=1. Note however, that such loading can produce an initial build-up of earthquake rates prior to decay. If stress decreases by logarithm of time rapid decay with p>1 is possible.

Earthquake clustering. *Kagan and Jackson* [1991] have assembled data on clustering of earthquakes. Their data employ several earthquake catalogues and give the

space and time statistics of earthquake pairs above some magnitude threshold. The following is based on the Kagan and Jackson plots of all earthquakes (*i.e.* not declustered) above a magnitude cutoff. Hence, the data include independent events, foreshocks, aftershocks and other possible types of clustered events. The data are presented as the ratio of observed number of pairs compared to expected number assuming the Poisson occurrence. The normalized number of pairs are computed for cumulative time and cumulative distances from the first event of each pair. Each data set shows significant clustering of earthquakes characterized by an interval in which frequency decays with time by $(1/t)^p$ with $p \sim 0.8$. Data for shallow earthquakes derived from the Harvard catalogue and for intermediate and deep earthquakes from the PDE catalogues are reproduced in Figure 9a, 9b and 9c, respectively.

These data have been modeled assuming the rate of occurrence of the second earthquake of all possible pairs is perturbed by the stress step of the previous earthquake as given by (21). Because the stress as given by (20) is singular at $x=c$, for this application (21) has been modified to limit the stress increase to a maximum value of $-\Delta\tau_e$. The simulations employ an idealized geometry of a seismogenic belt (Figure 10) which is represented as a surface of half-width W. The analysis assumes that before the first earthquake of any pair, the unperturbed background rate of seismicity is the same everywhere along the surface. The first earthquake in the pair has a radius c and is assumed to occur in the middle of the belt. Numerical integration of the modified version of equation (21) gives the cumulative number of earthquake pairs to time t from the first event and over the distance interval from $x=c$ to $x=2c$, $4c$, $8c$ etc. Because the Kagan and Jackson analysis began the count of pairs only after some finite interval of time had elapsed following the first event the integration for the simulations also began at finite elapsed time t_0. To obtain the model statistic equivalent to Kagan and Jackson, the net number of events cumulative to each time and distance was then normalized by the expected number assuming there was no interaction. All simulations assume the stressing rate before and after the first event are the same.

Results of simulations are plotted in Figure 9. Parameters t_a, $\Delta\tau_e/A\sigma = t_r/t_a$, and W were determined by trial and error to fit the data and are listed in Table 3. The source

radius c of the first event in a pair was taken to be the rupture radius of the average magnitude of the catalogue, where average magnitude is obtained from the Gutenberg-Richter magnitude frequency relation. To reduce the number free variables c was fixed as the minimum distance employed by Kagan and Jackson which was judged to represent a reasonable approximation of the source radius of the average catalogue magnitude. The simulations are only moderately sensitive to model parameters in that nearly as good fit to the data could be achieved with somewhat different parameter values (see Table 3).

The stress-step solution appears to provide a rather good representation of the data including intermediate and deep earthquakes which may involve mechanical processes that are significantly different from the shallow earthquakes. In each of the examples of Figure 9 the simulations agree to within 10 percent of the data for greater that 80 percent of the data points. The maximum deviations of the simulations from the data are about 50 percent of a data value. No attempt was made to model the data lying within the source radius of the first event because equation (21) applies to regions outside of the primary rupture area. Seismicity falling within the source region of a prior earthquake is discussed in a later section. For the shallow earthquake data, the results for W appear reasonably consistent with seismogenic zone width. Also for shallow earthquakes the estimates of t_a and t_r/t_a are consistent with the estimates of Figure 2 and Table 2. However, significantly different values of t_a, t_r/t_a and W are obtained for the intermediate and deep earthquake data. In particular, t_a appears to systematically decrease with increasing depth.

The characteristic shape of the data curves for variation of number of pairs with time is controlled by the stress sensitivity of earthquake rate to elastic stress changes near the first event. The apparent persistence of clustering to great distances shown in Figure 9 is wholly an artifact of summing the number of pairs cumulatively to some distance x. Highly perturbed seismicity close to the first event is lumped with essentially unperturbed seismicity at greater distances. Comparable effects are seen in the results for net aftershock rate by cumulative distance, (Figure 5). The decay of the normalized number of pairs by $(1/t)^p$ with p~0.8 derives from the characteristic stress change surrounding a shear rupture in conjunction with the time- and stress-dependence of seismicity rate of equation (12) as previously discussed for Figure 5. The peaking of number of pairs at finite times

following the first event, with fewer events at shorter times is also seen in the simulations and arises because of the count of earthquake pairs began following some finite time after the first event.

Foreshocks. Foreshock statistics appear very similar to that of aftershocks, and the clustering data discussed above. Histograms of the frequency of foreshock-mainshock pairs show rapid fall off of frequency of pairs with time and distance [*Jones and Molnar*, 1979; *Jones*, 1984; *Jones*, 1985]. For earthquakes in southern California *Jones* [1985] finds that the probability of a mainshock following a M≥3.0 earthquake decays by about $(1/t)^p$ with p~0.9 which is consistent with the result p=0.8 found for a finite region (Figure 5). In addition, *Jones* [1985] shows that relative to foreshock magnitude, mainshock magnitudes follow a normal b-value distribution down to the size of the foreshock. In the context of the model presented here, the occurrence of mainshock following a foreshock is interpreted as a perturbation of background seismicity by the stress change of the foreshock as represented equation (21).

DISCUSSION AND CONCLUSIONS

The approach presented here models seismicity as a sequence of earthquake nucleation events. The distribution of initial conditions over the population of nucleation sources and stressing history determine the timing of events in the sequence. If the nucleation process is assumed to be instantaneous at a critical stress, then rate of earthquake occurrence obtained from this model is simply proportional to stressing rate (assuming monotonic increase of stress). However, the model has been implemented for time-dependent earthquake nucleation. This yields a state-variable constitutive formulation for earthquake rate (equations 9-11) where state depends on stressing history. It is found that seismicity rate seeks a steady-state value that is proportional to the instantaneous stressing rate over the characteristic time t_a. An important consequence of the history dependence is that relatively modest jumps in stress result in large perturbations of rate of earthquake production.

Clustered earthquake phenomena have been modeled assuming earthquake rate is perturbed by the elastic stress change associated with prior earthquakes. The model (equations 12 and 13) yields Omori's Law and in combination with the characteristic elastic stress change in the vicinity of a shear rupture, it reproduces the time and distance statistics of earthquake pairs. These results suggest that the formulation contains a reasonable representation of time dependence and stress sensitivity of the earthquake nucleation processes in nature. Because deep earthquakes appear to cluster in a way that is simulated by the present model, but may involve different nucleation processes than shallow earthquakes, more than one time-dependent nucleation mechanism may yield similar results. In particular, if the various types of clustering considered here are driven by characteristic elastic stress changes in the vicinity of an earthquake, then the essential nucleation characteristic needed to model the clustering data is a dependence of the time to instability on an exponential function of the stress change (*i.e.* $t \propto exp\,[const. \times \tau\,]$). This is the sensitivity of the time to instability to stress obtained from equations (A13) and (A14) when the relation of initial slip speed to stress (equation A7) is used.

It is also possible that alternative models of earthquake occurrence might be found that satisfy the various clustering data and do not involve time-dependent nucleation. Time-dependent nucleation is a direct consequence of rate-and state-dependence of fault constitutive properties. To the extent that those properties exist on faults in nature, the nucleation process will be time dependent. An independent argument for the time-dependent nucleation model used here is based on corroboration of these constitutive properties in other applications. There is considerable experimental evidence indicating these properties are characteristic of sliding surfaces in non-metallic materials including laboratory faults with or without gouge layers. Additionally, various other studies [*Tse and Rice*, 1986; *Scholz*, 1988; *Stuart*, 1988; *Okubo*, 1989; *Marone and others*, 1991] have shown that this constitutive representation is effective in modeling fault creep, earthquake afterslip and various earthquake processes.

An outcome of the approach presented here is that parameters describing clustered phenomena have physical interpretations. For example, a predicted relationship between aftershock duration and stressing rate or recurrence time (equation 19) has been obtained.

In figure 3 the curves passing through the data for aftershock duration and recurrence time gives $t_r/t_a = -\Delta\tau_e/A\sigma$= 10-40. Similar values ($-\Delta\tau_e/A\sigma$= 25-75) were obtained with the models of the data for shallow earthquake pairs. Assuming average earthquake stress drops $-\Delta\tau_e$= 2.5MPa, with A=0.01 and $-\Delta\tau_e/A\sigma$= 25, these results suggest a rather low effective normal stress of about 10MPa. However, this estimate should probably be viewed with some caution until greater experience with this modelling approach is acquired.

Data for clustering of intermediate and deep earthquakes has been simulated. The direct relevance of the constitutive formulation to intermediate and deep earthquakes may be questioned, since mechanical processes and earthquake instability mechanisms at those depths may be quite different from those represented by the nucleation model. Nonetheless, the simulations appear to provide a good representation of the limited intermediate (70-280km) and deep (281-700km) earthquake pair data presented by *Kagan and Jackson* [1991]. From those simulations (Table 3) it is evident that t_a decreases with depth. This is generally consistent with observations that deep earthquakes have fewer aftershocks [*Frolich*, 1987]. Also the simulations clearly indicate that $t_r/t_a=-\Delta\tau_e/A\sigma$ has significantly larger values for deep earthquakes, with possible intermediate values for intermediate earthquakes. Assuming $-\Delta\tau_e/\sigma$ does not exceed order of unity, these results indicate that fault constitutive parameter A decreases to very small values for deep earthquakes.

Spatial dependence of earthquake clustering appears to derive from the spatial dependence of the stress changes around a prior earthquake source. Results have been presented for an approximate representation of shear stress change in the plane of a shear crack in an elastic medium. Hence, the model specifically applies to alteration of earthquake rates along the plane of the prior earthquake and outside of its rupture area. However, it is reasoned that all stress changes resulting from an earthquake will generally have similar spatial dependence because fall-off of stresses by $1/x^3$ is characteristic of finite sources in a three-dimensional body including the shear stress equation (20). Hence, distance effects found for the specific model will be generally applicable for perturbation of earthquakes from any stress change resulting from a prior earthquake.

Thus far only aftershocks lying outside of the zone of the mainshock rupture have been discussed. Many aftershocks originate within the mainshock source region, either on or near to the mainshock rupture surface. Two explanations for these aftershocks appear plausible. First, the aftershocks may occur on patches within the mainshock source region that did not slip during the mainshock. Such patches would therefor experience large stress increases at the time of the mainshock would have a high potential for aftershocks. The second and favored explanation is that aftershocks within the region of a mainshock may represent adjustments on secondary faults to stresses induced by mainshock slip. In particular it is reasoned no fault is perfectly planar and consequently mainshock slip will give rise to large local changes of shear and normal stress as non-matching geometry on opposite sides of the fault interfere [*Saucier and others*, 1992]. Those stresses will increase with each successive earthquake unless there is bulk flow or slip on secondary faults to relax the stress. Aftershock mechanisms that differ from that of the mainshock and originate near to but not on the mainshock plane [*Beroza and Zoback*, 1993] may be evidence of this process.

Aftershock decay is generally well-represented by $(1/t)^p$ with p ordinarily in the range 0.5 - 1.5. For the formulation developed here, equations (12) and (13) give p=1.0 if stress change and other model parameters are uniform over the volume considered. Deviations from p=1 and variability between aftershock sequences will arise from several causes. These include spatial variability of various model parameters over the volume considered and stressing histories not satisfying the simple conditions of (12) and (13). Spatial variability of model parameters results in an appropriately weighted average of the family of curves plotted in figure 2 and tends to decrease p relative to the homogeneous case. With the exception of stress change it is expected that model parameters (A, σ_0, r, $\dot{\tau}_r$ and $\dot{\tau}$) would probably not vary systematically with respect to distance from the mainshock. Consequently such effects might tend to cancel and any non-canceling effects would require analysis specific to a particular mainshock (*i.e.*, the effects would not be systematic to all aftershock sequences).

Use of non-uniform stress changes, characteristic of the elastic stresses around a shear

crack, yield $p \approx 0.8$ (Figure 5). Comparable decay rates are found for earthquake pair data compiled by *Kagan and Jackson* [1991] and for foreshock-mainshock pairs of *Jones* [1985] which suggest that rates of decay shown in those composite data sets show the systematic effect of the non-uniform elastic stress field near of a shear crack.

Another source of variability of p relates to non-constant stress or stressing rate following an earthquake stress step. Simulations with multiple stress steps, in which the later stress steps represent large aftershocks with secondary aftershock sequences (Figure 7) yield an apparent $p>1$ during secondary aftershock sequences. Recall that this effect is entirely an artifact of plotting the entire sequence by the logarithm of the time since the mainshock. As shown by Figure 8 relaxation of stresses with time can result in various rates of decay including cases where $p>1$.

The formulation developed here assumes that seismicity rate in the absence of stress perturbations is independent of time. Use of this steady-state assumption appears to be adequate for the applications explored here, at least over time intervals comparable to t_a which is small compared to the mean earthquake recurrence time. Hence, for those time intervals the reference seismicity rate is consistent with a Poisson model of earthquake occurrence and the perturbed seismicity is analogous to that of a non-stationary Poisson model. The introduction of the stochastic element in the formulation relates to the distribution initial conditions over the population of sources or equivalently to the uncertainty in initial conditions on a single source that nucleates a specific earthquake. It is emphasized that the nucleation process is not intrinsically uncertain. The underlying model is of fully deterministic nucleation of earthquake sources in which the stress on each source begins at some low value and increases with time until the conditions for onset of an earthquake are satisfied. Hence, conditions on an individual source are consistent with the stressing cycle often assumed for quasiperiodic earthquake occurrence.

In conclusion it is noted that applications of the seismicity rate constitutive formulation are not restricted to the simple stress step models investigated here. It may be applied to stressing histories of arbitrary complexity. The demonstrated capability for modeling the space and time characteristics of clustering phenomena suggests the feasibility of using observations of temporal variations of earthquake rate to invert for changes in driving

stress. Also, the formulation presented here could be employed to estimate short- to intermediate-term earthquake probabilities following prior earthquakes. Such probability estimates may serve as an alternative or adjunct to estimates that employ empirically derived relations for earthquake potential analogous to that obtained for this model [*e.g.Jones*, 1985; *Reasenberg and Jones*, 1989; *Working Group*, 1992].

ACKNOWLEDGEMENTS

This study profited from discussions with numerous people over a period of several years. I especially wish acknowledge the assistance provided by Mike Blanpied, John Dvorak, John Lahr, Paul Okubo, Paul Reasenberg, Bob Simpson and Will Tanigawa. Joe Andrews and Jim Savage provided reviews and several useful suggestions.

REFERENCES

Beroza, G. C. and M. D. Zoback, Mechanism diversity in the Loma Prieta aftershocks and mechanics of mainshock-aftershock interactions, Science, 259, 210-213.

Blanpied, M. L., D. A. Lockner and J. D. Byerlee, Fault stability inferred from granite sliding experiments at hydrothermal conditions, Geophys. Res. Lett., 18, 609-612, 1991.

Blanpied, M. L. and T. E. Tullis, The stability and behavior of a frictional system with a two state variable constitutive law, Pure Appl. Geophys., 124, 415-444, 1986.

Dieterich, J. H., Modeling of rock friction: 1 Experimental results and constitutive equations, J. Geophys. Res., 84, 2161-2168, 1979a.

Dieterich, J. H., Modeling of rock friction: 2 Simulation of preseismic slip, J. Geophys. Res., 84, 2169-2175, 1979b.

Dieterich, J. H., Constitutive properties of faults with simulated gouge, in: Mechanical Behavior of Crustal Rocks, edited by: N. L. Carter, M. Friedman, J. M. Logan and D. W. Stearns, Geophysical Monograph 24, 103-120, American Geophysical Union, Washington, D. C., 1981.

Dieterich, J. H., A model for the nucleation of earthquake slip, in: Earthquake Source Mechanics, edited by: S. Das, J. Boatwright and C. H. Scholz, Geophysical Monograph 37, Maurice Ewing Volume 6, 37-47, American Geophysical Union, Washington, D. C., 1986.

Dieterich, J. H., Nucleation and triggering of earthquake slip: Effect of periodic stresses, Tectonophysics, 144, 127-139, 1987.

Dieterich, J. H., Growth and persistence of Hawaiian volcanic rift zones, J. Geophys. Res., 93, 4258-4270, 1988a.

Dieterich, J. H., Probability of earthquake recurrence with non-uniform stress rates and time-dependent failure, Pure Appl. Geophys., 126, 589-617, 1988b.

Dieterich, J. H., Earthquake nucleation on faults with rate and state-dependent friction, Tectonophysics, 211, 115-134, 1992.

Dieterich, J. H. and M. F. Linker, Fault stability under condition of variable normal stress, Geophys. Res. Lett., 19, 1691-1694.

Dvorak, J. J. and W. R. Tanigawa, Generation of earthquake swarms along the south flank of Kilauea volcano, Hawaii (Abstract), Eos Trans. AGU, 66, 851, 1985.

Ellsworth, W. L., A. G. Lindh, W. H. Prescott and D. G. Herd, The 1906 San Francisco earthquake and the seismic cycle., in: Earthquake Prediction an International Review, edited by: D. W. Simpson and P. G. Richards, Maurice Ewing Volume 4, 126-140, American Geophysical Union, Washington, D. C., 1981.

Ellsworth, W. L. and L. D. Dietz, Repeating earthquakes: Characteristics and implications, in Proceedings of Workshop XLVI, The 7th U. S. - Japan Seminar on Earthquake Prediction, U. S. Geological Survey Open File Report, 90-98, 226-245, 1990.

Frolich, C., Aftershocks and temporal clustering of deep earthquakes, J. Geophys. Res., 92, 13944-13956, 1987.

Jones, L. M., Foreshocks (1966-1980) in the San Andreas system, California,, Bull. Seism. Soc. Am., 74, 1361-1380, 1984.

Jones, L. M., Foreshocks and time-dependent earthquake hazard assessment in southern California, Bull. Seism. Soc. Am., 75, 1669-1679, 1985.

Jones, L. M. and P. Molnar, Some characteristics of foreshocks and their possible relation to earthquake prediction and premonitory slip, J. Geophys. Res., 84, 5709-5723, 1979.

Kagan, Y. Y. and D. D. Jackson, Long-term earthquake clustering, Geophys. J. Int., 104, 117-133, 1991.

Linker, M. F. and J. H. Dieterich, Effects of variable normal stress on rock friction: observations and constitutive equations, J. Geophys. Res., 97, 4923-4940, 1992.

Marone, C. C., C. H. Scholz and R. Bilham, On the mechanics of earthquake afterslip, J. Geophys. Res., 91, 8441-8452, 1991.

Matsu'ura, M., D. D. Jackson and A. Cheng, Dislocation model for aseismic crustal deformation at Hollister, California, J. Geophys. Res., 91, 12,661-12,674, 1986.

Ogata, Y. and K. Shimazaki, Transition from aftershocks to normal activity: The 1965 Rat Islands earthquake aftershock sequence, Bull. Seism. Soc. Am., 74, 1757-1765,

1984.

Okubo, P. G., Dynamic Rupture modeling with laboratory derived constitutive relations, J. Geophys. Res., 94, 12321-12336, 1989.

Okubo, P. G. and J. H. Dieterich, State variable fault constitutive relations for dynamic slip, in: Earthquake Source Mechanics, edited by: S. Das, J. Boatwright and C. H. Scholz, Geophysical Monograph 37, Maurice Ewing Volume 6, 25-35, American Geophysical Union, Washington, D. C., 1986.

Reasenberg, P. and W. L. Ellsworth, Aftershocks of the Coyote Lake, California, earthquake of August 6, 1979: A detailed study, J. Geophys. Res., 87, 10637-10655, 1982.

Reasenberg, P. A. and L. M. Jones, Earthquake hazard after a mainshock in California, Science, 243, 1173-1176, 1989.

Reasenberg, P. A. and R. W. Simpson, Response of regional seismicity to the static stress change produced by the Loma Prieta earthquake, Science, 255, 1687-1690, 1992.

Rice, J. R. and J. -. Gu, Earthquake aftereffects and triggered seismic phenomena, Pure Appl. Geophys., 121, 187-219, 1983.

Rice, J. R. and A. L. Ruina, Stability of steady frictional slipping, Trans. ASME, J. Appl. Mech., 50, 343-349, 1983.

Ruina, A. L., Slip instability and state variable friction laws, J. Geophys. Res., 88, 10359-10370, 1983.

Saucier, F., E. Humphreys and R. Weldon, Stress Near geometrically complex strike-slip faults: Application to the San Andreas fault at Cajon Pass, southern California, J. Geophys. Res., 97, 5081-5094, 1992.

Scholz, C. H., The critical slip distance for seismic faulting, Nature, 336, 761-763, 1988.

Stein, R. S. and M. Lisowski, The 1979 Homestead Valley earthquake sequence, California: Control of aftershocks and postseismic deformation, J. Geophys. Res., 88, 6477-6490, 1983.

Stuart, W. D., Forecast model for great earthquakes at the Nankai trough subduction zone, Pure Appl. Geophys., 126, 619-641, 1988.

Tajima, F. and H. Kanamori, Global survey of aftershock area expansion patterns, Phys.

Earth Planet. Int., 40, 77-134, 1985.

Tse, S. T. and J. R. Rice, Crustal earthquake instability in relationship to the depth variation of frictional slip properties, J. Geophys. Res., 91, 9452-9472, 1986.

Tsukuda, T., Long-term seismic activity and present microseismicity on active faults in southwest Japan (Abstract), U.S.-Japan Seminar on Practical Approaches to Earthquake Prediction and Warning, 13-14, 1983.

Tullis, T. E. and J. D. Weeks, Constitutive behavior and stability of frictional sliding of granite, Pure Appl. Geophys., 124, 383-314, 1986.

Utsu, T., Aftershocks and earthquake statistics (I), J. Faculty of Sciences, Hokkaido Univ., Series VII, 3, 129-195, 1969.

Weeks, J. D. and T. E. Tullis, Frictional sliding of dolomite: A variation in constitutive behavior, J. Geophys. Res., 90, 7821-7826, 1985.

Wesson, R. L., Modelling aftershock migration and afterslip of the San Juan Bautista, California, earthquake of October 3, 1972, Tectonophysics, 144, 214-229, 1987.

Working Group, Probabilities of Large Earthquakes in the San Francisco Bay Region, California, U. S. Geological Survey Circular, 1053, 51 pages, 1990.

Working Group, Future seismic hazards in southern California, Phase I: Implications of the 1992 Landers earthquake sequence , California Division of Mines and Geology, Sacramento, California, 1992.

Wyss, M., Regular recurrence intervals between Hawaiian earthquakes: Implications for predicting the next event, Science, 234, 726-728, 1986.

Wyss, M., A proposed model for the great Kau, Hawaii, earthquake of 1868, Bull. Seism. Soc. Am., 78, 1450-1462, 1988.

Table 1 Mathematical symbols

Symbol	Equation First used	Description
a,b	15	Omori aftershock decay parameters
A, B	5	Fault constitutive parameters
c	20	Radius of shear crack
C	1	General representation of initial conditions on nucleation source
D_c	6	Characteristic sliding distance for evolution of fault state
G	A1	Shear modulus
H	7, A8	Term containing model parameters for nucleation source
k	7, A1	Effective stiffness of nucleation source
l	A1	Dimension fault patch
l_c	A2	Characteristic dimension of nucleation source
n	2	Earthquake sequence number indicating nth source in distribution
m	B20	Term used in solution for stressing by logarithm of time
r	2	Reference steady-state seismicity rate
R	11, B24	Seismicity rate
R_0	16	Seismicity rate immediately following a stress step
t	1	Time, time of instability
t_a	12	Characteristic time for seismicity to return to steady state
t_e	18	Characteristic time for initiation of aftershock decay
t_r	19	Mean earthquake recurrence time
u,w	B18	Parameters for characterization of stressing by the logarithm of time
x	20	Distance from center of center of shear crack
α	6	Constitutive parameter for evolution of state with normal stress
γ	7	State variable for seismicity formulation
γ_{ss}	10	Steady state value of γ
δ, $\dot{\delta}$	5	slip and slip speed
δ^*	5	Normalizing slip speed in constitutive formulation
η	A1	Crack geometry parameter
μ_0	5	Nominal coefficient of friction
θ	5	State variable in fault constitutive formulation
θ^*	5	Normalizing state variable in fault constitutive formulation
σ	5	Normal stress
τ, $\dot{\tau}$	1	Shear stress and shear stressing rate
$\dot{\tau}_r$	3	Reference stressing rate
$\Delta\tau_e$	19	Stress change on earthquake rupture (negative)
ξ	A2	Scaling parameter for critical fault length l_c for unstable slip

Table 2 Earthquake Recurrence and aftershock duration

Event	Magnitude	t_a (years)	t_r (years)	Data sources and method of estimation
1) Bear Valley, California, 1972	5.0	.2-.5	14-21	Recurrence times from *Ellsworth and Dietz* [1988]. Aftershock duration obtained by fit to aftershock equation (12).
2) Coyote Lake, California, 1979	5.7	1.4-2.5	54-82	Upper limit on recurrence time from *Reasenberg and Ellsworth* [1982]. Minimum recurrence time estimated assuming slip of 70 cm and Calaveras fault slip rate of 1.3cm/a from *Matsu'ura and others* [1986]. Aftershock duration obtained from fitting of aftershocks data [*Reasenberg and Ellsworth*, 1982] to equation (12).
3) Loma Prieta, California, 1989	7.1	1.7-3.5	84-100	Recurrence time from *Working Group* [1990]. Aftershock duration provided by P. Reasenberg [written communication].
4) Kalapana, Hawaii, 1975	7.5	8.5-11.2	50-100	Recurrence time estimated from from rift opening rate of 6-12cm/a and net offset of 6m [*Dieterich*, 1988a]. This is generally consistent with recurrence following the great earthquake of 1868 [*Wyss*, 1988]. Aftershock duration obtained by fitting aftershock decay to equation (12).
5) Koaiki, Hawaii, 1983	6.7	1-1.7	10.5-21	Recurrence time from *Wyss* [1986]. Aftershock duration obtained by fitting aftershock decay to equation (12).
6) Alaska, 1964	9.2	4.6-9.6	230-385	Recurrence time estimated assuming plate slip rate of 6.5cm/yr and earthquake slip of 15-25m. Aftershock duration is from data supplied by J. Lahr.
7) Nobi, Japan, 1891	~8	≥78	5,000-20,000	Recurrence time from [*Tsukuda*, 1983] based on dating of paleoseismic events. Aftershocks of this event continue to at least 1969 without showing any indication of returning to a background rate [*Utsu*, 1969].
8) Rat Islands, Alaska, 1965	8.7	2.7-5.5	72-120	Aftershock duration is obtained fitting of data from *Ogata and Shimazaki* [1984] to equation 14. Recurrence time estimated assuming plate motion rate of 8.3 cm/a and earthquake slip of 6-10m.
9) San Francisco, California, 1906	8	5-10	129-281	Recurrence time is taken to be range of estimates for recurrence on San Francisco Peninsula and North Coast segments from *Working Group* [1990]. Aftershock duration is from data of *Ellsworth and others* [1981].
10) San Juan Bautista, California, 1979	4.8	.5-.8	4-8	Recurrence time estimated from fault slip rate of 2.5cm/a [*Matsu'ura and others*, 1986] and estimated slip of 10-20cm. Aftershock duration obtained by fitting of aftershocks to equation (12).

Table 3 Parameters for simulation of clustering data

Range of parameters giving satisfactory fit to data of Figure 9. Preferred values are indicated in bold face type.

Data	t_a(years)	t_r/t_a $(-\Delta\tau_e/A\sigma)$	Source radius, c	W
Harvard, 0-70km, $M \geq 6.0$	**10.2**	**45**	**12.8**	**102**
	10.2	75	12.8	179
	10.2	25	12.8	57.8
PDE, 71-280km, $M \geq 5.3$	**0.11**	**50**	**3.2**	**6.4**
	0.07	150	3.2	12.8
	0.17	25	3.2	3.5
PDE, 281-700km, $M \geq 5.3$	**0.013**	**1000**	**6.4**	**38.4**
	0.012	3000	6.4	38.4

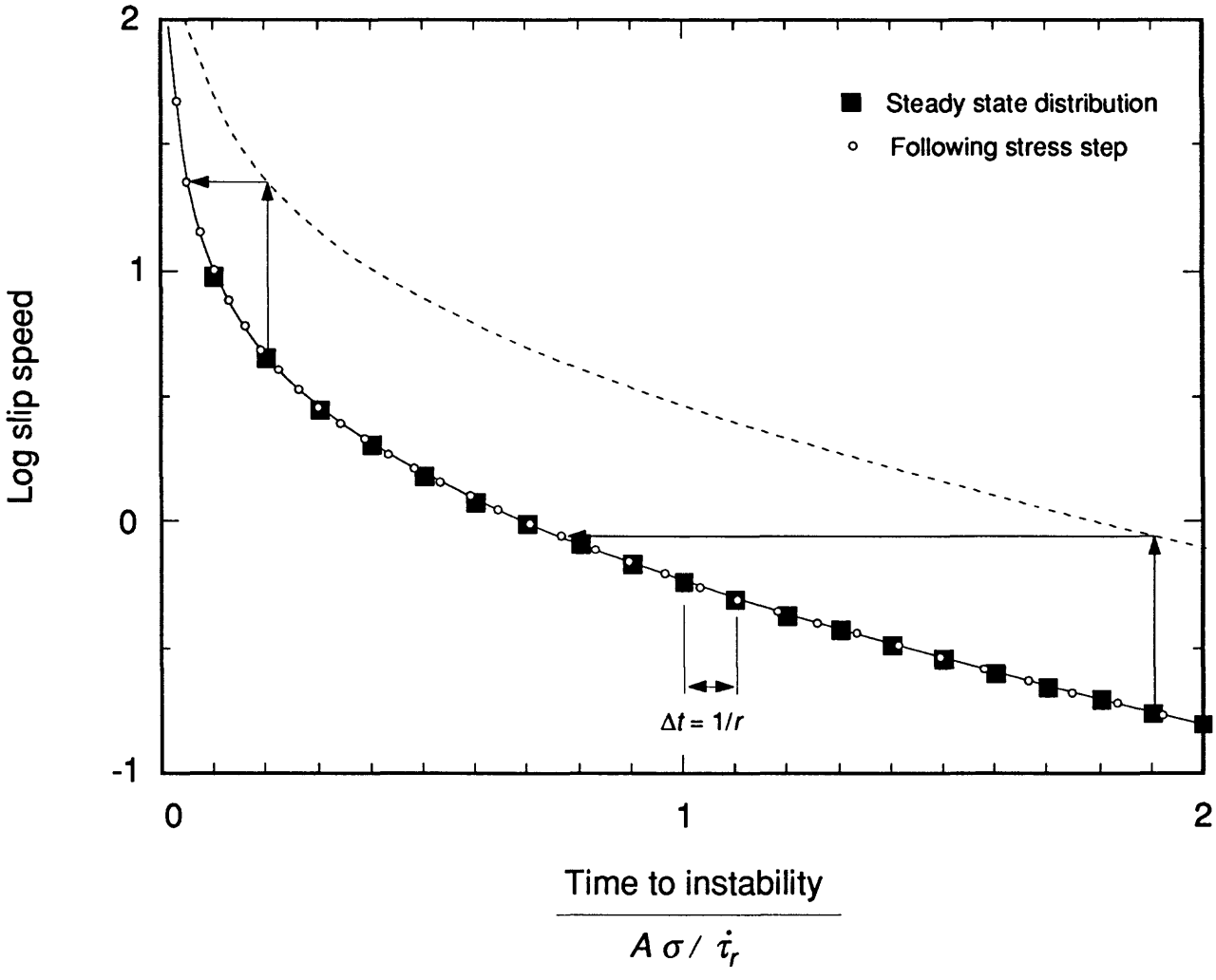

Figure 1 Distribution of slip speeds against time to instability. The solid curve is the solution for time to instability given an initial slip speed of the nucleation source (equation A11 of Appendix A). Solid squares give the distribution of slip speeds from equation (7) under the reference condition at constant seismicity rate r. Small circles show effect of stress step on the distribution from solution of evolution equation (9). This solution is given in Appendix B, equation (B11). The effect of a stress step is to increase slip speed (vertical arrows) of each source as given by equation (A17). This increase of slip speed decreases the time to instability (horizontal arrows) and results in higher density of points (higher seismicity rate) at short times, but does not affect density at larger times where the dependence of time to instability against log slip speed against is linear. Hence, with passage of time, the perturbation of seismicity rates from the stress step evolves out of the system.

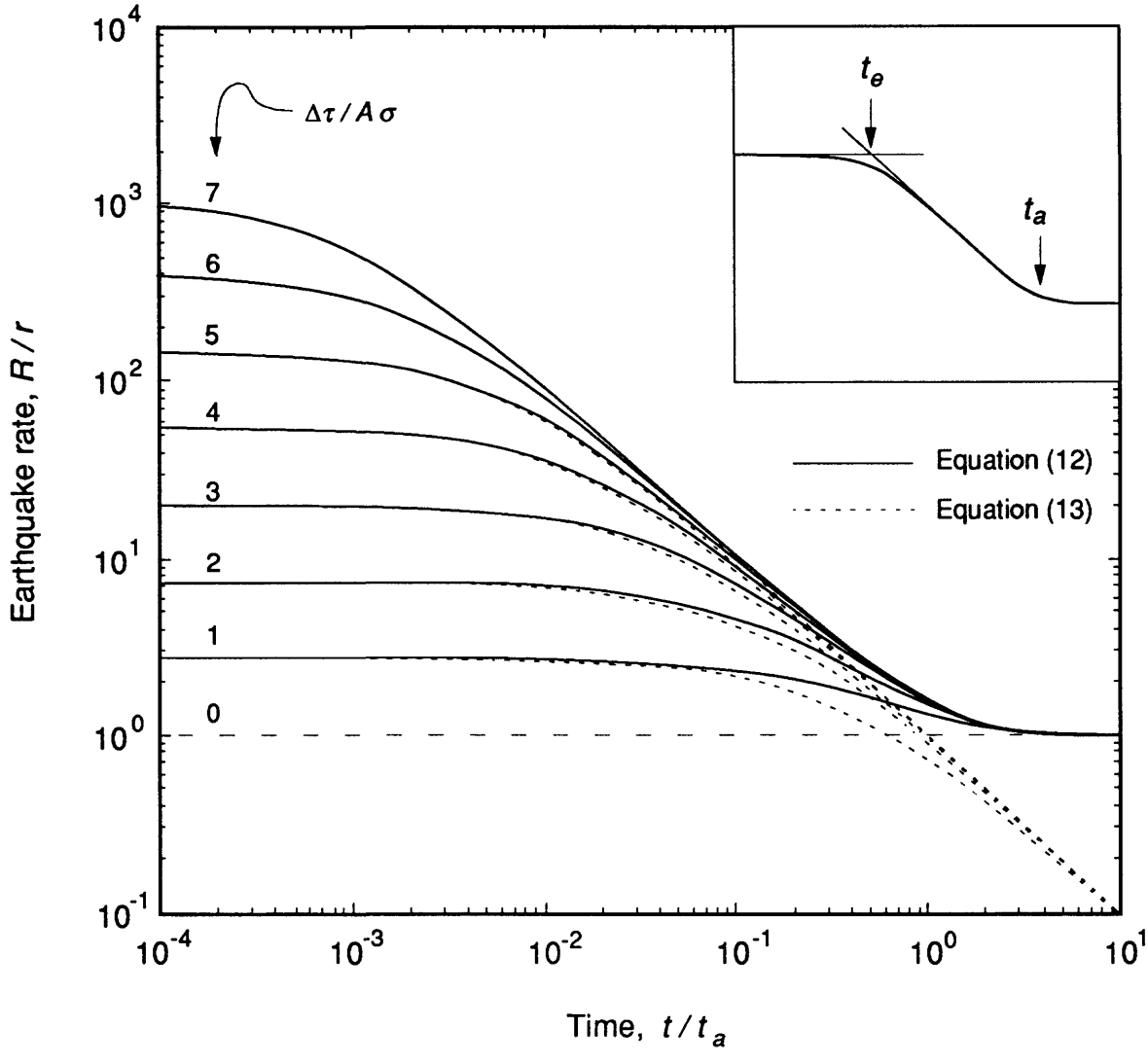

Figure 2 Seismicity rate following a stress step from equations (12) and (13). Inset illustrates the definition of t_e.

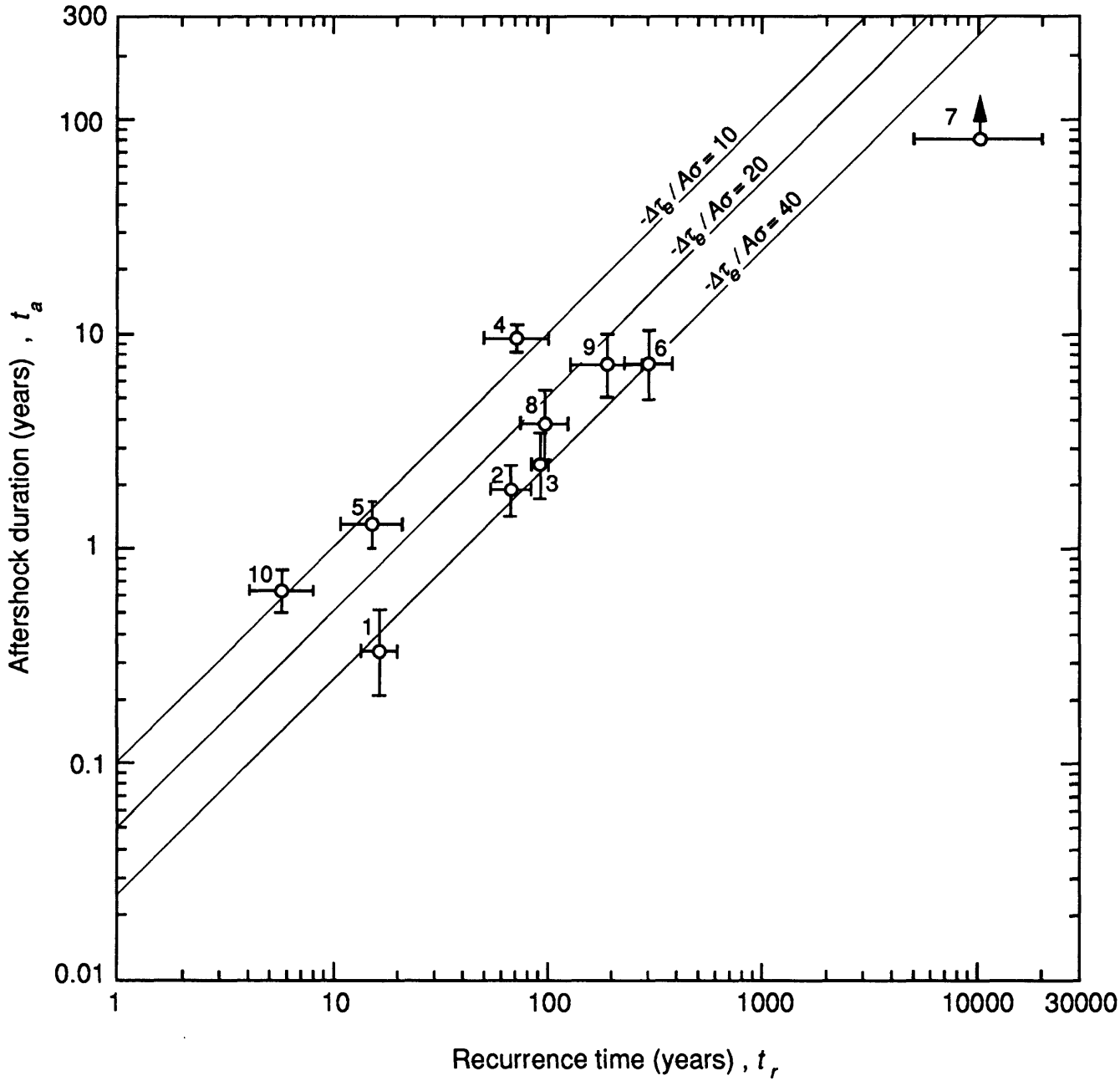

Figure 3 Aftershock duration against recurrence time. Sources of data are summarized in Table 2. Solid lines are obtained from equation (19) for different values of the term ($-\Delta\tau_e / A\sigma$).

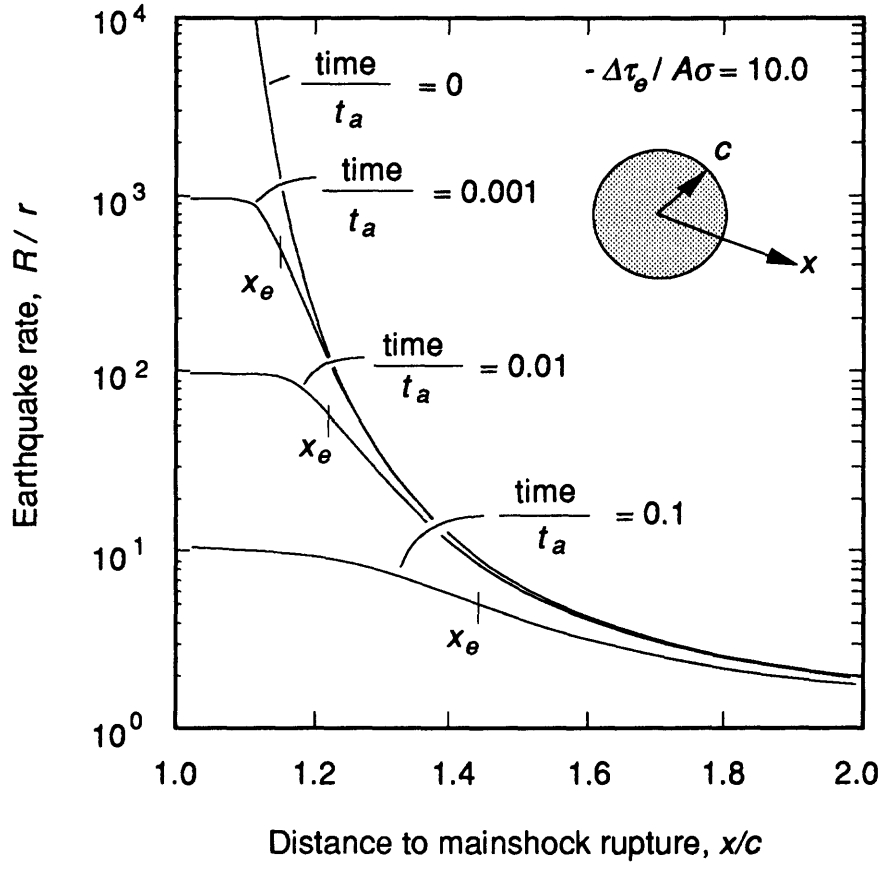

Figure 4 Earthquake rate from equation (21) against distance at different times following a prior earthquake. The points labeled x_e indicate the apparent edge of the aftershock zone as given by equation (22).

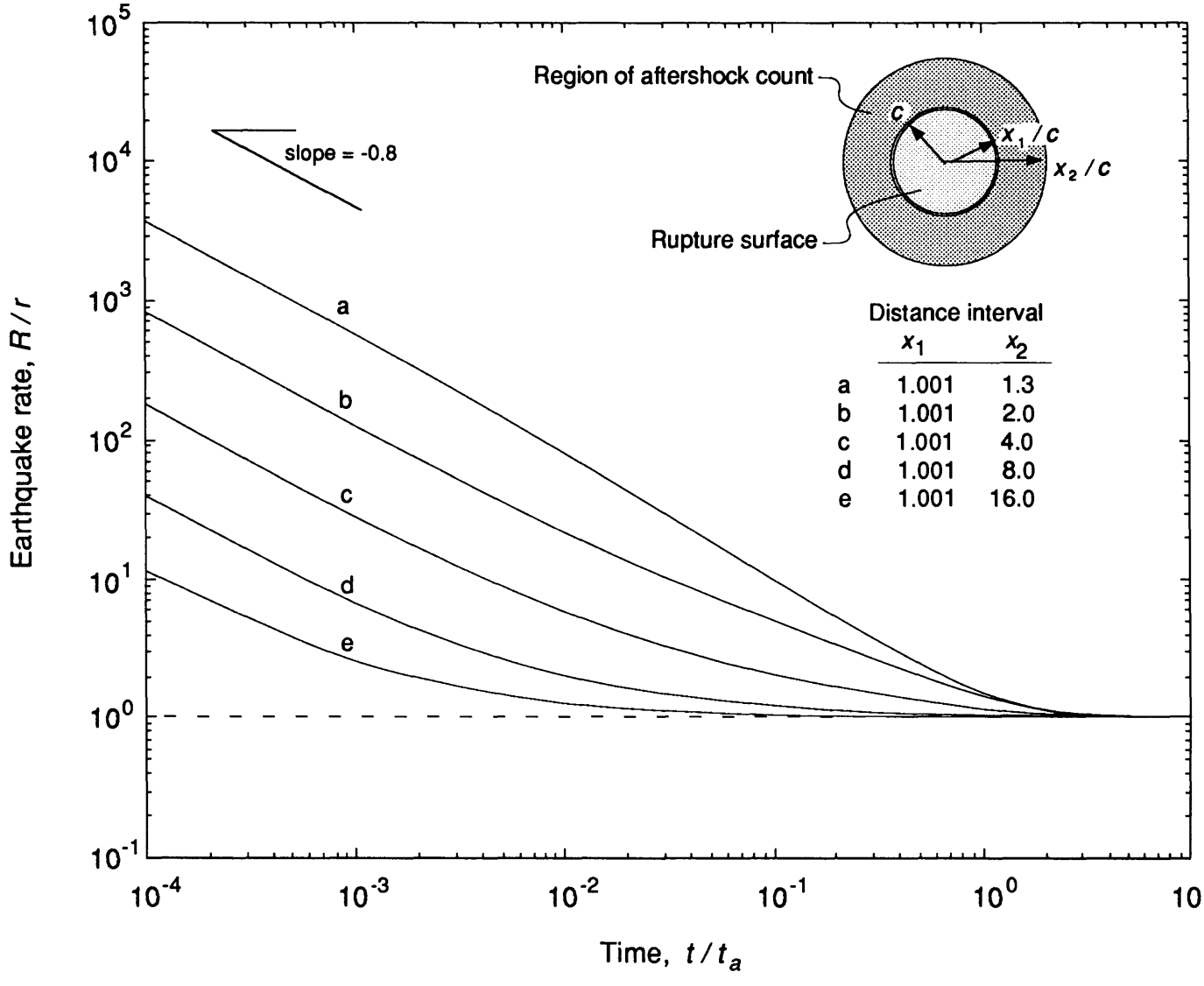

Figure 5 Net earthquake rate for finite regions surrounding a shear crack. a) Seismicity rate for cumulative distance from edge of crack.

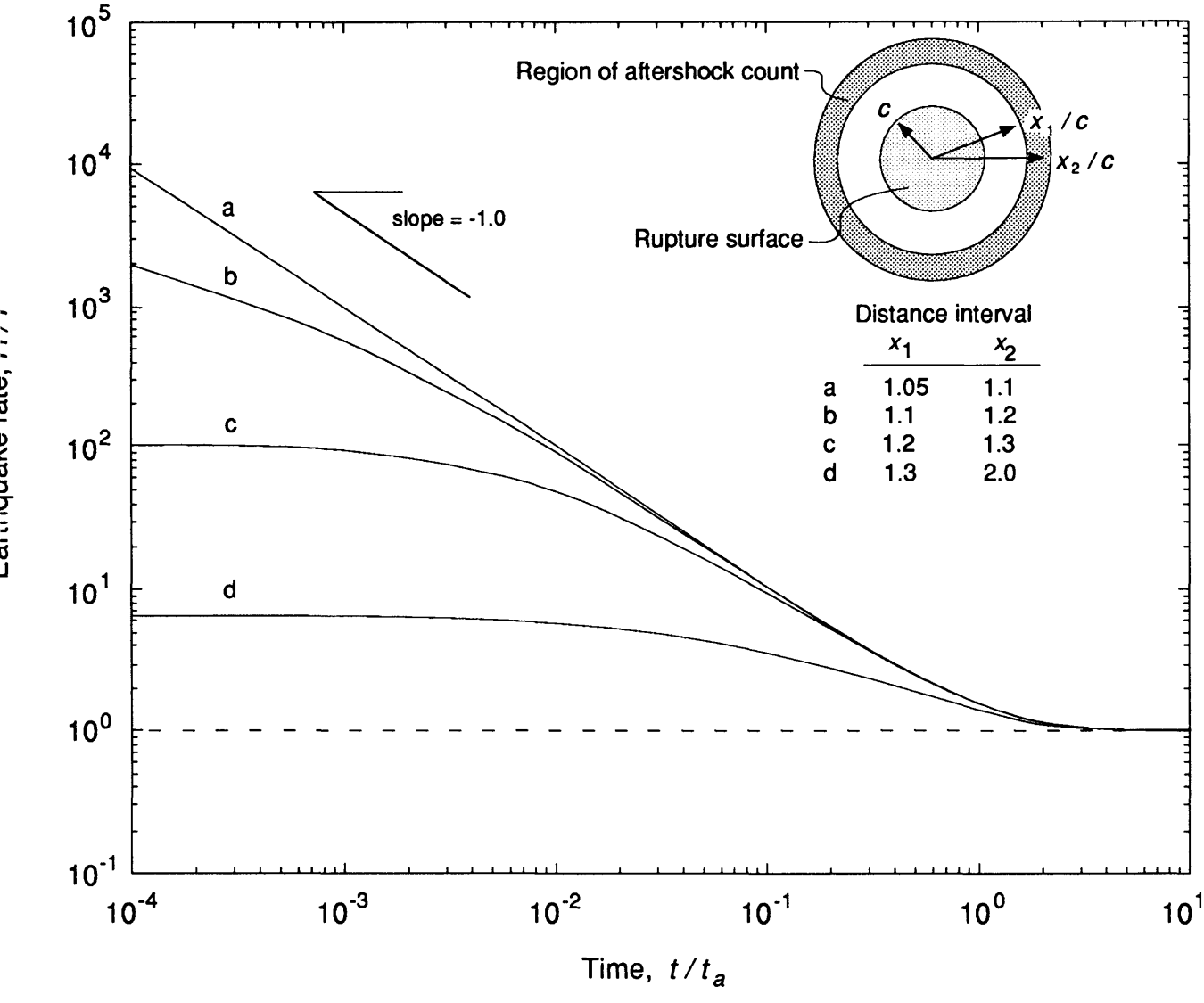

Figure 5 Net earthquake rate for finite regions surrounding a shear crack. b) Seismicity rate for annular distance segments.

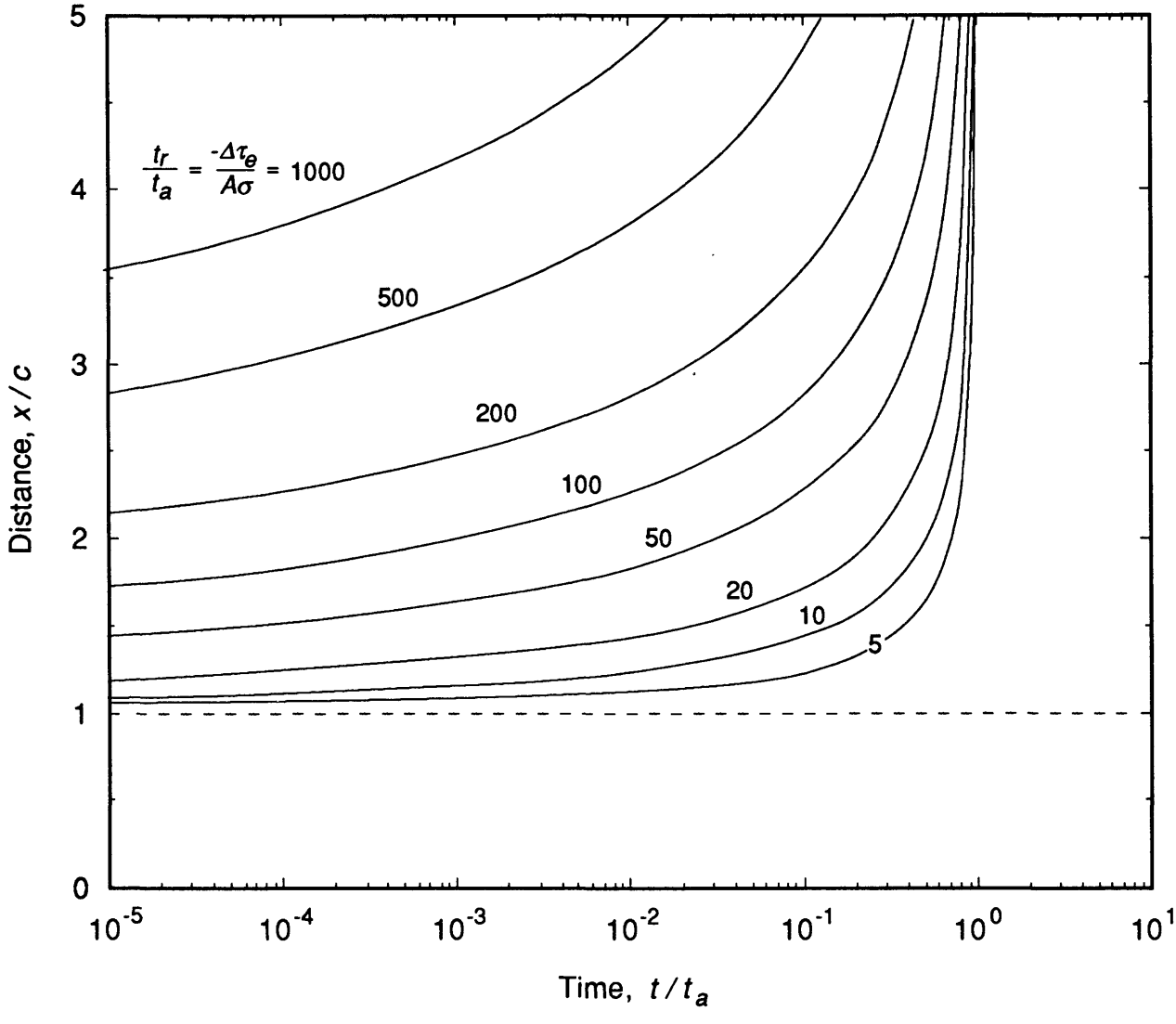

Figure 6 Expansion of aftershock zone from equation (22). Curves give the position of the edge of the aftershock zone as given by x_e where earthquake rate begins to merge with the $1/t$ asymptote.

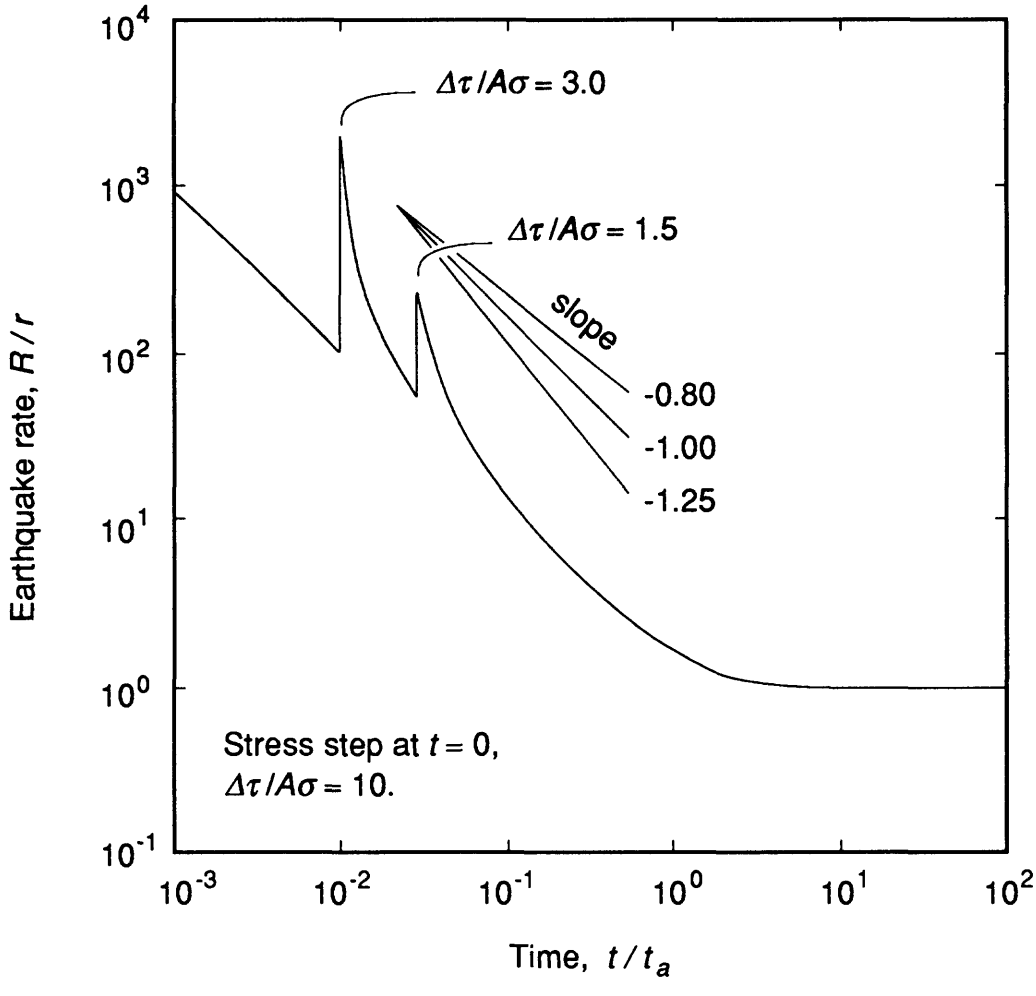

Figure 7 Seismicity rate for stressing history consisting of several stress steps. The second and third stress steps represent large aftershocks which give rise to secondary aftershock sequences.

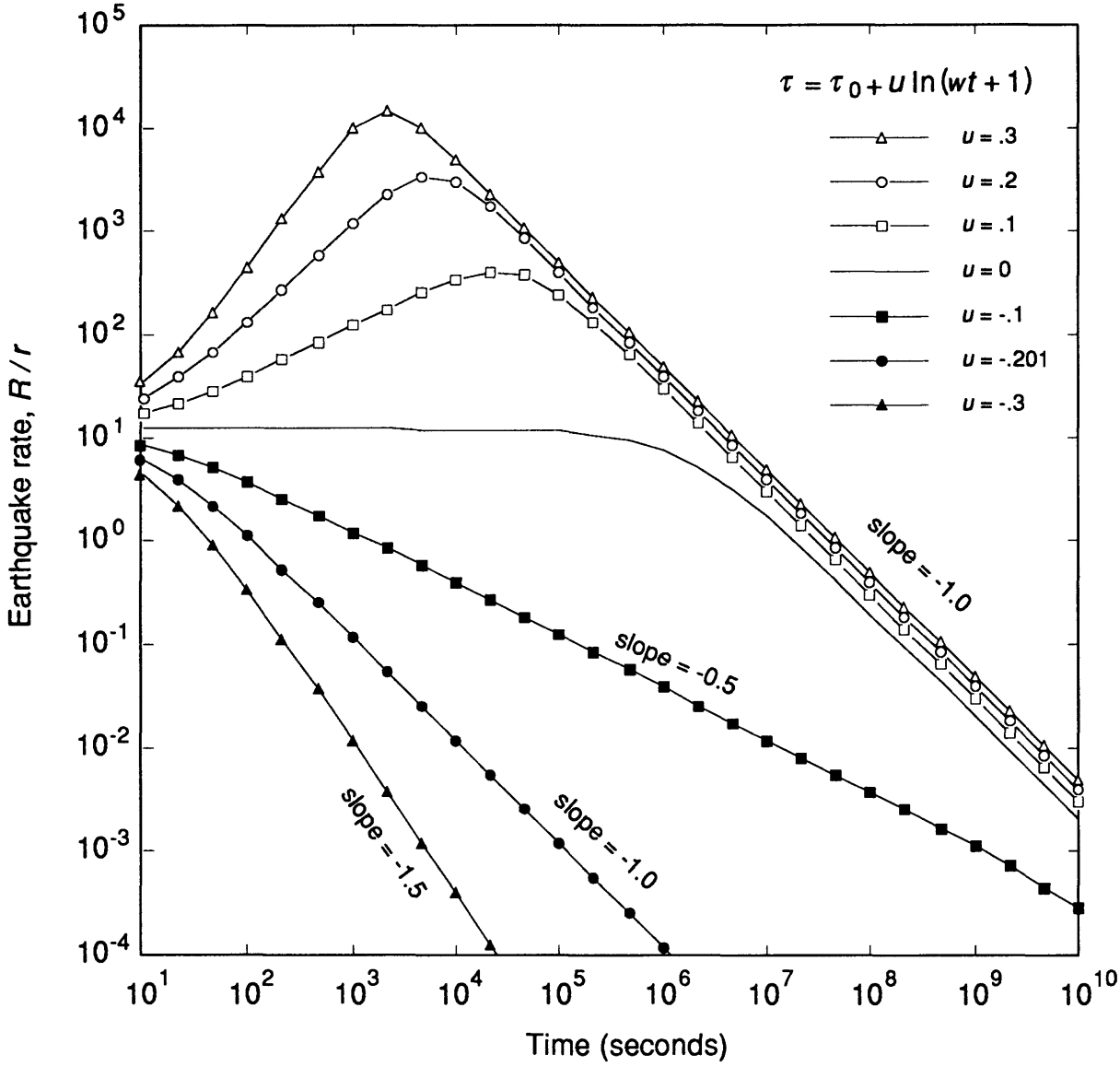

Figure 8 Seismicity rate for a stressing history composed of a stress step followed by change of stress with logarithm of time. Parameters for the computation are: A=0.01, σ=20 MPa, $\dot{\tau}_r$=10^{-8} MPa/s, $\Delta\tau$=0.5 MPa, w=10s.

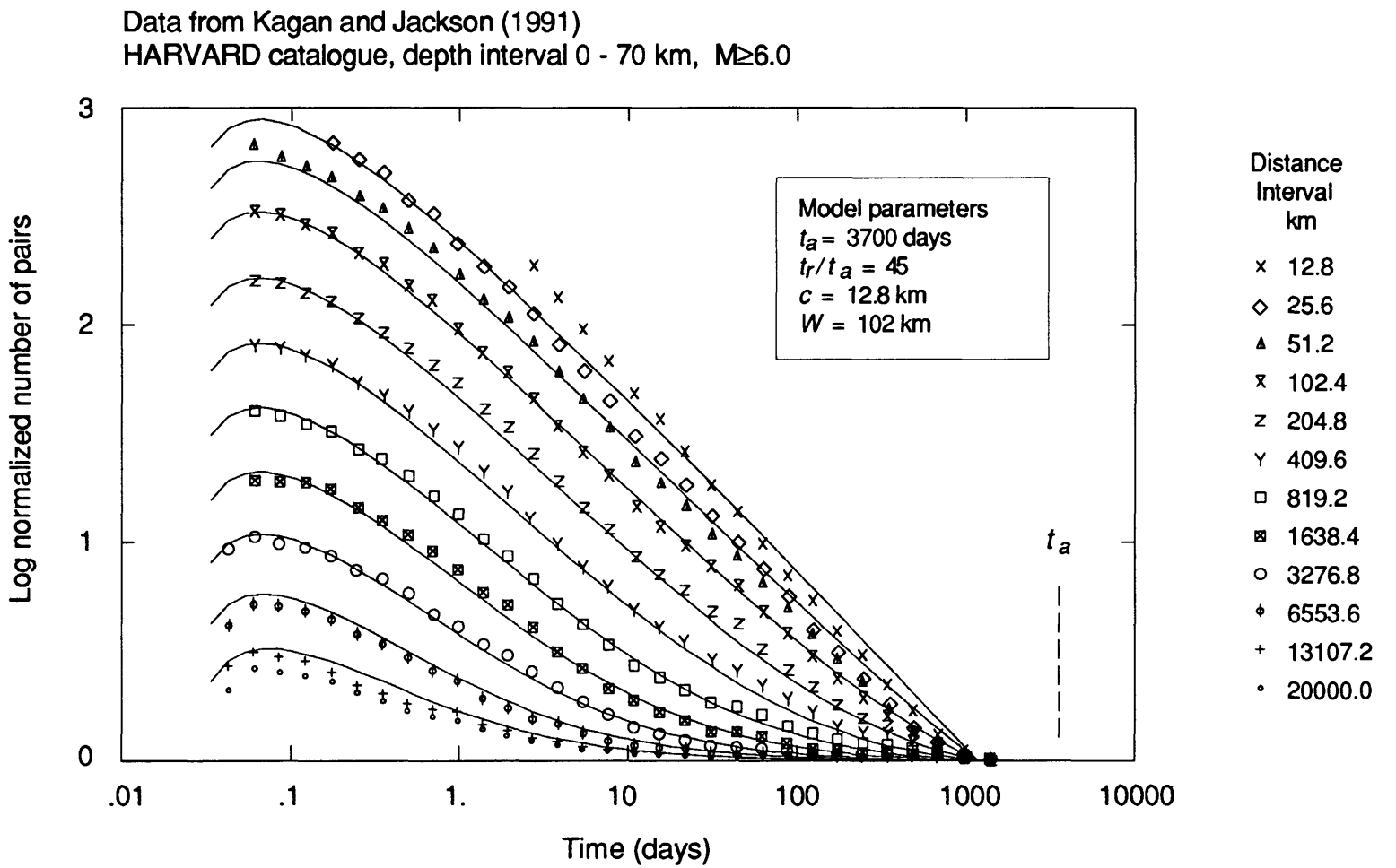

Figure 9a Clustering of shallow earthquake pairs. Data from *Kagan and Jackson* [1991]. Curves give examples of simulations using model of Figure 10.

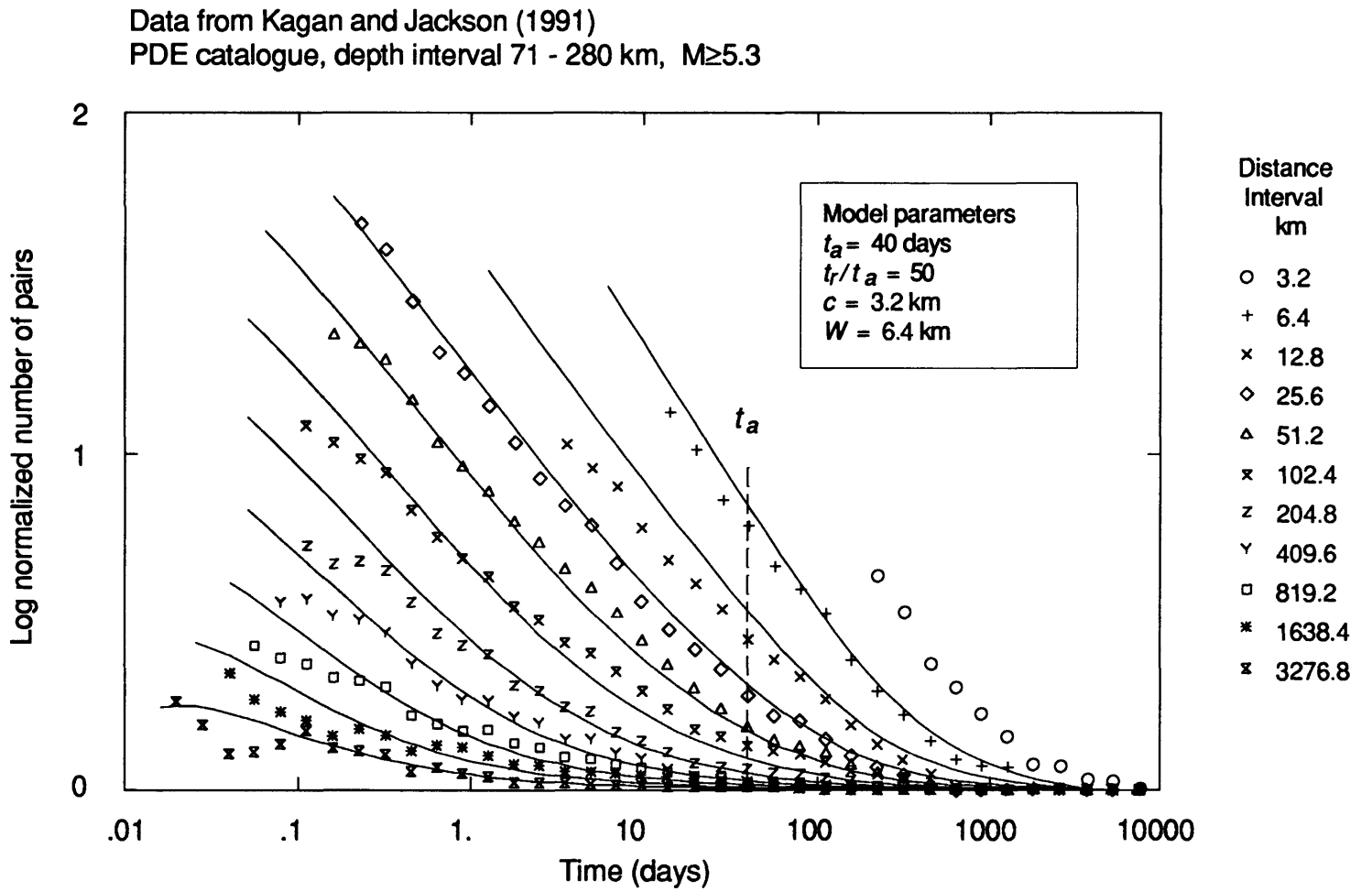

Figure 9b Clustering of intermediate depth earthquake pairs. Data from *Kagan and Jackson* [1991]. Curves give examples of simulations using model of Figure 10.

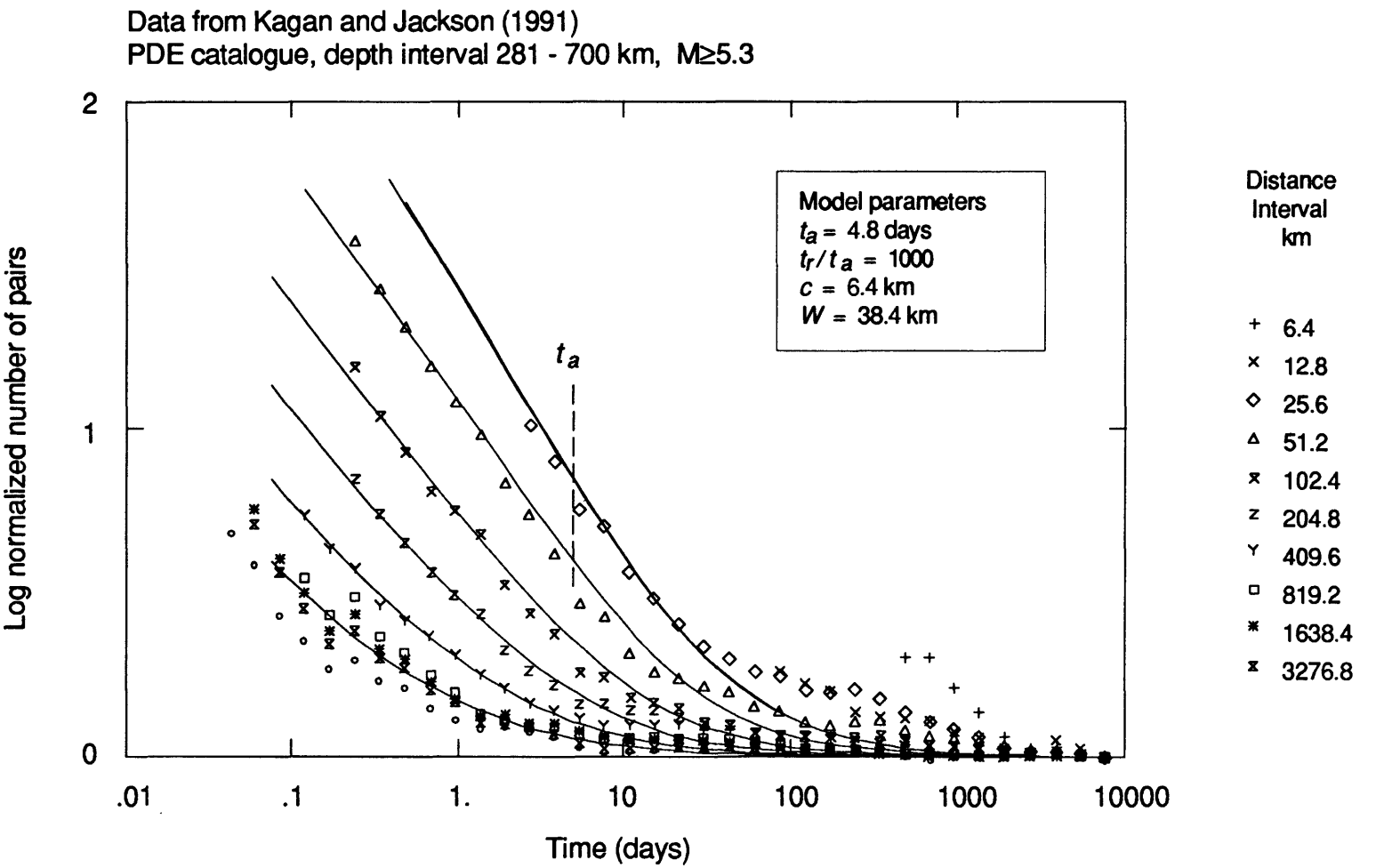

Figure 9c Clustering of deep earthquake pairs. Data from *Kagan and Jackson* [1991]. Curves give examples of simulations using model of Figure 10.

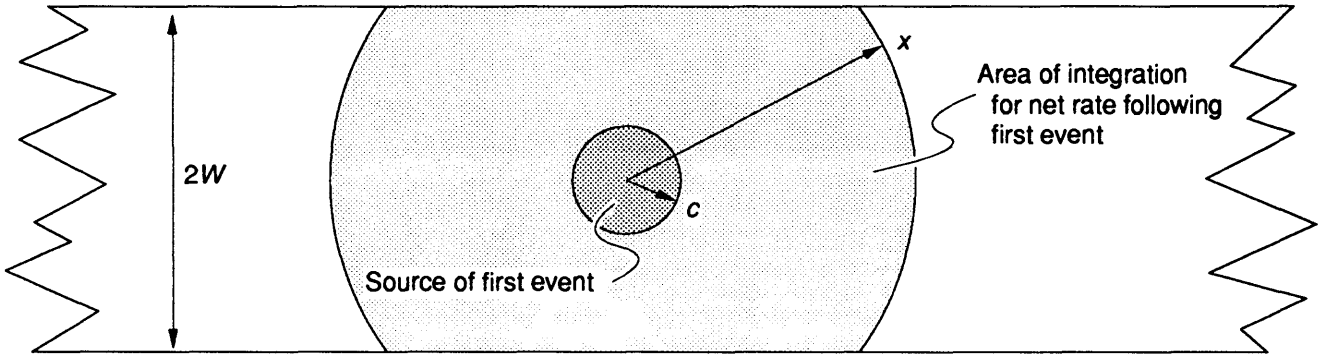

Figure 10 Model employed for simulation of clustering of earthquake pairs.

APPENDIX (A)
EARTHQUAKE NUCLEATION

Nucleation model. The following summarizes results obtained for a simplified model of a nucleation source that is represented as single spring-slider system. Details of the model and comparison of the simple model with plane strain numerical solutions of a fault with spatially variable conditions are given by *Dieterich* [1992]. Here the spring and slider results of *Dieterich* [1992] are generalized somewhat by incorporating of multiple state representation of fault friction (equation 5). Additionally, results are obtained for the change of conditions on a source arising from a step in both shear and normal stress.

Spring stiffness, k, may be scaled to crack length by:

$$k = \frac{\Delta\tau}{\delta} = \frac{G\eta}{l} \quad , \tag{A1}$$

where l is half-length or radius of the fault segment, G is shear modulus (Poisson's ratio of 0.25), and η is a crack geometry parameter with values near 1 [*Dieterich*, 1986; 1992]. For an instability to develop, k must be less than the critical stiffness for unstable slip [*Dieterich*, 1981; *Ruina*, 1983; *Rice and Ruina*, 1983; *Dieterich and Linker*, 1992]. Hence, from (A1) critical spring stiffness can be related to a minimum dimension for unstable slip giving

$$l_c = \frac{G\,\eta D_c}{\xi\,\sigma} \quad , \tag{A2}$$

where ξ is a parameter that depends on constitutive properties and loading conditions. It is found that the nucleation process is characterized by an interval of self-driven accelerating slip that precedes instability. The duration of the nucleation process is highly sensitive to initial stress and initial θ. The numerical simulations demonstrate that the

segment on which instability nucleates also has a characteristic length l_c that scales by (A2). Empirical evaluation of the size of the nucleation zone from the numerical models gives $\xi \sim 0.4B$. If accelerating slip initiates on a patch that exceeds l_c the zone of most rapid acceleration tends to shrink to the characteristic length as the time of instability approaches.

Equating constitutive law (5) for fault strength with fault stress gives

$$\frac{\tau(t) - k\delta}{\sigma} = \mu_0' + A \ln \dot{\delta} + \sum_{i=1}^{n} B \ln \theta_i \quad , \tag{A3}$$

where $\tau(t)$ is the remotely applied stress acting on the fault in the absence of slip and $-k\delta$ is the decrease in stress due to fault slip. In (A3) the constant terms μ_0, $A \ln \dot{\delta}^*$ and $B_i \ln \theta^*_i$ have been grouped into μ_0'. Normal stress is assumed to be constant. Recall that θ evolves with sliding history as given by equation (6). The problem may be solved numerically. However, when the nucleation process is under way and slip is accelerating, the slip speed soon greatly exceeds the steady state speed for all θ_i (*i.e.* $\theta_i >> D_{c_i}/\dot{\delta}$). As this happens, the $1/\dot{\delta}$ term in (6) will no longer contribute to the evolution and (6) is well-approximated by

$$\left(\frac{\partial \theta_i}{\partial \delta}\right)_{\sigma = const} = -\frac{\theta_i}{D_{c_i}} \quad , \quad \theta_i = \theta_{0_i} e^{-\delta / D_{c_i}} \quad . \tag{A4}$$

Hence, state is simply dependent on displacement, where θ_{0_i} is state at $\delta = 0$.

For slip at constant normal stress, substitution of (A4) into (A3) yields

$$\frac{\tau(t) - k\delta}{\sigma} = \mu_0' + A \ln \dot{\delta} + \sum_{i=1}^{n} B_i \ln \theta_i^0 - \delta \sum_{i=1}^{n} \frac{B_i}{D_{c_i}} \quad . \tag{A5}$$

For a variety of functions for the remote stressing term (A5) yields a separable differential equation that may be solved directly.

Constant stressing rate. For the case of constant rate of remote loading, $\tau(t) = \tau_0 + \dot{\tau} t$, (A5) may be rearranged by solving for $\dot{\delta} = d\delta/dt$ giving

$$\dot{\delta}_0 \int_0^t exp\left\{ \frac{\dot{\tau} t}{A\,\sigma} \right\} dt = \int_0^\delta exp\left\{ \frac{-H\,\delta}{A} \right\} d\delta \quad , \tag{A6}$$

where $\dot{\delta}_0$ and H contain terms for the initial conditions and model constants, respectively

$$\dot{\delta}_0 = \left[\left(\theta_1^0\right)^{-B_1/A} \left(\theta_2^0\right)^{-B_2/A} \ldots \right] exp\left\{ \frac{\tau_0/\sigma - \mu_0'}{A} \right\} \tag{A7}$$

$$H = -\frac{k}{\sigma} + \sum_{i=1}^{n} \frac{B_i}{D_{c_i}} \quad . \tag{A8}$$

Note in (A7) that the initial slip speed, $\dot{\delta}_0$, fully describes the initial conditions τ_0 and θ_i^0. Equation (A6) has the following solutions:

$$\delta = \frac{-A}{H}\, ln\left\{ \frac{\dot{\delta}_0 H\,\sigma}{\dot{\tau}} \left[1 - exp\left(\frac{\dot{\tau} t}{A\,\sigma} \right) \right] + 1 \right\} \quad , \quad \dot{\tau} \neq 0 \quad , \tag{A9}$$

$$\delta = \frac{-A}{H}\, ln\left\{ 1 - \frac{\dot{\delta}_0 H\, t}{A} \right\} \quad , \quad \dot{\tau} = 0 \quad . \tag{A10}$$

The slip speeds are:

$$\dot{\delta} = \left\{ \left[\frac{1}{\dot{\delta}_0} + \frac{H\sigma}{\dot{\tau}} \right] \left[exp\left(\frac{-\dot{\tau} t}{A\sigma} \right) \right] - \frac{H\sigma}{\dot{\tau}} \right\}^{-1} \quad , \quad \dot{\tau} \neq 0 \tag{A11}$$

$$\dot{\delta} = \left[\frac{1}{\dot{\delta}_0} - \frac{H t}{A} \right]^{-1} \quad , \quad \dot{\tau} = 0 \tag{A12}$$

The time of instability, t, is obtained by substituting $\dot{\delta}_i$, the slip speed at instability, into (A11) and (A12). The following employs $1/\dot{\delta}_i = 0$. Use of finite $\dot{\delta}_i$ while tractable, introduces additional terms into the equations and does not result in solutions that are numerically distinguishable from the simpler solutions provided $\dot{\delta}_i$ is much greater than the average long term fault slip rate. This condition is well satisfied for earthquake processes where $\dot{\delta}_i$ is cm/s to m/s and long term slip rates are mm/year to cm/yr. Time of instability is

$$t = \frac{A\sigma}{\dot{\tau}} ln\left(\frac{\dot{\tau}}{H\sigma\dot{\delta}_0} + 1 \right) \quad , \quad \dot{\tau} \neq 0 \quad , \tag{A13}$$

$$t = \frac{A}{H}\left(\frac{1}{\dot{\delta}_0} \right) \quad , \quad \dot{\tau} = 0 \quad . \tag{A14}$$

The evolution of state on a nucleation source after some time interval is readily obtained from the displacement solution and (A2). The results of (A13 and A14) are in surprisingly good agreement with the times to instability obtained from detailed numerical simulations of a fault with spatial variation of conditions [*Dieterich*, 1992].

The above solutions have the useful characteristic that they may be applied repeatedly, in a step-by-step manner, to approximate complicated stressing histories as a series of constant stressing rate increments. Recall that initial slip speed fully describes the initial

conditions. Hence, the initial slip speed, $\dot{\delta}_0$, at the start of each time interval in a loading history, is obtained from the solution for slip speed (A13, A12) at the end of the previous time interval.

The effects of jumps of normal stress and shear stress on slip speed may be found from the constitutive relations (A5 and A6). Before a stress jump, slip speed depends on initial stress and state as given by (A7) (taking $\sigma = \sigma_0$). Similarly, the slip speed following the stress jump depends on τ, σ and θ after the step. Jumps of τ do not affect state, but from (6) change of normal stress from σ_0 to σ, results in the change of state

$$\theta_i = \theta_i^0 \left(\frac{\sigma}{\sigma_0} \right)^{-\alpha_i/B_i} . \tag{A15}$$

Hence, from (A7) and (A15), after the stress jump

$$\dot{\delta} = \left[\left(\theta_1^0\right)^{-B_1/A} \left(\theta_2^0\right)^{-B_2/A} \cdots \right] \left[\left(\frac{\sigma}{\sigma_0} \right)^{\alpha_1/A} \left(\frac{\sigma}{\sigma_0} \right)^{\alpha_2/A} \cdots \right] exp\left\{ \frac{\tau}{A\sigma} - \frac{\mu_0'}{A} \right\} . \tag{A16}$$

Using (A7) the state terms in (A16) may be defined in terms of initial stresses and $\dot{\delta}_0$ giving:

$$\dot{\delta} = \dot{\delta}_0 \left(\frac{\sigma}{\sigma_0} \right)^{\alpha/A} exp\left(\frac{\tau}{A\sigma} - \frac{\tau_0}{A\sigma_0} \right), \quad \alpha = \sum_{i=1}^{n} \alpha_i . \tag{A17}$$

APPENDIX (B)
FORMULATION FOR EFFECT OF STRESSING HISTORY ON EARTHQUAKE RATE

Distribution of Conditions for Steady-State Seismicity. Taking $dn/dt = r$ as the reference rate of seismicity, the time of an earthquake at source n is,

$$t = \frac{n}{r} \quad . \tag{B1}$$

In Appendix A, initial slip speed is shown to fully describe the initial conditions for subsequent acceleration of slip to instability (equation A7). The distribution of initial conditions over the steady-state population of patches is obtained by equating the result for time of instability (A13) with (B1) and rearranging to give initial slip speed as the dependent variable:

$$\dot{\delta}(n) = \frac{1}{\left[\frac{H\sigma}{\dot{\tau}_r}\right]\left[exp\left(\frac{\dot{\tau}_r n}{A\sigma r}\right) - 1\right]} \quad , \quad \dot{\tau}_r \neq 0 \tag{B2}$$

where, $\dot{\tau}_r$ is the reference stressing rate. Hence, the time of instability at the nth source may be found by evaluating (B2) at n to obtain $\dot{\delta}_0$ and then substituting that value into the appropriate solution for time to instability, *e.g.* equation (A14). For later convenience, (B2) is rewritten as

$$\dot{\delta}(n) = \frac{1}{H\sigma\gamma\left[exp\left(\frac{\dot{\tau}_r n}{A\sigma r}\right) - 1\right]} \quad . \tag{B3}$$

Hence, for the reference steady-state distribution, $\gamma = 1/\dot{\tau}_r$. Below, the effects of stressing history on the distribution (B3) are examined. It is shown that the distribution of slip speeds is always of the form of (B3), but with different values of γ that evolve with stressing history.

Evolution equation for distribution. The general equation for evolution of γ is found by evaluating the partial derivatives in

$$d\gamma = \left(\frac{\partial \gamma}{\partial t}\right)_{\tau,\sigma} dt + \left(\frac{\partial \gamma}{\partial \tau}\right)_{t,\sigma} d\tau + \left(\frac{\partial \gamma}{\partial \sigma}\right)_{t,\tau} d\sigma \quad . \tag{B4}$$

To find $\left(\frac{\partial \gamma}{\partial t}\right)_{\tau,\sigma}$ the distribution $\dot{\delta}(n)$ of equation (B3) is substituted for $\dot{\delta}_0$ in (A12) giving the distribution of slip speeds after some elapsed time, t, at $\dot{\tau}=0$, $\dot{\sigma}=0$,

$$\dot{\delta}(n) = \frac{1}{H\sigma\gamma_0 \left[exp\left(\frac{\dot{\tau}_r n}{A\sigma r}\right) - 1 \right] - \frac{H t}{A}} \quad . \tag{B5}$$

The use of γ_0 indicates the value of γ at t=0. After time t has elapsed, some number of sources, I, will have nucleated earthquakes because the speed for onset of instability, $\dot{\delta}_i$ has been reached. Consequently, those sources will no longer be a part of the population. Setting $\dot{\delta}(n) = \dot{\delta}_i = \infty$ and $n = I$ in (B5) and solving for I gives

$$I = \frac{A\sigma r}{\dot{\tau}_r} ln\left[1 + \frac{t}{\gamma\sigma A}\right] . \tag{B6}$$

The updated distribution of slip speeds, after time increment t, is obtained by the substitution $I + n = n_{old}$ in (B5), where n_{old} now refers to n appearing in (B5), prior to the time step and using (B6) to evaluate I. Following some algebra, the new evolved distribution is found to have the form of (B3) as previously asserted with

$$\gamma = \gamma_0 + \frac{t}{\sigma A} \quad , \tag{B7}$$

which gives

$$\left(\frac{\partial \gamma}{\partial t}\right)_{\tau,\sigma} = \frac{1}{A\,\sigma} \quad . \tag{B8}$$

A similar procedure is used to evaluate $\left(\frac{\partial \gamma}{\partial \tau}\right)_{t,\sigma}$ and $\left(\frac{\partial \gamma}{\partial \sigma}\right)_{t,\tau}$. From (B3) and (A17) the distribution of slip speeds following a step in shear stress and normal stress is

$$\dot{\delta}(n) = \frac{\left(\frac{\sigma}{\sigma_0}\right)^{\alpha/A} exp\left(\frac{\tau}{A\sigma} - \frac{\tau_0}{A\sigma_0}\right)}{H\sigma\gamma\left[exp\left(\frac{\dot{\tau}_r\, n}{A\sigma r}\right) - 1\right]} \quad . \tag{B9}$$

Figure 1 illustrates the effect of a stress step on the distribution. A stress step that increases slip speed (an increase of shear stress or decrease of shear stress) will cause some number of patches, I, to nucleate earthquakes if the slip speed, $\dot{\delta}_i$ at instability is finite. Setting $\dot{\delta} = \dot{\delta}_i$ in (B9) and solving for the number sources, I, that have nucleated an earthquake gives:

$$I = \frac{A\,\sigma r}{\dot{\tau}_r} ln\left\{1 + \frac{1}{\gamma_0}\left[(H\sigma\dot{\delta}_i)^{-1}\left(\frac{\sigma}{\sigma_0}\right)^{\alpha/A}\right] exp\left(\frac{\tau}{A\sigma} - \frac{\tau_0}{A\sigma_0}\right)\right\} . \tag{B10}$$

The new distribution of conditions following the stress step is obtained by the substitution, $I + n = n_{old}$, in (B9) and using (B10) to evaluate I. Use of either finite or infinite $\dot{\delta}_i$ at

instability again yields an evolved distribution of the form of (B3) with

$$\gamma = \gamma_0 \left(\frac{\sigma}{\sigma_0} \right)^{-\alpha / A} exp\left(\frac{\tau_0}{A\sigma_0} - \frac{\tau}{A\sigma} \right) , \tag{B11}$$

where γ_0 denotes the value of γ immediately prior to the stress step. From this result

$$\left(\frac{\partial \gamma}{\partial \tau} \right)_{t,\sigma} = \frac{-\gamma}{A\,\sigma} , \tag{B12}$$

and

$$\left(\frac{\partial \gamma}{\partial \sigma} \right)_{t,\tau} = \frac{\gamma \tau}{A\,\sigma^2} - \frac{\gamma \alpha}{A\,\sigma} . \tag{B13}$$

In summary, the distribution of slip speeds retains the form of (B3) through time (with $\dot{\tau}=0$, $\dot{\sigma}=0$) and through steps in shear and normal stress. Because any loading history may be represented as a sequence of sufficiently small stress jumps and time steps (with $\dot{\tau}=0$, $\dot{\sigma}=0$), the distribution of slip speeds will retain the form of (B3) for any stressing history. From (B4), (B8), (B12) and (B13) the general evolution equation for γ is

$$d\gamma = \frac{1}{A\,\sigma} \left[dt - \gamma d\tau + \gamma \left(\frac{\tau}{\sigma} - \alpha \right) d\sigma \right] . \tag{B14}$$

Recall from (A17) that $\alpha = \alpha_1 + \alpha_2 + \ldots$ for applications employing friction formulations with multiple state variables.

Solutions for linear and logarithmic shear stressing. Solution of (B14) for change of γ for increase of shear stress at a constant rate and by logarithm of time are easy to obtain and of use for modeling earthquake processes. If shear stress is given by

$$\tau = \tau_0 + \dot{\tau} t \ , \tag{B15}$$

and $\dot{\sigma}=0$, then from (B14) evolution of γ is given by

$$d\gamma = \frac{1}{A\,\sigma}\left[\, 1 - \gamma \dot{\tau}\right] dt \quad , \tag{B16}$$

which has the solution

$$\gamma = \left[\, \gamma_0 - \frac{1}{\dot{\tau}} \right] exp\left[\frac{-\,t\,\dot{\tau}}{A\sigma} \right] + \frac{1}{\dot{\tau}} \ . \tag{B17}$$

For logarithmic stressing,

$$\tau = \tau_0 + u \ln (wt + 1) \ , \tag{B18}$$

and $\dot{\sigma}=0$, the evolution equation (B14) becomes

$$d\gamma = \frac{1}{A\,\sigma}\left[\, 1 - \frac{\gamma u\, w}{bt + 1}\right] dt \ . \tag{B19}$$

Using the integrating factor

$$(wt + 1)^{m}, \ \text{where} \ m = \frac{u}{A\sigma} \ , \tag{B20}$$

B(19) has the solution

$$\gamma = \gamma_0 (wt + 1)^{-m} + \frac{(wt + 1) - (wt + 1)^{-m}}{A\sigma w\, (m + 1)} \ . \tag{B21}$$

These solutions may also be obtained using the procedure of the previous section which evolves the distribution of initial slip speeds by employing the specific solutions for increase of slip speed with time of a source. Conversely, the earlier solutions for evolution of γ for constant stress and for stress steps, equations (B7) and (B11) respectively may of course be obtained by direct solution of (B14).

Seismicity rate. Under the condition $\dot{\tau}=0$, $\dot{\sigma}=0$, the distribution of earthquakes times, beginning at $t= 0$ is found from (A14) by substituting the distribution of slip speeds (B3) for initial slip speed, $\dot{\delta}_0$. In making this substitution note that the distribution of initial speeds is fixed at $t = 0$ and consequently γ is fixed at γ_0. The distribution of times of earthquakes is

$$t = \sigma A \gamma_0 \left[exp\left(\frac{\dot{\tau}_r\, n}{A\sigma r}\right) - 1 \right] \quad , \quad \dot{\tau}=0 \, , \, \dot{\sigma}=0 \quad . \tag{B22}$$

Rearranging for n

$$n = \frac{A\sigma r}{\dot{\tau}_r} ln\left[\frac{t}{A\sigma\gamma_0} + 1\right] \quad , \quad \dot{\tau}=0 \, , \, \dot{\sigma}=0 \, , \tag{B23}$$

and differentiating gives seismicity rate $R = dn/ dt$ normalized by the reference rate, r

$$\frac{R}{r} = \frac{1/\dot{\tau}_r}{\frac{t}{A\sigma} + \gamma_0} \quad , \dot{\tau} = 0 \, , \, \dot{\sigma} = 0 \quad . \tag{B24}$$

Note that the denominator of the solution for seismicity rate is simply the specific solution of $\gamma(t)$ given in (B7) for these stressing conditions ($\dot{\tau}=0$, $\dot{\sigma}=0$).

This suggests

$$R = \frac{r}{\dot{\gamma}\ \dot{\tau}_r} \quad , \tag{B25}$$

as a general formulation for any stressing history. Hence, it is proposed that at any instant seismicity rate depends on the current value of γ and is independent of current stressing rate. The validity of (B25) for any stressing history may be understood by considering the nucleation process during unconstrained loading histories. As implied by (B4) and as discussed previously, the evolution of γ for any loading history may be found by breaking the loading history into a series of sufficiently small stress jumps and time increments with $\dot{\tau}$=0, $\dot{\sigma}$=0. Because γ determines the initial conditions for the time to instability, (B25) will be generally valid if the time to instability becomes independent of stressing rate as time decreases to zero. The solutions for time of instability for $\dot{\tau}$=0 (A13) and for $\dot{\tau}\neq 0$ (A14) converge and become independent of stressing rate as slip speed approaches the critical speed for instability demonstrating that this condition is satisfied. Indeed, (B25) may be obtained following the above procedures using solutions for time to instability and evolution of γ under conditions where stressing rate is not zero (*i.e.*$\tau=\tau_0+\dot{\tau}t$, $\dot{\sigma}$=0 and $\tau=\tau_0+u\ \ln(wt+1)$, $\dot{\sigma}$=0).

Equations (B14) and (B25) comprise the general formulation for stressing history dependence of seismicity rates.

Foreshock Occurrence in Kanto, Cental Japan, and its Performance as a Precursor

Masajiro IMOTO

National Research Institute for Earth Science and Disaster Prevention

Tsukuba, Ibaraki,305, Japan

Abstract

A simple algorithm to issue short term alarms is applied to catalog data obtained from a local seismograph network in Kanto, central Japan. This algorithm is based on an assumption that the last interevent time of small seismic events preceding a large earthquake is shorter than the mean interevent time for small earthquakes before the large earthquake. To investigate this assumption, interevent times are studied for earthquakes preceding 14 moderately large earthquakes which occurred with magnitude 5.5 and larger during the period from 1982 to 1991 in a 180 x 180 x 100 km volume. The last interevent time associated with each large earthquake is compared with the mean interevent time between successive earthquakes within a certain distance from the respective earthquake. This comparison suggests that the last interevent times tends to be shorter than the respective mean times. The last interevent times however, vary from 0 to several days. Therefore obvious foreshocks are unable to be determined in the present study. In the algorithm all earthquakes larger than a threshold magnitude of 2.0 are defined as a potential foreshock and an alarm is issued for a small volume (10-20 km in radius) at every foreshock occurrence. This alarm persists for several days (5-10 days), but may be terminated before this limit by the occurrence of an earthquake in the same volume larger than the foreshock. By this simple algorithm values from 0.5 to 0.9 and from 5. to 18. depending on parameters are obtained for reliability and probability gain, respectively. An assumption is made that the large earthquakes may be modeled by two Poisson processes with different rates: the higher rate process simulates large earthquakes that occur in the time-space volume when an earthquake alarm has been declared and the lower rate process similates earthquakes that occur in a non-alarm time-space volume. The performance of the proposed algorithm is measured in terms of the likelihood ratio of the two Poisson rate model to a uniform Poisson model. The likelihood ratio obtained by this study shows that a high level of significance is attached to the two Poisson process model.

1. Introduction

An anomalous increase in local seismicity prior to a large earthquake is one of the best known phenomena among earthquake precursors. Foreshocks sometimes make it possible to predict an earthquake with pin-point accuracy. For example, foreshock activity played an essential role in issuing a short-term warning of the Haicheng earthquake. However, only rarely are forshocks recorgnized before the occurrence of their main shock, because a quantitative definition of foreshocks that distinguishes them from background seisimicity has not been established yet. A large number of studies have been attempted to find characteristic features of foreshocks based on seismicity patterns, wave forms and other data. Analyzing the spatial and temporal distributions of seismicity preceding moderate ($M \geq 5.0$) main shocks in the San Andreas fault system in California, Jones (1984) reported that of 20 main shocks, 7 had been preceded by immediate foreshock sequences that had included events within 1 day and 5 km of the main shock. Bowman and Kisslinger (1984) applied a statistical method for estimating the ocurrence of foreshocks to the catalog of earthquakes from a local seismograph network near Adak, Alaska. In this study, foreshocks were defined in a restricted sense based on time intervals between successive earthquakes. They concluded that detectable foreshocks preceded about 6 to 10 per cent of 53 main shocks of $mb \geq 4.5$ and 14 per cent of 23 main shocks of $mb \geq 5.0$. As they noted, their method for estimating foreshock occurrence can not be applied prospectively.

Assuming simple Poisson process models for earthquakes of $M \geq 2.0$ in Kanto, central Japan, Imoto (1992) reported that increases in the Poisson rate appear more frequently than decreases one or two years before prominent earthquakes of magnitude 6.0 and larger. Imoto (1991) also reported decreases in b-value before these earthquakes. These findings suggest that intermediate term changes in seismicity appeared around the source areas of these earthquakes. Since it is possible that these changes be followed by a short term change in seismicity, it is worthwhile investigating in foreshock activity in the Kanto area. From a viewpoint of earthquake prediction, definition of foreshocks in the present study is designed simple and applicable as a prediction tool. Any definition should be applied prospectively to data and results are measured in terms of parameters estimating performance of earthquake prediction such as validity and reliablity (Reasenberg and Matthews, 1988). In addition to these two parameters, a new scale based on information theory will be proposed. This scale is needed to make the best selection of parameters concerning each definition of anomalies.

2. Data

Occurrences of foreshocks are studied for data from the Kanto area in central Japan (Fig.1), which were collected by the network of the National Research Institute for Earth Science and Disaster Prevention. This area is characterized by its complex tectonic features: the Pacific and the Philippine Sea plates, which are subducting beneath the Eurasian plate (or the North American plate), a triple junction of trench-trench-trench type located to the east, and others (Okada, 1990). Taking into consideration the detection capabilities of the network, tectonic environment and other factors, a 180 x 180 x 100 km volume (the dashed box in Fig.1) is chosen for study, in which the earthquake records of magnitude 2.0 and larger are considered complete (Morandi and Matsumura 1991). Within this volume, about 20,000 earthquakes of magnitude above this threshold are located from January 1982 through December 1991. Among these events, 14 moderately large earthquakes of magnitude 5.5 and larger are listed as target events for forecasting (Fig.1 and Table 1). The size of target events, $M \geq 5.5$, is chosen from consideration of seismicity in this area. The largest event is recorded as a magnitude 6.7 by Japan Meteorological Agency on December 17, 1987 in the study area. This earthquake, named Chiba Toho Earthquake, was followed by the largest aftershock of magnitude of 5.2. Lowering the threshold magnitude of target events would require that large aftershocks be classified into target events. The physical process of an aftershock might differ from that of a main shock and our interest is focused on forecasting a main shock rather than its aftershock. Accordingly, the threshold of target events is tenyatively set at magnitude 5.5. It is claimed that errors in hypocentral coordinates are less than a few kilometers in most cases. In this study, assuming that possible foreshocks are at most 20 km away from their mainshock, our analysis of foreshock occurence will be made in this range. Since the above mentioned errors should not seriously effect the results, relocation of earthquakes was not made.

3. Time interval

By inspecting space-time plots of earthquakes within 30 days and 30 km of each target event separetely, no obvious foreshocks, as distinct from background seismicity, were found, except for a few cases. Therefore, it is unlikely that an algorithm issuing an alarm 1 or 2 days before target events would work at high performance.

To compare seimicity just before target events with background seismicity, interevent times are studied for earthquakes within 2 years and 20 km of target events. The last interevent time associated with each target event is compared with the mean interevent time.

Table 1 List of target events.

Date	Year	H M	Lat.(N)	Long.(E)	Depth	M
Feb.27	1983	21:14	35.99	140.10	67.0	5.8
Oct. 4	1985	21:25	35.91	140.11	71.6	6.3
Feb.12	1986	11:59	36.38	141.01	24.7	6.0
Nov.29	1986	7:29	36.41	141.22	28.2	5.6
Dec.17	1987	11:08	35.37	140.52	47.3	6.4
Mar.18	1988	5:34	35.67	139.63	90.5	6.4
Feb.19	1989	21:27	36.05	139.90	45.4	6.1
Mar. 6	1989	23:39	35.71	140.67	51.5	6.1
Dec. 9	1989	2:23	36.59	141.07	37.4	5.6
May 3	1990	16:45	36.47	140.63	49.9	5.5
June 1	1990	10:22	35.67	140.74	49.0	5.8
Aug. 5	1990	12:36	36.43	141.19	27.4	5.7
Aug.23	1990	8:47	35.34	140.45	45.9	5.5
Aug. 6	1991	23:49	35.87	141.15	26.5	5.8

This comparison suggests that the last interevent times tend to be shorter than the respective mean times. The last interevent times, however, vary depending on each case from several seconds to several days. To display this result, the last interevent time for earthquakes within 12 km of target events is normalized by respective mean interevent time since seismicity rate in diffrent sources ranges from 1.5×10^{-6} events/day/km^3 to 3.1×10^{-5} events/day/km^3. If an interevent time ν is taken from a uniform Poisson process with its rate equal to 1., probability density function of ν is expected to be an exponential function of $\exp(-\nu)$. Distribution function obtained by integral from ν to infinity is given by $\exp(-\nu)$. Figure 2 shows both the expected exponential function and cumulative frequencies obtained by accumulating from infinity 14 normalized times for the case of radius 12 km. The cumulative frequency diagram of composing shows a steeper slope than that of expected distribution. This means that the Poisson rate becomes higher just before the largest event than that of expected from background seismicity. Similar patterns are observed in other cases of different radii. These suggest possibility of an anomalous increase in seismicity which differs distinctly from

background seismicity.

4. Algorithm

In the present study, all earthquakes larger than a threshold magnitude of 2.0 are assumed as a foreshock and an alarm is issued for a small spherical volume (radius = R_s) at every foreshock occurrence. This alarm persists for several days (T_d) unless it is terminated earlier by the occurrence of an earthquake larger by *dm* than the foreshock. The parameters, R_s, T_d and *dm*, respectively ranging from 10 km, 5 days, and 0.5 to 20 km, 10 days, and 2.0 over intervals of 2 km, 1 day and 0.5 respectively are adopted in our analyses. No effort to remove aftershocks has been made.

At the beginning of each day the alarm state is assessed for each grid point in a 3-D spatial grid with 2-km spacing filling the study volume, using data obtained up through the previous day. The total volume in a state of alarm in each day is represented by the total number of grid points included in an alarm state. When a target event occurs on a certain day and the nearest grid point belongs to an alarm, which has been judged in advance, it is considered that the target event was successfully predicted. Summing up the volume of alarm and the number of successes for the whole period, the total volume of alarm v_a and the total number of target events predicted n_a are obtained. The reliability R_b and probability gain P_g of the algorithm are respectively defined by

$$R_b = \frac{n_a}{n_o} ,$$

and

$$P_g = \frac{n_a}{v_a} \cdot \frac{v_o}{n_o} ,$$

where v_o and n_o are the total space-time volume under study and the total number of target event (=14 for M≥5.5), respectively (Aki, 1980; Reasenberg and Matthews, 1988).

Figures 3a and 3b show contours of reliability and probability gain, respectively, on the R_s-T_d plane in the case of *dm* equal to 1.0. The values of R_b and P_g range from 0.5 to 0.9 and from 5 to 18, respectively. Roughly speaking, R_b appears inversely correlated with P_g. Similar patterns are obtained for different values of *dm*. For an excellent algorithm of earthquake prediction, it is desirable that both R_b and P_g become large. Along this line , it is not easy to select the best combination of R_s, T_d and *dm*. To do this reasonably, a new scale to measure performance of earthquake prediction will be proposed in the next section.

5. Performance

An assumption is made that the target events may be modeled by two Poisson

processes with different rates: the higher rate process simulates large earthquakes that occur in the space-time volume when an earthquake alarm has been declared, and the lower rate process similates earthquakes that occur in a non-alarm space-time volume. The performance of the proposed algorithm is measured in terms of the likelihood ratio of the two Poisson rate model to a uniform Poisson model.

In the case of the uniform Poisson model, the likelihood L_1 is defined by

$$L_1 = e^{-\lambda v_a}(\lambda v_a)^{n_a} \cdot e^{-\lambda(v_o - v_a)}\{\lambda(v_o - v_a)\}^{n_o - n_a} / \{n_a!(n_o - n_a)!\} \quad ,$$

where λ is given by n_o/v_o. The likelihood of the two Poisson rate model is defined by

$$L_2 = e^{-n_a} n_a^{n_a} \cdot e^{-(n_o - n_a)}(n_o - n_a)^{n_o - n_a} / \{n_a!(n_o - n_a)!\} \quad .$$

The difference in log likelihod between two models, l_2-l_1 is obtained as

$$l_2 - l_1 = n_o \log P_g + n_o(1 - R_b)\log\left(\frac{1 - R_b}{P_g - R_b}\right) \quad .$$

This value is connected with the difference in AIC (dAIC), which was proposed by Akaike for model selection, through a simple relation:

$$dAIC = AIC_1 - AIC_2 = -2\times(l_1 - l_2) + 2\times(1 - 2) \quad .$$

Figures 4 to 7 show contours of *dAIC* on R_s-T_d planes for different values of *dm*.
The maximum of *dAIC* is rising up more than 42. The likelihood ratio suggests a high level of significance is attached to the two Poisson process model with values around e^{21}. From contours as shown in Figs.4 to 7, we can determine 12 km, 9 days and 1.0 as the optimum values of the parameters, R_s, T_d and *dm*. Values of 0.8 and 11.4 are obtained in turn for reliability and probability gain, R_b and P_g, respectively.

6. Summary

A simple algorithm to issue short term alarms focused on foreshock occurrence is applied to data of microearthquakes from the Kanto area. The results of the study are summarized as folllows:

(1) The distribution of the last interevent time suggests the possibility of an anomalous short-term increase in seismicity before main shocks which differs distinctly from background seismicity;

(2) It is proposed to use the likelihood ratio as a scale to measure the performance of

methods to issue alarms, which has a close relation with AIC;

(3) From optimization of parameters, values of 0.8 and 11.4 are obtained for the reliability and probability gain associated with the algorithm in this case; and

(4) The likelihood ratio suggests a high level of significance is attached to the two Poisson process model.

The author would like to thank P.Reasenberg, S.Matsumura and D.Rosenblatt for discussion and constructive reviews of this manuscript.

References

Aki, K., A probabilistic synthesis of precursory phenomena, Earthquake Prediction, (eds.,D.W. Simpson and P.G. Richards), 566-574, AGU, 1981.

Bowman, J.R., and C. Kisslinger, A test of foreshock occurrence in the central Aleutian island arc, Bull. Seism. Soc. Am., 74, 181-197, 1984.

Imoto, M., Changes in the magnitude-frequency b-value prior to large ($M \geq 6.0$) earthquakes in Japan, Tectonophysics, 193, 311-325, 1991.

Imoto, M., Changes in seismicity of microearthquakes before major earthquakes in the Kanto area, Zisin, 45, 1992 (in Japanese).

Jones, L., Foreshocks (1966-1980) in the San Andreas system, California, Bull. Seism. Soc. Am., 74, 1361-1380, 1984.

Marandi, M.T., and S. Matsumura, Update on the examination of the seismic observational network of the National Research Institute for Earth Science and Disaster Prevention (NIED) - detection capability and magnitude correction -, Report of the Natl. Res. Inst. Earth Sci. & Disast. Prev., 47, 1-18, 1991.

Okada, Y., Seismotectonics in the Southern Kanto District, Central Japan, Zisin, 43, 153-175, 1990 (in Japanese).

Reasenberg, P.A. and M.V. Mattews, Precursory seismic quiescence: A preliminary assessment of the hypothesis, Pure and Appl. Geophys., 126, 373-406, 1988.

Sakamoto, Y., M. Ishiguro and G. Kitagawa, Akaike information criterion statistics, D.Reidel, Dordrecht, 290pp, 1983.

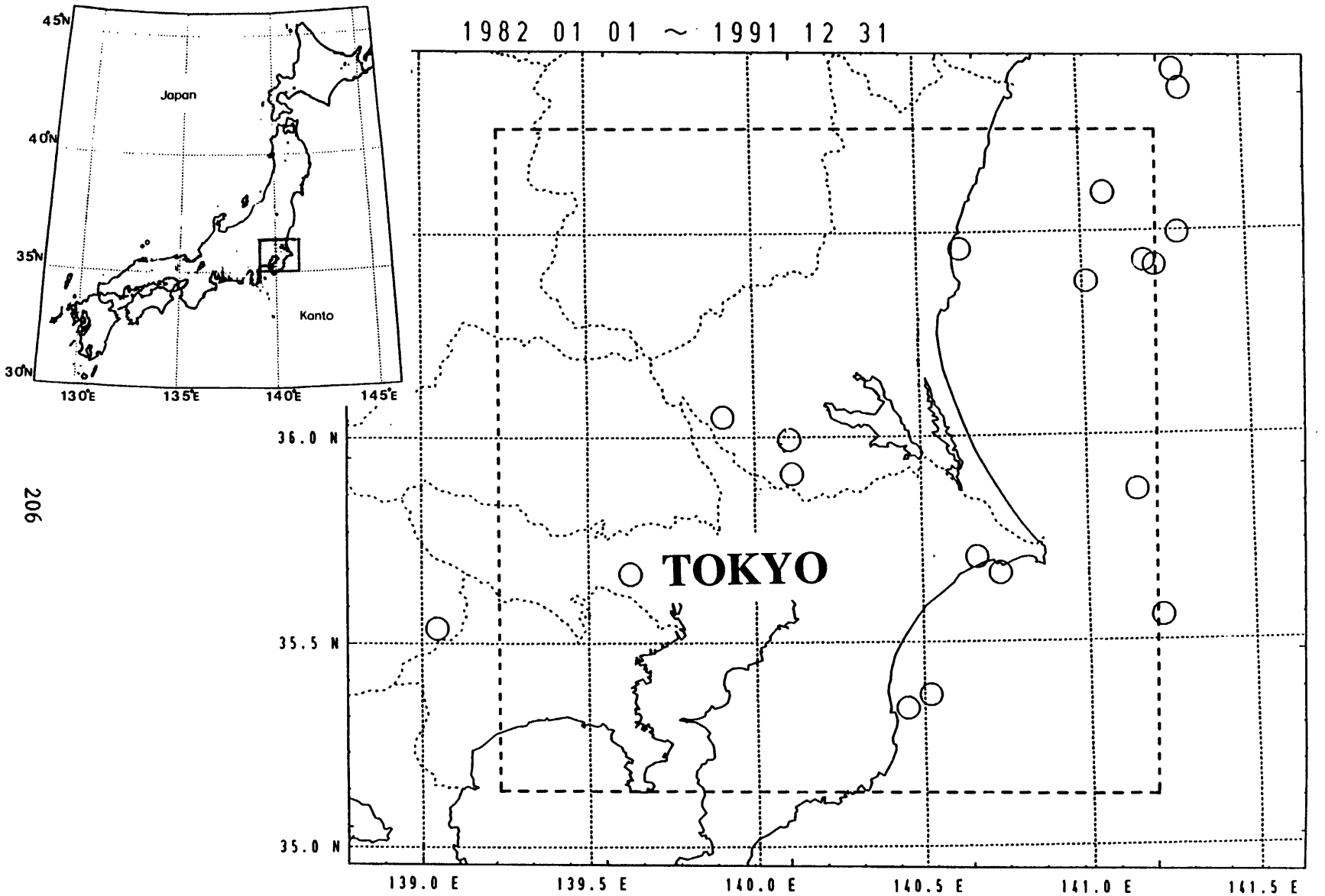

Fig.1 Map of larger earthquakes (M≥5.5) in the Kanto area, central Japan from January 1982 through December 1991. Dashes lines indicate the area for study. Earthquakes inside the dashed box were used as the set of target events.

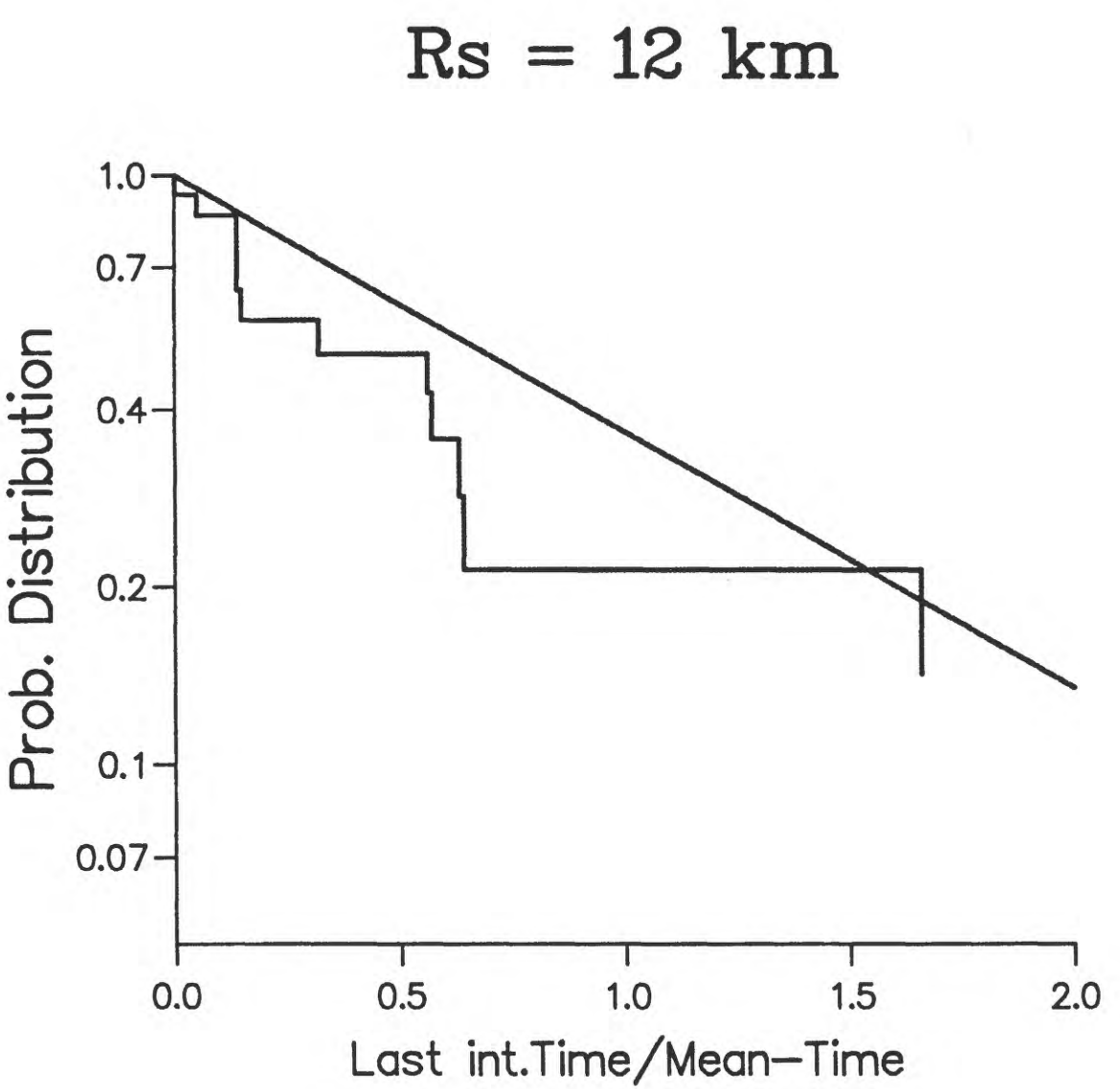

Fig.2 Distribution of the last interevent times in the case of radius 12 km. The last interevent times are normalized by the respective mean interevent times. The cumulative frequencies are obtained by accumulation from infinity. The expected function is shown by a straight line.

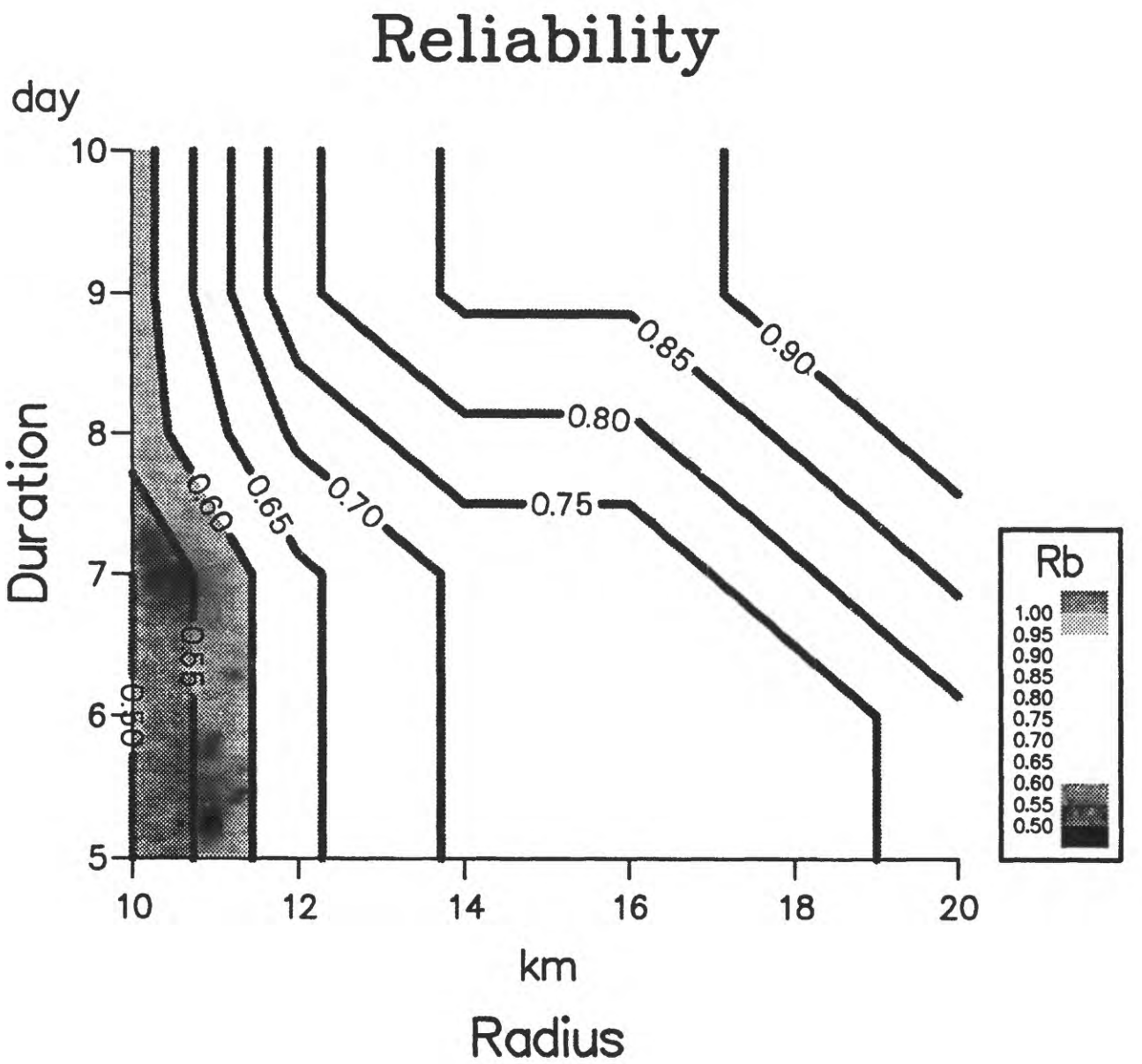

Fig.3a Contours of reliability on a R_s-T_d plane in the case of *dm* equal to 1.0. Countours are indicated at every 0.05.

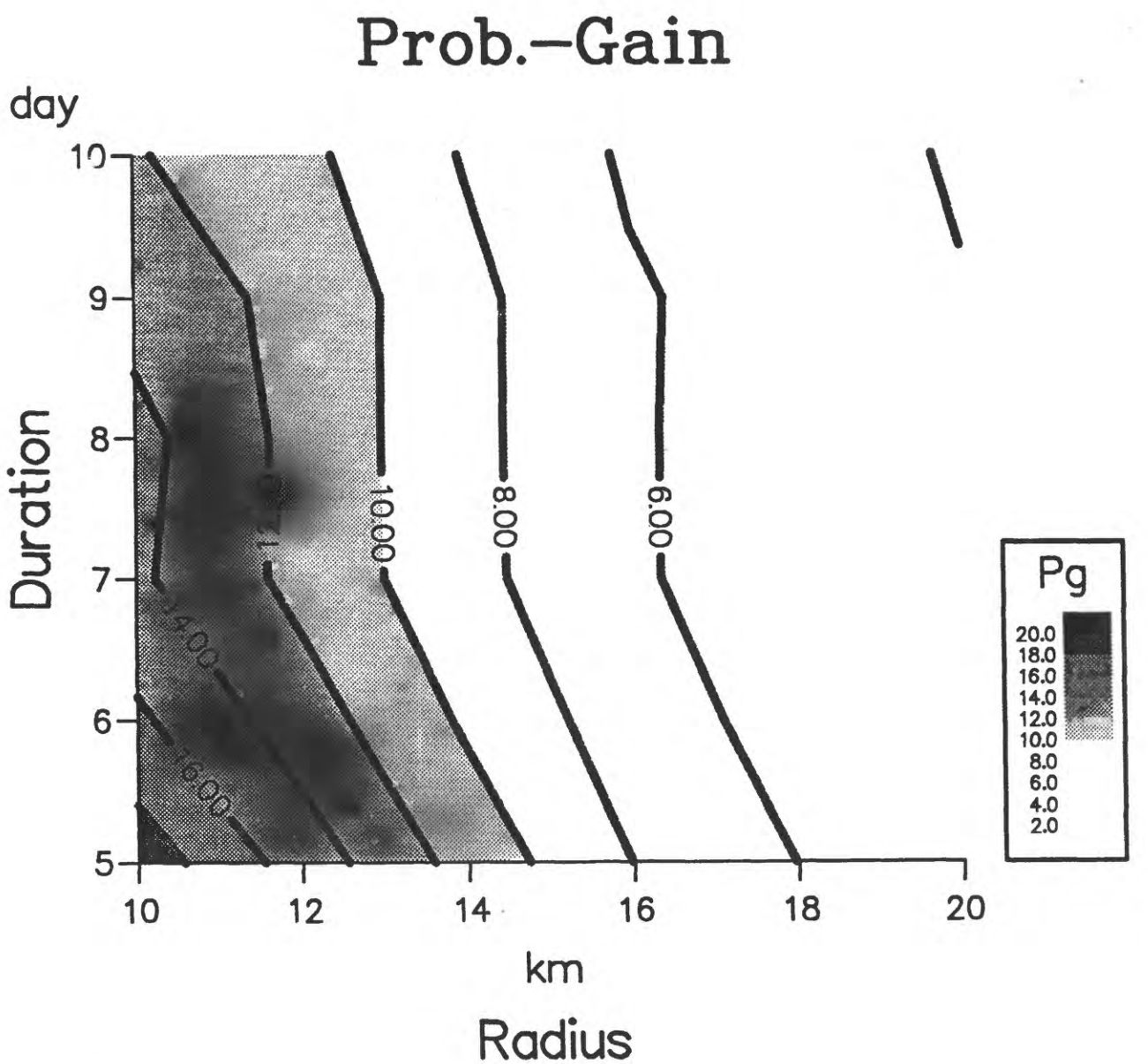

Fig.3b Contours of probability gain on a R_s-T_d plane in the case of *dm* equal to 0.5. Countours are indicated at every 2.

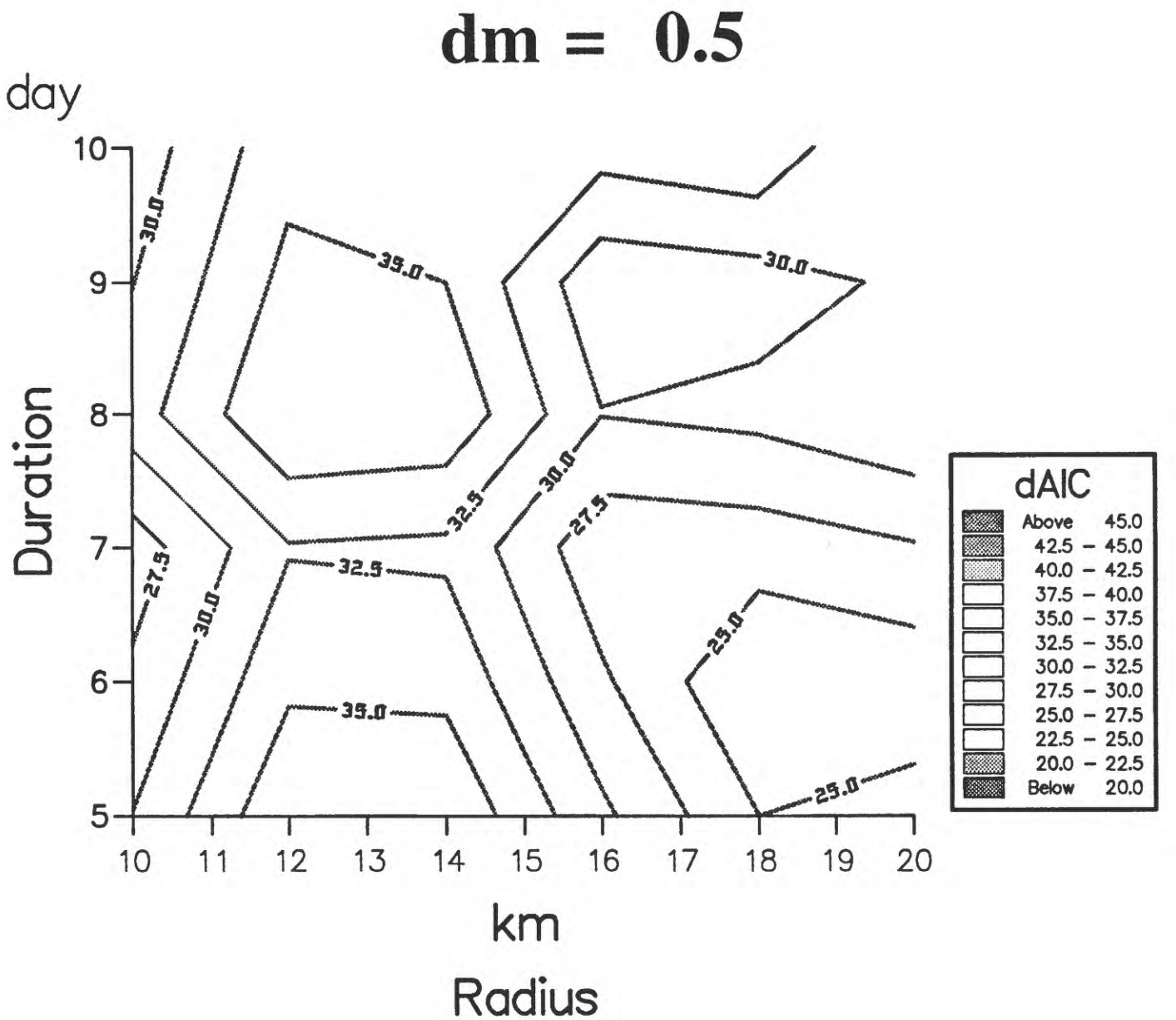

Fig.4 Contours of dAIC on a R_s-T_d plane in the case of *dm* equal to 0.5.

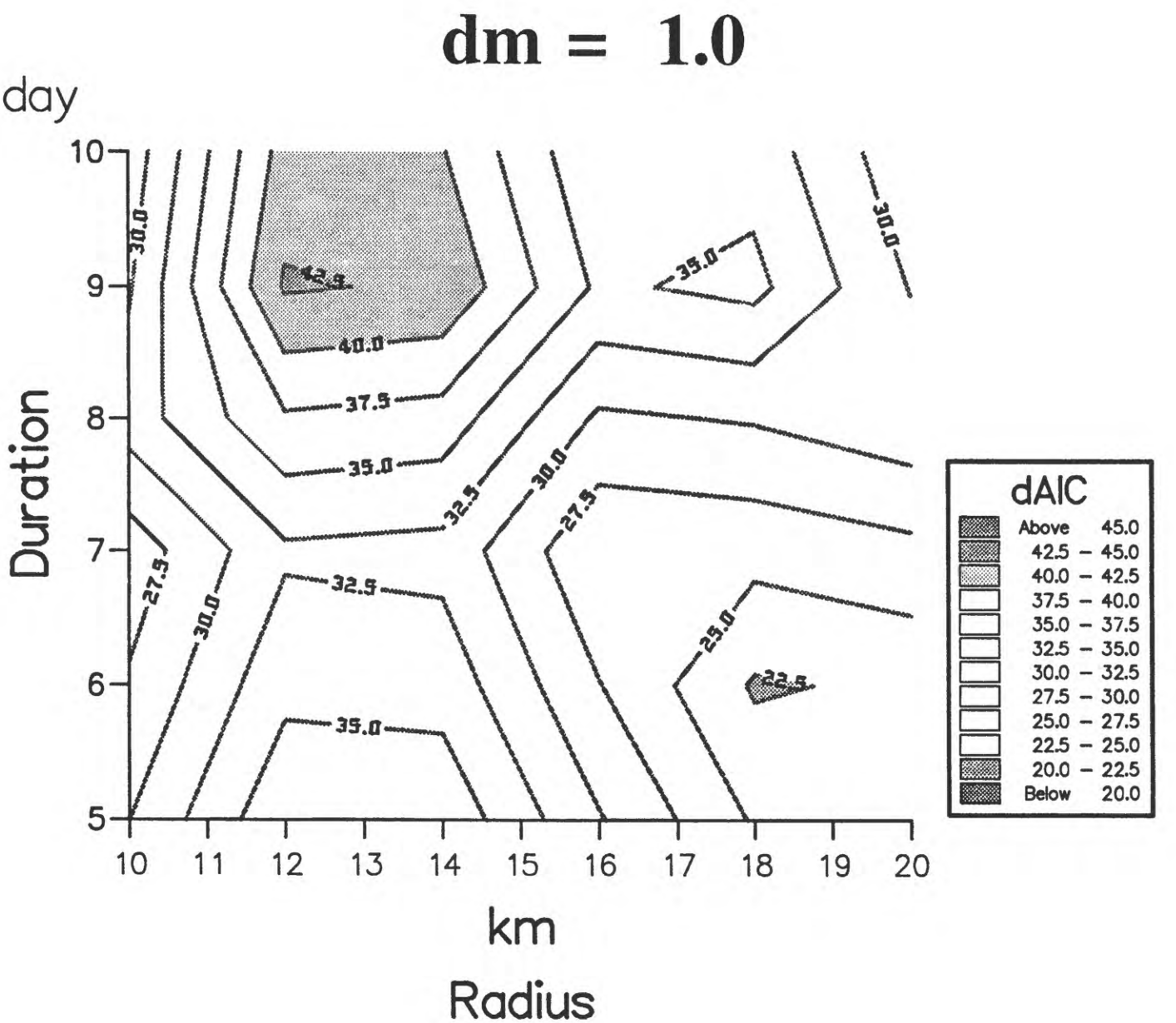

Fig.5 Same as Fig.4 but for *dm* equal to 1.0.

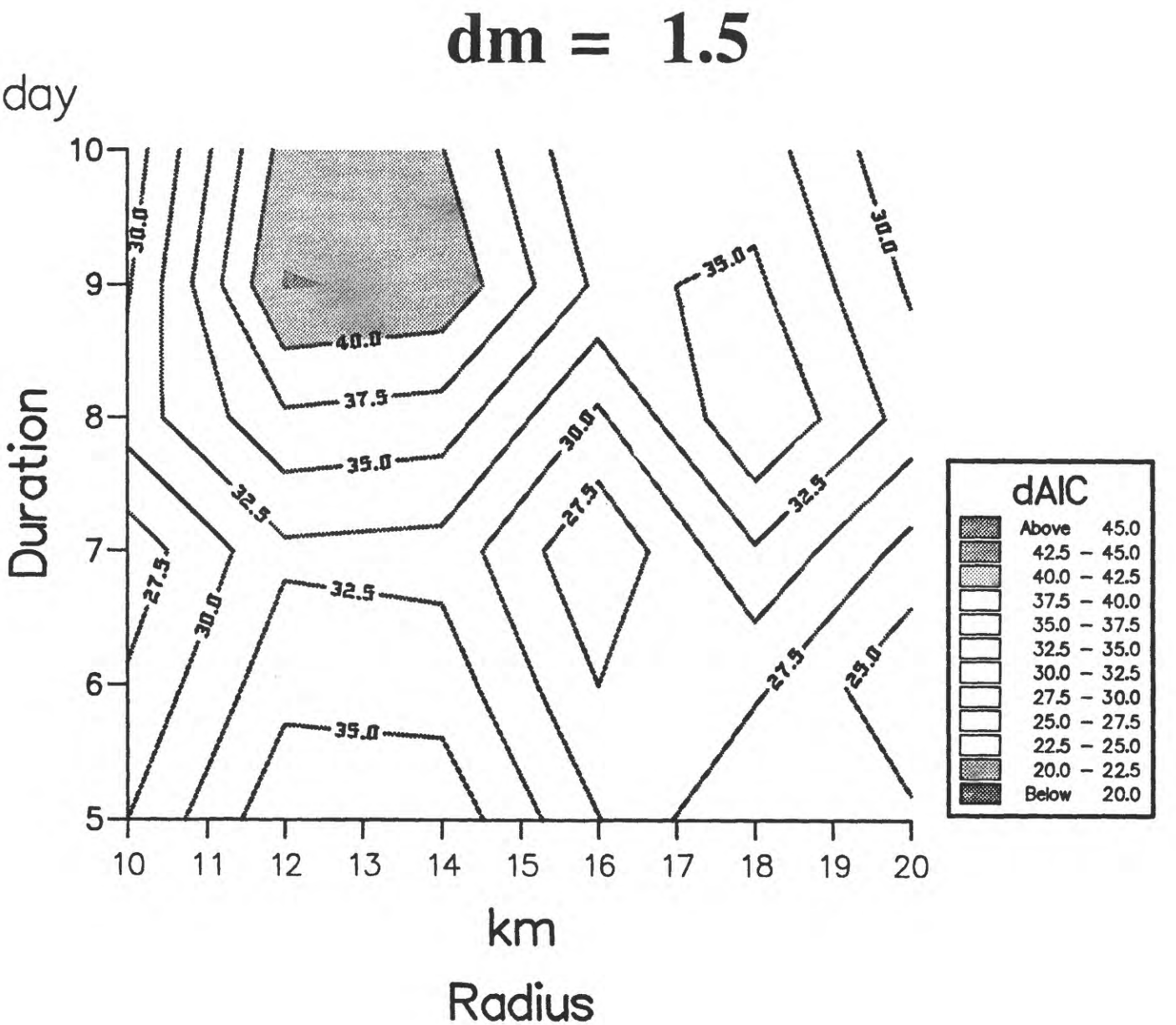

Fig.6 Same as Fig.4 but for *dm* equal to 1.5.

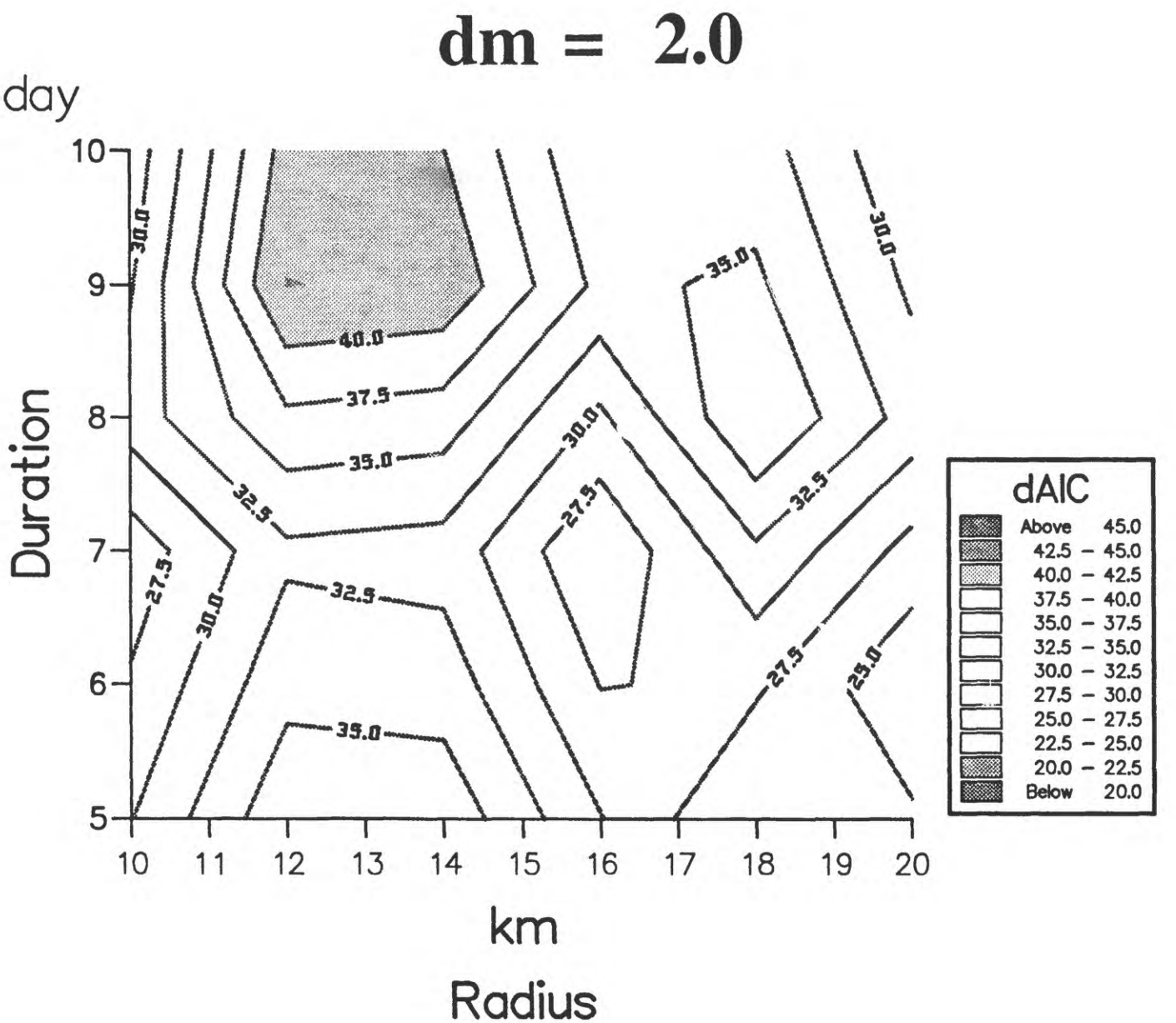

Fig.7 Same as Fig.4 but for *dm* equal to 2.0.

Seismicity and Creep at Parkfield

Allan G. Lindh, Kate Breckenridge, U.S. Geological Survey, Menlo Park, Calif. USA,
and Mick Gladwin, Queensland Univ., Queensland, Australia.

Since about 1980, the U.S.Geological Survey, in conjunction with University and other scientists and the State of California, has conducted a detailed earthquake prediction experiment near the small central California town of Parkfield (Bakun and Lindh, 1985). Two major components of this experiment are an array of seismometers around Middle Mountain, near the epicenter of the 1966 Parkfield earthquake, and an array of creepmeters -- low sensitivity extensometers placed obliquely across the surface trace -- deployed between Middle Mountain and the Cholame Valley. These instrumental arrays permit the routine location of microearthquakes of M1 and greater along this portion of the San Andreas, and the recording of creep events as small as 0.05 mm. Since about 1987 the creep meters have been supplemented by an array of downhole strainmeters and water wells, the data from which place some constraints on the dimension and moment of the largest creep events; preliminary analysis they extend to only about 1 km depth. Since 1 October 1992, a pair of creep events on Middle Mountain, and a sequence of earthquakes which included a M4.7 event, resulted in a public warning that there was a 37% chance that a M6 earthquake could occur within 72 hours. As of now (12 Nov 1992) no such earthquake has occurred, and the warning appears to have been a false alarm.

Each of the two creep events in the recent sequence was followed within about two hours by a pair of small earthquakes directly beneath the creep event at 4-10 km depth. These and other temporal correlations within the sequence suggest long distance communication within the fault zone that does not appear to be the result of far-field stress changes, and probably not propagating creep events. If recent suggestions concerning the dynamic role of confined high fluid pressures within active fault zones should prove applicable to real faults, the possibility of fault zone communication via fluid pressure transients should possibly be considered.

Relocation of Earthquakes in the Parkfield Region, Central California, 1932 - 1969

Karen L. Meagher
U.S. Geological Survey
Geophysics Program AK-50
University of Washington
Seattle, Washington 98195

South central California, defined as the area along the San Andreas fault from Bear Valley at the north to the northern edge of the Transverse Ranges to the south and from the coast landward to the Great Valley (Figure 1), is of clear importance in any effort to understand the behavior of the San Andreas fault system. At the center of this area, the section of the San Andreas fault near Parkfield is of particular seismological interest because a comprehensive experiment to predict a moderate magnitude earthquake has been deployed here (Bakun and Lindh, 1985a, 1985b). East of Parkfield the MS= 6.5 1983 Coalinga earthquake occurred on a shallow dipping thrust fault near the transition between the Coast Range and the Great Valley (Eaton, 1990). Recent studies of the probability of major earthquakes occurring between 1988 and 2018 have suggested that there is a 30 percent chance of an event of magnitude 7 on the San Andreas immediately south of Parkfield at Cholame (Working Group on California Earthquake Probabilities, 1988).

Both the Parkfield prediction experiment and the probability estimate at Cholame utilize the available historical record and the modern instrumental record of seismicity. The historical record of felt earthquakes in south central California suggests that since 1857 there has been a M= 5.5-6.0 earthquake at Parkfield approximately every 22 years (1857, 1881, 1901, 1922, 1934, and 1966; Bakun and McEvilly, 1984). The modern instrumental record for south central California dates from the late-1960s when the U.S. Geological Survey began recording microseismic data on the central California seismic network (CALNET). By 1969 enough stations had been installed in central California that wide areal coverage was available; as a result the U.S. Geological Survey catalog of earthquakes greater than magnitude 3.5 is considered complete for all of central California from the coast eastward to the Sierra Nevada (Figure 1) (Hill et al., 1991).

Prior to expansion of CALNET in south central California, earthquakes in the area near Parkfield had been located using relatively sparse seismic networks operated by the University of California (Berkeley) (Figure 2A) and the California Institute of Technology (Caltech) (Figure 2B). In 1932 the closest stations to the study area were at Mount Hamilton (MHC in Figure 2A) and Santa Barbara (SBC in Figure 2B). In 1935 Berkeley installed a station closer to the study area at Fresno (FRE in Figure 2A). The number of seismic stations operating in south central California remained the same from 1935 until after the MS= 7.8 1952 Kern County earthquake when Caltech installed King Ranch (KRC on Figure 2B) and two additional stations in the vicinity of the Kern County epicenter. KRC was the nearest station to the study area until late summer of 1961 when Berkeley completed the installation of three stations in south central California (Figure 2A). The dashed line represents the historical division between the two institutions geographical interests.

Each institution published their own local observatory bulletins containing seismicity data; Berkeley data were published in *Bulletin of the Seismographic Stations* beginning in 1910 and Caltech data appeared in *Bulletin of the California Institute of Technology, Seismological Laboratory, Pasadena and Auxiliary Stations* beginning in 1931. Compilations, additions, and corrections to the earlier published seismic data were provided by Bolt and Miller (1975) for the Berkeley network and by Hileman et al. (1973) for the Caltech network. The

earthquake parameters in these compilations along with corrections and additional earthquakes not previously listed were eventually transferred onto magnetic tape.

Earthquake epicenters for south central California for events with $ML \geq 3.5$ from 1932 through 1969 were selected and plotted (Figures 2A and 2B) from the Berkeley and Caltech magnetic tape catalogs. Although there are many Caltech locations reported north of the division line (Figure 2B), only a few Berkeley locations (Figure 2A) are reported south of the line. Figure 2C shows earthquake epicenters from both catalogs only for the study area. Many of the events in this figure are duplicate earthquakes; i.e., one earthquake that has been assigned a different location (and possibly a different magnitude) by each institution. Such duplicate events are relatively easy to identify if the two locations are close enough so that their symbols overlap on an epicenter map, such as Figure 2C. If the two locations are very different, it can be more difficult to identify the pair of earthquakes as duplicates. For example, in some cases one of the institutions located an earthquake inside of our study area, while the other institution located it outside of the area. There are 246 distinct earthquakes plotted in Figure 2C; within our study area only 22 published earthquake locations had been determined using phase data from both Berkeley and Caltech. This past failure to combine the phase data from Berkeley and Caltech may be the cause of the difference between the diffuse distribution of epicenters in the years 1932-1969 (Figures 2B and 2C) and the rather distinct zones of epicenters along the western edge of the Great Valley and along the San Andreas fault for earthquakes since 1970 (Figure 1). A careful merging of the Caltech and Berkeley data sets for the period 1932-1969 has the potential to either confirm or refute this apparent difference in the spatial distribution of earthquakes during the two time periods.

In an effort to build a complete catalog of earthquakes within the study area, I began compiling location data from the magnetic tape catalogs and phase data from the station bulletins for each of the 246 earthquakes in Figure 2C. To resolve conflicts in hypocentral parameters I checked original data sheets, laboratory notes from both Berkeley and Caltech, and original seismograms for selected earthquakes. Caltech P-arrivals were tabulated from microfilm copies of their phase cards (Goodstein and Roberts, 1988). Berkeley P-arrivals were obtained from microfiche copies of *Bulletin of the Seismographic Stations, vol. 3 - 39.* Raw P-arrival times, station clock corrections, and corrected P-arrival times were published in the Caltech bulletin. The clock corrections were reapplied to the raw readings for a comparison to the published P times and corrections made when necessary. I was not able to apply this checking procedure to Berkeley's published P times, since the raw readings and clock corrections were not published. Amplitude data for the Caltech Wood-Anderson seismographs were also obtained from microfilm, and Berkeley's Wood-Anderson amplitudes were retrieved from original archive files at the University. Additional P-arrival times not previously published in the Berkeley *Bulletins* were also obtained from the archives.

In addition to merging the Berkeley and Caltech data sets for the study area, I also looked for earthquakes in the Parkfield area that had been timed by Caltech but which never made it into the final bulletins (perhaps because the events were too small). I did this by scanning microfilm copies of Caltech phase cards (Goodstein and Roberts, 1988) for the period 1 January 1932 through 31 December 1969, looking for earthquakes with S-P intervals of 25-28 seconds, 30-33 seconds, and 26-29 seconds at SBC, PAS, and TIN respectively. These intervals correspond approximately to epicentral locations in a 40 km by 25 km region along the San Andreas fault, centered near the town of Parkfield. This search revealed no previously unreported earthquakes with $M \geq 3.5$ along the Parkfield segment of the San Andreas fault.

I recomputed locations for all events with the program HYPO71PC (Lee and Valdes, 1985) using the standard four-layer velocity model for central California (Wesson et al., 1973). The Parkfield earthquakes of 28 June 1966, a $ML = 5.1$ foreshock and a $ML = 5.6$ mainshock (Bakun and McEvilly, 1984), were centered at a depth of about 9 km and the zone of aftershock activity was concentrated at depths between 8 to 10 km (Eaton et al., 1970). Therefore, I fixed the hypocentral depth for all events in the 1932-1969 data set at 9 km. I

relocated the earthquakes with a master event procedure, using travel-time corrections estimated from station travel-time residuals for the 1934, 1966, and 1975 Parkfield earthquakes. All stations within 500 km of Parkfield for which travel-time corrections could be determined were used in the earthquake relocations. I also recalculated earthquake magnitudes from Wood-Anderson amplitude data by applying amplitude station corrections derived by Uhrhammer (written communication, 1989) and Richter (1958) to the raw magnitude determinations at each station.

A preliminary location run was made using all of the tabulated P-readings. Each event was then individually reviewed. Arrival times were rechecked on the original seismograms for all events that had any stations with P-residuals greater than three seconds. If an event was found to be without P-arrivals from either Berkeley or Caltech, an effort was then made to search the seismograms and time any available P-arrivals. Of the 246 published events in the study area (Figure 2C) all but ten earthquakes now have P-arrivals from both institutions. As noted earlier only 22 events originally had arrivals from both networks.

After all additions and corrections were completed the events were rerun. Twenty one relocations were rejected from the final data set. If a solution had very few readings (< 4) or a large RMS residual (> 1.2 seconds), then the event was eliminated with the exception of two aftershocks of the June 1934 earthquake. Seven of these 21 solutions had arrivals only from one institution. Station coverage in south central California was improved in the late summer of 1961, so relocations of earthquakes occurring after 1961 were deleted if the epicentral standard error was ≥ 7.0 km.

The results of the 225 accepted relocations are plotted in Figure 3. When we compare Figure 3 with the combined catalogs of Berkeley and Caltech (Figure 2C) we see the result of combining the P-arrival times from both institutions. There is a tightening of epicenters at both Parkfield and Bryson, and many events have been relocated to the north, out of the study area. The spatial distribution of the relocated earthquakes for the years 1932-1969 now bears a greater resemblance to the distribution of 1970-1992 events (compare Figures 1 and 3).

REFERENCES

Bakun, W.H. and T.V. McEvilly (1984). Recurrence models and Parkfield, California, earthquakes, *J. Geophys. Res., 89,* 3051-3058.

Bakun, W.H. and A.G. Lindh (1985a). The Parkfield, California, prediction experiment, *Earthq. Predict. Res., 3,* 285-304.

Bakun, W.H. and A.G. Lindh (1985b). The Parkfield, California Earthquake, prediction experiment, *Science, 229,* 619-624.

Bolt, B.A. and R.D. Miller (1975). Catalogue of earthquakes in northern California and adjoining areas, 1 January 1910 - 31 December 1972, *Seismographic Stations, University of California,* Berkeley, California, 567 pp.

The registration of earthquakes, *Bulletin of the Seismographic Stations, Volumes 3 - 39, 1932 - 1970,* University of California Press, Berkeley, California (Microfiche copy)

Eaton, J.P., M.E. O'Neill, and J.N. Murdock (1970). Aftershocks of the 1966 Parkfield-Cholame, California, earthquake: a detailed study, *Bull. Seism. Soc. Am., 60,* 1151-1197.

Eaton, J.P (1990) The earthquake and its aftershocks from May 2 through September 30, 1983, in M.J. Rymer and W.L. Ellsworth (Editors), The Coalinga, California, Earthquake of May 2, 1983, *U.S. Geol. Surv. Prof. Paper 1487,* 113-170.

Goodstein, J.R. and P. Roberts (1988). Filming seismograms and related materials at the California Institute of Technology, in W.H.K. Lee, H. Meyers, and K. Skimazaki (Editors), Academic Press, *Historical Seismograms and Earthquakes of the World,* 380-389.

Hileman, J.A., C.R. Allen, and J.M. Nordquist (1973). Seismicity of the southern California region 1 January 1932 to 31 December 1972, *Contribution No. 2385, Division of Geological and Planetary Sciences, California Institute of Technology,* Pasadena, California.

Hill, D.P, J.P. Eaton, W.L. Ellsworth, R.S. Cockerham, F.W. Lester, and E.J. Corbett (1991). The Seismotectonic fabric of central California, in D.B. Slemmons, E.R Engdahl, D. Blackwell, D. Schwartz, and M. Zoback (Editors), *Neotectonics of North America, DNAG Associated Volume GSMV-1,* The Geological Society of America, Boulder, Colorado.

Lee, W.H.K. and C.M. Valdes (1985). HYPO71PC: a personal computer version of the HYPO71 earthquake location program, *U.S. Geol. Surv., Open-File Rept. 85-749,* 43 pp.

Richter, C.F. (1958). *Elementary Seismology,* W.H. Freeman and Company, 343.

Wesson, R.L., J.C. Roller, and W.H.K. Lee (1973). Time-term analysis and geologic interpretation of seismic traveltime data from the coast ranges of central California, *Bull. Seism. Soc. Am., 63,* 1447-1471.

Working Group on California Earthquake Probabilities (1988). Probabilities of large earthquakes occurring in California on the San Andreas fault, *U.S. Geol. Surv. Open-File Rept. 88-398,* 62 pp.

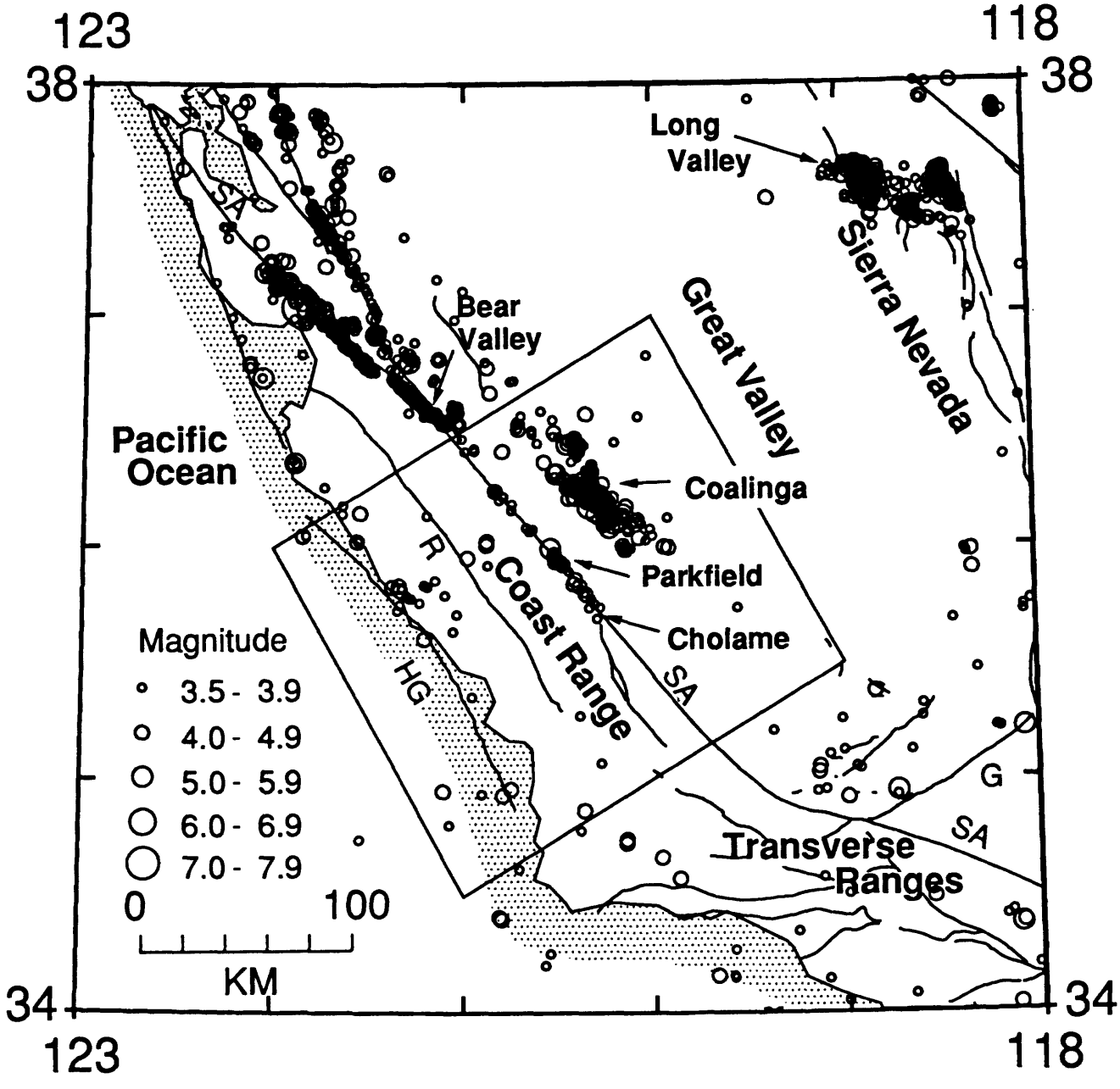

Figure 1. Earthquake epicenters in central California, magnitude 3.5 or greater, from 1 January 1970 through 31 December 1992 located by the U.S. Geological Survey. Only events with 6 or more stations, RMS less than 0.35 seconds, and ERH or ERZ less than 5 km are plotted. The group of earthquakes labeled "Coalinga" includes aftershocks of the M 6.5 1983 Coalinga earthquake. Study area enclosed by bold line. Major faults and physiographic features are identified. Faults are labeled: G, Garlock, HG, Hosgri; R, Rinconada; SA, San Andreas.

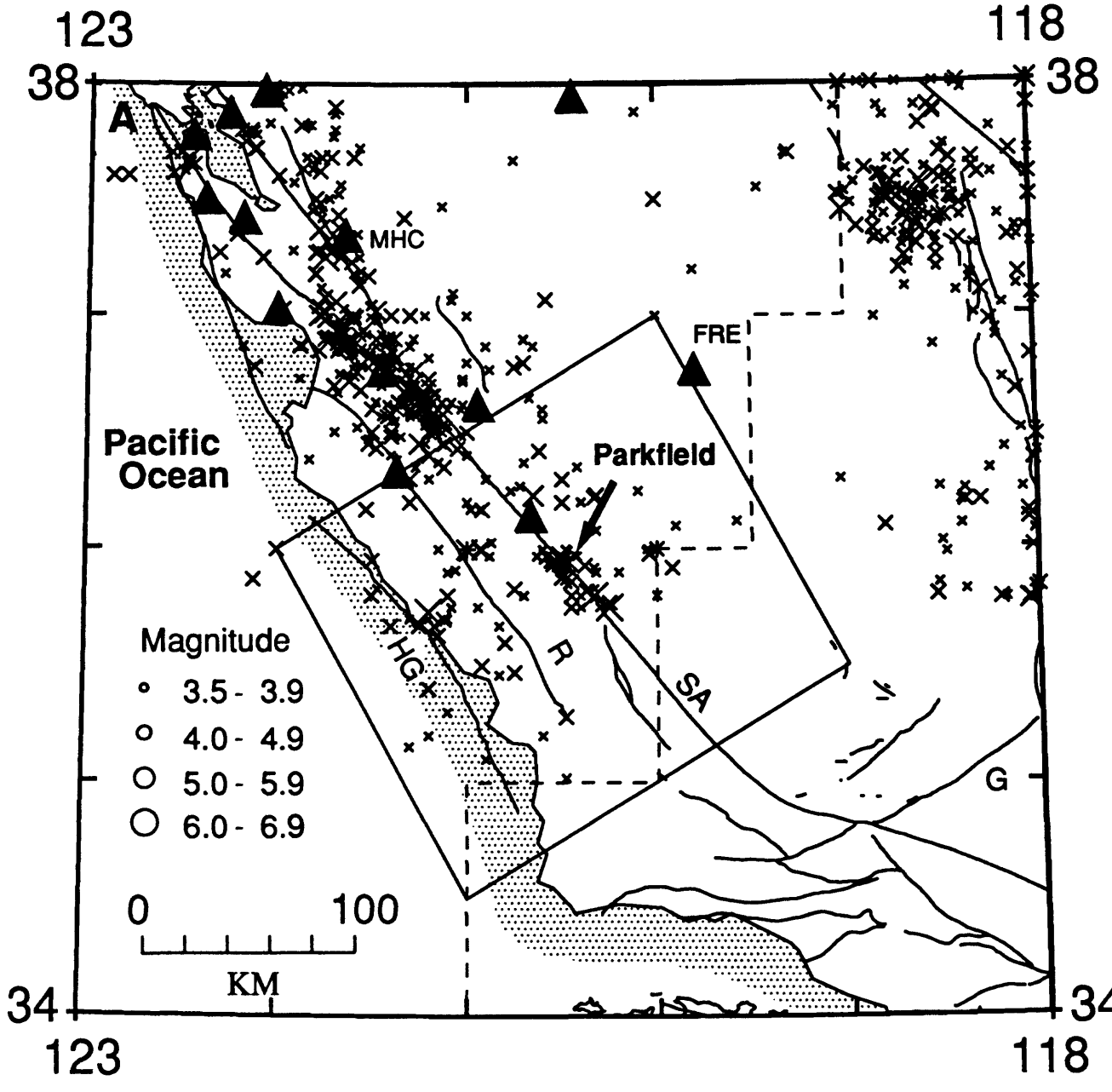

Figure 2. Earthquake epicenters in central California, greater than magnitude 3.5, from 1 January 1932 through 31 December 1969. Triangles are stations in operation during any time from 1932-1969. Study area enclosed by bold line. Faults identified in Figure 1. Dashed line is the historical division line between Berkeley and Caltech. A) University of California (Berkeley) earthquakes are plotted as crosses. B) California Institute of Technology (Caltech) locations are plotted as squares. C) Berkeley and Caltech earthquakes for study area only - criteria for selecting and plotting earthquakes are at least one institution reported location within the study area and a magnitude of 3.5 or greater. Corresponding magnitude by other institution may be less than 3.5.

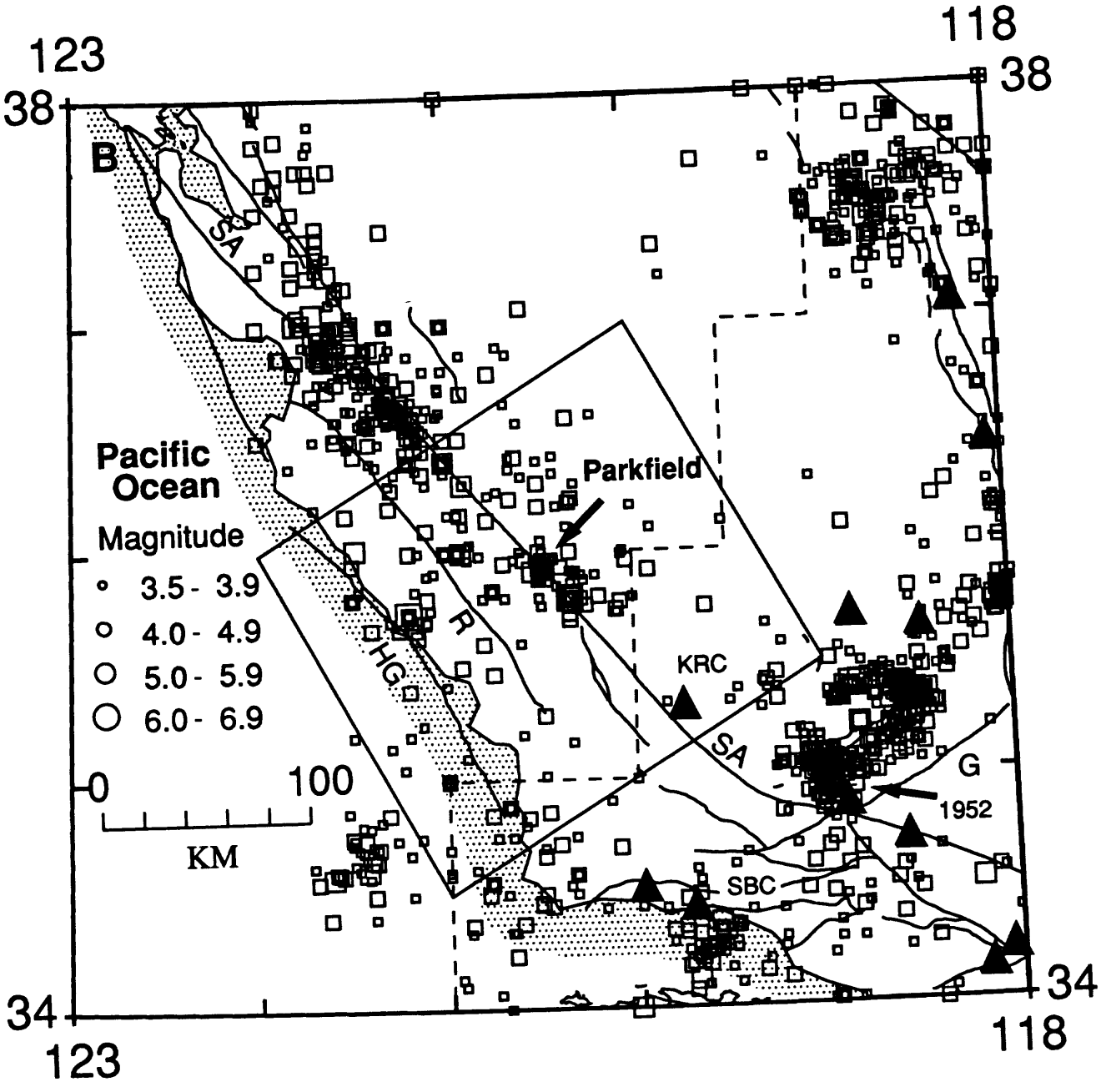

Figure 2. continued

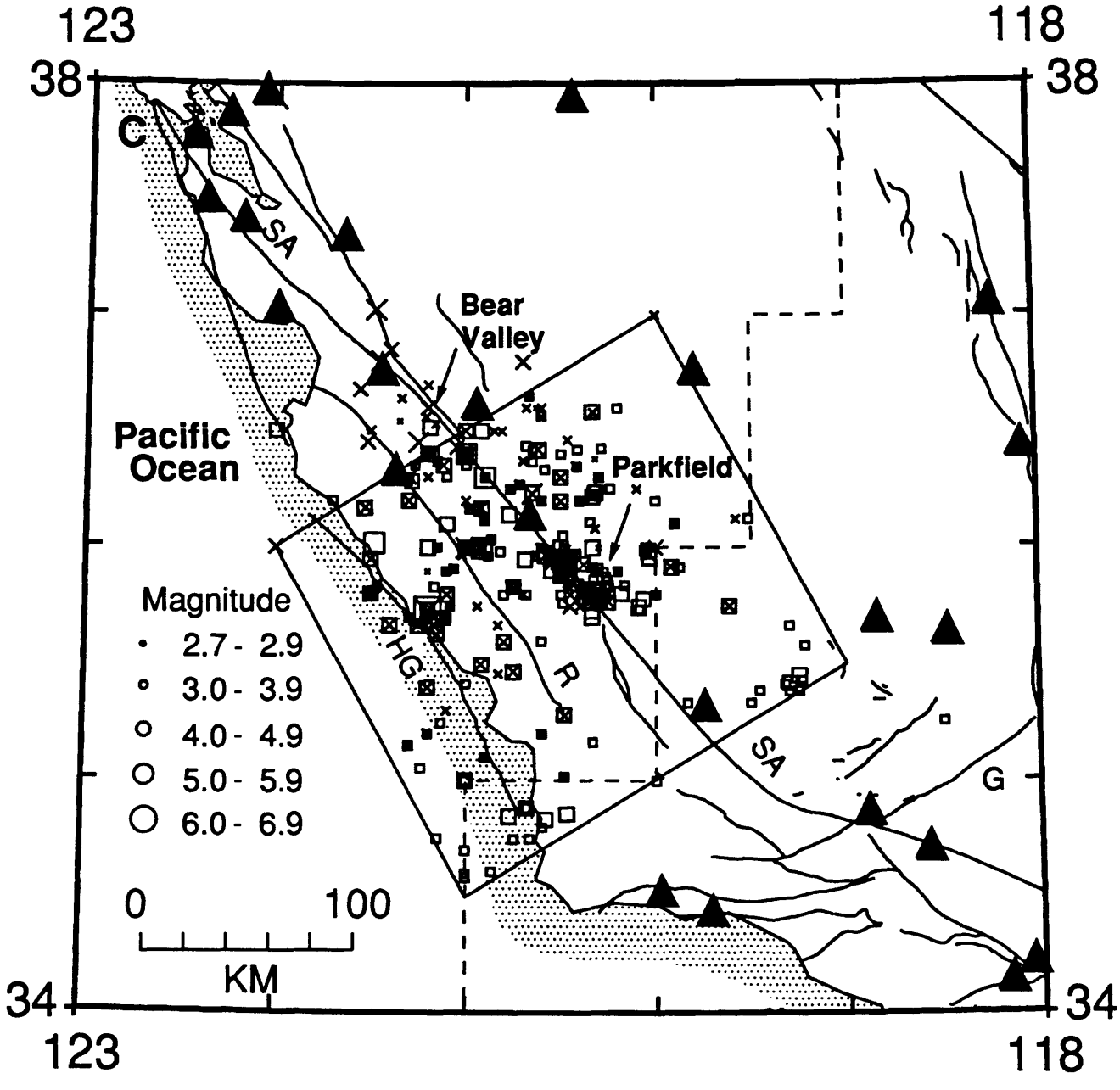

Figure 2. continued

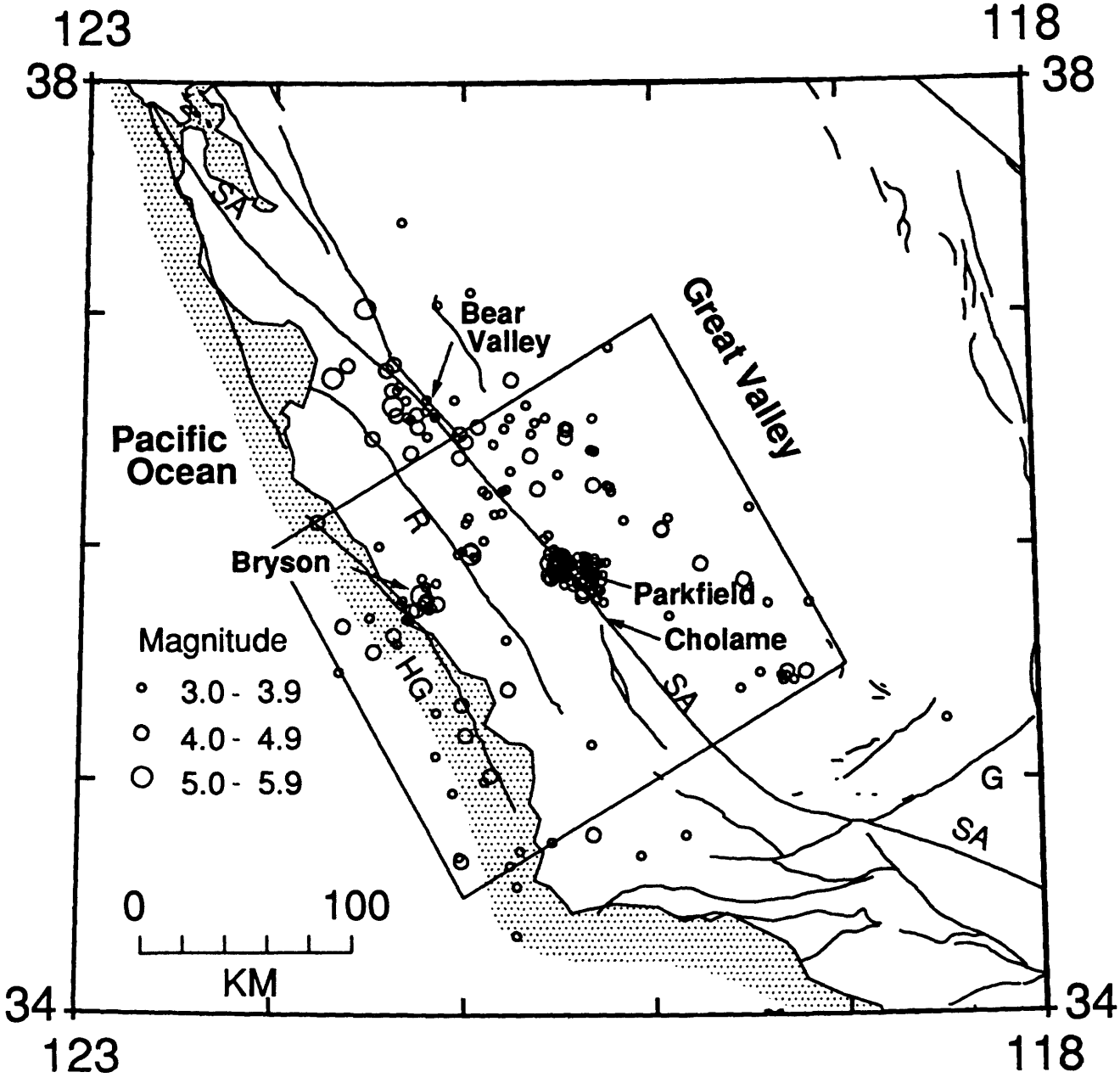

Figure 3. Earthquake relocations for south central California from 1932 through 1969. All events are plotted even if the recomputed magnitude is less than 3.5. Faults identified in Figure 1.

Probability Estimation of Large Earthquake Occurrence from the Viewpoint of Successiveness of Seismic Activity

Seismological and Volcanological Department, JMA
Noritake NISHIDE
Meteorological Research Institute, JMA
Masaaki SEINO

1 Introduction

The successiveness of seismic activity that one or more earthquakes take place successively after an earthquake occurrence in the vicinity of the earthquake, is a well known fact, and was researched in detail based on earthquake data in and around Japan by many seismologist (for example, Utsu;1961 & 1969, Mogi;1963). The successiveness of seismic activity is grouped into three types, namely, "Mainshock-Aftershock Type", "Foreshock-Mainshock-Aftershock Type" and "Swarm Type". There are especially recognized remarkable regional characteristics in the occurrence of "Foreshock-Mainshock-Aftershock Type" and "Swarm Type" (Mogi;1963 & 1967, Yoshida;1990).
The successiveness of earthquake occurrence in and around Japan was studied here based on earthquake data from 1926 to 1990. It will actually be not so easy to discuss the successiveness dividing into the above three types because there are many cases of overlapping the same types or other types (Utsu;1970), or many intermediate cases of two types. So, the time series analysis was done here for foreshocks, mainshocks, and aftershocks with magnitude near those of their mainshocks , not grouping into the above three types.
And then, to see the effectiveness of the method, forecasting seismic activity was tried by using methods and expressions of statistics and probability.

2 Data

Earthquakes with $M \geq 6.0$ and $h \leq 80$ km from 1926 to 1990 in and around Japan except for Ryukyu region shown in Fig.1 (area;$1.35 \times 10^6 km^2$) were extracted from the JMA catalogue of earthquake origins. Then, after recognizing all aftershocks, small aftershocks whose magnitudes were much smaller than that of their mainshocks ($\Delta M > 1.0$), were excluded from the data for the time series analysis. The number of earthquakes which were selected through these procedures is 532.

3 Point Process Analysis

The analysis method adopted here is the point process model composed of trend terms and response (successiveness) terms by Ogata & Katsura (1986). Fig.2 shows the results of the time series analysis about earthquakes shown in Fig.1. Fig.2a shows the trend of occurrence intensity (number of events per day) of earthquakes as independent events in the model which was determined as an optimum model by the above analysis. The occurrence intensity has been declining year by year, the number of independent events is estimated at 401 and the average through the whole period is 1.70×10^{-2} events/day. Fig.2b shows the response function as successiveness of seismic activity. The successiveness is large immediately after an earthquake occurrence, then decreasing rapidly, and almost vanish in 10 days. Therefore,

the duration when remarkable successiveness of seismic activity exists is determined here to be 10 days.

4 Identification of Successive Events

A successive event is defined as a group of earthquakes that take place in 10 days after an earthquake occurrence in the neighboring region which corresponds to the focal region of the earthquake. The group can contain not only aftershocks whose magnitudes were near those of their mainshocks ($\Delta M \leq 1.0$) but also foreshocks which took place within 10 days before their mainshocks. Under this definition, there are 53 successive events, among which "Mainshock–Aftershock Type","Foreshock–Mainshock–Aftershock Type" and "Swarm Type" coexist. Then, 532 earthquakes are divided into 401 independent events, and there are 348 (87%) single events and 53 (13%) successive events. 16 events among 53 successive events are "Foreshock–Mainshock–Aftershock Type", which amount to 4% of all independent events. ○ and ● denote single events and successive events, respectively in Fig.3.

5 Comparison with the Probability of Earthquake Occurrence calculated by the Poissonian Process Analysis

The probability of earthquake occurrence based on the Poissonian process is calculated here, and is compared with the empirical probability of "Foreshock–Mainshock– Aftershock Type". This comparison has equivalent significance as that between background seismicity and number of foreshocks in southern California done by Jones (1985).
Now, independent events of which number is estimated in Section 3 are assumed to take place at random according to the Poissonian process in the region shown in Fig.3. Averaged number of independent event occurrence in this region is 1.26×10^{-8} event/day·km^2. Under this assumption, the probability (P_0) that a next independent event will occur within 10 days after an independent event in the neighboring area which is defined as a circle with radius L centering the previous event, can be calculated. L is selected the length of focal region (Utsu, 1961) expressed as

$$L = 10^{(0.5M-1.0)}$$

And M in the above formula is selected the averaged magnitude expressed as

$$M_{ave} = 1/(b \cdot \ln 10) + M_{th}$$

By using magnitude data of 401 identified independent events which contain 98 estimated independent without magnitude data, the threshold value of magnitude M_{th}=5.95, M_{ave}=6.4 and L=25km, so the neighboring area (s) is 2.0×10^3km^2 in area. There occur 2.5×10^{-4} independent events during 10 days in this neighboring area. So, the probability that one independent event or more occur, is calculated as

$$P_0 = \{1 - \exp(-2.5\times10^{-4})\} \times 100 = 2.5\times10^{-2}\ (\%)$$

Comparing P and P_0, $P/P_0 \approx 160$, though the empirical probability (P) of "Foreshock–Mainshock–Aftershock Type" obtained in the section 4 is as small as 4%. That is, a forecast that an earthquake with not less magnitude than a previous one will occur within 10 days after the earthquake, will be improved about 160 times with regard to probability when the effect of successiveness of seismic activity is made use of, instead of a random process.

6 Successiveness of Earthquake Occurrence in the region off the Pacific coast of NE Japan

6.1 Point Process Analysis

The regional characteristic is seen in Fig.3 that there are remarkably a lot of successive events in the region off the Pacific coast of northern Japan, especially in two sub-regions (area;$1.30\times10^5 km^2$) enclosed by broken lines, namely, "Off Etorofu-Island" and "Off-Sanriku to Off-Ibaraki Prefecture". This characteristic has already been pointed out by Mogi (1967) and Utsu (1969). Fig.4 shows the results of the time series analysis using earthquake data in these sub-regions. Fig.4a shows the trend of occurrence intensity of earthquakes as independent events in the optimum point process model. The occurrence intensity in these sub-regions has also been declining year by year like the nationwide trend shown in the Fig.2a, the number of the events is estimated at 98 and the average value is 4.13×10^{-3} event/day. The successiveness shown in Fig.4b is large immediately after an earthquake occurrence, then decreasing rapidly, and almost vanish in 10 days. Therefore, the duration of successiveness in these sub-regions is determined to be 10 days just as the nationwide case.

6.2 Probability of Successive Occurrence

There occurred 186 earthquakes selected in Section 2, and these earthquakes are grouped into 92 independent events. Number of successive events under the same definition as that in Section 4 is counted up to 34 (37%), while there are 58 single events (63%). 12 events among successive events are "Foreshock-Mainshock- Aftershock Type", which are 13% of all independent events. In addition, there clearly seems to be a characteristic that the successiveness after earthquake occurrence in succession is stronger. Fig.5 shows the successiveness of a case that two earthquakes take place in succession. According to this example, integral value of the response function of successiveness within next 10 days is 0.47, so the probability that one earthquake or more will occur within next 10 days in the neighboring area is estimated 38% before the next earthquake occurrence, while the probability is estimated, from the integral value (0.74), to rise to 52% if the second earthquake follows half a day after the first earthquake. The fact in Table.1 indicates the existence of the mechanism that the occurrence of an earthquake excites the second earthquake occurrence and the second earthquake occurrence raises the potential to let the third earthquake occur, and it is the statistically averaged result of the mechanism.

6.3 Comparison with the Probability of Earthquake Occurrence calculated by the Poissonian Process Analysis

Averaged number of independent events in these sub-regions is calculated to be 3.18×10^{-8} event/day·km^2. Assuming independent events to take place at random according to the Poissonian process in these sub-regions, the probability (P_0) that a next independent event will occur within 10 days after an independent event in the neighboring area defined in Section 5 can be calculated. By using magnitude data of 92 identified independent events, M_{ave}=6.5, L=28km, and $s=2.5\times10^3 km^2$, there occur 7.8×10^{-4} independent events during 10 days in this neighboring area. So, the probability (P_0) that one independent event or more occur, is calculated as 7.8×10^{-2}%.

The empirical probability (P) of "Foreshock-Mainshock-Aftershock Type" obtained in the section 6.2, 13%, not only is not a low value but also 170 times higher than the probability

based on the Poissonian process.
That is to say, considering the characteristics of successiveness of seismic activity in these sub-regions, the forecast of seismic activity change in these sub-regions will be remarkably improved and may give a high percentage enough to trigger disaster prevention/mitigation measures.

6.4 Other Characteristics Concerning the Successive Earthquake Occurrence

In the case of using M≥7.0 earthquake data, among 17 (independent) events, there are 3 successive events (18%) and 1 "Foreshock-Mainshock" Type (5.9%). These percentages are about a half compared with those of independent events with magnitude more than 6. It implies that the intensity of successiveness can depend on magnitude of earthquakes.
Though the duration when the successiveness exists is determined 10 days in the section 6.1, there is one event (about 1%) which occurred between 10 and 20 days after the previous event. It is gathered that the probability of successive occurrence more than 10 days after the previous event could be one order larger than that calculated from the Poissonian process.

7 Application to Actual Seismic Activity and Conclusion

There occurred a sequence of earthquakes on 16-29 July 1992 (JST), in the sub-region examined in Section 6, that is, off-Sanriku region. Fig.6 shows the epicentral distribution of this seismic activity. The first M6.1 earthquake of this earthquake sequence took place at 0901h on 16 July 1992 (JST), and the M6.9 mainshock took place at 1736h on 18 July 1992 (JST). Table 2 shows examples of forecasts for this actual seismic activity as an application of the result of the analysis in Section 6, on a non-realtime basis. These forecasts could tell the real change of the seismic activity very well enough to be utilized for real forecasts for seismic activities.
The authors will consider the application to realtime earthquake information service, studying for other regions, different magnitudes, and hearing opinions of disaster prevention organizations as users.

8 Acknowledgements

The authors very much appreciate the cooperation of the staff of the Meteorological Research Institute, JMA, including Messrs. Hidemi Ito, Akihiko Wakayama, Hiromi Takayama, Kenji Maeda, Mitsuyuki Hoshiba and Dr. Akio Yoshida.

References

T. Utsu, 1961; A Statistical Study on the Occurrence of Aftershocks, Geophys. Mag., 30, 521-605.

T. Utsu, 1969; Aftershocks and Earthquake Statistics(I) -- Some Parameters Which Characterize an Aftershock Sequence and Their Interrelations --, J. Fac. Sci. Hokkaido Univ., Ser. VII (Geophysics) 3, 129-195.

K. Mogi, 1963; Some Discussions on Aftershocks, Foreshocks and Earthquake Swarms -- the Fracture of a Semi-infinite Body Caused by an Inner Stress Origin and Its Relation to the Earthquake Phenomena (Third Paper), Bull. Earthq. Res. Inst., Tokyo Univ. 41, 615-658.

K. Mogi, 1967; Regional Variation of Aftershock Activity, Bull. Earthq. Res. Inst., Tokyo Univ. 45, 711-726.

A. Yoshida, 1990; Characteristics of Foreshock Activities associated with Large Shallow Intraplate Earthquakes in the Japanese Islands, Pap. Met. Geophys.,41, 15-32.

T. Utsu, 1970; Aftershocks and Earthquake Statistics(II) -- Further Investigation of Aftershocks and Other Earthquake Sequences Based on a New Classification of Earthquake Sequences --, J. Fac. Sci. Hokkaido Univ., Ser. VII (Geophysics) 3, 197-266.

Y. Ogata and K. Katsura, 1986; Point-Process Models with Linearity Parameterized Intensity for Application to Earthquake Data, J. Applied Probability, Special Vol. 23A, 291-310.

L. M. Jones, 1985; Foreshocks and Time-dependent Earthquake Hazard Assessment in Southern California, Bull. Seism. Soc. America, 75, 1669-1679

Captions

Fig. 1 Epicentral distribution of earthquakes in and around Japan, used for this study. The earthquakes with $M \geq 6.0$, $h \leq 80$km, from 1926 to 1990 are selected from JMA catalogue of earthquakes, and moreover small aftershocks with $\Delta M > 1.0$ are excluded.

Fig. 2 Time series analysis by point process model.
Fig. 2a shows intensity of earthquake occurrence as trend of seismic activity. Intensity; frequency per day, and time; total days from Jan. 1, 1926.
Fig. 2b shows response function as successiveness of seismic activity. Response; frequency per day, and time; lapse days after an earthquake occurring.

Fig. 3 Distribution of epicenters of earthquakes as independent events. Open circles and closed circles show single events and successive events, respectively. The successive events are remarkable in the regions enclosed by broken lines.

Fig. 4 Time-sequence analysis by Point-process model, based on data of the independent events in the regions enclosed by broken lines in Fig. 3 and the successive earthquakes following them.
Fig.4a shows intensity of earthquake occurrence as trend of seismic activity, and Fig. 4b shows response as successiveness of seismic activity.

Fig. 5 Intensity variation in the case that a successive earthquake follows 0.5 day after an earthquake occurrence. The intensity integral within 10 days after an earthquake occurrence is estimated at 0.47, and the intensity integral within 10 days after a successive earthquake occurrence is estimated at 0.75.

Fig. 6 Epicentral distribution of a series of earthquakes in the region off Sanriku on July 16-29, 1992. The M6.9 mainshock occurred at 1736(JST), July 18.

Table.1 Successiveness of earthquake in the region off Etorofu Island and off Sanriku–Ibaraki Prefecture

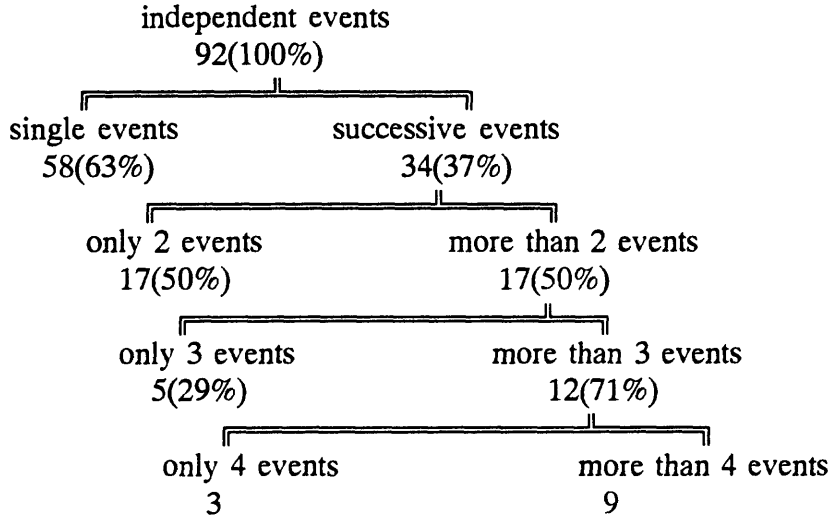

Table.2 Application to forecasts of earthquakes off Sanriku region, July, 1992

Facts and Information

(Fact 1) The M6.1 earthquake occurred at 09h01m, July 16, 1992.

(Information 1) The probability that one or more earthquakes with Magnitude 6 or more will occur within the following 10 days in the neighboring region is estimated to be usually about 0.1%.
(Information 2) The probability is estimated to be about 40% using the successiveness of seismic activity in this region.
(Information 3) There were 4 cases among 26 cases which were followed by one or more magnitude 7 earthquakes.

(Fact 2) The M6.9 earthquake occurred at 17h36m, July 18, 1992. The JMA issued the Tsunami Attention, and small tsunami was observed.

(Information 4) The probability is re-estimated to be about 50% using the successiveness of seismic activity in this region.
(Information 5) (Assuming the above M6.9 earthquake be an M7 class earthquake,) There was one case among 17 cases that was followed by a larger earthquake or more after M7 class earthquake occurrence, namely, the 1978 Etorofu Earthquake.

(Fact 3) The M6.6 earthquake occurred at 17h39m, July 18, 1992.

(Information 6) The probability is re-estimated to be about 70% using the successiveness of seismic activity in this region.

(Fact 4) The M6.3 earthquake occurred at 19h20m, July 18, 1992.
(Fact 5) The M6.1 earthquake occurred at 22h56m, July 18, 1992.
(Fact 6) The M6.0 earthquake occurred at 11h53m, July 25, 1992.
(Fact 7) The M6.2 earthquake occurred at 13h30m, July 29, 1992.
(Fact 8) No earthquake with magnitude 6 or more occurred during 10 days until August 8, 1992.
(Information 7) The probability is estimated to decrease to about 1%.

h 0≤ o <81

M 8 o , 7 o , 6 o

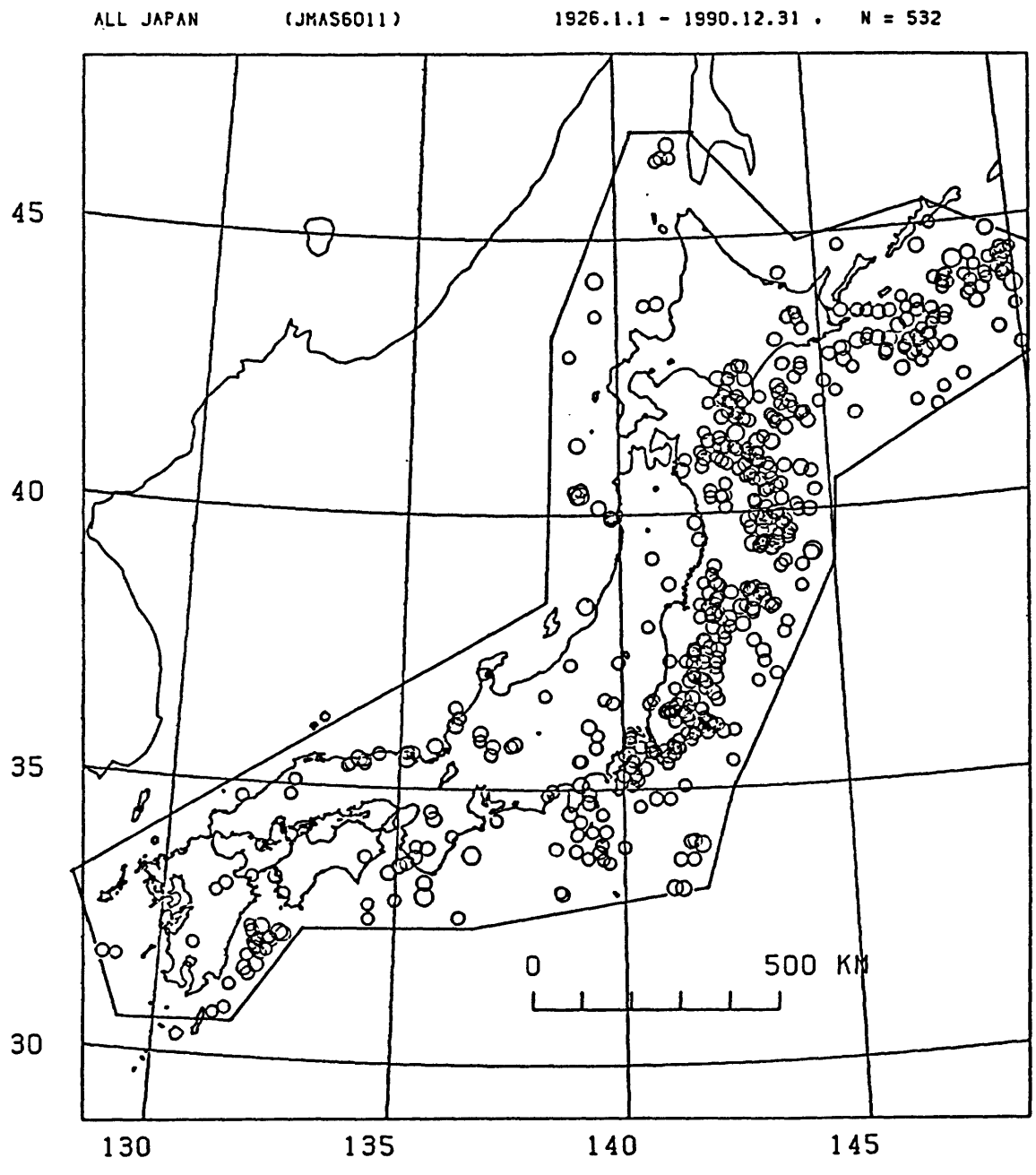

Figure 1

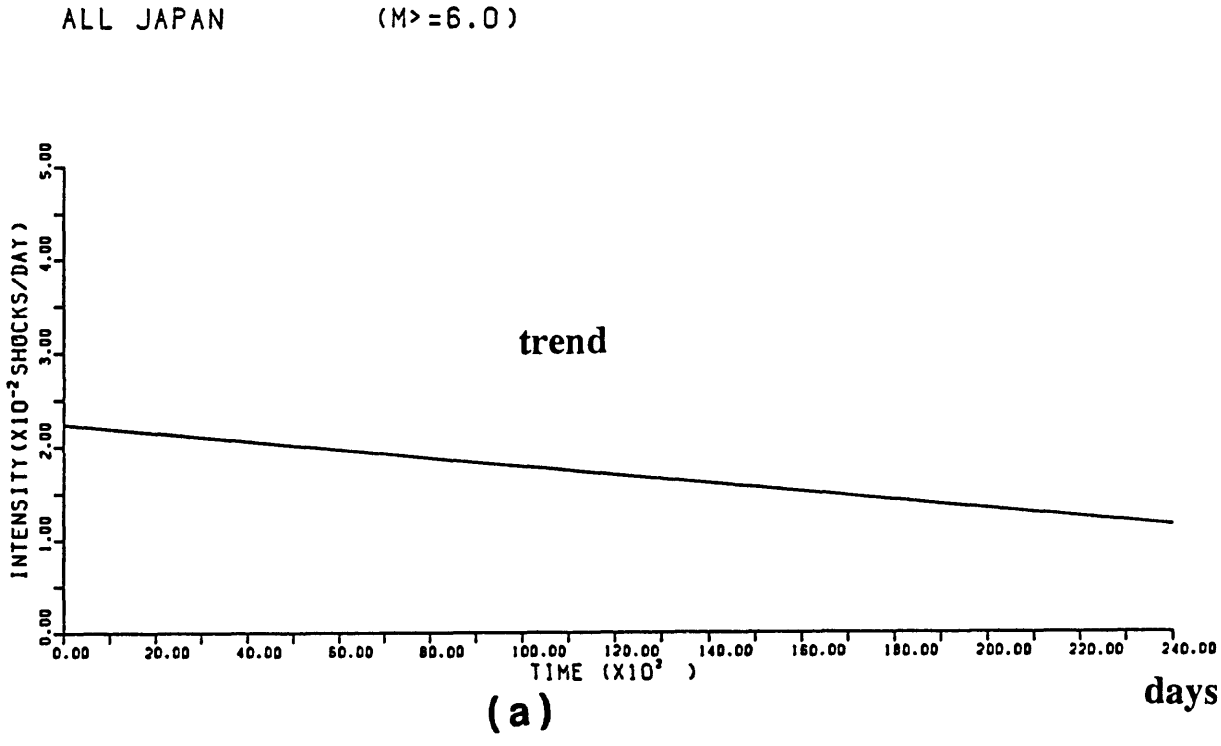
ALL JAPAN (M>=6.0)
INTENSITY (X10⁻² SHOCKS/DAY)
0.00
1.00
2.00
3.00
4.00
5.00
0.00
20.00
40.00
60.00
80.00
100.00
120.00
140.00
160.00
180.00
200.00
220.00
240.00
TIME (X10²)
trend
days
(a)

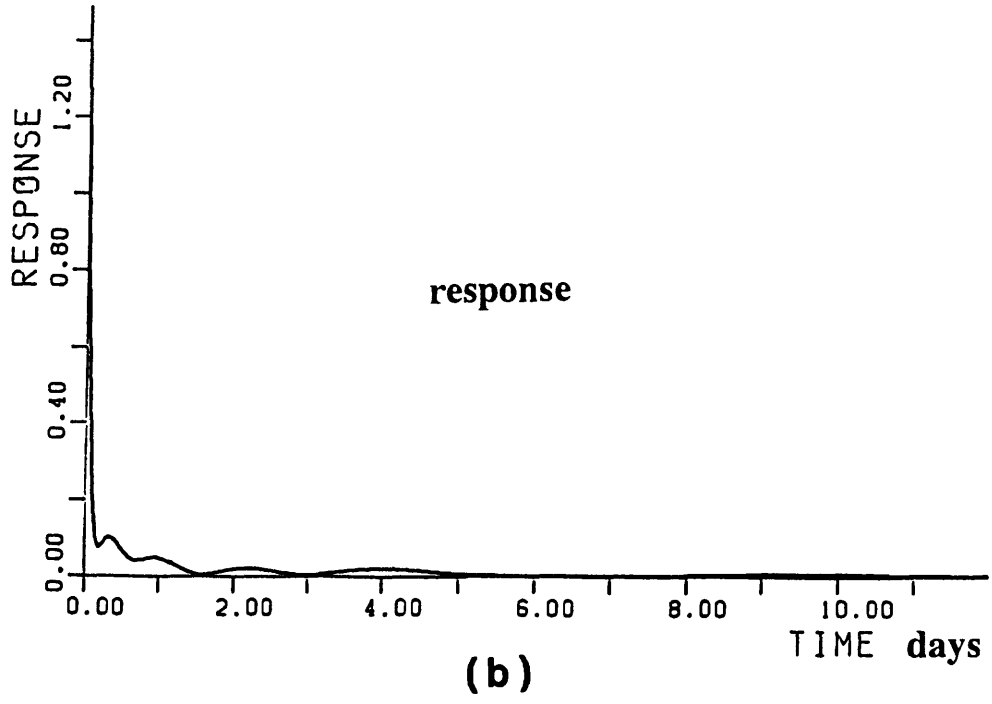
RESPONSE
0.00
0.40
0.80
1.20
0.00
2.00
4.00
6.00
8.00
10.00
TIME days
response
(b)

Figure 2

h 0≤ o <81

M 8 o , 7 o , 6 o

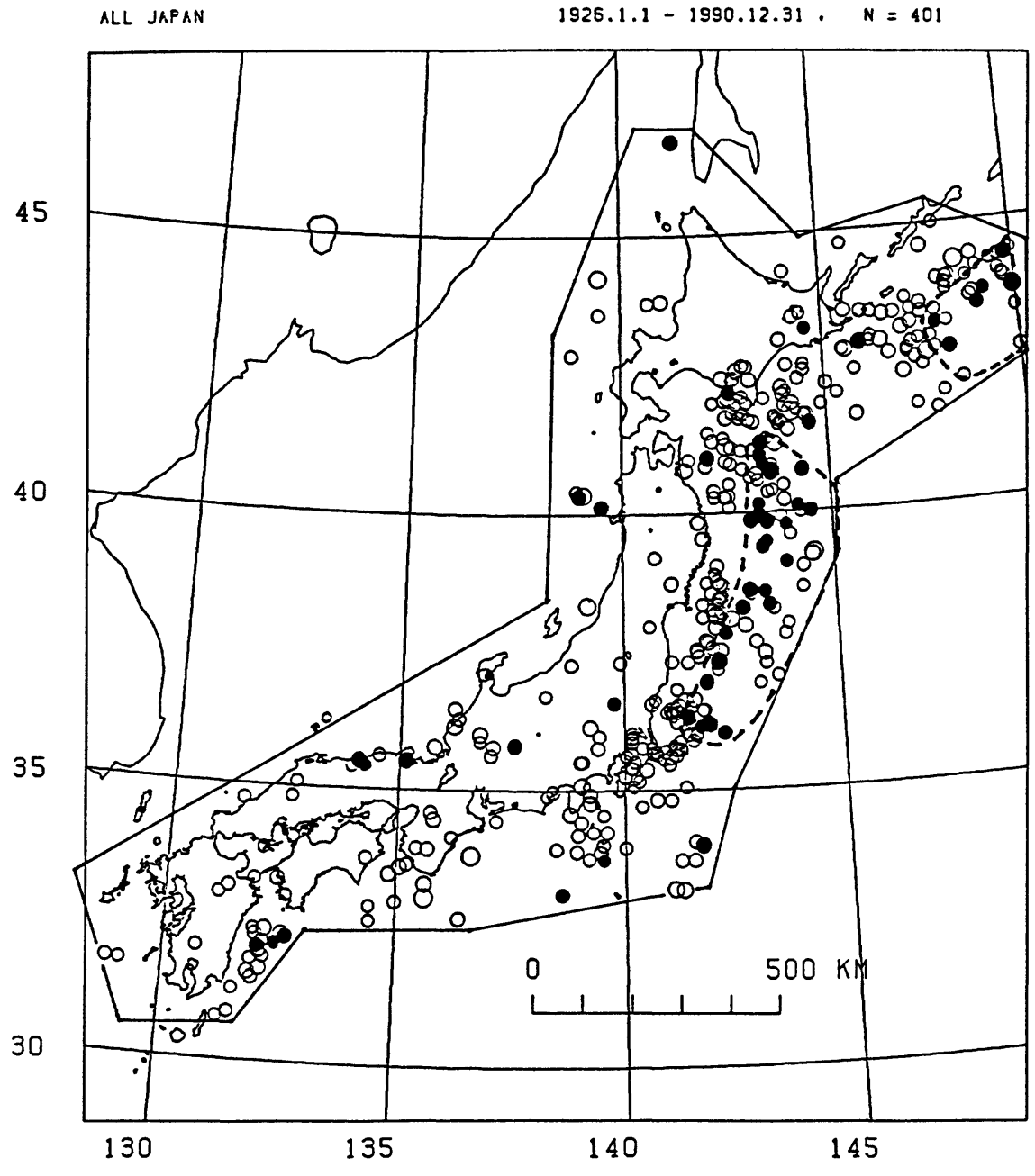

Figure 3

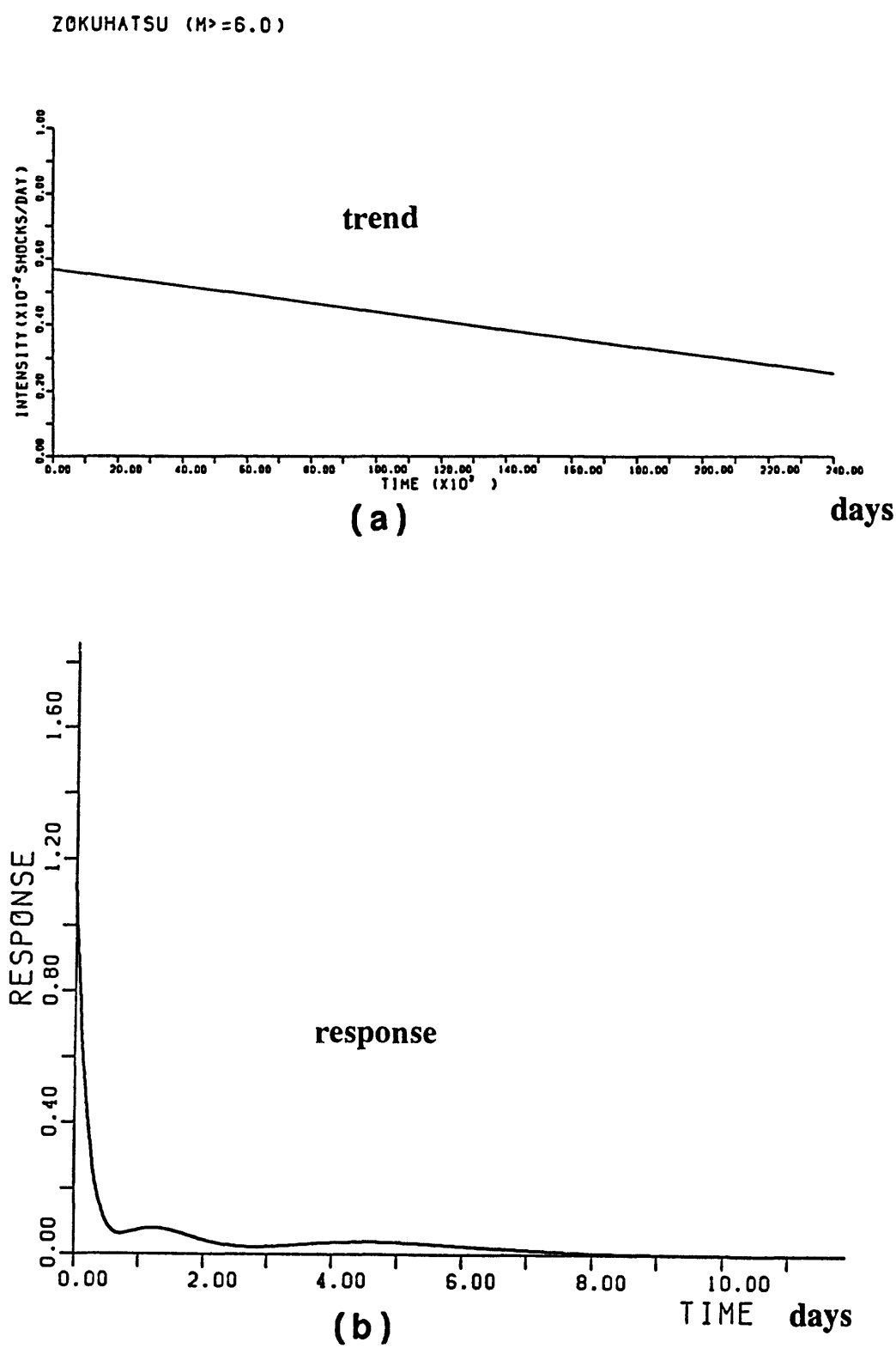
ZØKUHATSU (M>=6.0)
INTENSITY (X10⁻² SHOCKS/DAY)
trend
0.00
20.00
40.00
60.00
80.00
100.00
120.00
140.00
160.00
180.00
200.00
220.00
240.00
TIME (X10²)
(a)
days
RESPØNSE
0.00
0.40
0.80
1.20
1.60
response
0.00
2.00
4.00
6.00
8.00
10.00
TIME days
(b)

Figure 4

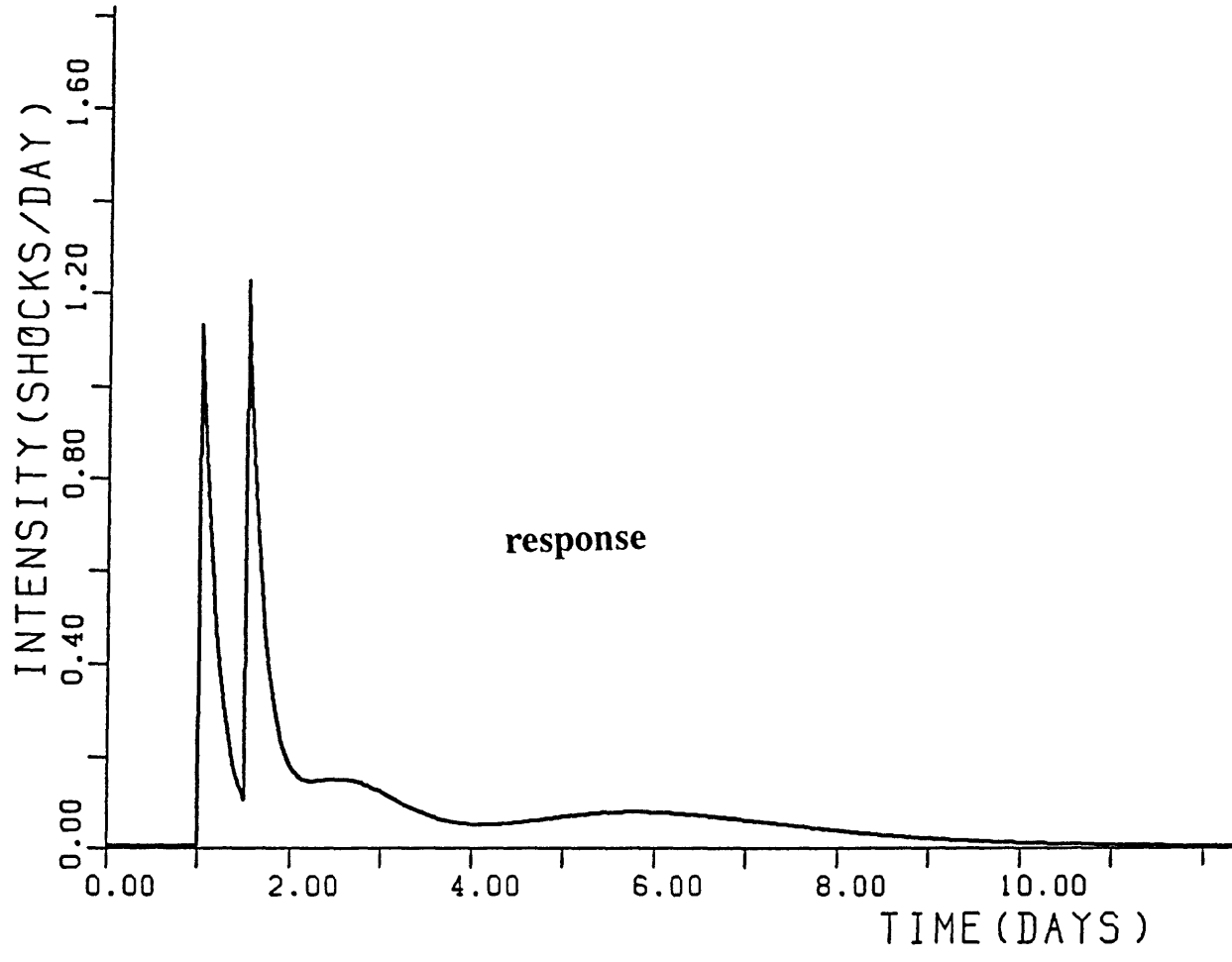
INTENSITY(SHOCKS/DAY)
0.00
0.40
0.80
1.20
1.60
response
0.00
2.00
4.00
6.00
8.00
10.00
TIME(DAYS)

Figure 5

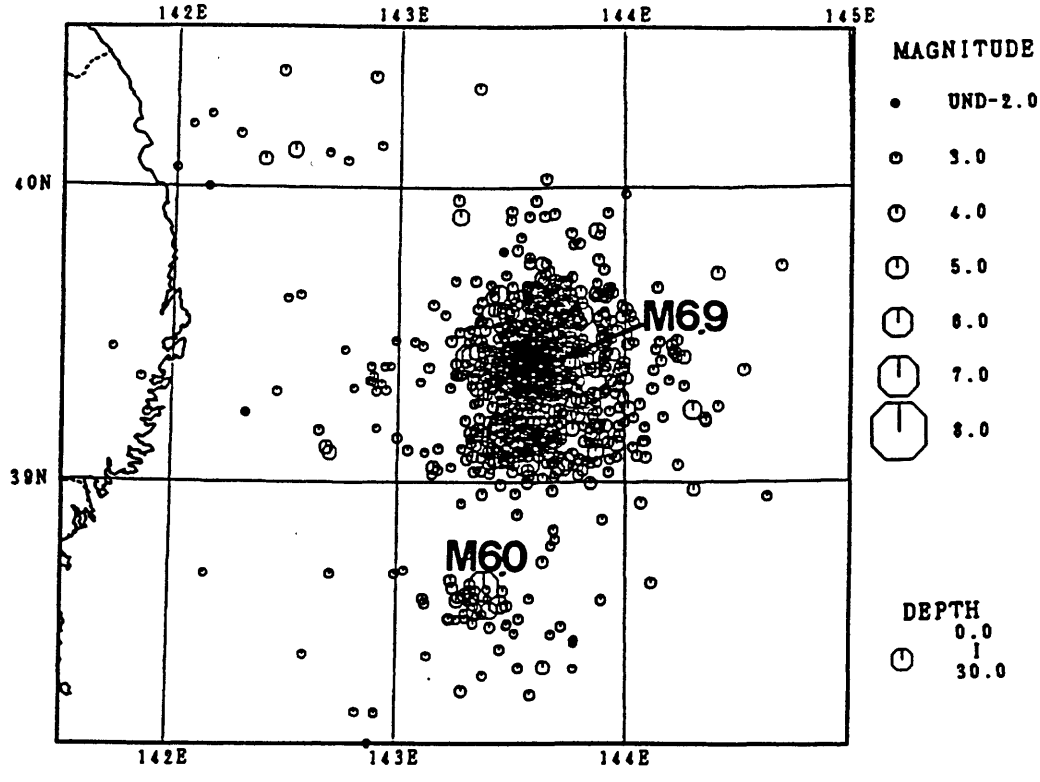
142E
143E
144E
145E
40N
39N
M6.9
M6.0
MAGNITUDE
UND-2.0
3.0
4.0
5.0
6.0
7.0
8.0
DEPTH
0.0
30.0

Figure 6

An Overview of the 1992 Joshua Tree, Landers, and Big Bear Earthquake Sequences

Lorraine J. Hwang, and the Staff of the U.S. Geological Survey, Pasadena, CA
and the California Institute of Technology, Pasadena, CA

The 1992 sequence of moderate to large earthquakes that shook Southern California began with the ML 6.1 Joshua Tree earthquake on 23 April 1992 04:50 GMT. The earthquake was preceded by several foreshocks including a ML 4.6 event more than 2 hrs before the main shock. The main shock was a right-lateral strike-slip event (strike: N14W, dip: 80W, rake: 175) at a depth of 12-13 km that propagated northward along an unknown fault that did not rupture the surface. Aftershocks along the main fault plane extend to a depth of 13 km while aftershocks on adjacent secondary structures were shallower (< 8 km). Aftershocks migrated to the south near the San Andreas fault and north eventually crossing the Pinto Mountain fault.

The MS 7.5, MW 7.3 Landers event of 28 June 1992 11:58 GMT (1 x 10 ** 27 dyne-cm) is the largest earthquake in the sequence and the largest in the region in 40 yrs. The Landers earthquake was preceded by a tight cluster of foreshocks beginning 12 hrs before the main shock. The main shock started as a small event that within seconds grew to a MS 7.5 event whose rupture propagated towards the north rupturing segments of the Johnson Valley, Homestead Valley, Emerson and Camp Rock faults. Source studies show the event ruptured along an almost vertical, right-lateral strike-slip fault that initially trended NS. The strike of the event changed about 26 degrees as the rupture jumped along fault strands that strike progressively westward. Aftershocks extend 65 km to the north of the main shock epicenter and 40 km to the south crossing the Pinto Mountain fault through the Joshua Tree aftershock zone. The estimate of slip distribution determined from empirical Green's functions is consistent with teleseismic data and the surface offsets mapped in the field and geodectic observations.

The largest cluster of off-fault aftershocks for the Landers event is due to the M6.6 Big Bear event on 28 June 1992 (3 x 10 ** 25 dyne-cm) that occurred just 3 hrs (15:05 GMT) after the Landers main shock. Its epicenter lies 30 km west of the Landers main shock and its aftershocks extend 20 km along a northeast trend. Its focal mechanism and aftershocks indicate rupture along a northeasterly striking, steeply dipping, left-lateral strike-slip fault.

The Joshua Tree and Landers event occurred on the southernmost end of the Mojave shear zone. These events are thought to represent transfer of motion from the San Andreas fault in the Imperial Valley to the Basin and Range province in eastern California, Nevada, and Utah.

Seismicity in the Western United States Remotely Triggered by the M 7.4 Landers, California, Earthquake of June 28, 1992

Submitted to Science, February 2, 1993

David P. Hill, Paul A. Reasenberg, Andrew Michael, Walter J. Arabasz, Greg Beroza, James N. Brune, David Brumbaugh, Raul Castro, Scott Davis, Diane dePolo, William L. Ellsworth, Joan Gomberg, Steve Harmsen, Leigh House, Suzette M. Jackson, Malcolm Johnston, Lucy Jones, Randy Keller, Steve Malone, Luis Munguia, Susan Nava, James C. Pechmann, Alan Sanford, Robert W. Simpson, Robert S. Smith, Mitchell Stark, Mike Stickney, Antonio Vidal, Steve Walter, Victor Wong, and James Zollweg

ABSTRACT

The M 7.4 Landers earthquakes of June 28, 1992, triggered a remarkably sudden and widespread increase in earthquake activity across much of the western United States. The triggered earthquakes, which occurred at distances up to 1250 km (seventeen source dimensions) from the Landers mainshock, were confined to areas of persistant seismicity and strike-slip to normal faulting. Many of the triggered areas also are sites of geothermal and recent volcanic activity. Static stress changes calculated for elastic models of the earthquake appear too small to cause the triggering. The most promising models involve non-linear interactions between large dynamic strains accompanying seismic waves from the mainshock and crustal fluids (perhaps including crustal magma).

At 1158 UT (04:58 PDT) on June 28, 1992, southern California was rocked by the magnitude (M) 7.4 Landers earthquake, the largest earthquake to strike the region in 40 years (1). The earthquake resulted from a northward propagating rupture producing up to 6 m of right-lateral, strike-slip displacement on a series of faults extending over 70 km north-northwest into the Mojave desert from its epicenter 5 km southwest of the town of Landers (Figure 1). Within minutes after the Landers mainshock, earthquake activity abruptly increased at widely scattered sites across the western United States (2). This abrupt, widespread and unexpected increase challenges the skeptical view held by many seismologists regarding triggered seismic activity at great distances from an earthquake. Indeed, the observations presented here strongly point to a direct physical (causal) link between the Landers earthquake and the sudden increase in seismicity throughout the western United States.

That earthquake activity can be triggered by a nearby source is well known. Aftershocks of large and moderate earthquakes commonly occur at distances of one or two source dimensions from a mainshock (3). Seismicity induced by human activities (which include the underground detonation of nuclear explosions, filling or emptying of water reservoirs, injecting and extracting fluids in deep boreholes, and mining) is usually confined to an area within a few tens of km or less of the inducing source (4). In marked contrast, the widespread surge in post-Landers seismic activity extended over 1250 km (17 source dimensions) from the mainshock.

Traditional skepticism regarding remotely triggered activity has its roots, in part, in the lack of statistical significance associated with an increase in earthquake activity

at a solitary, remote site after a large earthquake, and, in part, in the lack of a plausible physical model for remote triggering. In particular, earth models based on linear elasticity, which have enjoyed enormous success in explaining a vast range of seismological phenomena, seem incapable of explaining triggered seismicity beyond a few source dimensions of an earthquake rupture (5). The simultaneous increase in seismic activity at many remote sites following the Landers earthquake thus forces consideration of new models that include non-linear interactions to explain remote triggering.

In this paper we document the spatial distribution and temporal evolution of the seismic activity that followed the Landers mainshock and the tectonic settings in which the activity occurred. We argue that this activity is not explained by random coincidence, and we comment briefly on evidence for remote triggering by other major ($M \geq 7$) earthquakes. We conclude by exploring some possible physical processes that might explain remote triggering.

Distribution and nature of triggered seismicity. Recognition of remotely triggered seismicity depends critically on the distribution of seismic networks. Because the networks operating in the western United States and northern Mexico (Figure 1) do not provide spatially uniform coverage and their detection thresholds vary, our recognition of seismicity triggered by the Landers event is probably incomplete. For example, a sequence of $M < 2$ earthquakes triggered in southeastern Oregon or southern Arizona would not be detected by any of the operating networks. Furthermore, before the late 1970's many of the present networks were sparse or non-existent. Had the Landers earthquake occurred prior to then, the chances are poor that triggered activity would

have been recognized.

The most dramatic increase in earthquake activity occurred in the Landers aftershock zone (Figure 2), which we exclude from further consideration in this paper (6). We also exclude from consideration possible triggered activity in southern California between the Garlock fault and Mexico, for which a complete earthquake catalog is not yet available. We note, however, two candidates for triggered activity in southern California: a cluster beneath Pasadena 60 km west of the aftershock ellipse that included a M=3.9 event on June 29, and a lineation of earthquakes along and east of the White Wolf fault (source of the M = 7.5 Kern County earthquake of 1952).

North of the Garlock fault, post-Landers earthquake activity was concentrated within a belt of persistent seismicity and Holocene faulting that extends north-northwest from the southern margin of the Great Basin (7) along the Sierra Nevada-Great Basin boundary zone (SNGBZ) as far north as the southern Cascade volcanoes in northern California (10). Triggered activity outside the SNGBZ occurred in more isolated sites, each also with a history of persistent seismic activity (Figures 2 and 7). Particulary noteworthy aspects of the triggered sites include: 1) all sites of (recognized) remote triggering are north of the Landers mainshock, and 2) all are sites of persistent seismicity showing strike-slip to normal faulting (i.e., having horizontal least principal stress). At the same time, many sites of persistent seismicity north of Landers did not respond with triggered seismicity. Most notably, the active sections of the San Andreas fault system in central and northern California, the Intermountain seismic belt in central Utah, and the central Nevada belt (8) showed no response. Many sites of remotely

triggered activity are closely associated with areas of geothermal activity and/or young volcanism (last 1 my). Sites of triggered activity not closely associated with geothermal activity or post 1-my volcanism are concentrated just east of the California-Nevada border from the eastern side of the the White Mountains northwest to the Excelsior Mountains and beyond to Lake Tahoe. The association is marginal for triggered sites in southern Nevada (Little Skull Mountain) and western Utah (Cedar City), which have no nearby geothermal systems but are within 20 km of Pliestocene ($\leq$ 1 my) basaltic vents (9). Only a fraction of the seismically active geothermal and young volcanic systems, however, responded with triggered activity. The seismogenic Brawley and Cierro Prieta geothermal areas in the Imperial Valley - Salton Trough south of Landers (Δ = 150 ~ 250 km) are particularly notable for the absence of triggered activity (9a).

Both the maximum magnitude and the total seismic moment of the remotely triggered earthquakes decreased with distance from the Landers epicenter (Table 1 and Figure 4). The largest triggered earthquake was a M = 5.6 event beneath Little Skull Mountain in southern Nevada (Δ = 240 km) on 29 June at 1014 UT located approximately 20 km east of a group of basaltic vents with date estimates ranging from 0.02 to 1.0 my (9). This earthquake, which had an oblique normal mechanism with an NW-SE T-axis orientation, was preceded by at least 19 smaller events within 100 km of Little Skull Mountain beginning at most 91 minutes after the Landers mainshock (earlier events could have been obscured by seismic waves generated by the intense Landers aftershock activity). It is the largest earthquake to occur in this secton of the southern Great Basin since 1868.

Triggered activity along the eastern margin of the Sierra Nevada and adjacent sections of western Nevada (the Sierra Nevada-Great Basin boundary zone, or SNGBZ) was concentrated in scattered clusters from the Indian Wells Valley-Coso area north of the Garlock fault (Δ = 150 km) to the vicinity of Lake Tahoe (Δ = 500 km). The SNGBZ is marked by numerous Quaternary basaltic and rhyolitic volcanic centers and geothermal areas, and has been a persistent source of moderate-to-large earthquakes throughout historic time, which dates from the mid-1800's (10). Long Valley caldera has been the most active area within the SNGBZ over the last decade with recurring earthquake swarms and over 0.5 m of ground uplift, and it is the site of the most recent volcanism within the SNGBZ with eruptions just 500-600 years ago (11). The triggered seismicity within the SNGBZ, which included numerous events in the M = 3-4 range, coincides closely with the locations and depths of earthquakes located there over the past several decades. Specific areas of triggered activity within the SNGBZ include (see Figure 2): a 60-km-long, north-northwest-trending lineation along the base of the Sierra Nevada from Indian Wells Valley (I) to the vicinity of Coso Hot Springs (C); a diffuse cluster cutting westward from the California-Nevada border near 37° N across the northern end of Death Valley (D) through the Inyo Mountains into Owens Valley (OV); a dense cluster concentrated in the south moat of Long Valley (LV) caldera; three clusters along the California-Nevada border, two east of Long Valley along the east margin of the White Mountains (W) and one north of Long Valley in the Mono Basin (M); a cluster elongated to the northeast in the Excelsior Mountains (E) in western Nevada; and a diffuse lineation along the eastern margin of the Sierra Nevada between Bridgeport and Lake Tahoe (LT).

The triggered swarm near Cedar City in southwestern Utah ($\Delta = 470$ km) included more than 60 earthquakes (at least 7 of which were felt locally) within the Hurricane fault zone, the principal bounding fault between the Colorado Plateau and the eastern Great Basin, and within 15 to 20 km of Quaternary basalt flows with dates of 1.0 to 1.2 my (9). No other sites along the seismically active, eastern margin of the Great Basin (the Intermountain seismic belt [12]) showed evidence of triggered activity.

Beyond 600 km, isolated clusters of less intense activity occurred in the Geysers geothermal area ($\Delta = 740$ km), the southern Cascade range ($\Delta = 810$–920 km), Yellowstone National Park ($\Delta = 1270$ km), and western Idaho ($\Delta = 1100$ km). The triggered activity at the Geysers consisted of a surge of $M < 1$ earthquakes that began 30 s after the Landers S-wave arrival, and decayed to background levels three hours later (Figure 6a). This is the only triggered activity recognized within the northern San Andreas fault system. In the southern Cascade Range, earthquake activity increased at Lassen Peak, Medicine Lake caldera, and near Burney (an area covered by Quaternary lava flows). Triggered seismicity near Cascade, Idaho, was located in the western part of the Idaho batholith (see Figure 7) some 15 km west of the nearest hot spring. The most distant candidate for activity triggered by the Landers mainshock occurred in a small cluster ($\Delta = 1250$ km) 15 km northwest of Yellowstone caldera in Yellowstone National Park (13) (see Figure 7).

Temporal patterns in triggered activity. The apparent onset of triggered seismicity (time of the first detected earthquake after Landers) varied from site to site

(Figure 3, Table 1), from 30 s after passage of the Landers S wave to 33 hours after the Landers main shock. Establishing the onset time is important both for judging statistically whether triggering has taken place (ruling out random coincidence) and for constraining physical models for remote triggering. In general, the recognized onset time will depend on the local rate of seismicity and the sensitivity of the seismic network, both of which vary regionally. In addition, the temporary obscuring effect of coda waves from the Landers mainshock and its largest aftershocks may have masked otherwise detectable local earthquakes at some sites.

The strong direct waves and the reflected and scattered coda waves produced by the mainshock and its large aftershocks tended to obscure the onset time of the triggered activity. Our approach to this problem takes advantage of the fact that seismic waves from nearby earthquakes are relatively rich in high frequency energy, while waves from the Landers mainshock, having traveled a long distance, are relatively depleted in high frequency energy due to intrinsic attenuation and scattering. Applying a 5 to 30 Hz band-pass filter to seismograms effectively eliminates the mainshock coda at distances beyond 500 km and enhances the local earthquakes (Figure 5). The result shows that in Long Valley caldera (Δ = 415 km) and the Geysers (Δ = 740 km), the triggered activity began 30 to 40 s after the S-wave arrival from the Landers earthquake and during the passage of the large-amplitude Lg and Rg surface wave trains (14). No evidence for such early activity was found at Parkfield, the White Mountains, Mono Basin, western Nevada, Lassen, Burney, or Yellowstone. Inadequate station coverage or severe signal clipping made this analysis impossible at the other sites listed in Table 1.

Using the earthquake catalog data, we tested the hypothesis that the observed onset of activity at each site is consistent with an instantaneous increase in local seismicity rate at the time of the Landers earthquake (15). We were unable to reject the hypothesis at all but one of the sites, a result consistent with a causal link between the Landers earthquake and the remote earthquake activity.

It is possible that the increased seismicity rate at some sites is merely coincidental (having no causal link) with the Landers earthquake. Although the post-Landers surge in seismicity is unusual at each site, all of the sites are seismically active and have had seismicity surges (swarms) in the past (see, for example, the swarm on day 35 at Lassen Peak in Figure 3). Considering the relative infrequency of these seismicity surges, however, we believe non-causal coincidence to be unlikely for the post-Landers activity (16).

The duration of the triggered activity at a given site showed no clear correlation with distance from the Landers rupture (Figure 3,6, Table 1). At Long Valley and the Geysers, where seismicity is normally high, the triggered seismicity occurred as smooth transient surges in seismicity with durations of a few days and a few hours, respectively (Figure 6), while at Mono Basin and Burney, triggered activity showed little sign of diminishing after three weeks or more. The increase in number of events after the Landers earthquake varied widely from site to site, apparently uncorrelated with distance from Landers. As summarized in Table 1, however, the maximum magnitude of triggered earthquakes at each site generally decreased with distance from Landers.

Supporting observations. Observations of both permanent and dynamic strain changes at sites of remotely triggered seismicity help constrain possible triggering processes. Of all the sites showing triggered activity, however, only Long Valley caldera has continuous deformation-monitoring instrumentation. Here, data from daily measurements of a two-color geodimeter network showed no strain changes above its resolution of about 0.3 microstrain (17). Continuous data from a 200-m-deep borehole dilatometer 4 km west of the caldera show an instantaneous compressional strain step of about 3×10^{-9} between the Landers P and S waves, followed by a slower compressional pulse that builds to about 2×10^{-7} during the five days after the mainshock and returns to the background level over the next few weeks (Figure 6).

Information on dynamic stresses comes from on-scale records of the Landers mainshock recorded on both broad-band, digital seismometers and dilatometers (Table 1; 18). The dilatometers provide a direct measurement of dilatational strain, θ, and the associated dynamic mean stresses are $\bar{\sigma} = k\theta$, where k is the bulk modulus. The seismometers provide data on particle velocities, which are proportional to dynamic stresses (19). Peak particle velocities and dilatational strains (and thus peak dynamic stresses) occur within the S-wave coda at distances beyond about 300 km, and include early parts of the fundamental-mode Rayleigh (Rg) and Love (Lg) wave train, with dominant periods in the range 5 to 20 s (see Table 2).

The distribution of peak dynamic stresses from the Landers mainshock (Figure 7) shows a strong directivity effect associated with the northward propagation of the mainshock rupture. Peak dynamic stress values north-northwest of the mainshock are

roughly twice those at comparable distances to the west, and over three times those to the south. For example, at $\Delta = 410$ km the peak dynamic stress was 1–2 bars at Parkfield, but 3–4 bars in Long Valley caldera. Peak dynamic stresses in the San Francisco Bay area produced by the Landers mainshock (1.2-1.5 bars) are roughly twice those produced by the M = 7.0 Petrolia (Cape Mendocino) earthquake (0.5-0.6 bars), while the distance from the Bay area to Landers is nearly twice that to Cape Mendocino.

Well-aquifer systems can behave as band-limited volume strain meters, and the response of such systems to the dilatational strains of Rayleigh waves from distant earthquakes is well documented (20). Preliminary data from water wells at Yucca Mountain (25 km northwest from Little Skull Mountain) and Long Valley caldera show pronounced transient fluctuations (amplitudes from less than one cm to several m) associated with seismic waves from the Landers mainshock, but no clear evidence for static offsets in local water table levels (21).

Remote triggering by previous large ($M \geq 6.5$) earthquakes? It might at first appear from the paucity of examples in the literature that the triggering of remote seismicity by large earthquakes is exceptional. The activity triggered by the Landers earthquake, however, consists largely of small ($M \leq 3$) events in relatively remote areas, and, as noted earlier, our ability to recognize reliably this level of seismic activity dates only from the late 1970s with the deployment of dense, telemetered seismic networks and computer-based, real-time data processing systems (22). Indeed, pushing the search for evidence of remote triggering further back in time forces us to

consider progressively larger (and thus less common) earthquakes, in turn pressing the issue of statistical significance.

Four other $M \approx 7$ earthquakes have occurred in the western United States since 1980: the $M = 7.3$ Eureka, California, earthquake (located 50 km west of Cape Mendocino) of 8 November 1980, the $M = 7.0$ Borah Peak, Idaho, earthquake of 28 October 1983, the $M = 7.0$ Loma Prieta, California, earthquake of 18 October 1989, and the $M = 7.0$ Petrolia, California, earthquake of 25 April 1992. However, with the possible exception of minor swarm activity at the Geysers geothermal field coincident with the 1989 Loma Prieta and 1992 Petrolia earthquakes (distances of 220 and 230 km from the Geysers, respectively), none of these $M \approx 7$ earthquakes appears to have triggered remote seismicity (23). The 1980 Eureka earthquake was essentially the same size as the Landers earthquake (both with seismic moments $M_0 = 1 \times 10^{27}$ dyne-cm). The other three events are smaller by factors of 2 to 5, with seismic moments ranging from $M_0 = 2 \times 10^{26}$ (Loma Prieta) to $M_0 = 5 \times 10^{26}$ dyne-cm (Petrolia). It is particularly noteworthy that neither the 1980 Eureka nor the 1992 Petrolia earthquakes near Cape Mendocino triggered seismicity in the vicinity of the southern Cascade volcanoes (distances 200 to 250 km), while just 64 days after the Petrolia event the Landers earthquake did trigger activity in the southern Cascades ($\Delta = 800$ to 900 km). It is perhaps also noteworthy that the Eureka and Petrolia ruptures propagated to the southwest and west, respectively, (away from the continental United States) while the Landers rupture propagated to the north and in the direction of the triggered activity. In any case, it appears that the conditions for remote triggering involve more than simply the occurrence of a $M \geq 7.3$ (or $M_0 \geq 1 \times 10^{27}$ dyne-cm) earthquake.

Remote triggering may have occurred after the 1906 San Francisco M8¼ earthquake. Eight felt earthquakes occurred during the first 2 days within 700 km of San Francisco, most notably including a M6.2 event in the Imperial Valley 11 hours after the mainshock. Similarly, seven M2–3 events near Riverside, California (distance 100 km) occurred within the first 6 hours after the M7.7 1952 Kern County earthquake. If the Imperial Valley and Reverside events were triggered, the triggering is not very "remote", as they lie within 2 and 2.5 rupture lengths from their respective mainshock sources.

Two additional candidates for remote triggering that have come to our attention involve an abrupt seismicity increase in Rabaul caldera (Papua New Guinea) on 10 May 1985 following a M = 7.2 earthquake in New Britain 180 km away (24) and a swarm of some 30, locally felt earthquakes on Kyushu, Japan, that began about 16 minutes after the the great (M = 8) Nankaido earthquake of 21 December 1946 at a distance of 450 km (25). In both cases, the putative triggered activity occurred in close association with sites of young volcanism and geothermal activity.

Triggering mechanisms. Competitive models for the remote triggering process fall into two broad classes: one involving the static stress changes in the crust produced by the dislocation along the Landers rupture surface, and the other involving the dynamic stresses associated with the propagating seismic waves generated by abrupt slip along the rupture surface. In both, remote triggering involves brittle slip on local, favorably oriented faults induced by an incremental change in the local stress field sufficient to overcome frictional strength and/or an incremental reduction in effective

frictional strength.

Static stress changes decrease rapidly with distance (as r^{-3}, compared to r^{-2} and r^{-1} for dynamic stresses associated with body and surface waves, respectively) for a dislocation in an elastic half space. Maximum static shear stress changes calculated for the Landers earthquake, for example, fall below daily tidal stress changes (26) at distances beyond about 250 to 300 km (Table 1; Figure 7). The dilatational component of the static strain change calculated for this model in the vicinity of Long Valley caldera ($\Delta = 420$ km) agrees in both sense and magnitude with the -3×10^{-9} compressional strain step detected by the borehole dilatometer in the caldera.

The small size of static stress (or strain) changes for the Landers mainshock at distances beyond about 250 km argues against their efficacy as a triggering mechanism for remote seismicity. Before completely discounting the role of static stress changes in remote triggering, however, it is worth noting that 1) static changes act for much longer times than either tidal or dynamic changes, and 2) the continental crust in tectonically active areas may behave more like an array of blocks with relatively weak boundaries (faults) than a homogeneous elastic half space (27). Static strain changes within weak boundaries (fault zones) between blocks may show considerable deviations from those predicted for a homogeneous half space. The ability of static strain changes within weak zones to trigger local seismicity may be further enhanced if the weak zones are relatively impermeable such that the strain changes drive large changes in local pore pressure (28).

The relatively large, northward-directed dynamic stresses associated with the shear-wave coda and the fundamental mode Love (Lg) and Rayleigh (Rg) waves with periods in the range 5 to 20 s (Figure 7) admit several possible mechanisms for the triggering process. In principal, an S wave (or Lg wave) polarized in the plane of maximum tectonic shear stress could trigger slip on favorably oriented faults that were close to the failure threshold. S- or Lg-waves propagating through a locally heterogeneous stress field will generate particle accelerations in the direction of propagation and transient stresses normal to the shear plane (29). The combination would facilitate slip on an optimally oriented fault by temporarily reducing the normal stress acting across the fault plane. The non-linear nature of constitutive laws for fault friction (30) admits the possibility that the frictional strength of faults can be lowered as the fault planes are "worked" by the dynamic strains of the passing wave field, thereby triggering slip on faults near the failure threshold.

An important set of non-linear processes that may contribute to remote triggering involves the interaction of the dilatational component of crustal Rayleigh (Rg) waves with fluids in the crust. Peak dynamic stresses associated with Rg (and Lg) waves at mid-crustal depths are on the order of a few bars at distances to at least 500 km (Figure 7, Table 1) (19). We noted earlier (20) the pronounced transient response of water wells and unconfined aquifers to passing Rayleigh waves from large, distant earthquakes. In the case of confined fluids, the Rayleigh waves may act as a hydraulic pump, with the compressional phase irreversibly driving pore fluids to shallower depths, thereby lowering the effective strength of faults in the upper (brittle) crust. Vertical fluid motion may be favored in tectonic environments characterized by strike-

slip to normal faulting (least principal stress horizontal) where fluid-filled cracks tend to grow in vertical planes. Hydrothermal systems may be particularly susceptible to such a process because super-hydrostatic pore fluids associated with rocks in the plastic domain (temperatures above 350-400° C) may exist at relatively shallow depths (31). At a somewhat more speculative level, the large dilatational strains associated with Rg waves interacting with magma bodies in the upper crust may accelerate the exsolution of volatile components, temporarily increasing pressure within the magma body or pore pressure in the overlying rock due to an increased flux of volatile components out of the magma body (32). Alternatively, crustal magma bodies that are predominately crystalline with only a small melt fraction behave as solids rather than as liquids at small strain levels (i.e., they transmit shear waves). If the large dynamic strains associated with the surface waves caused such a magma chamber to liquify, this would release any differential stress it supported and transfer this load to the surrounding crust, triggering earthquakes in much the same way that stress redistribution in an earthquake triggers aftershocks.

Possibly, a combination of processes contribute to the observed triggering, with the dominant process at a given site determined by the local crustal environment and location (both distance and azimuth) with respect to the mainshock source. The close association of most sites of triggered activity with recent volcanism and geothermal systems, for example, suggests that the interaction of the dilatational components of the strain field from the Landers earthquake with geothermal fluids or crustal magma bodies may be an important triggering process. At Long Valley caldera, the close temporal association between seismicity rate and the increasing portion of the transient

compressional strain pulse (Figure 6) strongly points to an increase in fluid pressure somewhere in the upper crust driving the triggered seismicity.

The fact that the triggered activity persisted hours to a week or more after seismic waves from the Landers event subsided (and apparently in some cases may not have begun until after the seismic waves had subsided) emphasizes that the triggered activity was not driven directly by the dynamic stresses. Indeed, all of the triggered sites coincide with regions of persistent, low-level seismic activity, indicating that local stresses were close to the threshold for brittle failure immediately prior to the Landers earthquake. Whatever the triggering processes were, their result was a cascading failure sequence (earthquake swarm) within a crustal volume already loaded to a critical stress state (33). The form and duration of individual triggered sequences are probably influenced by the same factors (the degree and characteristic dimension of fracturing, pore pressure, permeability, etc.) that influence the evolution of an aftershock sequence.

Our observations of remote triggering of seismicity after the Landers earthquake focus attention on the nature of earthquake fault interaction and the mechanics of the seismogenic crust. While elastic dislocation models in homogeneous media may explain the occurrence of aftershocks within one to two rupture lengths away from a fault, the predicted static stress changes at greater distances seem too small to explain remote triggering. The temporal form and spatial distribution of the remote triggering point, instead, to an alternate class of explanations involving critically loaded faults in a heterogeneous crust, static strain amplification within weak boundaries (fault zones)

between crustal blocks, and the non-linear interaction between dynamic stresses in seismic waves and crustal fluids. Although no single model seems capable of explaining all the triggered activity following the Landers earthquake, this general class of explanations is appealing because it involves geologically more realistic crustal models than does the classical, homogeneous view. Indeed, the greatest importance of the Landers triggering observations may be in the new, clear evidence they provide leading toward a view of crustal mechanics more geologically and structurally complex, and away from the classical paradigm of a homogeneous, linear elastic halfspace.

REFERENCES AND NOTES

1. H. Kanamori, H.-K. Thio, D. Dreager, E.H. Hauksson, *Geophys. Res. Lett.*, in press (1993). In this paper we use M for moment-magnitude (T. Hanks and H. Kanamori, *Jour. Geophys. Res.* **84** 2348 (1979)) and *M* for local network magnitudes based on either amplitude or coda duration measurements.

2. Earthquake data used in this study were provided by regional seismograph networks operated by the U.S. Geological Survey, California Institute of Technology, the University of Nevada, the University of Utah, the University of Washington, Boise State University, The University of Texas at El Paso, Idaho National Engineering Laboratory, Los Alamos National Laboratory, Montana Bureau of Mines and Geology, Centro de Investigacion Cientifica y de Educacion Superior de Ensenada, B.C., Mexico, Unocal Corporation, U.S. Bureau of Mines, and the Montana Bureau of Mines and Geology.

3. The source dimension of an earthquake is usually defined as the maximum linear measure of fault surface that slipped. The source dimension of the Landers earthquake is approximately 70 km. For comparison, the source dimension of a $M \approx 3$ earthquake (generally the smallest earthquake to produce locally felt shaking) is a few hundred meters, while that of a great ($M \geq 8$) earthquake is a few hundred km.

4. C. Kisslinger, *Eng. Geol.* **10** 85 (1976).

5. R.A. Harris and R.W. Simpson, *Nature*, **360** 251, (1992); P.A. Reasenberg and R.W. Simpson, *Science* **255**, 1687 (1992); R. S. Stein and M. Lisowski, *J. Geophys. Rev.* **88**, 6477 (1983); K. W. Hudnut, L. Seeber, J. Pacheco, *Geophys. Res. Letters* **16**, 199-202 (1989); also R. Stein, G.C.P. King and J. Lin, *Nature* **258**, 1328 (1992).

6. K. Sieh, et al., *Science*, in press (1993).

7. We take the southern margin of the Great Basin as defined by the belt of pronounced geophysical anomalies that cut across the southern tip of Nevada the between 36.5° and 37° N (the dash-dot line in Figures 1 and 2). These coincidental anomalies include pronounced gravity and topographic gradients and the southern Nevada transverse seismic belt [G.P. Eaton, R.R. Wahl, H.J. Prostka, D.R. Mabey, M.D. Kleinkopf, in *Cenozoic Tectonics and Regional Geophysics of the Western Cordillera*, R.S. Smith and G.P. Eaton Eds., (Geological Soc. Am. Memoir 152, 1978), pp. 51-91; R.S. Smith and M.L. Sbar, *Geol. Soc. Am. Bull.* **85** , 1205 (1974).]

8. R.E. Wallace *Jour. Geophys. Res.* **89**, 5763 (1984).

9. Maps showing the distribution of geothermal areas and late Cenozoic volcanic centers are found in L.J.P Muffler, Ed., *Assessment of Geothermal Resources of the United States - 1978* U.S. Geological Survey Circular 790, 1979), and R.G. Luedke and R.L. Smith, U.S. Geological Survey Misc. Inv. Series, MAP I-1091B, C (1978, 1981) respectively; S. Hecker, *Utah Geol. Surv. Bull.* (in press);

B.D. Turin, D. Champion, and R.J. Fleck, *Science*, **253**, 654 (1991).

9a. A small swarm occured in the Brawley seismic zone beginning a week after the Landers mainshock. This swarm appears in Figure 2 as a cluster of epicenters in the Imperial Valley (IV).

10. J.D. VanWormer and A.S. Ryall, *Bull. Seismol. Soc. Am.*, **70** 1557 (1980); A.M. Rogers, S.C. Harmsen, E.J. Corbett, D.M. dePolo, K.F. Priestley in *Neotectonics of North America,* D.B. Slemmons, E.R. Engdahl, M.D. Zoback, D.D. Blackwell Eds. (Geol. Soc. Am. 1991) pp. 153-184. This zone is also known as the Eastern California- Central Nevada seismic belt [D.P. Hill, R.E. Wallace, R.S. Cockerham *Earthq. Predct. Res.*, **3** 571 (1985)] and the Eastern California Shear Zone [R.K. Dokka and C.J. Travis, *Tectonics*, **9**, 311 (1990)].

11. J.B. Rundle and D.P. Hill, *Ann. Rev. Earth Planet. Sci.*, **16** 251 (1988). R.A. Bailey and D.P. Hill *Geoscience Canada* **17** 175 (1990).

12. R.B. Smith and W.J. Arabaz, in Neotectonics of North America, D.B. Slemmons, E.R. Engdahl, M.D. Zoback, D.D. Blackwell, Eds., (Geol. Soc. Am., 1991), 185.

13. In addition, less certain observations include a swarm of $M \geq 1.7$ events near Wallace, Idaho (Δ = 1400 km), beginning 4 days after the Landers earthquake [P. Swanson, personal communication, 1992], and three $M2-3$ events in southeastern Oregon near Crump's Hot Springs (Δ = 940 km).

14. Before transforming the seismograms to the frequency domain a 20% cosine taper was applied in the time domain. In the frequency domain cosine tapers were applied between 4 and 5 Hz and 30 and 35 Hz. Between 5 and 30 Hz the filter was flat.

15. We defined the onset delay T_1 at each site as the time interval between the Landers mainshock and the first detected post-Landers earthquake. We represented the post-Landers seismicity at each site by a Poisson process, and estimated its rate, λ, from the first 10 events located at that site. Interevent times in a Poisson process are expected to exceed $3/\lambda$ five percent of the time. We compared the quantity $3/\lambda$ to the onset delay, T_1, at each site, and found $T_1 < 3/\lambda$ at all but one of the sites tested; the swarm near Cascade, Idaho was the exception (see Table 1).

16. We have not attempted to test the hypothesis that a regional strain event acted as a common trigger to both the Landers mainshock and the remote seismicity. Two observations stand against this hypothesis, however: 1) The Parkfield and Long Valley borehole dilatometers showed no evidence for a regional strain event prior to the Landers mainshock; and 2) in no case did triggered seismicity begin before the shear wave arrival from the Landers mainshock.

17. J. Langbein, *J. Geophys Res.* **94**, 9453 (1989).

18. The Landers mainshock did not trigger strong-motion seismometers at distances beyond about 200 km [A. Shakal, *CSMIP Strong-motion Records from the*

Landers, California Earthquake of 28 June 1992, Report No. OSMS 92-09, (Calif. Dept. of Conservation, CDMG, Sacramento CA, 1992)].

19. The relation between mean stress, $\bar{\sigma}$, and dilatational strain is $\bar{\sigma} = k\theta$, where $\bar{\sigma} = \frac{1}{3}(\sigma_{11}+\sigma_{22}+\sigma_{33})$. The stress tensor for a plane shear wave has the form $\mathbf{T} = -\dot{\mathbf{u}}\,(\mathbf{x},t)\,(\mu/\beta)\,[\hat{\mathbf{b}}\hat{\mathbf{k}} + \hat{\mathbf{k}}\hat{\mathbf{b}}]$, where $\hat{\mathbf{k}}$ and $\hat{\mathbf{b}}$ are unit vectors in the propagation and polarization directions, respectively, $\mathbf{u}(\mathbf{x},t)$ is particle displacement, μ is the shear modulus, and β is shear velocity. Taking values appropriate for mid-crustal depths (Poisson ratio = 0.25, $\mu = 3.3\times10^{11}$ dyne/cm^2, $\rho = 2.7$ gm cm^{-3}, and $\beta = 3.5$ km/s) gives $\bar{\sigma} = 0.5\,\theta$ bars with θ in microstrain, and $|\mathbf{T}| \approx c\,\dot{\mathbf{u}}(\mathbf{x},t)$ bars, where $c = 1$ (bar s/cm). Note that the relation between dynamic stress and particle velocity does not depend on frequency for harmonic, plane waves [J.N. Brune, *J. Geophys. Res.*, **75** 4997 (1970).]

20. L-B Liu, E. Roeloffs, X-Y Zheng, *J. Geophys. Res.* **94**, 9453 (1989)

21. M.L. Sorey, personal communication, 1992; G.M. O'Brian and P. Tucci, EOS, 73, 157 (1992).

22. E.R. Engdahl and W.A. Rinehart, in *Neotectonics of North America* D.B. Slemmons, E.R. Engdahl, M.D. Zoback, D.D. Blackwell, Eds., (Geol. Soc. Am., 1991).

23. The interval between eruptions of the Old Faithful geyser in Calistoga, California, (30 km south-southwest of the Geysers geothermal field) also seems to be sensitive to large ($M \geq 5.5$), regional earthquakes [P.G. Silver and N.J. Valette-Silver,

Science, **257** (1992), 1363]. The Calistoga geyser, however, failed to respond to the Landers mainshock (P.G. Silver, personal communication, 1992).

24. J. Mori et *al.*, in *Volcanic Hazards*, J.H. Latter, Ed., (Springer-Verlag, 1989), pp. 429-462.

25. K. Abe, K. Mogi, personal communication, 1992.

26. Peak stresses due to the solid earth tides typically range from 0.01 to 0.03 bar (strains in the range 0.02 to 0.06 microstrain). Peak tidal stresses the day of the Landers mainshock were about 0.02 bar (0.04 microstrain).

27. D.P. Hill, *J. Geophys. Res.* **87**, 5433 (1982). A. Nur, H. Ron and O. Scotti, Geology 14, 746 (1986).

28. S.C. Jaume and L.R. Sykes, *Science* **258**, 1325 (1992); M.L. Blanpied, D.A. Lockner, J.D. Byerlee, *Nature* **358**, 574 (1992).

29. C. Kisslinger and J.T. Cherry, *Trans. Am. Geophys. Union* **51**, 353 (1970).

30. P. Okubo and J.H. Dieterich, in *Earthquake Source Mechanics*, S. Das, J. Boatwright, C. Scholz, Eds., (Am. Geophys. Union, 1986) pp. 37-48.

31. R.O. Fournier, *Geophys. Res. Lett.* **18**, 955 (1991).

32. R.I. Tilling, J.M. Rhodes, J.W. Sparks, J.P. Lockwood, P.W. Lipman, *Science* **235**, 196 (1987); D.L. Sahagiam and A.A. Proussevitch, *EOS* **73**, 627 (1992).

33. In the terminology of non-linear dynamics, the sites that responded to the Landers earthquake with triggered seismicity had reached a state of self-organized criticality sometime prior to the Landers earthquake, with a correlation length spanning much of the Great Basin [see, for example, J.B. Rundle, in *Chaotic Processes in the Geological Sciences*, D.A. Yuen, Ed., (Springer-Verlag, 1992), 293-303.]

34. Y. Okada, *Bull. Seismol. Soc. Am.* **82**, 1018 (1992).

35. We wish to thank Jim Savage, Paul Spudich, and Tom Hanks (add others as appropriate) for their helpful comments in review.

TABLES

Table 1. Summary of earthquake data and modeling results.

Table 2. Observations of dynamic stress.

FIGURE CAPTIONS

Fig. 1. Map showing seismograph stations in the western United States and Mexico at the time of the Landers earthquake (2). The Landers mainshock rupture is shown by heavy solid line. Major physiographic provinces are outlined by dashed lines. Abbreviations: CP-SRP = Columbia Plateau-Snake River Plain.

Fig. 2. Map showing earthquake earthquake activity detected by the combined seismic network in the 10-day period immediately after the Landers earthquake. Major physiographic provinces are outlined by dashed lines. Faults with quaternary movement are shown by solid lines. Shaded ellipse extending approximately 100 km beyond the Landers rupture represents the aftershock zone. Abbreviations: AZ = Arizona; B = Burney; C = Coso Hot Springs; CA = California; CC = Cedar City, Utah; CM = 1992 Cape Mendocino earthquake epicenter; CNSB = Central Nevada seismic belt; D = Death Valley; E = Excelsior Mountains; G = Geysers; GF = Garlock fault; HFZ = Hurricane fault zone; I = Indian Wells Valley; IV = Imperial Valley; K = 1952 Kern County earthquake epicenter; LP = 1989 Loma Prieta earthquake epicenter; L = Lassen Peak; LV = Long Valley caldera; LT = Lake Tahoe; M = Mono Basin; ML = Medicine Lake caldera; MS = Mount

Shasta; NV = Nevada; OV = Owens Valley; P = Parkfield; PA = Pasadena; SAF = San Andreas fault zone; SCR = Southern Cascade Range; SM = Little Skull Mountain; UT = Utah; W = White Mountains; WF = Wasatch fault zone; WW = White Wolf fault.

Fig. 3. Cumulative number of earthquakes in selected zones, beginning January 1, 1992. Numbers in parentheses are distances (km) from Landers earthquake. Total number of earthquakes in each zone is shown at right. Vertical lines mark times of the April 25, 1992 Petrolia (Cape Mendocino) (M = 7.0) and Landers (M = 7.4) earthquakes.

Fig. 4. Cumulative seismic moment in selected zones, beginning January 1, 1992. Numbers in parentheses are distances (km) from Landers earthquake. Total seismic moment (in dyne-cm) for each zone is shown at right. Vertical lines mark times of the Petrolia (Cape Mendocino) (M = 7.0) and Landers (M = 7.4) earthquakes.

Fig. 5. Unfiltered and filtered vertical-component, ground-velocity seismograms from low-gain Calnet stations at Long Valley caldera, the Geysers geothermal area, and Parkfield. Number next to filtered trace indicates its magnification relative to corresponding unfiltered trace. "S" indicates arrival of Landers S-wave. "1" indicates first identified triggered event at each site.

Fig. 6. Response of seismicity and strain to the Landers earthquake. (A) Cumulative number of earthquakes detected at the Geysers geothermal area in a 24-hour

period surrounding the Landers earthquake. (B) Cumulative number of earthquakes detected at Long Valley caldera between June 1 and August 20, 1992. (C) Dilatational strain recorded at Devils Postpile, located approximately 10 km west of the triggered seismicity in Long Valley caldera, during the same interval. Increasing values correspond to increasing compression. Tidal strains and a secular dilatational strain rate of –0.007 microstrain/day have been removed, but a residual tidal strain signal remains. The transient dynamic Landers signal (6.4 microstrain) is not shown on this record.

Fig. 7. Map showing static mean stress change and peak dynamic stress in bars for the Landers mainshock at mid-crustal depth together with the first 10 days of post-Landers seismicity. The static mean stress change was calculated for an elastic half-space using the three-dimensional boundary element subroutines of Okada (34) and a model for the Landers rupture based on Caltech Terrascope data and surface slip observations (1). "T" indicates typical range of tidal streses. Shading shows the expansional quadrants; the compressional quadrants can be filled in by 90° rotation of the shaded pattern and a sign change. (Maximum static shear stress changes resolved onto vertical planes based on the same model are listed in Table 1.) Numbers indicate peak dynamic mean stress from borehole dilatometer data (triangles) and peak dynamic shear stress from regional digital seismic stations (diamonds). Value at Parkfield is mean of 6 dilatometer observations. Parenthetic numbers are peak dynamic stresses for the M = 7.0 Petrolia (Cape Mendocino) earthquake, shown for comparison. Contours suggest general pattern of peak dynamic stresses from the Landers mainshock without distinguish-

ing between mean and shear stresses.

Table 1.— *Summary of earthquake data and modeling results.*

Region	Approximate Distance (km)	Source Lengths (1)	Static Stress Change (2) (bar)	Fraction of Tidal (3)	Maximum Magnitude (4)	N_b (5)	N_a (6)	T_1 (hr)(7)	T_m (hr)(8)
China Lake	165 – 205	2.2 – 2.8	$2 - 6 \times 10^{-2}$	1 – 3	4.4	4	44	8.6	4.6
Skull Mountain	240	3.2	2.8×10^{-2}	1.4	5.6	10	59	1.5	0.9
Death Valley	300	4.1	8.0×10^{-3}	0.4	3.6	6	11	5.3	12.4
White Mountains †	380 – 420	5.1 – 5.7	$2.3 - 3.0 \times 10^{-4}$	0.3	3.7	0	27	11.6	12.0
Parkfield †	410	5.5	6.9×10^{-3}	0.35	—	8	11	—	—
Long Valley †	415	5.6	2.8×10^{-3}	0.14	3.4	38	340	0.15	0.052
Mono Basin †	450	6.1	1.9×10^{-3}	0.05	3.1	3	12	19.1	12.0
Cedar City	490	6.6	3.6×10^{-3}	0.18	4.1	0	39	0.63	1.3
Western Nevada †	450 – 650	6.1 – 8.8	$0.6 - 2.0 \times 10^{-3}$	0.03 – 0.1	4.0	58	504	0.15	0.10
Geysers (9) †	740	10.0	8.7×10^{-4}	0.04	1.6	70	60	0.05	0.01
Lassen †	840	10.9	3.9×10^{-4}	0.02	2.8	0	14	0.2	5.4
Burney †	900	12.4	2.9×10^{-4}	0.015	2.8	1	9	23.0	21.0
Cascade, Idaho	1100	14.9	2.5×10^{-4}	0.01	1.7	0	38	33.3	1.2
Yellowstone †	1250	16.9	2.3×10^{-4}	0.01	2.1	0	16	1.8	2.1

1. Assumes a source length of 74 km based on surface faulting observations.

2. Maximum static horizontal shear stress change on optimally oriented vertical planes.

3. Assumes daily tidal stress variation of 2×10^{-2} bar.

4. During first week of triggered activity.

5. Numbers of events located during 7 days preceeding the Landers mainshock (June 21 to June 28).

6. Numbers of events located during 7 days following the Landers mainshock (June 28 to July 5).

7. T_1 is defined as time between Landers mainshock and first located post-Landers earthquake.

8. T_m is defined as mean interevent time of first 10 local earthquakes in post-Landers activity. T_1 and T_m reflect only earthquakes included in catalogs.

9. N_a and N_b reflect Calnet data. T_1 and T_m reflect Unocal data.

† Indicates regions where high-pass filtering of seismograms was used to extract early events from Landers coda.

Table 2.— *Observations of dynamic stress.*

Station	Type	Latitude	Longitude	Epicentral Distance (km)	Peak stress (bar)
SVD	3	34.104	117.100	63	9.4
PFO	3	33.609	116.460	67	5.8
GSC	3	35.300	116.810	125	19.1
PUBS	1	34.434	117.874	135	2.5
PAS	3	34.148	118.170	161	7.5
ISA	3	35.643	118.480	245	3.6
SBC	3	34.422	119.710	303	4.1
RHDS	1	35.624	120.255	382	1.5
JCDS	1	35.716	120.205	382	1.4
GH1S	1	35.831	120.346	399	2.0
DLDS	1	35.940	120.423	411	2.5
FRDS	1	35.911	120.486	415	1.6
VCDS	1	35.922	120.533	419	1.6
POPS	1	37.632	119.079	448	3.2
SAO	3	36.765	121.440	535	1.4
CMB	2	38.035	120.390	553	3.0
MHC	2	37.342	120.640	585	1.5
STAN	2	37.404	122.170	628	1.2
BKS	2	37.877	122.240	662	1.2
ASC	2	40.877	124.070	1000	0.8

Station types: 1 = U.S. Geological Survey borehole strainmeter; 2 = Berkeley Digital Seismic Network seismometer; 3 = Caltech Terrascope Network seismometer.

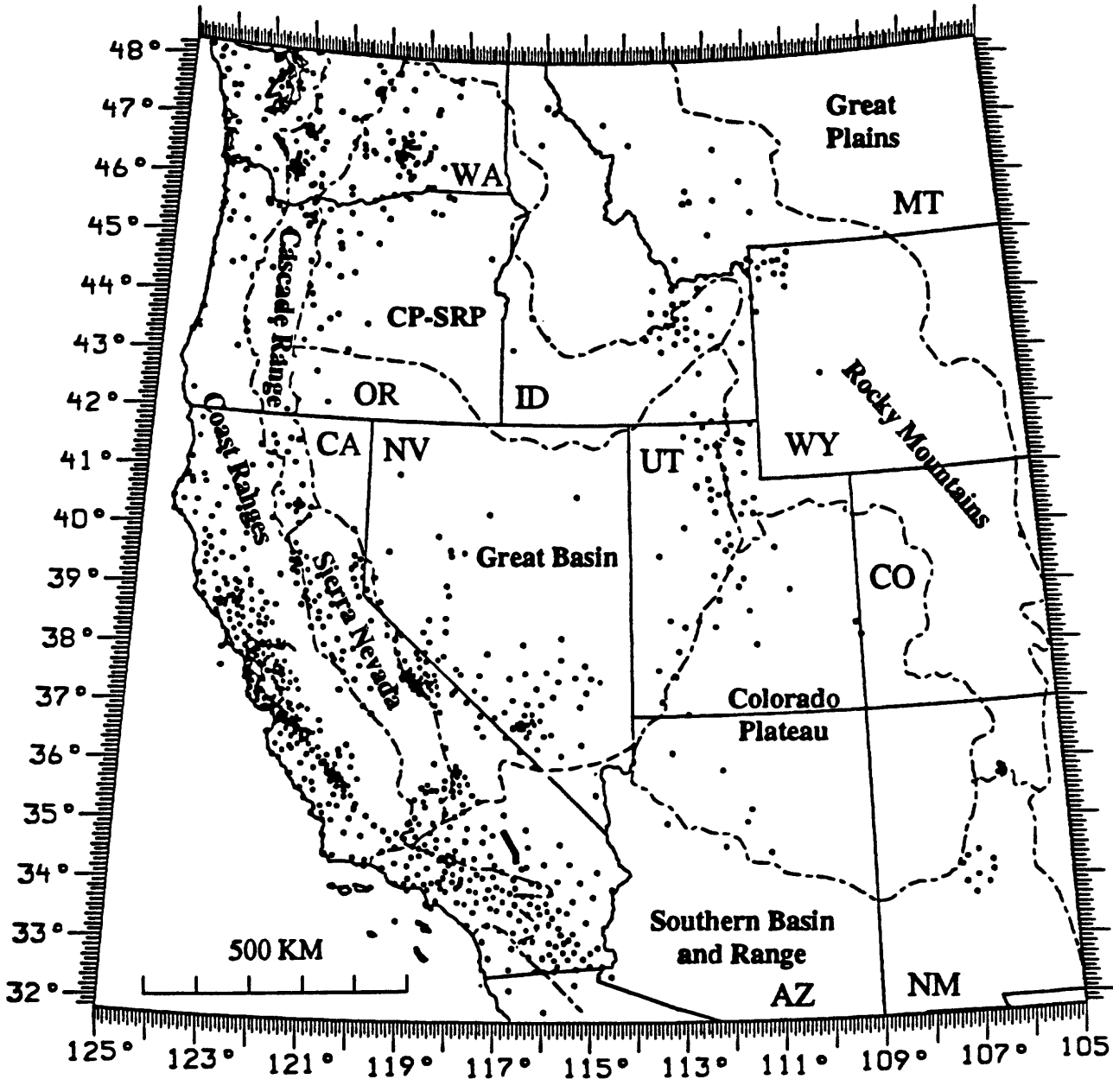
48°
47°
46°
45°
44°
43°
42°
41°
40°
39°
38°
37°
36°
35°
34°
33°
32°
125°
123°
121°
119°
117°
115°
113°
111°
109°
107°
105°
Great Plains
WA
MT
CP-SRP
Cascade Range
OR
ID
Rocky Mountains
Coast Ranges
CA
NV
UT
WY
Great Basin
Sierra Nevada
CO
Colorado Plateau
Southern Basin and Range
AZ
NM
500 KM

Figure 1

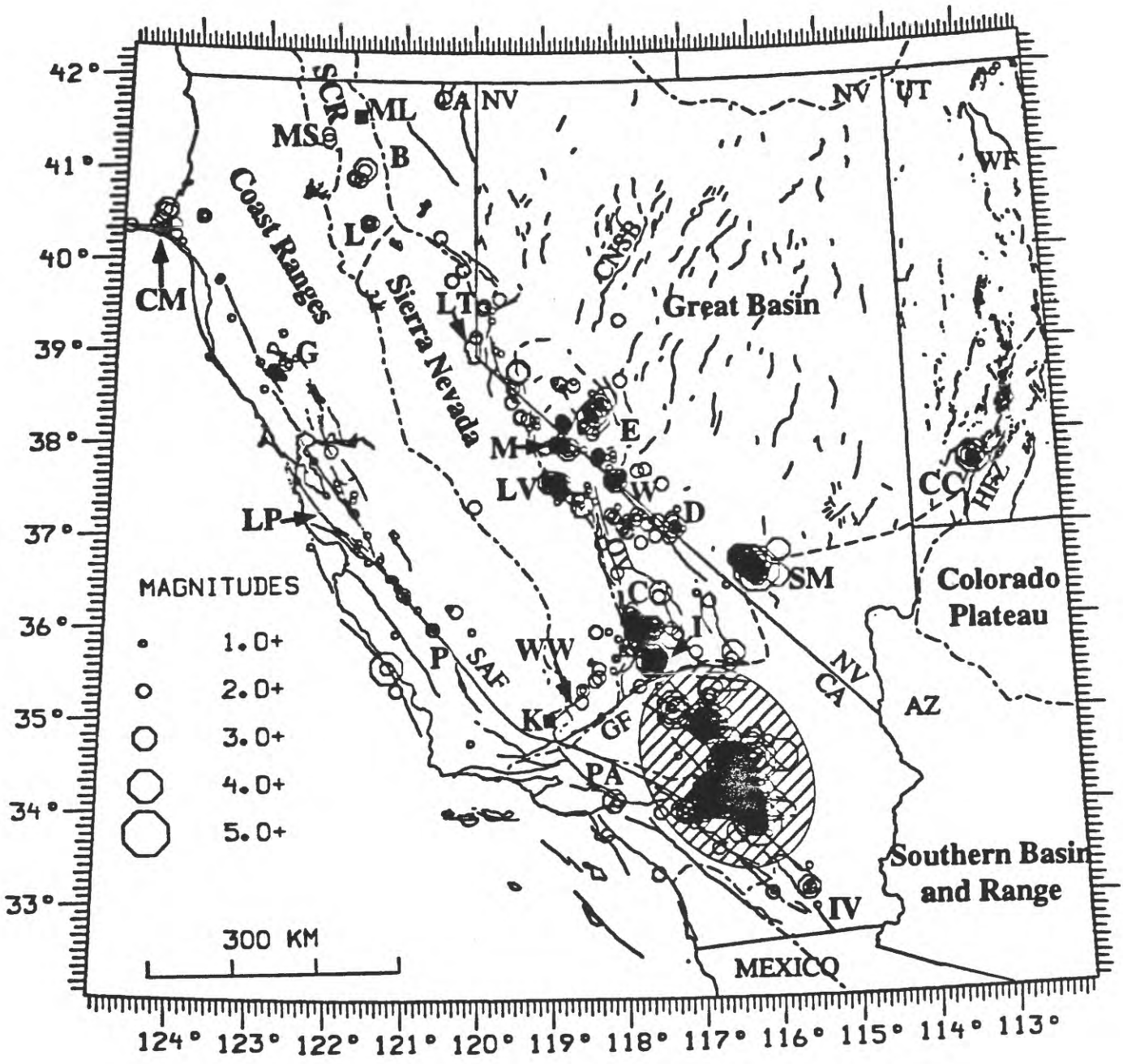
42°
41°
40°
39°
38°
37°
36°
35°
34°
33°
CA
NV
NV
UT
CR
ML
MS
B
L
CM
Coast Ranges
Sierra Nevada
LT
CNSB
Great Basin
G
E
M
LV
W
D
LP
SM
Colorado
Plateau
CC
HR
WF
MAGNITUDES
1.0+
2.0+
3.0+
4.0+
5.0+
C
I
P
SAF
WW
NV
CA
AZ
K
GF
PA
Southern Basin
and Range
IV
300 KM
MEXICO
124° 123° 122° 121° 120° 119° 118° 117° 116° 115° 114° 113°

Figure 2

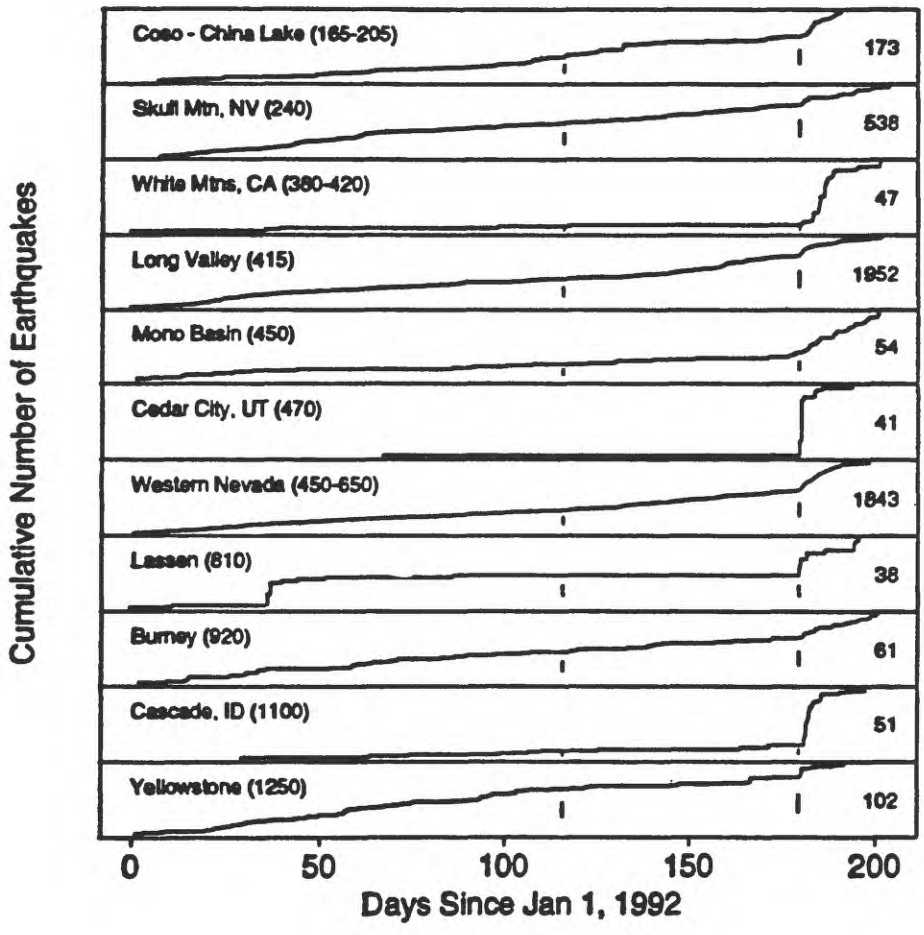
Coso - China Lake (165-205)
173
Skull Mtn, NV (240)
538
White Mtns, CA (380-420)
47
Long Valley (415)
1952
Mono Basin (450)
54
Cedar City, UT (470)
41
Western Nevada (450-650)
1843
Lassen (810)
38
Burney (920)
61
Cascade, ID (1100)
51
Yellowstone (1250)
102
Cumulative Number of Earthquakes
0
50
100
150
200
Days Since Jan 1, 1992

Figure 3

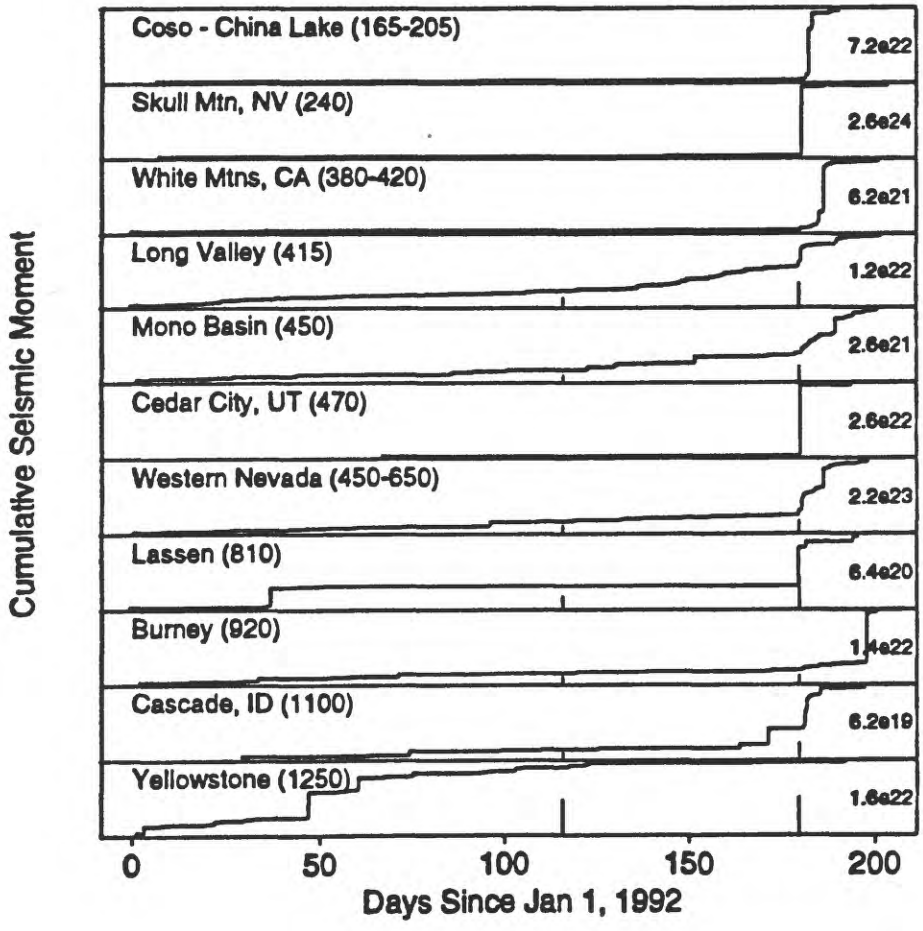
Coso - China Lake (165-205)
7.2e22
Skull Mtn, NV (240)
2.6e24
White Mtns, CA (380-420)
6.2e21
Long Valley (415)
1.2e22
Mono Basin (450)
2.6e21
Cedar City, UT (470)
2.6e22
Western Nevada (450-650)
2.2e23
Lassen (810)
6.4e20
Burney (920)
1.4e22
Cascade, ID (1100)
6.2e19
Yellowstone (1250)
1.6e22
Cumulative Seismic Moment
0
50
100
150
200
Days Since Jan 1, 1992

Figure 4

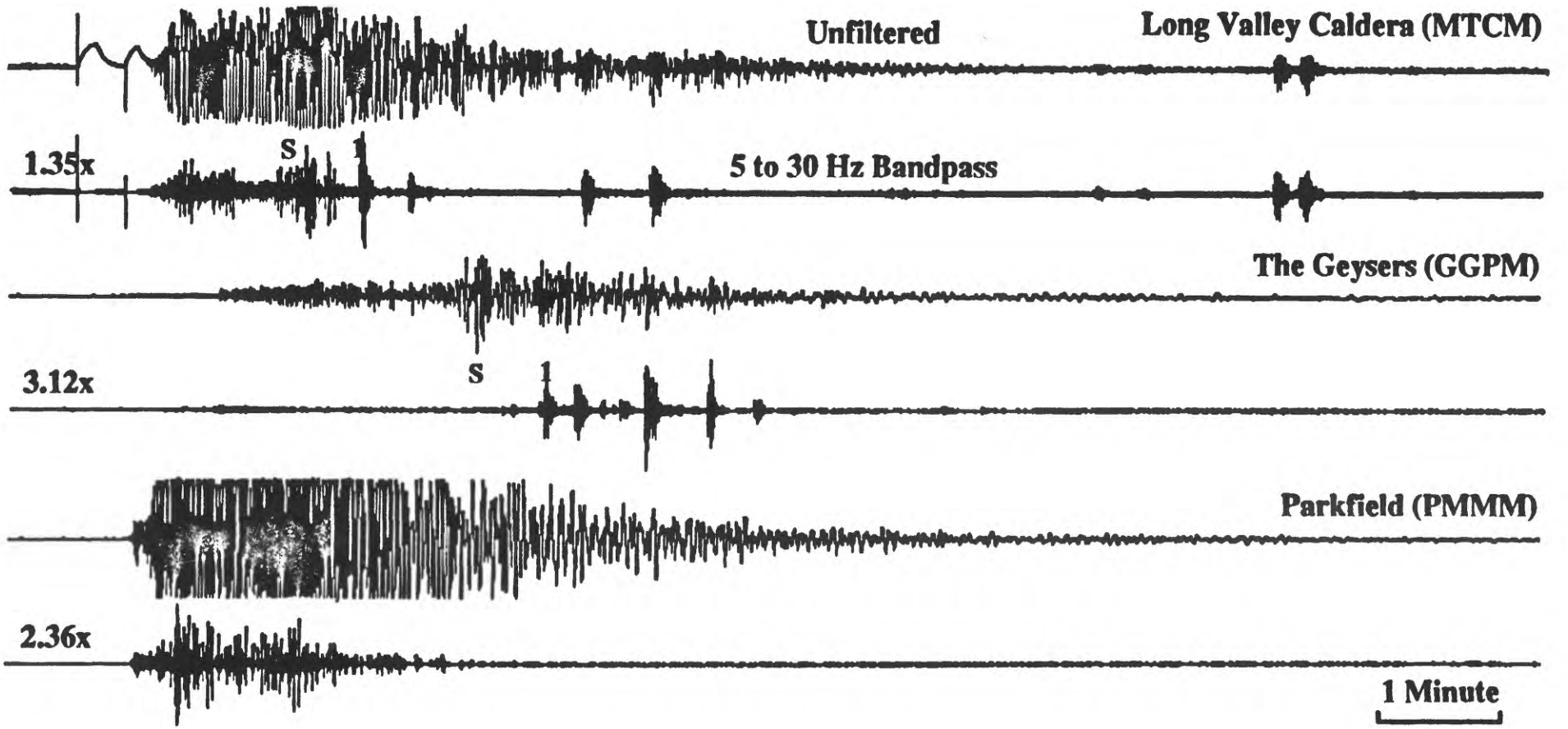
Unfiltered
Long Valley Caldera (MTCM)
1.35x
S
1
5 to 30 Hz Bandpass
The Geysers (GGPM)
3.12x
S
1
Parkfield (PMMM)
2.36x
1 Minute

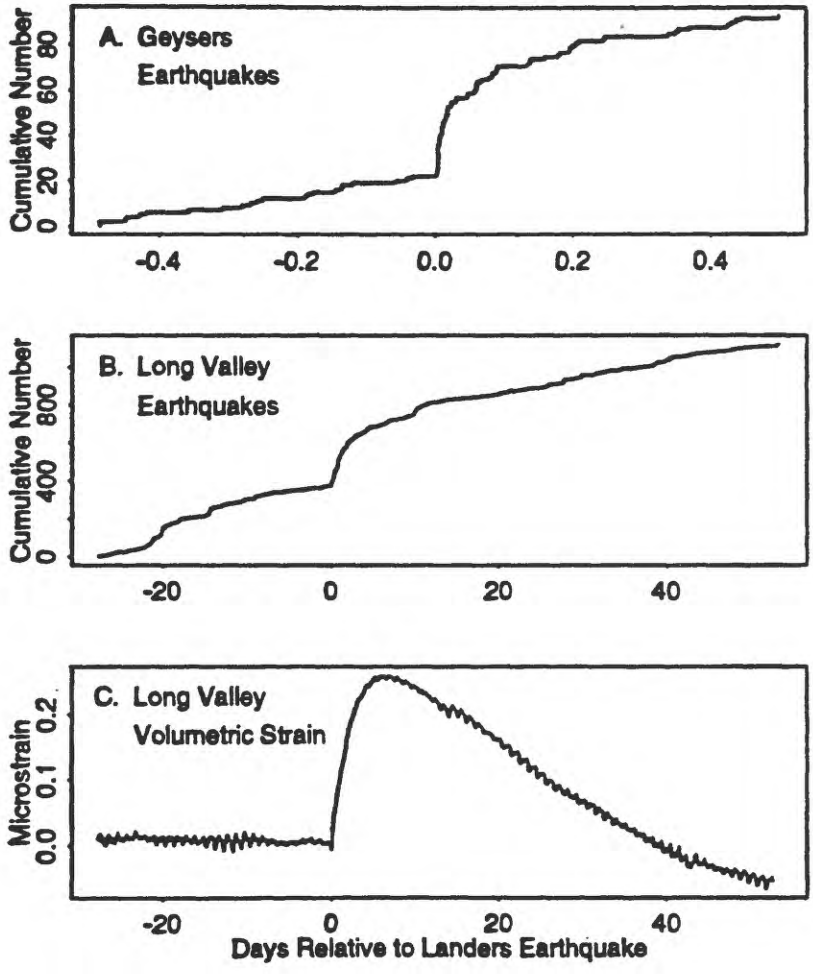
A. Geysers
Earthquakes
Cumulative Number
0 20 40 60 80
-0.4 -0.2 0.0 0.2 0.4
B. Long Valley
Earthquakes
Cumulative Number
0 400 800
-20 0 20 40
C. Long Valley
Volumetric Strain
Microstrain
0.0 0.1 0.2
-20 0 20 40
Days Relative to Landers Earthquake

Figure 6

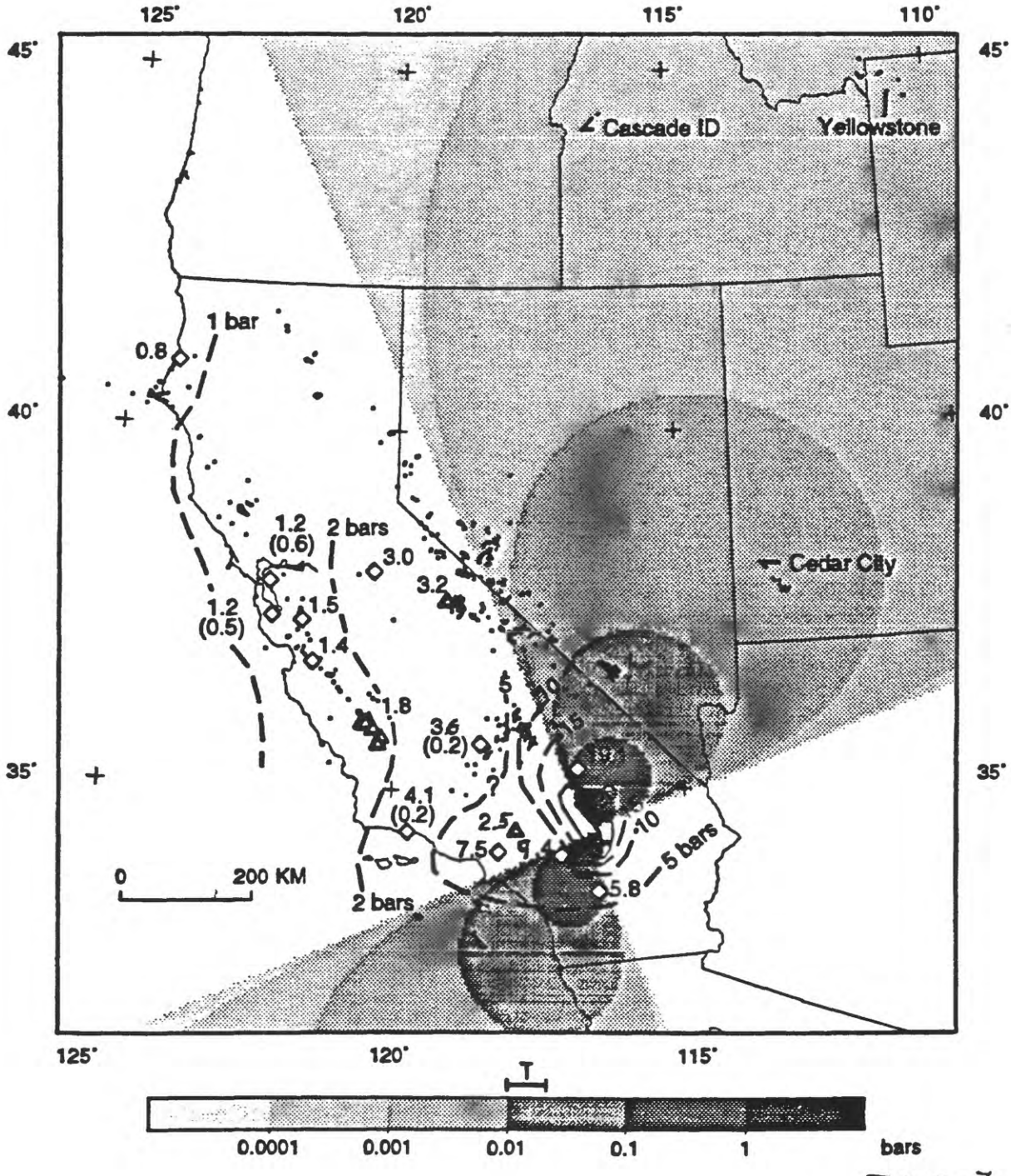
125°
120°
115°
110°
45°
40°
35°
Cascade ID
Yellowstone
Cedar City
1 bar
0.8
1.2
(0.6)
2 bars
3.0
3.2
1.2
(0.5)
1.5
1.4
1.8
3.6
(0.2)
4.1
(0.2)
2.5
7.5
10
5 bars
5.8
2 bars
0
200 KM
T
0.0001
0.001
0.01
0.1
1
bars

Figure 7

CONFERENCES TO DATE

Conference I	Abnormal Animal Behavior Prior to Earthquakes, I Not Open-Filed
Conference II	Experimental Studies of Rock Friction with Application to Earthquake Prediction Not Open-Filed
Conference III	Fault Mechanics and Its Relation to Earthquake Predition Open-File No. 78-380
Conference IV	Use of Volunteers in the Earthquake Hazards Reduction Program Open-File No. 78-336
Conference V	Communicating Earthquake Hazard Reduction Information Open-File No. 78-933
Conference VI	Methodology for Identifying Seismic Gaps and Soon-to-Break Gaps Open-File No. 78-943
Conference VII	Stress amd Strain Measurements Related to Earthquake Prediction Open-File No. 79-370
Conference VIII	Analysis of Actual Fault Zones in Bedrock Open-File No. 79-1239
Conference IX	Magnitude of Deviatoric Stresses in the Earth's Crust and Upper Mantle Open-File No. 80-625
Conference X	Earthquake Hazards Along the Wasatch and Sierra-Nevada Frontal Fault Zones Open-File No. 80-801
Conference XI	Abnormal Animal Behavior Prior to Earthquakes, II Open-File No. 80-453
Conference XII	Earthquake Prediction Information Open-File No. 80-843
Conference XIII	Evaluation of Regional Seismic Hazards and Risk Open-File No. 81-437
Conference XIV	Earthquake Hazards of the Puget Sound Region, Washington Open-File No. 82-19
Conference XV	A Workshop on "Preparing for and Responding to a Damaging Earthquake in the Eastern United States" Open-File No. 82-220
Conference XVI	The Dynamic Characteristics of Faulting Inferred from Recording of Strong Ground Motion Open-File No. 82-591
Conference XVII	Hydraulic Fracturing Stress Measurements Open-File No. 82-1075
Conference XVIII	A Workshop on "Continuing Actions to Reduce Losses from Earthquakes in the Mississippi Valley Area" Open-File No. 83-157
Conference XIX	Active Tectonic and Magmatic Processes Beneath Long Valley Open-File No. 84-939

Conference XX	A Workshop on "The 1886 Charleston, South Carolina, Earthquake and its Implications for Today" Open-File No. 83-843
Conference XXI	A Workshop on "Continuing Actions to Reduce Potential Losses from Future Earthquakes in the Northeastern United States" Open-File No. 83-844
Conference XXII	A Workshop on "Site-Specific Effects of Soil and Rock on Ground Motion and the Implications for Earthquake-Resistant Design" Open-File No. 83-845
Conference XXIII	A Workshop on "Continuing Actions to Reduce Potential Losses from Future Earthquakes in Arkansas and Nearby States" Open-File No. 83-846
Conference XXIV	A Workshop on "Geologic Hazards in Puerto Rico" Open-File No. 84-761
Conference XXV	A Workshop on "Earthquake Hazards in the Virgin Islands Region" Open-File No. 84-762
Conference XXVI	A Workshop on "Evaluation of the Regional and Urban Earthquake Hazards in Utah" Open-File No. 84-763
Conference XXVII	Mechanics of the May 2, 1983 Coalinga Earthquake Open-File No. 85-44
Conference XXVIII	A Workshop on "The Borah Peak, Idaho, Earthquake" Open-File No. 85-290
Conference XXIX	A Workshop on "Continuing Actions to Reduce Potential Losses from Future Earthquakes in New York and Nearby States" Open-File No. 85-386
Conference XXX	A Workshop on "Reducing Potential Losses from Earthquake Hazards in Puerto Rico" Open-File No. 85-731
Conference XXXI	A Workshop on "Evaluation of Regional and Urban Earthquake Hazards and Risk in Alaska" Open-File No. 86-79
Conference XXXII	A Workshop on "Future Directions in Evaluating Earthquake Hazards of Southern California" Open-File No. 86-401
Conference XXXIII	A Workshop on "Earthquake Hazards in the Puget Sound, Washington Area" Open-File No. 86-253
Conference XXXIV	A Workshop on "Probabilistic Earthquake-Hazards Assessments" Open-File No. 86-185
Conference XXXV	A Workshop on "Earth Science Considerations for Earthquake Hazards Reduction in the Central United States" Open-File No. 86-425

Conference XXXVI	A Workshop on "Assessment of Geologic Hazards and Risk in Puerto Rico" Open-File No. 87-007
Conference XXXVII	A Workshop on "Earthquake Hazards Along the Wasatch, Utah" Open-File No. 87-154
Conference XXXVIII	A Workshop on "Physical & Observational Basis for Intermediate Term Earthquake Prediction" Open-File 87-154
Conference XXXIX	Directions in Paeloseismology Open-File No. 87-673
Conference XL	A Workshop on "The U.S. Geological Survey's Role in Hazares Warnings" Open File No. 87-269
Conference XLI	A Review of the Earthquake Research Applications in the National Earthquake Hazard Reduction Program: 1977-1987 Open-File No. 88-13-A
Conference XLII	A Workshop on "Evaluation of Earthquake Hazards and Risk in the Puget Sound and Portland Areas" Open File No. 88-541
Conference XLIII	A Workshop on "Earthquake Risk: Information Needs of the Insurance Industry" Open-File No. 88-669
Conference XLIV	A Workshop on "Geological, Geoophysical, and Tectonic Settings of the Cascade Range" Open-File No. 89-178
Conference XLV	A Workshop on "Fault Segmentation and Controls of Rupture Initiation and Termination" Open-File No. 89-315
Conference XLVI	The 7th U.S.- Japan Seminar on Earthquake Prediction Open-File No. 90-98
Conference XLVII	A Workshop on "USGS'S New Generation of Probabilistic Ground Motion Maps and their Applications to Building Codes" Open-File No. 89-364
Conference XLVIII	A Workshop on "Earthquake Hazards in the Puget Sound, Portland Area" Open-File No. 89-465
Conference IL	A Meeting of the U.S. AD HOC Working Group on: "Earthquake Related Casualties" Open-File No. 90-244
Conference LX	4th Annual Workshop on "Earthquake Hazards in the Puget Sound, Portland Area" Open-File No. 90-xxx
Conference LXI	A Workshop on " Role of State Geological Surveys in Postearthquake Investigations" Open-File No. 93-346
Conference LXII	Proceeding of the "Eighth Joint Meeting of the U.S.-Japan Conference on Natural Resources (UJNP) Open-File No. 93-xx

For information on ordering the above publications, please contact:

U.S. Geological Survey
Books and Open-File Reports Service Section
Building 41, Box 25425
Federal Center
Denver, Colorado 80225

☆U.S. GOVERNMENT PRINTING OFFICE: 1993-787-197/99215